

THE UNIVERSITY OF HULL

New Inorganic Nanomaterials for Low-Voltage Transistor Applications

Being a Thesis submitted for the Degree of
Doctor of Philosophy (PhD)
In the University of Hull

By

Fahad Ahmed A Alharthi, B.Sc., M.Sc.

May 2016

Acknowledgments

Firstly, I thank ALLAH for giving me the strength, patience, courage and maturity to face and undergo one of the most challenging events of my life.

Also, I would like to thank my supervisor, Professor Stephen M Kelly for providing me the freedom to carry out interesting and unique research. Professor Kelly has provided guidance and support, which has made my research for my PhD studies very interesting and enjoyable.

Also, I would like to thank Professor Gillian M Greenway for their help and advices. As well, I would like to thank Dr Fei Cheng for his useful discussion, suggestions and valuable advices.

I would also like to thank some members of the Organophotonics group. Special thanks are reserved for Professor Mary O'Neill, Dr Neil T Kemp and Dr Emanuele Verrelli and Mohammed A Ibrahim for useful suggestions valuable advices. A great thank to Dr Emanuele Verrelli to provide electrical characterisation.

I would like to thank all the staff in the Department of Chemistry at the University of Hull. I would like to thank the technical staff of the chemistry department for providing analysis of the resultants synthesised in this thesis. This includes Dr Adam Lee (XPS), Mrs Carol Kennedy (Elemental analysis) and Mr Bob Kinght (ICP), Mrs Ann Lowry (TEM) and Mr Ian Dobson (TGA).

Also, a countless thanks to my parents, Salehah and Ahmed, for their help, support and patience while I am away from them. As well, would like my uncles, Fahad and Mussaed for their support. In addition, great thanks to my brothers, sisters and my cousins my family for support and prays.

A huge thanks to Dr Awadh Ali a consultant in Abu Dhabi Authority for Culture and Heritage in UAE for his useful help and advice. A lovely thank you for my wife, Reem, and my children, Hadeel, Yam and Tallal, for their help and patience. Thanks for every how ask about me and help me during PhD journey.

Finally, I would like to thank King Saud University (KSU) and the Royal Embassy of Saudi Arabia Cultural Bureau in London for the financial support.

Abstract

This research aims to synthesise and characterise solution-processable high- k dielectric nanorods, which are potentially suitable for use as the dielectric layer in low-voltage Organic Field-Effect Transistor (OFET) applications. Oleic acid-stabilised titanium dioxide nanorods ($\text{TiO}_2\text{-OA}$), metal-doped anatase titanium oxide ($\text{TiO}_2\text{-OA-M}$; $\text{M}=\text{Nb}$, In , or Nb/In) nanorods, rutile titanium oxide nanorods (TiO_2) and barium titanium oxide nanorods (BaTiO_3) have been prepared and investigated.

Solution processable oleic acid-stabilised titanium dioxide nanorods ($\text{TiO}_2\text{-OA}$) have been prepared by hydrolysis of titanium (IV) tetraisopropoxide (TTIP) with oleic acid (OA) as surfactant in the presence of trimethylamine N-oxide (TMAO). Furthermore, a series of ligand exchange reactions were carried out to replace the oleic acid bonded on the surface of $\text{TiO}_2\text{-OA}$ with diethyl 2-phenylethyl phosphonate (DEPPNA), octadecylphosphonic acid (ODPA) or octylphosphonic acid (OPA). The ligand exchange rate was characterised by a combination of ^{31}P liquid NMR, ICP, CHN, and FT-IR. The solubility of the ligand-exchanged products in chlorobenzene was also investigated.

A novel method based on the co-hydrolysis of titanium (IV) tetraisopropoxide (TTIP) and niobium or/and indium isopropoxide or ethoxide has been investigated to prepare solution-processable, oleic acid-stabilised, niobium- and indium-doped, anatase TiO_2 nanorods ($\text{TiO}_2\text{-OA-M}$; $\text{M} = \text{Nb}$, In or Nb/In). The effect of niobium and indium precursors, the molar ratio of Nb or In precursors/TTIP and reaction time on the composition, structure and morphology of the Nb or In doped TiO_2 products have been investigated by a combination of XPS, XRD, ICP, CHN, FT-IR and TEM. Furthermore, a series of ligand exchange reactions were carried out to replace the oleic acid, which is bonded on the surface of $\text{TiO}_2\text{-OA-M}$, with diethyl 2-phenylethyl phosphonate (DEPPNA) or octadecylphosphonic acid (ODPA). The solubility of the products in chlorobenzene was also investigated.

Rutile titanium dioxide nanorods with different sizes were prepared by three different approaches. In the first approach, hair-like rutile nanorods TiO_2 were prepared by simple hydrolysis of a TiOCl_2 solution at low temperature (50, 70 and 90 °C). In the second approach,

rutile nanorods TiO_2 with a length of 150-200 nm and a width of 25-40 nm were prepared by using a hydrothermal treatment of TiOCl_2 at 220 °C. In the third approach, rutile nanorods TiO_2 with length of 80 nm and diameter of 20 nm were prepared by using an hydrothermal reaction of TiOCl_2 in the presence of 3-hydroxytyramine hydrogen chloride, $[(\text{HO})_2\text{C}_6\text{H}_3\text{CH}_2\text{CH}_2\text{NH}_2\cdot\text{HCl}]$ at 150°C. In order to improve the solubility of the obtained rutile titanium dioxide nanorods in organic solvents, different surface-modification methods have been investigated to coat the surface of the rutile titanium dioxide nanorods with various organic ligands. In the first method, a modification of the TiO_2 nanorods with oleic acid (OA) in chlorobenzene was investigated. In the second method, a two-stage treatment of TiO_2 nanorods in an acidic medium was studied, using a selection of oleic acid (OA), diethyl 2-phenylethyl phosphonate (DEPPNA), octylphosphonic acid (OPA) and decylphosphonic acid (ODPA) as ligands. In the third method, wet TiO_2 nanorods before dry was directly modified with a range of oleic acid and amines, *e.g.*, octylamine, dodecylamine and hexadecylamine, as ligands. All the products were characterized by a combination of XRD, ICP, CHN, FT-IR and TEM.

The preparation of barium titanium oxide nanorods (BaTiO_3) has been investigated by different approaches. In the first approach, a hydrothermal reaction was carried out to convert the titanium dioxide nanorods prepared in the first and third parts in this research into BaTiO_3 nanorods. The effect of the molar ratio of Ba/Ti, the reaction pH, reaction time and temperature on the composition, structure and morphology of the products were fully investigated. In the second approach, a hydrothermal reaction using a single source Ba/Ti precursor, *i.e.*, barium titanium ethylhexano-isopropoxide $\text{BaTi}(\text{O}_2\text{CC}_7\text{H}_{15})(\text{OC}_3\text{H}_7)_5$, was carried out to prepare barium titanium oxide nanorods. In the third approach, barium titanium oxide nanorods were prepared by using a hydrothermal reaction between barium chloride (BaCl_2) and titanium oxy chloride (TiOCl_2) in the presence of ethylene glycol as surfactant. All the products have been characterised by a combination of XRD, ICP, CHN, FT-IR and TEM.

List of Abbreviations

Some common abbreviations used in this report are shown below:

CHN	Carbon, hydrogen and nitrogen
DEPPNA	Diethyl 2-phenylethyl phosphonate
EDX	Energy-dispersive X-ray spectroscopy
FT-IR	Fourier transform infrared spectroscopy
ICP	Inductively coupled plasma
INEO	Indium (III) ethoxide
INIO	Indium (III) isopropoxide
<i>k</i>	Dielectric constant
NBEO	Niobium (V) ethoxide
NBIO	Niobium isopropoxide
NMR	Nuclear magnetic resonance
NP	Nanoparticles
NW	Nanowires
OA	Oleic acid
ODPA	Decylphosphonic acid
OPA	Octylphosphonic acid
OFET	Organic Field Effect Transistors
TEM	Transmission electron microscopy
TGA	Thermal gravimetric analysis
TiO ₂ -M	Metal-doped (Nb/In) anatase titanium dioxide nanorods
TiO ₂ -OA	The oleic acid-stabilised titanium dioxide nanorods
TTIP	Titanium tetraisopropoxide

XPS	X-Ray photoelectron spectroscopy
XRD	X-Ray diffractometer
1D	One-dimensional

Aims

The main aim of this thesis is the synthesis and characterisation of solution-processable titanium dioxide and barium titanium oxide nanorods with a very high dielectric constant, k . The solution-processable high- k materials should be potentially useful as substitute gate insulator in Organic Field Effect Transistors (OFETs). In order to achieve this main aim, the preparation and characterisation of titanium dioxide nanorods (TiO_2) in both the anatase and rutile polymorphs, niobium-, indium- and niobium/indium-doped anatase titanium dioxide nanorods ($\text{TiO}_2\text{-M}$, where $\text{M} = \text{Ni}, \text{In}$ and Ni/In) and barium titanium oxide nanorods (BaTiO_3) will be investigated.

The preparation of solution-processable titanium dioxide nanorods, oleic acid-stabilised titanium dioxide nanorods ($\text{TiO}_2\text{-OA}$), in the anatase phase will be investigated. The obtained anatase titanium dioxide nanorods should exhibit an aspect ratio of at least 5 and be easily dissolvable at relatively high concentration, *e.g.*, ca. 10 wt%, in common organic solvents used for the deposition from solution of thin, uniform films of defined thickness and configuration on a substrate surface, such as chlorobenzene, using standard techniques, such spin coating, drop casting, doctor blade, inkjet printing processes, etc. In addition, ligand-exchange reactions involving anatase oleic acid-stabilised titanium dioxide nanorods ($\text{TiO}_2\text{-OA}$) and a variety of ligands with different head-groups and alkyl chain lengths, such as phosphonic acid; octylphosphonic acid (OPA) and decylphosphonic acid (ODPA) and phosphonate ligand; 2-phenylethyl phosphonate (DEPPNA), will also be investigated to prepare titanium dioxide nanorods with improved dielectric properties. The anatase oleic acid-stabilised titanium dioxide nanorods ($\text{TiO}_2\text{-OA}$) should ideally be about 20 nm in length and 3-4 nm in diameter for practical applications. Hair-like rutile titanium dioxide nanorods (TiO_2) (Rutile-NRs-1) and rutile titanium dioxide nanorods (TiO_2) (Rutile-NRs-2) with 150-200 nm and 25-40 nm, in length and diameter, restrictively will be prepared. Surface modification of the prepared rutile titanium dioxide nanorods (TiO_2) (Rutile-NRs-1 and Rutile-NRs-2) will be carried out using wet rutile titanium dioxide nanorods (TiO_2) with ligands, such as oleic acid and alkyl amines *i.e.*, octyl amine, dodecyl amine and hexadecyl amine.

The preparation of solution-processable metal-doped anatase nanorods ($\text{TiO}_2\text{-M}$; where $\text{M} = \text{Ni}$, In and Ni/In) will be investigated using a novel sol-gel process. The intention is to produce titanium dioxide nanorods doped with *n*-type, indium, and *p*-type, niobium dopants with a lower dielectric loss compared with that of the corresponding pure anatase titanium dioxide nanorods. Titanium dioxide nanorods with *n*-type indium and *p*-type niobium dopants is expected to exhibit an advantageous combination of high dielectric constant and low dielectric loss. The ligand exchange of oleic acid on metal doped anatase titanium dioxide nanorods ($\text{TiO}_2\text{-M}$) surface with phosphonic acid; decylphosphonic acid (ODPA) and phosphonate ligand; 2-phenylethyl phosphonate (DEPPNA) will be investigated.

The preparation of solution-processable titanium dioxide nanorods (TiO_2) in the rutile, rather than the anatase, phase with different dimensions will be investigated. Surface modification of the rutile titanium dioxide nanorods using with different ligands, such as oleic acid and alkyl amines will also be investigated in order to improve the solubility of these titanium oxide nanorods in common organic solvents.

The synthesis of barium titanium oxide (BaTiO_3) will be investigated using different procedures. A novel method for transforming titanium dioxide nanorods (TiO_2) into barium titanium oxide (BaTiO_3) nanorods using a hydrothermal reaction will be developed. The main challenge in adopting this approach will be to ensure the complete conversion of titanium dioxide nanorods to the corresponding barium titanium oxide nanorods while retaining the original shape and size of the original titanium dioxide nanorods in the final barium titanium oxide products.

The preparation of barium titanium oxide (BaTiO_3) will be investigated using three general approaches. In approach 1 (NRs- $\text{BaTiO}_3\text{-1}$), barium titanium oxide nanorods will be prepared by converting titanium dioxide nanorods (TiO_2) to barium titanium oxide. There different types of titanium dioxide nanorods (TiO_2) will be used as starting material, *i.e.*, anatase oleic acid-stabilised titanium dioxide nanorods ($\text{TiO}_2\text{-OA}$), rutile titanium dioxide nanorods. In Approach 2 (NRs- $\text{BaTiO}_3\text{-2}$) preparation of barium titanium oxide will be investigated using hydrothermal reaction of Ba/Ti single source precursor, barium titanium ethylhexanoisopropoxide $\text{BaTi}(\text{O}_2\text{CC}_7\text{H}_{15})(\text{OC}_3\text{H}_7)_5$. In Approach 3 (NRs- $\text{BaTiO}_3\text{-3}$) preparation of barium titanium oxide will be investigated using hydrothermal reaction between barium chloride (BaCl_2) and titanium oxy chloride (TiOCl_2) in presence of ethylene glycol as surfactant.

The synthesis challenge for the preparation of both titanium dioxide nanorods (TiO_2) and barium titanium oxide (BaTiO_3) is to prepare nanorods with less than 100 nm in length and less than 10 nm in diameter with a very degree of dispersity. Another main challenge is that the nanorods should be soluble enough in organic solvents to permit the formation of homogenous thin films on a given substrate surface to function as highly efficient gate insulators in Organic Field Effect Transistors (OFETs).

Contents

Acknowledgment.....	i
Abstract.....	ii
List of abbreviations.....	iv
Aims.....	vi
1.1 Introduction.....	2
1.2 One-Dimensional Nanostructures (1D).....	3
1.3 Titanium Dioxide TiO ₂	4
1.3.1 Crystal Structures.....	4
1.3.2 Titanium Dioxide TiO ₂ Nanomaterials Properties.....	9
1.3.3 Titanium Dioxide Nanorods - Methods of Synthesis.....	13
1.3.4 Applications of Titanium Dioxide 1D-Nanorods.....	18
1.3.5 Metal-Doped Titanium Dioxide (TiO ₂ -M).....	20
1.4 Barium Titanium Oxide BaTiO ₃	22
1.4.1 Perovskite Structure of Barium Titanium Oxide BaTiO ₃	22
1.4.2 Preparation of Barium Titanium Oxide (BaTiO ₃) Nanowires.....	23
1.5 Organic Field Effect Transistors (OFET).....	24
1.5.1 Organic Field Effect Transistors (OFET).....	24
1.5.2 Organic Field Effect Transistors (OFET) - Challenges.....	25
1.6 High-k Dielectric Materials.....	26
1.6.1 High-k Dielectric Materials for Organic Field Effect Transistors OFETs.....	26
1.7 References.....	28
2.1 Measurement and Instruments.....	42
2.1.1 X-Ray Diffraction (XRD).....	42
2.1.2 Transmission Electron Microscopy (TEM).....	42
2.1.3 Fourier Transform Infrared Spectroscopy (FT-IR).....	43
2.1.4 X-ray Photoelectron Spectroscopy (XPS).....	43
2.1.5 Thermal Gravimetric Analysis (TGA).....	44

2.1.6 Inductively Coupled Plasma (ICP)	44
2.1.7 Elemental Analyser (CHN Analyser)	44
2.1.8 Nuclear Magnetic Resonance Spectroscopy (NMR).....	45
2.1.9 Centrifugation.....	45
2.1.10 Ultrapure Water	45
2.2 References	46
3.1 Introduction	48
3.2 Experimental	48
3.2.1 Materials	48
3.2.2 Synthesis of TiO ₂ /OA Nanocomposites Consisting of Anatase Titanium Dioxide Nanorods Coated with a Monolayer of Oleic Acid	49
3.3 Results and Discussion.....	52
3.3.1 Characterisation of Anatase Titanium Dioxide Nanorods Capped with Oleic Acid TiO ₂ /OA FA3-1	52
3.3.2 Characterisation of the Ligand Exchanged FA3-2 TiO ₂ /OA/OPA, FA3-3 TiO ₂ /OA/DEPPNA and FA3-4, FA3-5 and FA3-6 TiO ₂ /OA/ODPA nanocomposites ...	58
3.3.3 Possible Mechanism for Ligand Exchange Reaction of the Anatase Titanium Dioxide Nanorods FA3-1 TiO ₂ /OA nanorods with OPA, DEPPNA and ODPA to produce the Ligand Exchanged FA3-2 TiO ₂ /OA/OPA, FA3-3 TiO ₂ /OA/DEPPNA and FA3-4, FA3-5 and FA3-6 TiO ₂ /OA/ODPA nanocomposites, respectively.	65
3.4 Conclusion and Summary	68
3.5 References	69
4.1 Introduction	72
4.2 Experimental	72
4.2.1 Materials	72
4.2.2 Solution-Processable, Metal-Doped Anatase Titanium Dioxide Nanorods Synthesis (TiO ₂ -M; M = Nb, In or Nb/In)	73
4.3 Results and Discussion.....	79

4.3.1	Characterisation of Metal-Doped Titanium Dioxide Nanorods (TiO ₂ -L-M)	79
4.4	Conclusion and Summary	107
4.5	References	109
5.1	Introduction.....	112
5.2	Experimental.....	112
5.2.1	Materials	112
5.2.2	Synthesis of Rutile TiO ₂ Nanorods.....	113
5.3	Results and Discussion	126
5.3.1	Approach 1: Synthesis of Rutile TiO ₂ Nanorods from TiOCl ₂ and H ₂ O (NRs-Rutile-1).....	126
5.4	Conclusion and Summary	173
5.5	References.....	175
6.1	Introduction	178
6.2	Experimental	180
6.2.1	Materials	180
6.2.2	Synthesis of Barium Titanium Oxide (BaTiO ₃) Nanorods.....	180
6.3	Results and Discussion.....	184
6.3.1	Approach 1: Characterisation of Barium Titanium Oxide Nanorods BaTiO ₃ Transferred from Titanium Dioxide Nanorods TiO ₂	184
6.3.2	Approach 2: Barium Titanium Oxide Nanorods from a Single-source Ba/Ti Precursor.....	209
6.3.3	Approach 3 - Barium Titanium Oxide Nanorods BaTiO ₃ using Ethylene Glycol	211
6.4	Conclusions	213
6.5	References	215
	Appendix 1	I

List of Figures

Figure 1-1: Images of titanium dioxide (TiO_2) in naturally occurring crystalline forms, <i>e.g.</i> , anatase (A-B), rutile (C) and brookite (D) crystalline structures.....	3
Figure 1-2: The unit cell of titanium dioxide rutile phase.	5
Figure 1-4: The unit cell of titanium dioxide anatase phase.	6
Figure 1-3: The three faces of titanium dioxide rutile phase: (a) (110), (b) (100) and (c) (001).	7
Figure 1-5: The three faces of titanium dioxide anatase phase: (a) (101), (b) (100) and (c) (001).	8
Figure 1-6: The unit cell of titanium dioxide brookite.	9
Figure 1-7: The three faces of titanium dioxide brookite phase: (a) (100), (b) (010) and (c) (110).....	10
Figure 1-8: The density of states (DOS) of titanium dioxide TiO_2	12
Figure 1-9: molecular band bonding structure for titanium dioxide.....	12
Figure 1-10: Perovskite structure of barium titanium oxide BaTiO_3	23
Figure 1-11: Schematic representation of the Organic Field Effect Transistor (OFET) Structure.	25
Scheme 3-1: Schematic diagram of synthesis of the oleic acid-capped anatase titanium dioxide nanorods FA3-1 TiO_2/OA	50
Scheme 3-2: Diagram shows ligands exchange of oleic acid capped anatase titanium dioxide nanorods FA3-1 $\text{TiO}_2\text{-OA}$ with (A) octylphosphonic acid (OPA), (B) decylphosphonic acid (ODPA) and (C) 2-phenylethyl phosphonate (DEPPNA) ligands to produce the FA3-2 $\text{TiO}_2/\text{OA}/\text{OPA}$, FA3-3 $\text{TiO}_2/\text{OA}/\text{DEPPNA}$ and FA3-4, FA3-5 and FA3-6 $\text{TiO}_2/\text{OA}/\text{ODPA}$ nanocomposites, respectively.	52
Figure 3-1: XRD pattern of FA3-1 TiO_2/OA nanocomposites consisting of anatase titanium dioxide nanorods capped with oleic acid.	54
Figure 3-2: FT-IR pattern of FA3-1 TiO_2/OA nanocomposites consisting of anatase titanium dioxide nanorods capped with oleic acid.	54

Figure 3-3: TEM images of FA3-1 TiO ₂ /OA nanocomposites consisting of anatase titanium dioxide nanorods capped with oleic acid.	55
Figure 3-4: The aspect ratio distribution of FA3-1 TiO ₂ /OA nanocomposites consisting of anatase titanium dioxide nanorods capped with oleic acid.	56
Figure 3-5: TGA analysis of FA3-1 TiO ₂ /OA nanocomposites consisting of anatase titanium dioxide nanorods capped with oleic acid.	56
Figure 3-6: Dielectric constant <i>k</i> with frequency for the oleic acid-stabilised titanium dioxide nanorods TiO ₂ -OA, FA3-1.....	57
Figure 3-6: The XRD patterns of the FA3-1 TiO ₂ /OA nanorods, the FA3-3 TiO ₂ /OA/DEPPNA and FA3-5 TiO ₂ /OA/ODPA nanocomposites.	61
Figure 3-7: FT-IR patterns of FA3-1 TiO ₂ /OA nanorods and the FA3-2 TiO ₂ /OPA nanocomposites.	61
Figure 3-8: FT-IR patterns of the FA3-1 TiO ₂ /OA nanorods and the FA3-3 TiO ₂ / DEPPNA nanocomposites.	62
Figure 3-9: FT-IR patterns of FA3-1 TiO ₂ /OA nanorods and the FA3-4 (4:1), FA3-5 (3:1) and FA3-6 (2:1) TiO ₂ /ODPA nanocomposites.	62
Figure 3-10: ³¹ P NMR of (a) FA3-3 TiO ₂ /DEPPNA nanocomposites, before separation treatment (b) FA3-3 TiO ₂ /DEPPNA nanocomposites after separation treatment, (c) FA3-5 TiO ₂ /ODPA nanocomposites (3:1) before separation treatment.	63
Figure 3-13: 40% Solutions of the FA3-3 TiO ₂ /DEPPNA and FA3-5TiO ₂ /ODPA (3:1) nanocomposites in chlorobenzene.	63
Figures 3-11: TEM images of the FA3-3 TiO ₂ /DEPPNA (A-B) and the FA3-5 TiO ₂ /ODPA nanocomposites (3:1) (C-D).	64
Figure 3-12: The aspect ratio distribution of the FA3-5 TiO ₂ /ODPA (3:1) nanocomposites..	64
Scheme 3-3: Some possible modes of binding between the titanium dioxide surface with phosphorus ligands, i.e., monodentate (1-2), bidentate (3-4) and tridentate bonding modes..	67
Figure 4-1: XRD patterns of the oleic acid-stabilised, niobium-doped titanium dioxide nanorods (TiO ₂ -OA-Nb) FA4-2 and FA4-4 and the non-doped, oleic acid-stabilised titanium dioxide nanorods (TiO ₂ -OA) FA3-1.	83

Figure 4-2: XRD patterns of the oleic acid-stabilised, niobium-doped titanium dioxide nanorods (TiO ₂ -OA-Nb) FA4-3, FA4-5 and FA4-7.....	83
Figure 4-3: FT-IR patterns of the oleic acid-stabilised, niobium-doped titanium dioxide nanorods (TiO ₂ -OA-Nb) FA4-1 and FA4-4.	84
Figure 4-4: FT-IR patterns of the oleic acid-stabilised, niobium-doped titanium dioxide nanorods (TiO ₂ -OA-Nb) FA4-5 and FA4-6.	84
Figure 4-5: TEM images of the oleic acid-stabilised, niobium-doped titanium dioxide nanorods (TiO ₂ -OA-Nb), FA4-1 (A), FA4-2 (B), FA4-3 (C) and FA4-4 (D).	85
Figure 4-6: TEM images of the oleic acid-stabilised, niobium-doped titanium dioxide nanorods (TiO ₂ -OA-Nb) FA4-5 (A), FA4-6 (B), FA4-7 (C) and FA4-8 (D).	85
Figure 4-7: EDX results of the oleic acid-stabilised, niobium-doped titanium dioxide nanorods (TiO ₂ -OA-Nb) FA4-1 (A), FA4-2 (B), FA4-3 (C), FA4-4 (D), FA4-5 (E), FA4-6 (F), FA4-7 (G) and FA4-8 (H).	86
Figure 4-8: XPS data for Nb 3d spectra (3d _{5/2} and 3d _{3/2}) of the oleic acid-stabilised, niobium-doped, anatase titanium dioxide nanorods (TiO ₂ -OA-Nb), (A) FA4-3, (B) FA4-4, (C) FA4-5 and (D) FA4-6.....	88
Figure 4-9: XPS data for Ti 2p spectra (2p _{5/2} and 2p _{3/2}) of the oleic acid-stabilised, niobium-doped, anatase titanium dioxide nanorods (TiO ₂ -OA-Nb), (A) FA3-1 (B) FA4-3, (C) FA4-4, (D) FA4-5 and (E) FA4-6.	89
Figure 4-10: Proportion between Nb (IV) wt. % (XPS) and Ti (III) wt. % (XPS) for non-doped, oleic acid-stabilised titanium dioxide nanorods (TiO ₂ -OA) FA3-1 and the oleic acid-stabilised, niobium-doped titanium dioxide nanorods (TiO ₂ -OA-Nb) FA4-3 – FA4-6.	90
Figure 4-11: Solutions of the oleic acid-stabilised, niobium-doped titanium dioxide nanorods (TiO ₂ -OA-Nb) FA4-3, (NBEO, 9:1, 24 h), FA4-4, (NBEO, 9:1, 72 h), FA4-5, (NBEO, 18:1, 24 h), FA4-6, (NBEO, 18:1, 72 h) FA4-7, (NBEO, 45:1, 24 h), and FA4-8, (NBEO, 45:1, 72 h).	90
Figure 4-12: XRD patterns of the ODPA-stabilised, niobium-doped titanium dioxide nanorods (TiO ₂ -ODPA-Nb) FA4-11 and FA4-13 - FA4-15.	94

Figure 4-13: FT-IR patterns of the DEPPNA-stabilised, niobium-doped titanium dioxide nanorods (TiO ₂ -DEPPNA-Nb) FA4-10 and the ODPA-stabilised, niobium-doped titanium dioxide nanorods (TiO ₂ -ODPA-Nb) FA4-9 and FA4-11.	94
Figure 4-14: FT-IR patterns of the OPDA-stabilised, niobium-doped titanium dioxide nanorods (TiO ₂ -OPDA-Nb) FA4-12 - FA4-15.	95
Figure 4-16: Solutions of the ligand exchanged products of the ODPA-stabilised, niobium-doped titanium dioxide nanorods (TiO ₂ -ODPA-Nb) FA4-9, FA4-12 and FA4-13 in chlorobenzene.	95
Figure 4-15: TEM images of the ODPA-stabilised, niobium-doped titanium dioxide nanorods (TiO ₂ -ODPA-Nb) FA4-13 (A-B) prepared by a ligand exchange reaction using the oleic acid-stabilised, niobium-doped titanium dioxide nanorods (TiO ₂ -OA-Nb) FA4-5 (C-D).	96
Figure 4-17: XRD patterns of the oleic acid-stabilised, indium-doped titanium dioxide nanorods (TiO ₂ -OA-In) FA4-16 and FA4-17.	98
Figure 4-18: FT-IR patterns of the oleic acid-stabilised, indium-doped titanium dioxide nanorods (TiO ₂ -OA-In) FA4-16 and FA4-17.	98
Figure 4-19: TEM images of the oleic acid-stabilised, indium-doped titanium dioxide nanorods (TiO ₂ -OA-In) FA4-16.	99
Figure 4-20: Solutions of the oleic acid-stabilised, indium-doped titanium dioxide nanorods (TiO ₂ -OA-In) FA4-16 and FA4-17.	99
Figure 4-21: XRD pattern of the oleic acid-stabilised, niobium/indium-doped titanium dioxide nanorods (TiO ₂ -OA-Nb/In) FA4-18.	101
Figure 4-22: FT-IR pattern of the oleic acid-stabilised, niobium/indium-doped titanium dioxide nanorods (TiO ₂ -OA-Nb/In) FA4-18.	102
Figure 4-23: TEM images of the oleic acid-stabilised, niobium/indium-doped titanium dioxide nanorods (TiO ₂ -OA-Nb/In) FA4-18.	102
Figure 4-24: Solution of the oleic acid-stabilised, niobium/indium-doped titanium dioxide nanorods (TiO ₂ -OA-Nb/In) FA4-18 in chlorobenzene.	103
Figure 4-25: XRD patterns of the oleic acid-stabilised, niobium/indium-doped titanium dioxide nanorods (TiO ₂ -OA-Nb/In) FA4-18, the ODPA-stabilised, niobium/indium-doped titanium	

dioxide nanorods (TiO ₂ -ODPA-Nb/In) FA4-19 and the DEPPNA-stabilised, niobium/indium-doped titanium dioxide nanorods (TiO ₂ -DEPPNA-Nb/In) FA4-20.	105
Figure 4-26: FT-IR patterns of the ODPA-stabilised, niobium/indium-doped titanium dioxide nanorods (TiO ₂ -ODPA-Nb/In) FA4-19 and the DEPPNA-stabilised, niobium/indium-doped titanium dioxide nanorods (TiO ₂ -DEPPNA-Nb/In) FA4-20.	106
.....	106
Figure 4-27: Solution of the ODPA-stabilised, niobium/indium-doped titanium dioxide nanorods (TiO ₂ -ODPA-Nb/In) FA4-19 and the DEPPNA-stabilised, niobium/indium-doped titanium dioxide nanorods (TiO ₂ -DEPPNA-Nb/In) FA4-20 in chlorobenzene.....	106
Figure 5-1: A photo of process of transferring titanium (IV) chloride (TiCl ₄) to a stable solution of titanium oxychloride (TiOCl ₂).....	113
Figure 5-2: XRD patterns of the rutile TiO ₂ nanorods FA5-1 - FA5-3 (NRs-Rutile-1).	127
Figure 5-3: FT-IR patterns of the rutile TiO ₂ nanorods FA5-1 - FA5-3(NRs-Rutile-1).	127
Figure 5-4: TEM images of the rutile TiO ₂ nanorods FA5-1 (A-B), FA5-2 (C-D) and FA5-3 (E-F) (Rutile-NRs-1).....	128
Scheme 5-1: The formation of TiO ₂ rutile phase.	129
Figure 5-5: XRD patterns of the surface modification of the rutile TiO ₂ nanorods FA5-2 (NRS-Rutile 1) and the oleic acid-capped TiO ₂ /OA nanocomposites FA5-4 and FA5-6 prepared using surface treatment method 1.	132
Figure 5-6: FT-IR patterns of the surface modification of the rutile TiO ₂ nanorods FA5-2 (NRS-Rutile 1) and the oleic acid-capped TiO ₂ /OA nanocomposites FA5-4 - FA5-6 prepared using surface treatment method 1.	132
Figure 5-7: TGA of the surface modification of the rutile TiO ₂ nanorods FA5-2 (NRS-Rutile 1) and the oleic acid-capped TiO ₂ /OA nanocomposites FA5-4 and FA5-6 prepared using surface treatment method 1.	133
Figure 5-8: TEM images of the surface modification of the rutile TiO ₂ nanorods FA5-2 (NRS-Rutile 1) (A-B) and the oleic acid-capped TiO ₂ /OA nanocomposites FA5-4 (C-D) prepared using surface treatment method 1.	133

Schema 5-2: Schematic diagram of synthesis of processable solution of rutile TiO ₂ /ligand nanocomposites, oleic acid (A), octylamine (B), dodecylamine (C) and hexadecylamine (D)	134
Figure 5-9: colloidal solution of the oleic acid-capped TiO ₂ /OA nanocomposites FA5-7 and FA5-9 and the dodecyl amine-capped TiO ₂ /AA(12) nanocomposite FA5-13 (<i>n</i> -C _n H _{2n+1} NH ₂ ; <i>n</i> = 12) in chlorobenzene (C ₆ H ₅ Cl).....	139
Figure 5-10: XRD patterns of the surface modification of the rutile TiO ₂ nanorods FA5-2 (NRS-Rutile 1) and the oleic acid-capped TiO ₂ /OA nanocomposites FA5-7, FA5-9 and FA5-11 prepared using surface treatment method 2.	139
Figure 5-11: XRD patterns of the rutile TiO ₂ nanorods FA5-2 (NRs-Rutile-1) and the primary <i>n</i> -alkyl amines-capped TiO ₂ /AA(12, 8 and 16) nanocomposites FA5-13, FA5-15 and FA5-16 modified with primary <i>n</i> -alkyl amines (C _n H _{2n+1} NH ₂ ; <i>n</i> = 12, 8 and 16, respectively) using surface treatment method 2.....	140
Figure 5-12: FT-IR patterns of the rutile TiO ₂ nanorods FA5-2 (NRs-Rutile-1) and the oleic acid-capped TiO ₂ /OA nanocomposites FA5-7, FA5-9 and FA5-11 using surface treatment method 2.....	140
Figure 5-13: FT-IR patterns of the rutile TiO ₂ nanorods FA5-2 (NRs-Rutile-1) and the primary <i>n</i> -alkyl amines-capped TiO ₂ /AA(12, 12, 8 and 16) nanocomposites FA5-13 - FA5-16, respectively, modified with primary <i>n</i> -alkyl amines (C _n H _{2n+1} NH ₂ ; <i>n</i> = 12, 12, 8 and 16, respectively) using surface treatment method 2.....	141
Figure 5-14: TGA of the oleic acid-capped TiO ₂ /OA nanocomposites FA5-7, FA5-9 and FA5-11 modified with oleic acid using surface treatment method 2.	141
Figure 5-15: TGA of the primary <i>n</i> -alkyl amines-capped TiO ₂ /AA(12, 12, 8 and 16) nanocomposites FA5-13 - FA5-16, respectively, modified with primary <i>n</i> -alkyl amines (C _n H _{2n+1} NH ₂ ; <i>n</i> = 12, 12, 8 and 16) using surface treatment method 2.	142
Figure 5-16: TEM images of the oleic acid-capped TiO ₂ /OA nanocomposites FA5-7 (A-B), TiO ₂ /OA nanocomposites FA5-9 (C-D) using surface treatment method 2 and the dodecylamine-capped TiO ₂ /AA(12) nanocomposite FA5-14 (E-F) also using surface treatment method 2.....	143

Scheme 5-3: Possible binding mode of TiO ₂ surface modification by carboxylic acid; (1) electrostatic attraction, (2 and 6) H-Bonding, (3) monodentate (ester-like linkage) (4) bidentate bridging (5) bidentate chelating.	145
Scheme 5-4: Possible binding mode of TiO ₂ surface modification by primary <i>n</i> -alkyl amines.	145
Figure 5-17: Dielectric constant <i>k</i> with frequency for rutile TiO ₂ /ligand nanocomposites preparation – surface treatment method 2 product FA5-9.	146
Figure 5-18: XRD patterns of the rutile TiO ₂ nanorods FA5-2 (NRs-Rutile-1) and the oleic acid/dodecyl amine-capped TiO ₂ /OA/AA(12) nanocomposite FA5-19 as well as that of the doubly oleic acid-capped TiO ₂ /OAx2 nanocomposite FA5-20 prepared using surface treatment method 3.....	150
Figure 5-19: FT-IR patterns of the rutile TiO ₂ nanorods FA5-2 (NRs-Rutile-1) and the doubly oleic acid-capped TiO ₂ /OAx2 nanocomposites FA5-17, FA5-18 and FA5-20, prepared using surface treatments using methods 3.	151
Figure 5-20: FT-IR patterns of the rutile TiO ₂ nanorods FA5-2 (NRs-Rutile-1), the dodecyl amine-capped TiO ₂ /AA(12) nanocomposite FA5-14, prepared using surface treatment method 2, and oleic acid/dodecylamine-capped TiO ₂ /OA/AA(12) nanocomposite FA5-19 prepared using surface treatment method 3.	151
Figure 5-21: TGA of the oleic acid/dodecylamine-capped TiO ₂ /OA/AA(12) nanocomposite FA5-19 as well as that of the doubly oleic acid-capped TiO ₂ /OAx2 nanocomposites FA5-17 and FA5-20 prepared using surface treatment method 3.	152
Figure 5-22: TEM images of doubly oleic acid-capped TiO ₂ /OA x 2 nanocomposites FA5-17(A-B), FA5-18 (C-D) and the oleic acid/dodecylamine-capped TiO ₂ /OA/DA nanocomposite FA5-19 (E-F) prepared using surface treatment method 3.	153
Figure 5-23: XRD pattern of the rutile TiO ₂ nanorods FA5-21 (NRs-Rutile-2).	155
Figure 5-24: FT-IR pattern of the rutile TiO ₂ nanorods FA5-21 (NRs-Rutile-2).....	155
Figure 5-25: TEM images of the rutile TiO ₂ nanorods FA5-21 (NRs-Rutile-2).	156
Figure 5-26: XRD patterns of the rutile TiO ₂ FA5-21 nanorods (Rutile-NRs-2) and the oleic acid-capped TiO ₂ /OA nanocomposites FA5-22 – FA5-25 prepared using surface treatment method 1.....	158

Figure 5-27: FT-IR patterns of the rutile TiO ₂ FA5-21 nanorods (Rutile-NRs-2) and the oleic acid-capped TiO ₂ /OA nanocomposites FA5-22 – FA5-25 prepared using surface treatment method 1.....	159
Figure 5-28: TGA of the oleic acid-capped TiO ₂ /OA nanocomposites FA5-24 and FA5-25, prepared using surface treatment method 1.	159
Figure 5-29: TEM images of the oleic acid-capped TiO ₂ /OA nanocomposites FA5-22, prepared using surface treatment method 1.	160
Figure 5-30: XRD patterns of the rutile TiO ₂ FA5-26 nanorods (Rutile-NRs-3).....	161
Figure 5-31: FT-IR patterns of the rutile TiO ₂ FA5-26 nanorods (Rutile-NRs-3).	162
Figure 5-32: TEM images of the rutile TiO ₂ FA5-26 nanorods (Rutile-NRs-3).	162
Scheme 5-5: Structures of ligands that used in acid-stabilisation of the FA5-26 TiO ₂ nanorods (Rutile-NRs-3); (A) oleic acid (OA), (B) decylphosphonic acid (ODPA), (C) 2-(phenyl)ethyl phosphonate (DEPPNA) and (D) octylphosphonic acid (OPA).	166
Figure 5-34: XRD pattern of the octylphosphonic acid and oleic acid-capped TiO ₂ /OPA/OA nanocomposites FA5-34, FA5-37 and FA5-41 and the octylphosphonic acid and 2-(phenyl)ethyl phosphonate TiO ₂ /OPA/DEPPNA nanocomposite FA5-35, prepared using surface treatment method 2.	169
Figure 5-35: FT-IR pattern of the octylphosphonic acid-capped TiO ₂ /OPA nanocomposites FA5-27 and FA5-28 and the decylphosphonic acid-capped TiO ₂ /ODPA nanocomposite FA5-29, prepared using surface treatment method 1.	170
Figure 5-36: the octylphosphonic acid and oleic acid-capped TiO ₂ /OPA/OA nanocomposites FA5-34, FA5-36 and FA5-41, the octylphosphonic acid and 2-(phenyl) ethyl phosphonate-capped TiO ₂ /OPA/DEPPNA nanocomposite FA5-35 and the octylphosphonic acid and decylphosphonic acid-capped TiO ₂ /ODPA/OA nanocomposite FA5-40, prepared using surface treatment method 2.	170
Figure 5-37: TEM images of the octylphosphonic acid-capped TiO ₂ /OPA nanocomposites FA5-27 (A-B), FA5-28 (C-D) and the decylphosphonic acid-capped TiO ₂ /ODPA nanocomposite FA5-29 (E-F) prepared using surface treatment method 1.	171
Figure 5-38: TEM images of the octylphosphonic acid and oleic acid-capped TiO ₂ /OPA/OA nanocomposites FA5-36 prepared using surface treatment method 2.	172

Schema 6-1: Schematic diagram of synthesis of barium titanium oxide from the oleic acid-stabilised titanium dioxide nanorods TiO ₂ -OA.....	178
Figure 6-1: XRD spectra of the oleic acid-stabilised titanium dioxide nanorods (TiO ₂ -OA) FA3-1 and the barium titanium oxide (BaTiO ₃) nanorods FA6-1 and FA6-1 AW, before and after washing with formic acid, respectively, produced using FA3-1 as the starting material.	188
Figure 6-2: XRD spectra for the barium titanium oxide nanorods FA6-2 - FA6-7 produced from FA3-1 as the starting material.....	188
Figure 6-3: XRD spectra of the oleic acid-stabilised titanium dioxide nanorods (TiO ₂ -OA) FA3-1 and the barium titanium oxide nanorods FA6-1 and FA6-8 produced from FA3-1 at different pH values, i.e., pH = 12.3 and pH = 7.8, respectively, produced using FA3-1 as the starting material.	189
Figure 6-4: XRD spectra of the oleic acid-stabilised titanium dioxide nanorods (TiO ₂ -OA) FA3-1 and the barium titanium oxide nanorods FA6-9 - FA6-11 produced from FA3-1 as the starting material.	189
Figure 6-5: FT-IR spectra of the barium titanium oxide nanorods sample FA6-1 and the oleic acid-stabilised titanium dioxide (TiO ₂ -OA) nanorods sample FA3-1 used as the starting material.	190
Figure 6-6: FT-IR spectra of the barium titanium oxide nanorods samples FA6-2, FA6-3 and FA6-8, produced using FA3-1 as the starting material.....	190
Figure 6-7: FT-IR spectra of the barium titanium oxide nanorods samples FA6-5 - FA6-7, produced using FA3-1 as the starting material.	191
Figure 6-8: FT-IR spectra of the barium titanium oxide nanorods samples FA6-9 - FA6-11, produced using FA3-1 as the starting material.	191
Figure 6-9: TEM images of the oleic acid-stabilised titanium dioxide (TiO ₂ -OA) nanorods FA3-1 (A-B), barium titanium oxide nanorods FA6-1 (C-D) and FA6-2 (E-F).	192
Figure 6-10: TEM Images of barium titanium oxide nanorods FA6-3 (A-B), FA6-4 (C-D) and FA6-5 (E-F).	193
Figure 6-11: TEM Images of barium titanium oxide nanorods FA6-6 (A-B), FA6-7 (C-D) and FA6-8 (E-F).	194

Figure 6-12: TEM images of barium titanium oxide nanorods FA6-9 (A-B), FA6-10 (C-D) and FA6-11 (E-F).	195
Figure 6-13: XRD spectra of the barium titanium oxide samples FA6-12 and FA6-13 prepared using approach 1-2 and the rutile titanium dioxide nanorods FA5-2 used as the starting material in these reactions.....	198
Figure 6-14: FT-IR spectra of barium titanium oxide samples FA6-12 and FA6-13 prepared using approach 1-2 and the rutile titanium dioxide nanorods FA5-2 used as the starting material in these reactions.....	198
Figure 6-15: TEM images of rutile titanium dioxide nanorods FA5-2 (A-B) and barium titanium oxide nanoparticles FA6-12 (C-D) and FA6-13 (F-D).....	199
Figure 6-16: XRD spectra of the barium titanium oxide samples FA6-14 and FA6-15 prepared using approach 1-3 and the rutile titanium dioxide nanorods FA5-26 used as the starting material in these reactions.....	202
Figure 6-17: XRD spectra of the barium titanium oxide samples FA6-16 and FA6-17 prepared using approach 1-3 using FA5-26 as the starting material in these reactions.....	202
Figure 6-18: FT-IR spectra of the barium titanium oxide samples FA6-14 and FA6-15 prepared using approach 1-3 and the rutile titanium dioxide nanorods FA5-26 used as the starting material in these reactions.....	203
Figure 6-19: FT-IR spectra of the barium titanium oxide samples FA6-16 and FA6-17 prepared using approach 1-3 using FA5-26 as the starting material in these reactions.....	203
Figure 6-20: TEM images of rutile titanium dioxide nanorods FA5-26 used as the starting material in these reactions (A-B), barium titanium oxide (FA6-14 (C-D) and FA6-15 (E-F).	204
Figure 6-21: TEM images of rutile titanium dioxide nanorods FA5-26 used as the starting material in these reactions (A-B), barium titanium oxide FA6-16 (C-D) and FA6-17 (E-F).	205
Scheme 6-2: Possible mechanisms for the conversion of titanium dioxide nanorods into barium titanium oxide nanoparticles <i>via</i> a hydrothermal reaction.	208
Figure 6-22: XRD spectra of the barium titanium oxide sample FA6-18.	209
Figure 6-23: FT-IR spectra of the barium titanium oxide sample FA6-18.....	210

Figure 6-24: TEM images of the barium titanium oxide sample FA6-18.	210
Figure 6-25: XRD spectra of the barium titanium oxide sample FA6-19 and FA6-19 AW, before and after washing with formic acid, respectively.	211
Figure 6-26: FT-IR spectrum of the barium titanium oxide sample FA6-19.	212
Figure 6-27: TEM images of the barium titanium oxide sample FA6-19.	212

List of Tables

Table 3-1: Ligand exchange conditions of the reactions of the oleic acid-capped anatase titanium dioxide nanorods FA3-1 TiO ₂ /OA with the OPA, DEPPNA and ODPA ligands to produce the FA3-2 TiO ₂ /OA/OPA, FA3-3 TiO ₂ /OA/DEPPNA and FA3-4, FA3-5 and FA3-6 TiO ₂ /OA/ODPA nanocomposites, respectively.	51
Table 3-2: Chemical analysis of FA3-1 TiO ₂ /OA nanocomposites consisting of anatase titanium dioxide nanorods capped with oleic acid.	55
Table 3-3: Chemical analysis of the FA3-1 TiO ₂ /OA nanorods modified with the OPA, DEPPNA and ODPA ligands to produce the FA3-2 TiO ₂ /OA/OPA, FA3-3 TiO ₂ /OA/DEPPNA and FA3-4, FA3-5 and FA3-6 TiO ₂ /OA/ODPA nanocomposites.	60
Table 3-4: The rate of ligand exchange in the reactions of the anatase nanorods FA3-1 TiO ₂ /OA nanorods with the ligands OPA, DEPPNA and ODPA to produce the ligand exchanged FA3-2 TiO ₂ /OA/OPA, FA3-3 TiO ₂ /OA/DEPPNA and FA3-4, FA3-5 and FA3-6 TiO ₂ /OA/ODPA nanocomposites, respectively.	67
Table 4-1: Reaction conditions for the synthesis of niobium-doped titanium dioxide nanorods (TiO ₂ -OA-Nb).	74
Table 4-2: Reaction conditions for the ligand-exchange reactions between the niobium-doped titanium dioxide nanorods (TiO ₂ -OA-Nb) FA4-1 – FA4-6, see table 4-1, and either octadecylphosphonic acid (ODPA) or diethyl 2-phenylethyl phosphonate (DEPPNA) to produce the ODPA-stabilised, niobium-doped titanium dioxide nanorods (TiO ₂ -ODPA-Nb) FA4-9 and FA4-11 – FA4-15 or the DEPPNA-stabilised, niobium-doped titanium dioxide nanorods (TiO ₂ -ODPA-Nb) FA4-10.	76

Table 4-3: Reaction conditions for the synthesis of the oleic acid-stabilised indium-doped titanium dioxide nanorods (TiO ₂ -OA-In) FA4-16 and FA4-17.....	76
Table 4-6: Chemical analysis of the oleic acid-stabilised, niobium-doped titanium dioxide nanorods (TiO ₂ -OA-Nb) FA4-1 – FA4-8.	82
Table 4-7: The binding energy position (eV) and elemental concentration (%) for Ti (IV), Ti (III), Nb (V) and Nb (IV) ions present in the non-doped, oleic acid-stabilised titanium dioxide nanorods (TiO ₂ -OA) FA3-1 and the oleic acid-stabilised, niobium-doped titanium dioxide nanorods (TiO ₂ -OA-Nb) FA4-3 – FA4-6.	87
Table 4-8: The binding energy position (eV) and elemental concentration (%) for O 1s, Ti 2p, C 1s, Nb 3d and N 1s of the non-doped, oleic acid-stabilised titanium dioxide nanorods (TiO ₂ -OA) FA3-1 and the oleic acid-stabilised, niobium-doped titanium dioxide nanorods (TiO ₂ -OA-Nb) FA4-3 – FA4-6.	88
Table 4-9: Chemical analysis of the ligand-stabilised, niobium-doped, anatase titanium dioxide nanorods (TiO ₂ -DEPPNA-Nb) FA4-10 and (TiO ₂ -ODPA-Nb) FA4-9 and FA4-11 - FA4-15 derived from ligand exchange reactions between oleic acid-stabilised niobium doped anatase titanium dioxide nanorods (TiO ₂ -OA-Nb) FA4-1 - FA4-6 and diethyl 2-phenylethyl phosphonate (DEPPNA) and octadecylphosphonic acid (ODPA), respectively.	93
Table 4-10: Chemical analysis of the oleic acid-stabilised, indium-doped titanium dioxide nanorods (TiO ₂ -OA-In) FA4-16 and FA4-17.	98
Table 4-11: Chemical analysis of the oleic acid-stabilised, niobium/indium-doped titanium dioxide nanorods (TiO ₂ -OA-Nb/In) FA4-18.	101
Table 4-12: Chemical analysis of the ODPA-stabilised, niobium/indium-doped titanium dioxide nanorods (TiO ₂ -ODPA-Nb/In) FA4-19 and the DEPPNA-stabilised, niobium/indium-doped titanium dioxide nanorods (TiO ₂ -DEPPNA-Nb/In) FA4-20, prepared by ligand-exchange reactions of the oleic acid-stabilised, niobium/indium doped titanium dioxide nanorods (TiO ₂ -OA-Nb/In) FA4-18 using octadecylphosphonic acid (ODPA) and diethyl 2-phenylethyl phosphonate (DEPPNA) used as ligands, respectively.....	105
Table 5-1: Reaction conditions for the surface modification of the rutile TiO ₂ nanorods (NRS-Rutile 1) FA5-2, prepared using Approach 1 to yield the desired oleic acid-capped TiO ₂ /OA nanocomposites FA5-4 - FA5-6 prepared using surface treatment method 1.	116

Table 5-2: Reaction conditions for the surface modification of the rutile TiO₂ nanorods FA5-2 (NRs-Rutile-1), prepared as described in section 5.2.2.2.1, to yield the desired oleic acid-capped TiO₂/OA nanocomposites FA5-7 - FA5-12 and the primary *n*-alkyl amine-capped TiO₂/AA(12, 12, 8 and 16) nanocomposites FA5-13 – FA5-16, respectively, prepared using surface treatment method 2 under identical reaction conditions. 117

Table 5-3: Reaction conditions for the surface modification of the rutile TiO₂/OA nanocomposites FA5-8 (dry) and FA5-9 (dry), prepared using surface treatment method 2, or TiO₂/OA nanocomposites FA5-10 (wet) and FA5-14 (dry), prepared using surface treatment method 2, to yield the doubly oleic acid-capped TiO₂/OAx2 nanocomposites FA5-18, FA5-20 and FA5-17, respectively, or the oleic acid- and dodecyl amine-capped TiO₂/OA/AA(12) nanocomposite FA5-19, respectively, prepared using surface treatment method 3. 118

Table 5-4: Reaction conditions for the surface modification of the rutile TiO₂ nanorods FA5-21 (NRs-Rutile-2) to yield the desired oleic acid-capped TiO₂/OA nanocomposites FA5-22 - FA5-25 prepared using surface treatment method 1 under identical reaction conditions. 120

Table 5-5: Conditions for the surface modification of rutile TiO₂ nanorods FA5-2 (NRs-Rutile-1), prepared using Approach 1 described in section 5.2.2.2.1, and FA5-26 TiO₂ nanorods (NRs-Rutile-3) prepared using Approach 3 described in section 5.2.2.4.1 with either octylphosphonic acid or decylphosphonic acid to yield the TiO₂/OPA nanocomposites FA5-27 – FA5-31 and FA5-33 and the TiO₂/ODPA nanocomposite FA5-32 using surface treatment method 1..... 123

Table 5-6: Conditions for the surface modification of the TiO₂/OPA nanocomposites FA5-27 – FA5-31 and FA5-33 and the TiO₂/ODPA nanocomposite FA5-32 using oleic acid to yield the TiO₂/OPA/OA nanocomposites FA5-34, FA5-36 – FA5-39 and the FA5-41 and for the surface modification of the TiO₂/OPA nanocomposite FA5-27 with diethyl 2-phenylethyl phosphonate to yield the TiO₂/ODPA/OA nanocomposite FA5-40, respectively, using surface treatment method 2. 125

Table 5-7: chemical analyses for the oleic acid-capped TiO₂/OA nanocomposites FA5-4 - FA5-6 prepared using surface treatment method 1. 131

Table 5-8: Chemical analyses for the oleic acid-capped TiO₂/OA nanocomposites FA5-7 - FA5-12 and the primary *n*-alkyl amine-capped TiO₂/AA(12, 12, 8 and 10) nanocomposites FA5-13 – FA5-16, respectively, using surface treatment method 2. 138

Table 5-9: Chemical analyses for the doubly oleic acid-capped TiO ₂ /OAx ₂ nanocomposites FA5-17, FA5-18 and FA5-20 and the oleic acid/dodecyl amine-capped TiO ₂ /OA/AA(12) nanocomposite FA5-19, prepared using surface treatment method 3.....	150
Table 5-10: Chemical analyses of the oleic acid-capped TiO ₂ /OA nanocomposites FA5-22 – FA5-25, prepared using surface treatment method 1.....	158
Table 5-11: Chemical analyses for the octylphosphonic acid-capped TiO ₂ /OPA nanocomposites FA5-27, FA5-28, FA5-31 and FA5-33, the decylphosphonic acid-capped TiO ₂ /ODPA nanocomposites FA5-29 and FA5-32, prepared using surface treatment method 1.	164
Table 5-12: Chemical analyses for the TiO ₂ /OPA/OA nanocomposites FA5-34, FA5-36, FA5-38, FA5-39 and FA5-41, the TiO ₂ /OPA/DEPPNA nanocomposite FA5-35, the TiO ₂ /ODPA/OA nanocomposites FA5-37 and FA5-40, prepared using surface treatment method 2.....	165
Table 6-1: Reaction conditions for the preparation of the barium titanium oxide (BaTiO ₃) nanorods FA6-1 - FA6-11.....	182
Table 6-2: Reaction conditions for the preparation of the barium titanium oxide (BaTiO ₃) nanorods FA6-12 and FA6-13.	182
Table 6-3: Reaction conditions for the preparation of the barium titanium oxide (BaTiO ₃) nanorods FA6-14 and FA6-17.	183
Table 6-4: Chemical analysis of the barium titanium oxide nanorods FA6-1 - FA6-11 prepared from the oleic acid-stabilised titanium dioxide (TiO ₂ -OA) nanorods FA3-1.....	187
Table 6-5: Chemical analysis of the barium titanium oxide samples FA6-12 and FA6-13 prepared using approach 1-2 using the rutile titanium dioxide nanorods FA5-2 as the starting material in these reactions.....	197
Table 6-6: Chemical analysis of the barium titanium oxide products FA6-14 - FA6-17, prepared using different reaction times and Ba/Ti ratios, using the rutile titanium dioxide nanorods FA5-26 as the starting material.	201

Chapter 1

Introduction

1.1 Introduction

Nanoscience and nanotechnology focusing on materials with dimensions between some nanometres to some hundred nanometres have been rapidly developed in last few decades due to their promising and attractive properties and applications.¹ The physical properties of nanomaterials are different from those of their bulk counterparts due to a change from Newtonian physics to quantum-confined physics.² Since carbon nanotubes were discovered by Iijima³ in 1991, there has been an enormous interest in the synthesis and characterisation of nanomaterials with one-dimensional (1D) structures, e.g., nanowires, nanorods and nanobelts, which make up a significant group of 1D nanostructures. These new nanostructures facilitate the study of the relationship between the physical properties of nanostructures, such as electrical transport and optical properties, and their quantum-confined dimensionality, shape and size. Such inorganic nanowires have been used as active components in devices as reported in recent investigations⁴ in which a variety of inorganic nanowires has been synthesized and characterised over the previous decade.⁴

Titanium is the ninth most common element in the crust of the Earth in terms of concentration. Titanium dioxide (TiO₂) is the most widespread compound of titanium found in nature.⁵ Figure 1-1 shows images of naturally occurring forms of titanium dioxide.⁶⁻⁸ Bulk titanium dioxide is a commercially important product being used in variety of important industrial applications.⁹ However, there is an increasing interest in synthesising new types of titanium dioxide nanomaterials with finely controlled structures on a nanometre scale in order to utilise them in novel electro-optic or electronic devices. A variety of 1D titanium dioxide nanotubes, nanorods, nanosheets, nanowires, nanoribbons and nanofibers have been synthesised and their physical properties studied as titanium dioxide is an *n*-type semiconductor.^{2, 10, 11}

Titanium nanoparticles are of considerable interest for use as *n*-type semiconductors in a multitude of technical and commercial applications, such as photovoltaic applications (solar cells), photocatalysis, electrochromic devices, anti-fogging, self-cleaning surfaces, such as windows and vehicle windscreens, selective adsorption filters, biological coatings, sensors, photoluminescence ion exchange, ultraviolet blockers and smart surface coatings, etc.¹²



Figure 1-1: Images of titanium dioxide (TiO_2) in naturally occurring crystalline forms, *e.g.*, anatase (A-B), rutile (C) and brookite (D) crystalline structures.

Furthermore, nanostructures of titanium dioxide are interesting from a fundamental scientific point of view due to their potential to display unique, quantum-confined properties and also to facilitate the study of physical and chemical properties of size-confined semiconductor networks.¹³⁻¹⁵ The combination of the exceptional chemical stability of titanium dioxide, its mechanical strength and its large band gap render it an interesting material to study in a wide variety of nanostructures and electro-optic and electrical devices containing it.

1.2 One-Dimensional Nanostructures (1D)

Nanoscale structures consist of three basic nanoshapes, *i.e.*, zero-dimensional (0D) quantum dots and nanoparticles, one-dimensional (1D) nanorods and nanotubes and two-dimensional (2D) nanosheets, nanofilms and nanoplatelets.¹⁶

One-dimensional (1D) nanostructures are found in numerous morphologies, *e.g.*, hollow one-dimensional (1D) nanotubes and solid nanorods, nanowires, nanobelts and nanofibers.¹⁷ Such

(1D) nanostructures can be used for effective transport of electrons and holes in one direction and to generate polarised optical excitations in nanoscale devices.¹⁸ The usage of one-dimension (1D) nanostructures in functional technology strategies is currently still at an early developmental stage. However, they are likely to play a significant role in the realisation of the fabrication of new electronic, optoelectronic, electrochemical, and electromechanical devices with nanostructured dimensions.² Innovation around these novel one-dimension (1D) nanostructures has the real potential to create remarkable application in various areas as electronics, photonics, sensors, catalysts, and energy harvesting and data storage.

The use of titanium dioxide nanorods might well lead to significant advantages in some technological devices – due to one-directional charge-transport - over the corresponding spherical nanocrystals. Nanorods also have higher surface/volume ratio than that of the corresponding nanospheres and with a higher density of active sites for surface reactions and a high interfacial charge carrier transfer rate.¹⁹ Furthermore, the increased delocalisation of charge carriers in nanorods, where they are free to move throughout the length of the nanocrystalline structure, is expected to reduce the probability of electron and hole recombination, which would possibly compensate for the existence of surface trap states and guarantee a more efficient charge-separation. In addition, nanorods could facilitate one-directional charge transport in photovoltaic devices.²⁰

1.3 Titanium Dioxide TiO₂

1.3.1 Crystal Structures

The three crystalline forms of titanium dioxide are the anatase, rutile and brookite mesomorphs. The anatase and rutile forms of titanium dioxide are the most common forms found in nature, whereas the brookite form is relatively uncommon and unstable. The average crystal size of the three crystalline forms is dependent upon the stability of their structures: rutile titanium dioxide is stable with a diameter, $d > 35$ nm²¹, anatase titanium dioxide is stable with a diameter, $d < 11$ nm and brookite titanium dioxide TiO₂ is stable with a diameter 11 nm $< d < 35$ nm.^{22,23} These different polymorphs have different degrees of activity as catalysts for photocatalytic reactions. The density of the rutile and anatase polymorphs of titanium dioxide is 4.26 g cm⁻³ and 3.90 g cm⁻³, respectively. The anatase form of titanium dioxide is more

photocatalytically active than the rutile form, due to its more open structure compared with that of the rutile phase.²⁴

Degussa P25 is a commercially obtainable photocatalyst and it is a composite of two forms of TiO₂, *i.e.*, 25% of the rutile and 75% of the anatase polymorphs.²⁵ It is widely used in photocatalytic degradation reactions due to the fact that it is chemically stable, readily available, cost-effective and an efficient catalyst for oxidation processes.²⁶ There is growing interest in the further development of existing photocatalytic semiconducting materials as well as the preparation of new materials, which can be used in photovoltaics to convert solar energy to electricity and also to reduce the time needed for the photo-degradation of impurities, *e.g.*, in smart windows and vehicle windscreens.

1.3.1.1 Rutile Titanium Dioxide

The unit cells of both the rutile and anatase polymorphs of titanium dioxide are shown in figures 1-2 and 1-4²⁷, respectively. Both the rutile and anatase polymorphs exhibit tetragonal structures. In each unit cell, there are six titanium atoms and twelve oxygen atoms, respectively, *i.e.*, every titanium atom is coordinated to six oxygen atoms and every oxygen atom is coordinated to three titanium atoms. In each phase, there is a slight distortion of the TiO₆ octahedron, which is manifested in the fact that two Ti-O bonds are slightly longer than the other four Ti-O bonds and some O-Ti-O bond angles are not 90° as required.

The anatase phase is more distorted than the rutile phase. The rutile and anatase crystal structures have been reported generally in terms of octahedral TiO₆ chains with shared edges. The rutile and anatase polymorphs share two and four edges, respectively.²⁸

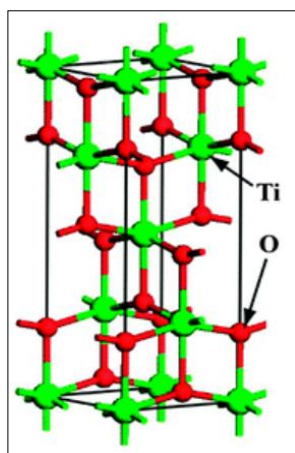


Figure 1-2: The unit cell of titanium dioxide rutile phase.

There are three faces of rutile phase: (110), (100) and (001), shown in figure 1-3²⁹. (110) and (100) faces have low energy rather than (001) and are hence reflected to be significant for practical polycrystalline or powder materials.³⁰

The (110) face is the most thermally stable and, consequently, it has been the most investigated. It has lines of crossing oxygen atoms, which are bonded to only two titanium atoms. The corresponding titanium atoms are 6-coordinate. In order to compare, there are lines of 5-coordinate titanium atoms running parallel to the lines of crossing oxygen atoms and alternating with these. The (100) face similarly has alternating lines of crossing oxygen atoms and 5-coordinate titanium atoms. However these are present in an altered symmetrical relationship with each other. The (001) face is less thermally stable and starts to rearrange above 475 °C.³⁰ There are paired lines of crossing oxygen atoms alternating with single lines of exposed titanium atoms, which are of the equatorial type rather than the axial type.

1.3.1.2 Anatase Titanium Dioxide

The anatase phase of titanium dioxide has three faces, (101), (011) and (100), as shown in figure 1-5²⁹. The faces (101) and (001) have a low energy in the natural crystalline polymorphs.^{23, 31} The (101) face, which is the most predominant face for anatase nanocrystals²², is wavy, also with interchanging lines of 5-coordinate titanium atoms and crossing oxygen atoms, which are at the edges of the folds. The (001) face is slightly planar, but can be shaped as a (1-4) restoration.^{31, 32}

The (100) face is less common in typical nanostructures. However, it is noted that it is present in rod-shape anatase polymorphs grown under in some circumstances using hydrothermal synthetic methods.²³ This face has double lines of 5-coordinate titanium atoms interchanging with double lines of crossing oxygen atoms. It can be shaped as a (1-2) restoration.³³

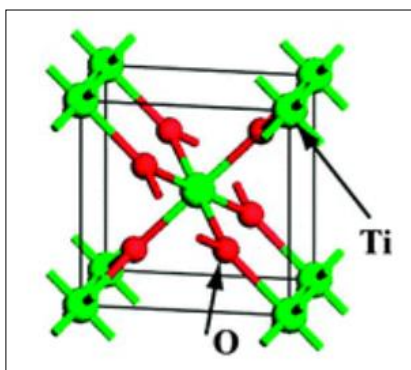


Figure 1-4: The unit cell of titanium dioxide anatase phase.

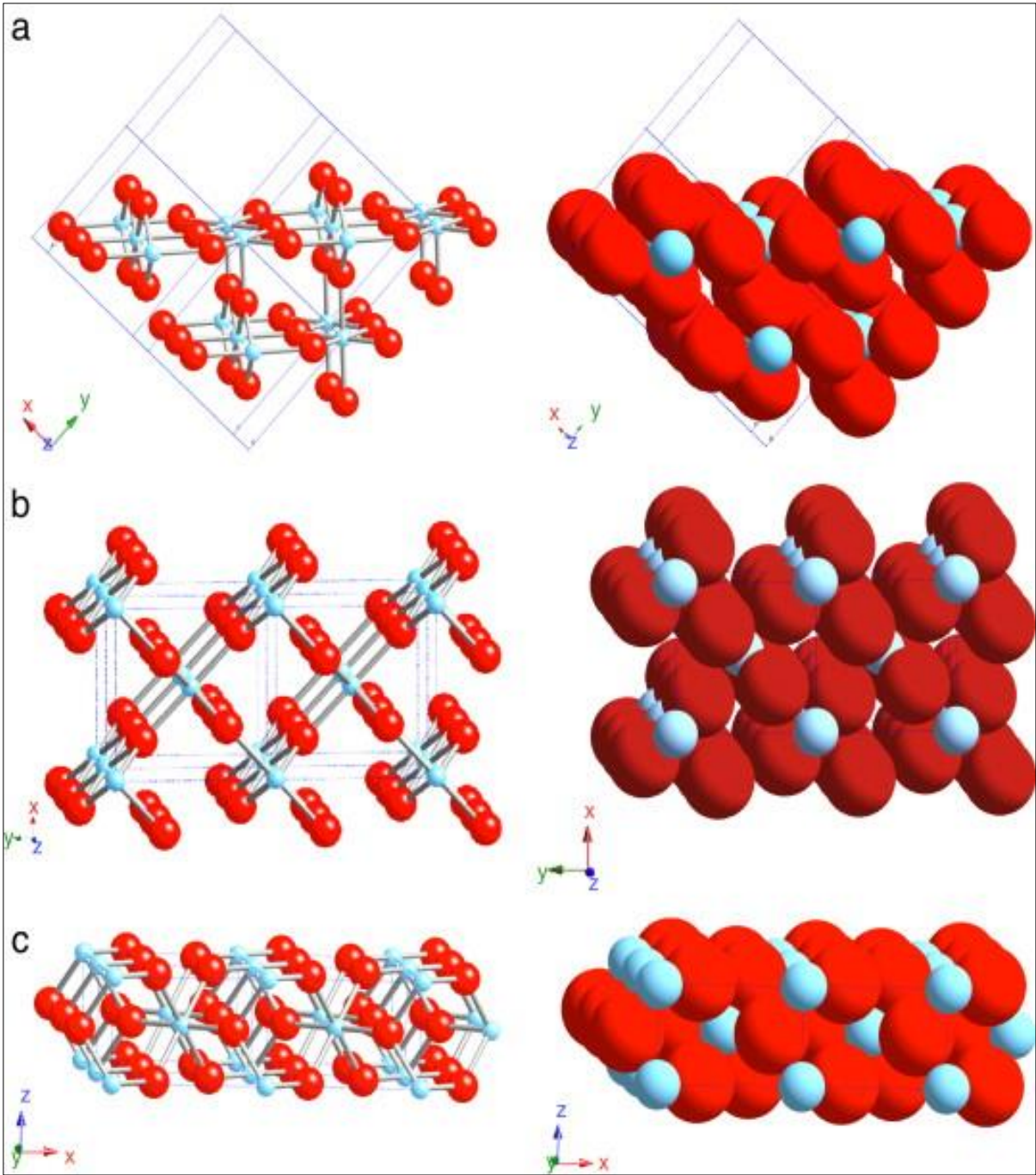


Figure 1-3: The three faces of titanium dioxide rutile phase: (a) (110), (b) (100) and (c) (001).

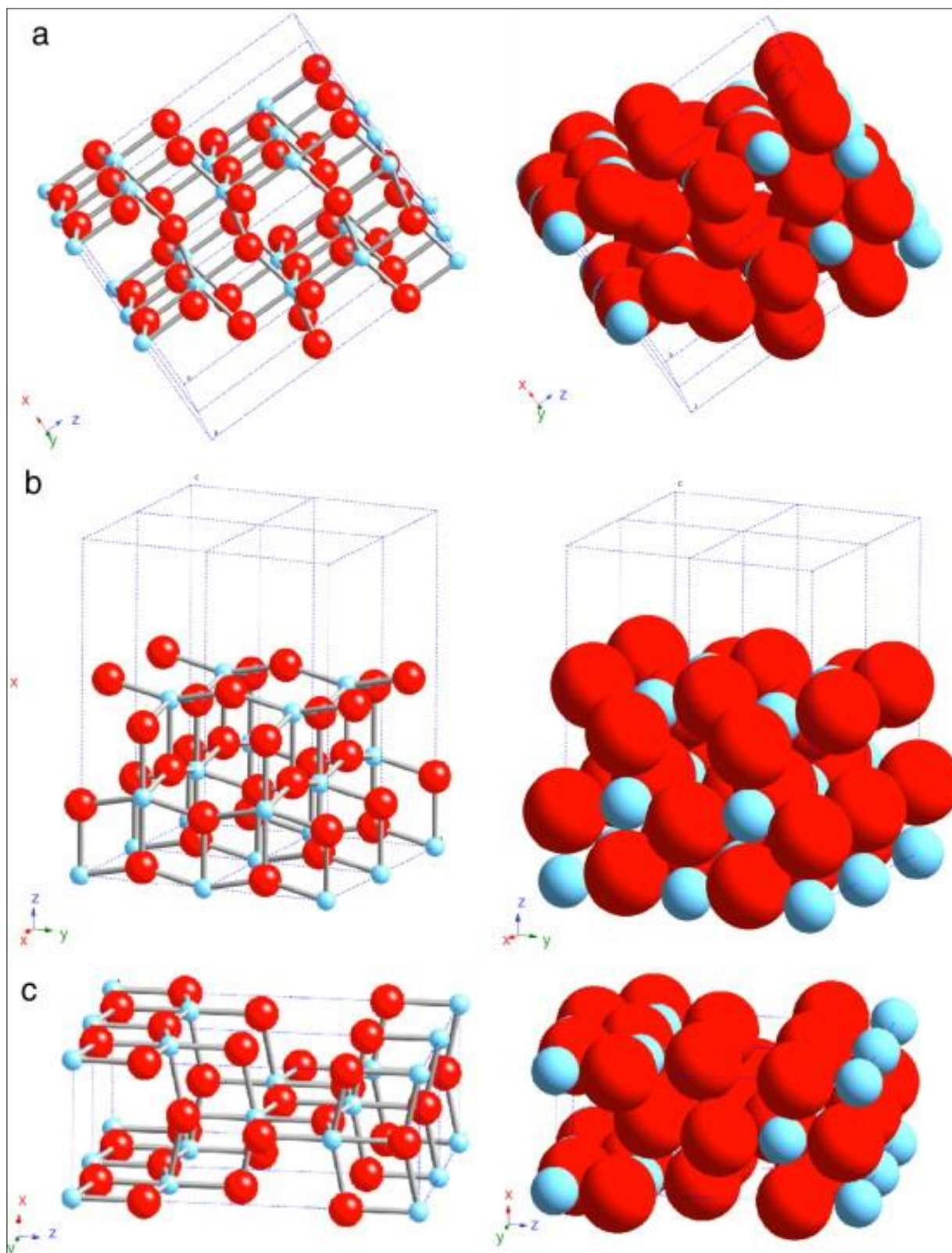


Figure 1-5: The three faces of titanium dioxide anatase phase: (a) (101), (b) (100) and (c) (001).

1.3.1.3 Brookite Titanium Dioxide

Brookite, the third phase of TiO_2 , shown in figure 1-6²⁷, has a more complex crystal structure. It has an orthorhombic cell, which contains eight formula units. The critical difference between the brookite and the anatase and rutile crystal structures is that there are six different Ti-O bonds with a bond length between 1.87 Å and 2.04 Å. Consequently, there are 12 O-Ti-O bond angles between 77° and 105°. However, only two types of Ti-O bonds and O-Ti-O bond angles exist for both the rutile and anatase crystalline structures. It can be supposed that brookite structure is composed of a distortion of TiO_6 octahedral sharing three edges.³⁴ The brookite phase has three faces shown in figure 1-7²⁹, (010), (110) and (100), which is scarcer and more difficult to synthesise. The order of stability of the crystal faces is (010) < (110) < (100).³⁵

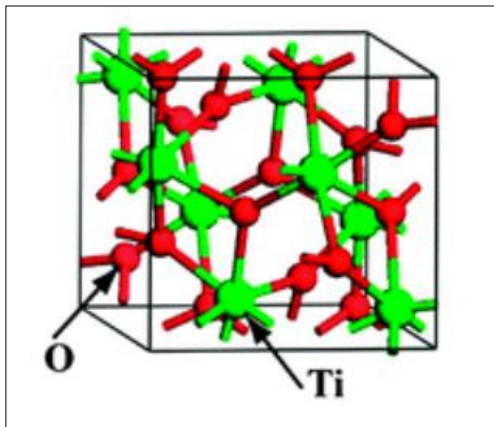


Figure 1-6: The unit cell of titanium dioxide brookite.

1.3.2 Titanium Dioxide TiO_2 Nanomaterials Properties

1.3.2.1 Titanium Dioxide TiO_2 Nanomaterials Structural Properties

The unit's cell structures of the rutile and anatase polymorphs of titanium dioxide are shown in figures 1-2 and 1-4, respectively.²⁷ These rutile and anatase structures can be defined by TiO_6 octahedral chains, where each of Ti^{4+} cation is bonded to six O^{2-} anions. The rutile and anatase crystal structures are different in the alternation of each octahedron and by the assembly pattern of the octahedral chains. The octahedron illustrates a slight orthorhombic alteration in the rutile phase. However, in the anatase polymorph the octahedron is significantly distorted,

so that its symmetry is lower than orthorhombic. The Ti-Ti distances in the rutile polymorph are shorter, whereas the Ti-O distances are larger than those in anatase phase. For the rutile structure, each octahedron has interaction with 10 neighbouring octahedrons (two sharing edge-oxygen pairs and eight sharing corner-oxygen atoms), whereas, for the anatase structure, each octahedron has interaction with eight neighbours (four sharing an edge and four sharing a corner). These dissimilarities in unit cell structures are the reason for the different densities and electronic band structures between the rutile and anatase polymorphs of titanium dioxide.

36

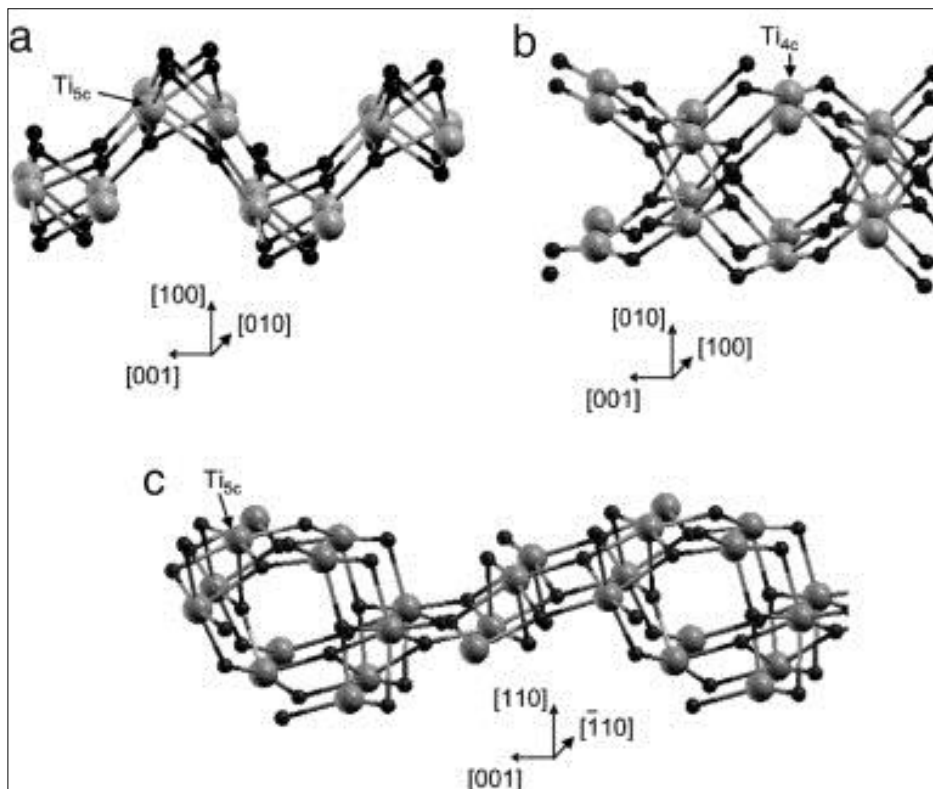


Figure 1-7: The three faces of titanium dioxide brookite phase: (a) (100), (b) (010) and (c) (110).

1.3.2.2 Titanium Dioxide TiO₂ Nanomaterials Thermodynamic Properties

The rutile phase of titanium dioxide is the most thermally stable polymorph. However, the anatase phase and brookite phases are very common in both naturally occurring and synthetic small-grained (nanoscale) samples of titanium dioxide. During the coarsening of the nanoparticles, the resulting phase changes are all observed: anatase to brookite to rutile, brookite to anatase to rutile, anatase to rutile, and brookite to rutile. These phase change sequences suggest that their energies are very close and size dependent. When the particles size is small, the free energy of the rutile phase will be higher than that of anatase phase. Thus it will be the most stable phase at small nanoparticle size.^{21,37}

1.3.2.3 Titanium Dioxide TiO₂ Nanomaterials Electronic Structures

The density of states (DOS) of TiO₂ consists of Ti e_g, Ti t_{2g} [d_{yz}, d_{zx}, and d_{xy}], O p_σ (in the Ti₃O group plane), and O p_π (out of the Ti₃O group plane) as shown in Figure 1-8.³⁸

The top of the valence band is separated into three main areas: the lower energy areas, the σ bonding, coming from oxygen p_σ bonding; the mid energy area is the π bonding and the higher energy area is oxygen p_π non-bonding states where hybridisation with d states is negligible.³⁸

The π-bonding contribution is considerably smaller than contribution from the σ-bonding. The conduction bands are separated into Ti e_g (>5 eV) and t_{2g} (<5 eV). The states of d_{xy} are predominantly located in the lowest conduction bands, i.e., the vertical dashed line in Figure 1-8. The other t_{2g} bands, d_{yz} and d_{zx}, are non-bonding with p states. The major peak of the t_{2g} bands is due mainly to the d_{yz} and d_{zx} states.³⁸

A schematic diagram of molecular band bonding is shown in Figure 1-9.³⁸ An obvious feature can be noticed in the non-bonding states near the band gap: the non-bonding orbital of oxygen pp orbital at the upper of the valence bands and the non-bonding d_{xy} states at the lowest of the conduction bands.³⁹ A comparable mark can be noticed in rutile; though, it is less remarkable than in anatase.³⁹ In the rutile polymorph, every octahedron shares corners with eight neighbours and shares edges with two other neighbours, creating a linear chain. On the other hand, in the anatase phase, every octahedron shares corners with four neighbours and shares edges with four other neighbours, creating a zigzag chain with a screw axis. Consequently, the anatase polymorph is less dense than the corresponding rutile polymorph of titanium dioxide. Furthermore, metal-metal distance in anatase is larger, 5.35 Å.³⁹

Consequently, the orbitals of titanium d_{xy} at the lowest of the conduction band are fairly isolated, whereas in the rutile phase, the orbitals of t_{2g} at the lowest of the conduction band exhibit a metal-metal interaction at a shorter distance of 2.96 Å.

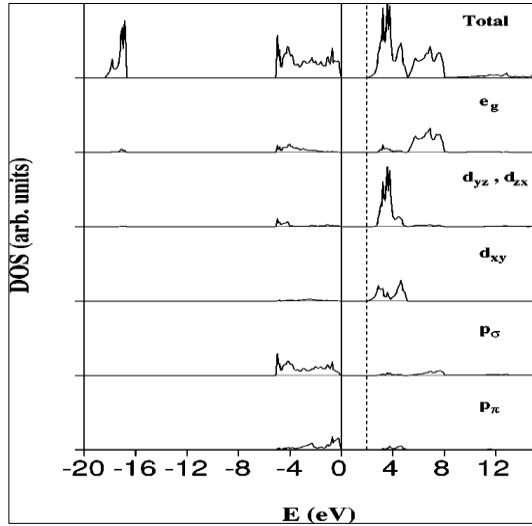


Figure 1-8: The density of states (DOS) of titanium dioxide TiO_2 .

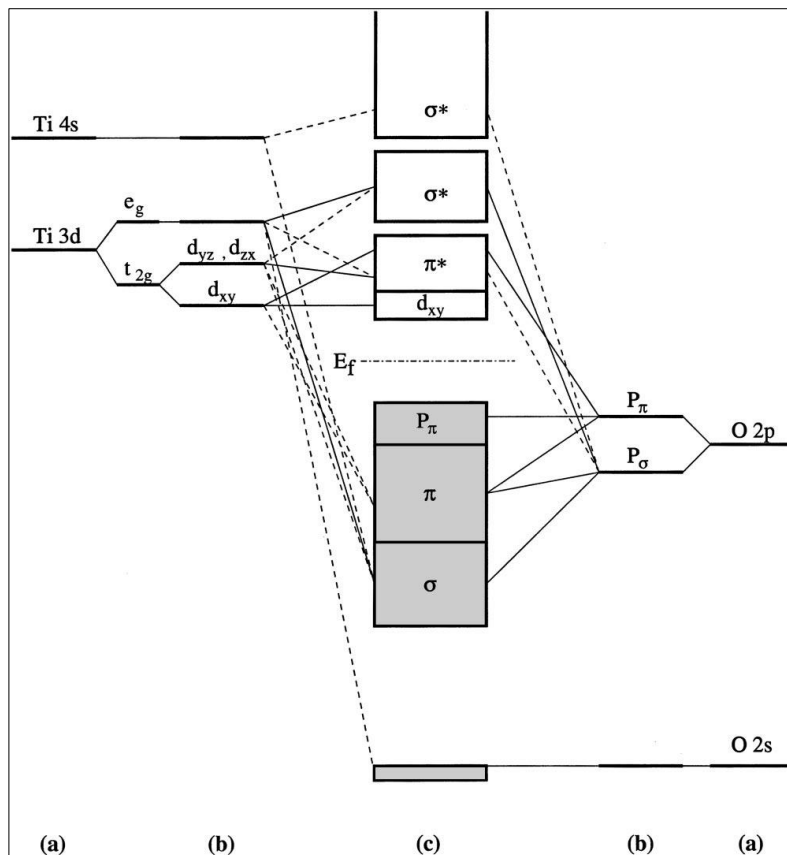
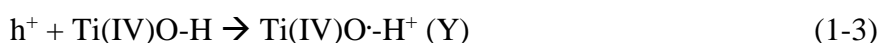
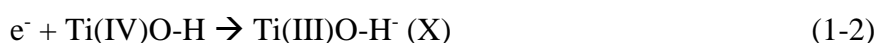


Figure 1-9: molecular band bonding structure for titanium dioxide.

1.3.2.4 Titanium Dioxide Nanomaterials - Electron and Hole Transport

On the absorption of photons with energies equivalent to, or higher than, the band gap of titanium dioxide, $E_g > 3.2 \text{ eV}$ ⁴⁰, electrons are excited from the valence band into the unoccupied conduction band, leading to the presence of excited electrons in the conduction band and positive holes in the valence band. These charges can recombine, either non-radiatively, *i.e.*, dissipating the input energy as heat, with the emission of a photon, by or becoming trapped and reacting with electron donors or acceptors adsorbed on the titanium dioxide surface. The competition between these excited-state dissipation routes, as illustrated below, controls the overall efficacy for several applications of titanium dioxide nanoparticles⁴¹.



Reaction (1-1) represents the absorption of a photon. Reactions (1-2)-(1-6) are photocatalytic redox pathways, while reactions (1-7)-(1-9) show charge recombination mechanisms. Reactions (1-3) and (1-4) are the competition ways for holes, leading to bound hydroxyl (OH) radicals and oxygen vacancies, respectively. The inverse of reaction (1-4) produces oxygen atom intermediates upon exposing defective surfaces to O_2 (g). The electrons and holes created in titanium dioxide nanoparticles by the absorption of incident photons are localised at different defect sites on the surface and in the bulk.⁴¹

1.3.3 Titanium Dioxide Nanorods - Methods of Synthesis

1.3.3.1 Aqueous Sol-Gel Routes

In recent times, sol-gel chemistry has made very significant progress as a very versatile and useful method for synthesising inorganic nanomaterials and is now regarded as a multipurpose

method used in producing numerous ceramic substances. The sol-gel method involves two main reactions. The first reaction is hydrolysis of soluble precursor molecules to produce a colloidal dispersion of small particles called the sol. The second reaction involves the formation of bonds between the particles in the sol to form a network of cross-linked particles called the gel. A subsequent heat treatment (pyrolysis) of the gel forms the desired solid material. There are several main advantages in using this method for the synthesis of inorganic materials compared with other methods, *e.g.*, good control over crystal structure, selective shape and size. The synthesis of titanium dioxide nanorods has been achieved by means of this wet chemistry approach to the preparation of nanocrystalline materials.

The synthesis of titanium dioxide nanorods has been achieved by hydrolysis and polycondensation using various titanium tetraalkoxides as starting materials. The growth of Ti-O-Ti bonds is facilitated using small volumes of water, a slow hydrolysis speed and a surplus of titanium tetraalkoxide in the reaction mixture. These anatase groups are prepared so as to favour hypothetically expected condensation and development paths.⁴²⁻⁴⁴ Due to the great reactivity of titanium starting materials, such as titanium chloride and titanium tetraalkoxides, control of the reaction speed is an important factor in the formation of TiO₂ nanorods with the preferred nanocrystalline structure and/or shape. Titanium dioxide nanocrystals with a uniform-sized have been prepared whereby their shape depends on the relative proportions of tetramethylammonium hydroxide (TMAH) to titanium alkoxide.⁴⁵

Recently, nanocrystals of transition metal oxides have been successfully prepared using a non-hydrolytic sol-gel process. A hydrolysis reaction of titanium tetraisopropoxide (TTIP), using oleic acid (OA) as a stabilising surfactant has used to control the organised growth of titanium dioxide TiO₂ nanorods.⁴⁶ This chemical modification of titanium tetraisopropoxide by oleic acid is a sensitive approach to adjust the reactivity of the starting material in water as the reaction solvent. The most significant aspects of shape control of titanium dioxide nanocrystals have been studied by simply changing their growing dynamics in water. Tertiary amines or quaternary ammonium hydroxides were used as catalysts to facilitate rapid crystallisation under mild reaction conditions.⁴⁷⁻⁵⁰

The controlled growth of anatase nanocrystals of titanium dioxide was carried out at 300 °C under non-aqueous conditions using two surfactants¹¹, *i.e.*, lauric acid (ABL) as the selective surfactant and trioctylphosphine oxide (TOPO) as the non-selective surfactant. The growth of titanium dioxide nanocrystals as either rods or as with branched shapes can be controlled by adjusting the relative proportions of a non-selective and a surface-selective surfactant, which

in turn is based on the fundamental anisotropic character of the anatase polymorph of titanium dioxide.

1.3.3.2 Chemical Vapour Synthesis (CVS)

Nanorods of titanium dioxide in the rutile phase have been prepared using various thermal evaporation methods at high-frequency, *e.g.*, 350 kHz and at high temperatures, *e.g.*, 1050 °C, in two stages carried out in a tube-shaped quartz furnace to control the growth of the titanium dioxide nanorods. The reaction progress can be controlled using a high heating rate, *e.g.* 100 °C min⁻¹, to reach 1050 °C due to the low vapour pressure, 10⁻³ Torr at 1577 °C, as well as the high melting point of titanium 1668 °C. The titanium powder was reacted on an alumina substrate for 30 min at 1050 °C throughout the first stage. The purpose of the first stage was to produce some titanium dioxide seeds, which would serve as active nucleation and reaction sites in the second stage, whereby the new sample of titanium powder and substrate of alumina were split and placed in the graphite vessel in the high-temperature (HT) zone and the low-temperature (LT) zone, respectively. The first stage is used to produce titanium dioxide seeds with a high surface energy, which nucleate the growth of the titanium dioxide nanorods in the second stage of the reaction. The nanorods formed using this two-stage process are 70-150 nm in diameter and 2 µm in length. The morphology of titanium dioxide products depends on the length of the growing period, *e.g.*, nanorods with a brick-like morphology were formed at a reaction time of 20 min in the second stage and nanorods with a rod-like morphology were formed at a reaction time of 40 min.⁵¹⁻⁵³

1.3.3.3 Metal Organic Chemical Vapour Deposition (MOCVD)

Rutile and anatase titanium dioxide nanorods have also been prepared using a Metal Organic Chemical Vapour Deposition (MOCVD) process.⁵⁴ Nanostructures of titanium dioxide can be grown-up in a two-temperature-zone furnace. The precursor, titanium acetylacetonate Ti(C₁₀H₁₄O₅) located on a Pyrex glass vessel was loaded into the low-temperature zone of the furnace, where the evaporation of the solid reactant can be controlled. The vapour was taken under a N₂/O₂ flow into the high-temperature zone of the furnace where substrate was situated. For example, nanostructures of titanium dioxide were grown directly on plain fused silica substrates at a high temperature of 500-700 °C.⁵⁴ Nanorods of titanium dioxide have also been

grown using MOCVD techniques on a WC-Co substrate using titanium tetraisopropoxide (TTIP) as a starting material. The growth progress of the titanium dioxide nanorods was catalysed by using cobalt as a nucleating centre. The diameter and length of nanorods were 50-100 nm and 0.5-2.0 mm, in that order. ⁵⁵

1.3.3.4 Template Method

The main advantages of the template method for the synthesis of titanium dioxide nanorods is that size and shape of the nanorods can be directly controlled using pre-designed template membranes, such as porous alumina membranes and “track-etched” polycarbonate filters, in the sol-gel preparation of the micro- and nanoscale products. Porous alumina membranes with a very high pore density, *e.g.*, 10^{11} pores cm^{-2} , can be formed electrochemically from aluminium metal. ⁵⁶ Two main template methods have been reported: direct sol-filling and sol electrophoresis, which combine a template method with sol-gel techniques. In the first method, nanorods of titanium dioxide have been prepared through direct filling of template pores by immersion in a metal oxide sol. ^{5, 56} Some of the problems encountered using sol-gel methods of this kind can be overcome by the use of electrophoresis in the second general template method. For example, sol-gel electrophoresis has been presented an effective way of making thick films. These films often have better thickness, density and quality than those shaped using tradition sol-gel methods. ⁵⁷⁻⁵⁹

1.3.3.5 Aerosol-Flame Synthesis Processes

Flame synthesis is a method that can be scaled up to yield nanosizes materials in high volume at comparatively low cost. Several morphologies of titanium dioxide nanoparticles have been prepared using a reaction of an aerosol-assisted vapour phase. Source materials vapour and/or droplets of aerosol are fed into a quartz tube and heated in a two-temperature-region furnace. The reaction consists of a combination of the decomposition of gas phase and crystal growth in the liquid droplet phase. The controlled formation of titanium dioxide nanoparticles has yielded a variety of shapes, from single crystal nanoparticles to complex dendritic nanostructures grown out of a core nanoparticle. ⁶⁰

1.3.3.6 Anodic Oxidation

Titanium dioxide nanostructures can be formed by oxidation of titanium metal or under anodisation. Titanium anodic oxidation in numerous electrolytes has received significant attention of late, e.g., a thin titanium foil after an anodisation treatment in HF in aqueous solutions. Nanostructured arrays with an adjustable pore diameter of ca, 25-65 nm have been formed by adjusting the anodising voltage.^{13, 61, 62} Optically transparent nanostructured titanium dioxide films with a negatively charged surface have been prepared using anodic oxidation of titanium sheets in an aqueous solution of hydrofluoric acid. Titanium nanorods with a diameter of 30-60 nm and length of 70-250 nm have been prepared using related methods.⁶³

1.3.3.7 Thermal Oxidation of Titanium Substrates

A one-step, simple technique was used to synthesise large-scale, uniform and well-ordered titanium dioxide nanorods by the oxidation of a titanium substrate at 850 °C using acetone as the oxygen source. Titanium dioxide nanorods were also formed by the oxidation of titanium substrates using either pure oxygen or a mixture of argon containing a low concentration of oxygen. The use of pure oxygen led to the formation of crystalline grain films, while the use of a low concentration of oxygen with argon formed random nanofibers developing from the ledges of the titanium dioxide grains. In contrast, highly dense and well-aligned titanium dioxide nanorods arrays were formed using acetone as the oxygen source.⁶⁴⁻⁶⁷

1.3.3.8 Hydrothermal Method

The hydrothermal technique is one of the most potential and favourable approaches for synthesising nanostructures of the titanium dioxide. The hydrothermal technique is generally carried out in autoclaves with Teflon liners under well-controlled temperature and/or pressure in the reaction with aqueous solution. The hydrothermal technique using aqueous NaOH or KOH solution yields nanostructures of titanium dioxide exhibits several advantages in terms of meeting the requirements for titanium dioxide nanostructures as electrode materials, photocatalyst, and hydrophobic surface etc. The resulting titanium dioxide nanorods are several hundreds of nanometres in length and the diameter is typically several nanometres.⁶⁸⁻⁷¹

The anatase or rutile polymorphs of titanium dioxide nanoparticles have been synthesised selectively using a hydrothermal treatment of titanium sols with either tetraalkyl ammonium hydroxides (TENOH) or nitric acid, respectively. Rutile nanorods can be simply created by the hydrothermal treatment of titanium sols with nitric acid, while the favoured growing of nanorods anatase is much more challenging in the absence of an external initiator.⁷²⁻⁷⁴

1.3.4 Applications of Titanium Dioxide 1D-Nanorods

In general, bulk titanium dioxide is an *n*-type semiconductor with a large band gap.⁷⁵ Nanomaterials such as spherical nanoparticles (NPs) and 1D-nanowires (NWs) are significant as they offer greater surface area, more reaction sites, and greater depletion regions and, if they are small enough, quantum confined properties compared with those of the bulk structures. These advantageous properties are of use for a wide range of applications, such as photovoltaics, sensors and catalysis. Unlike the nanoparticle (NP) films in which electrons move randomly in any direction and frequently interact with scattering sites, which increase the chance of charge recombination, 1D-nanowire (NW) structures provide directional conductive channels with a reduced probability of charge recombination and, hence, they should facilitate charge transport. Consequently, titanium dioxide 1D nanostructures have been the subject of intense study as a very effective nanowire framework in developing applications such as photovoltaics, photocatalysis, energy storage systems, electrochromic devices and sensors.^{76, 77}

1.3.4.1 Titanium Dioxide TiO₂ Nanomaterials Photocatalytic Applications

Titanium dioxide nanoparticles are widely used photocatalytic materials owing to their exceptional photochemical, thermal and chemical stability, appropriate electronic properties and environmentally friendly nature.⁷⁸⁻⁸⁰ Electron and hole pairs formed inside the titanium dioxide nanoparticles after absorbing photons with energy larger than the band gap⁴⁰, separate and then migrate to the very large surface of the nanoparticles where they can react with substances that have adhered on the titanium dioxide surface.⁸¹ In principle, the photocatalytic efficacy and efficiency is measured *via* light absorption, charge transport, surface reaction sites, number and rates of redox reaction, *etc.*⁸² The number of reaction sites is directly related to the size of the active surface area. Titanium dioxide nanorods in particular have been the subject

of extensive investigations in advanced photocatalysis applications and are available as commercial products.⁸²

1.3.4.2 Titanium Dioxide Nanomaterials in Photovoltaics Applications

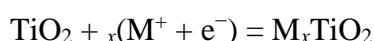
Different kinds of titanium dioxide nanoparticles have been broadly used in different kinds of photovoltaic structures as the charge collector due to their chemical, photochemical and thermal stability and suitable electronic band structure. The titanium dioxide nanoparticles contribute to good photovoltaic performance due to high charge carrier collection, low optical reflection and efficient absorption of incident photons across a wide optical spectrum due to the wide band gap. While issues still remain in terms of reducing the level of charge recombination, surface scattering and interface imperfection, understanding 1D charge transport property and discovering new configurations of titanium dioxide for effective solar energy absorption, conversion and charge collection remain active areas of investigation in terms of photovoltaic devices with a much higher level of performance.⁸³ There are three main types of photovoltaics application; dye-sensitised solar cells⁸⁴, polymer-based solar cells⁸⁵ and quantum dot solar cells.⁸⁶

1.3.4.3 Titanium Dioxide Nanomaterials Energy Storage Applications

The next generation of electrochemical energy storage applications, *e.g.*, batteries or supercapacitors, requires high energy density storage, high power, high charging/discharging rate, low weight and compact size. Nanomaterials 1D are presently investigated as the structure blocks for battery electrodes.^{87, 88} 1D Nanomaterials might offer advantages in terms of electrode design, high surface area and shorter ion diffusion path lengths compared to conventional thin film configurations. These qualities might lead to higher capacities with high charge/discharge rates. While titanium dioxide is not generally considered as a core electrode material, the 1D morphology of titanium dioxide nanorods is still expected to deliver significant improvements in high-performance electrode architectures.^{89, 90}

1.3.4.4 Titanium Dioxide Nanomaterials Electrochromism and Electrochromic Devices

Electrochromism is the phenomenon whereby a material can change colour by oxidation or reduction reactions in the electrochromic crystal lattices. When monovalent ions are intercalated into titanium dioxide, its colour often changes from transparent to blue, which gives the titanium dioxide an electrochromic property. The well-accepted model through this route ⁹¹ is:



The electrochromism properties of titanium dioxide might find application in smart windows, displays, sunroofs, mirrors, *etc.* ⁹²

1.3.5 Metal-Doped Titanium Dioxide (TiO₂-M)

Bulk titanium dioxide band exhibits a wide band gap (E_g) in the UV region of the electromagnetic spectrum, *i.e.*, $E_g = 3.0$ eV for the rutile phase and $E_g 3.2$ eV for the anatase phase. ⁹³ However, this significant absorption represents only a small fraction of the sun's energy (<10%). ³⁶ Consequently, one of the objectives of research on titanium dioxide nanomaterials is to increase their optical adsorption by shifting the onset of the band edge from the UV into the visible region ⁹⁴⁻⁹⁶. Various methods have been used in attempts to realise this objective, *e.g.*, doping titanium dioxide nanomaterials with other chemical elements can change the optical and electronic properties; doping titanium dioxide with other coloured inorganic or organic compounds can increase its optical absorption in the visible region of the electromagnetic spectrum; coupling collective oscillations of the electrons in the conduction band of metal nanoparticle surfaces to those in the conduction band of metal-doped titanium dioxide nanomaterials (TiO₂-M) can also modulate the performance; modification of the titanium dioxide nanoparticle surface with other semiconductors can alter the charge-transfer properties between the titanium dioxide nanoparticles and the surrounding environment. Each of these modifications can lead to improvements in the performance of electro-optic or electronic devices incorporating titanium dioxide nanomaterials as functional semiconductor components. ^{96, 97}

The range of applications of titanium dioxide can be widened by improving its properties by doping with transitional metal cations, *e.g.*, iron, niobium, vanadium, *etc.* Among these,

niobium-doped titanium dioxide (TiO₂-Nb) is one of the most studied transparent conductive oxides and has found application in electro-optic devices as a replacement for high-cost indium tin oxide as electrodes.⁹⁸

The recent discovery of the almost metallic conductivity and high optical transparency of niobium-doped titanium dioxide (TiO₂-Nb) nanoparticles in the anatase phase has inspired intense research on this material for applications as transparent conducting metal oxide electrodes.^{99,100} The Nb⁵⁺ anions act as an *p*-type dopant in titanium dioxide. They modify the band structure of the titanium dioxide nanoparticles and thereby produce additional charge carriers in the conduction band.^{100,101}

1.3.5.1 Preparation of Metal-Doped Titanium Dioxide (TiO₂-M)

Niobium-doped (3 wt%) titanium dioxide nanorods (TiO₂-Nb) have been prepared by a low-temperature (120 °C), surfactant-directed, hydrolysis method followed by calcination at 600–900 °C. The resultant titanium dioxide nanorods have a high aspect ratio ~ 10 with a length of up to 40 nm and a diameter of 3–4 nm.¹⁰² Niobium-doped (5 wt %) anatase titanium dioxide (TiO₂-Nb) nanorods have been synthesised by electrospinning a polymeric solution of titanium and niobium precursors and subsequent annealing. The resultant titanium dioxide nanofibers have diameter ~ 150 nm.¹⁰³ Niobium-doped (10 wt % and 20 wt %) titanium dioxide (TiO₂-Nb) nanorods have also been formed by using a solvothermal method using *tert*-butyl alcohol as the reaction medium. The solvothermal method enables the formation of crystalline Niobium-doped titanium dioxide (TiO₂-Nb) nanoparticles have a diameter varying from 4 nm to 15 nm depending on the reaction temperature and time.¹⁰⁴ Niobium-doped (5 wt% and 10 wt%) titanium dioxide (TiO₂-Nb) nanoparticles have been also synthesised using a sol-gel method combined with annealing at different temperatures, *e.g.*, at 450, 650 and 1050 °C.¹⁰⁵ Niobium-doped titanium dioxide (TiO₂-Nb) nanoparticles have also been synthesised *via* a continuous spray-drying method using titanium oxysulfate and ammonium niobate (V) oxalate as water-soluble starting materials.¹⁰⁶ The preparation of niobium-doped titanium dioxide (TiO₂-Nb) nanoparticles have been carried out using a co-hydrolysis method; mixing titanium dioxide nanoparticles (20-50 nm) with different concentrations of a gel containing small concentrations, *e.g.*, 0.5, 1, 5 and 5 mol%, of niobium.¹⁰⁷ Niobium-doped (10 wt %) titanium dioxide (TiO₂-Nb) nanoparticles have also been synthesised using a hydrothermal method. Solutions of TiOSO₄ and NbCl₅ were treated under three different hydrothermal conditions for

5 h at 180°C in the absence and/or presence of urea and aqueous ammonia. The resultant niobium-doped titanium dioxide (TiO₂-Nb) nanoparticles were formed as small, d ~11 nm, fine crystallites with a relatively large surface area, *e.g.*, 135 m² g⁻¹.¹⁰⁸

1.4 Barium Titanium Oxide BaTiO₃

1.4.1 Perovskite Structure of Barium Titanium Oxide BaTiO₃

Barium titanium oxide (BaTiO₃) has been of practical attention for more than 60 years due to its promising physical properties, such as good dielectric and ferroelectric properties at and above room temperature, its high chemical, thermal and mechanical stability, *etc.* Additionally, it can be synthesised simply and used in the form of a polycrystalline ceramic in a variety of commercial applications.¹⁰⁹ For example, owing to its combination of a very high dielectric constant and low dielectric loss, barium titanium oxide has been used in applications, such as capacitors and multilayer capacitors (MLCs).¹¹⁰

Ceramic materials with a perovskite structure, such as barium titanium oxide, represent a very important class of functional electronic materials.¹¹¹ The perovskite-like structure, named after the calcium titanium oxide (CaTiO₃) perovskite mineral¹¹², is a ternary inorganic compound with a general formula of ABO₃, where the A and B cations are of different sizes. Perovskite are considered to exhibit an FCC derivative structure in which the larger A cation and oxygen together form an FCC lattice, while the smaller B cation occupies the octahedral interstitial sites in the FCC array where the oxygen atom is the B cation's nearest neighbour. This structure is a network of octahedrons, corner-linked with oxygen atoms, with the smaller cations B filling the octahedral holes and the larger cations A filling the dodecahedral holes. The unit cell of perovskite cubic structure is shown below in figure 1-10.¹¹³ The coordination number of A (Ba⁺²) is 12, while the coordination number of B (Ti⁺⁴) is 6, although in most cases these values are somewhat idealized. In fact, any structure consisting of the corner-linked oxygen octahedral with a small cation filling the octahedral hole and a large cation, if present, filling the dodecahedral hole is usually regarded as a perovskite, even if the oxygen octahedral is slightly distorted.¹¹¹

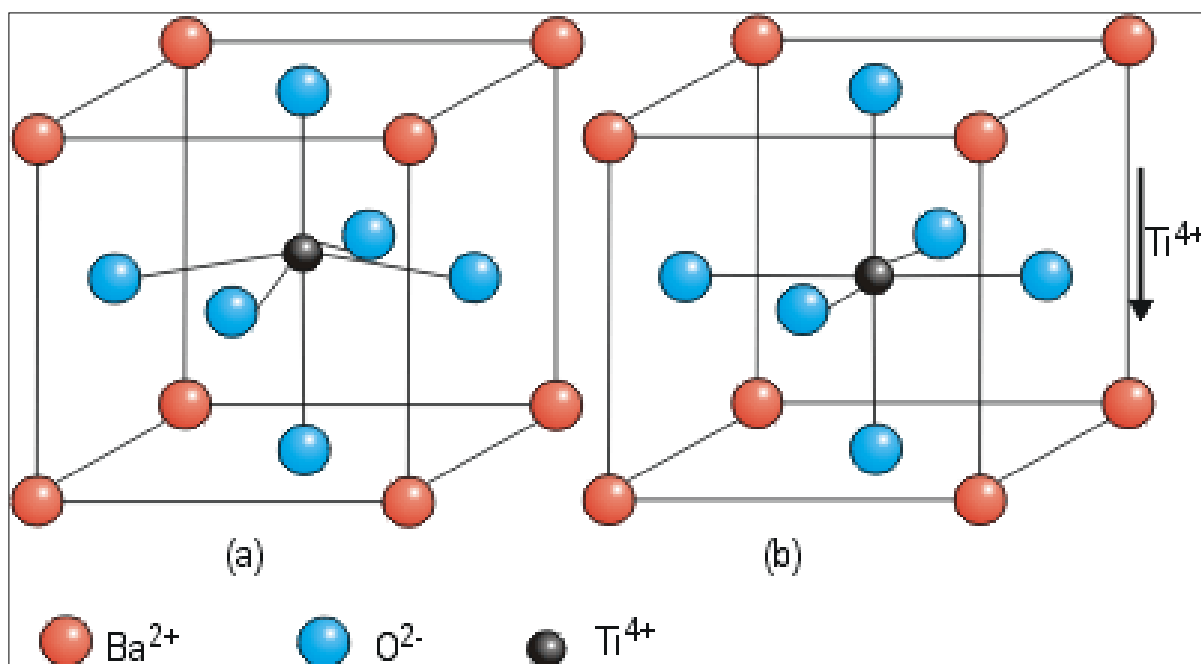


Figure 1-10: Perovskite structure of barium titanium oxide BaTiO₃.

1.4.2 Preparation of Barium Titanium Oxide (BaTiO₃) Nanowires

Single-crystalline barium titanium oxide (BaTiO₃) nanowires have been obtained by using a solution-phase method.^{114, 115} The decomposition of barium titanium isopropoxide in the presence of coordinating ligands results in the formation of nanowires of BaTiO₃ with a range of diameters, $5 \text{ nm} < d < 70 \text{ nm}$ and lengths, l , of up to tens of micrometres. This method facilitated the study of the ferroelectric properties of individual single, crystalline barium titanium oxide nanowires prepared in this way.^{114, 115} Single-crystalline perovskite barium titanium oxide nanorods have also been synthesised at low temperature by a combined method based on a combination of sol-gel and surfactant-templated methods. The preparation was achieved by using a combination of barium acetate (Ba(CH₃COO)₂) and tetrabutyl titanate (Ti[O(CH₂)₃CH₃]₄) as the starting materials and laurylamine as the surfactant. The resultant, single-crystalline cubic perovskite barium titanium oxide nanorods have diameters ranging between 20 and 80 nm and lengths reaching up to $>10 \mu\text{m}$.¹¹⁶ A solution-based preparation of single-crystalline barium titanium oxide nanorods was also investigated to produce nanorods with a broad range of diameters, $5 \text{ nm} < d < 60 \text{ nm}$ and lengths reaching up to ca. $10 \mu\text{m}$.¹¹⁷ The preparation of single-crystal barium titanium oxide nanorods was also investigated using K₂Ti₄O₉ and K₂Ti₆O₁₃ as precursors¹¹⁸ in a sol-gel method combined with electrophoretic

deposition. This new synthetic method was developed in order to increase the degree of control of the growth of barium titanium oxide nanorods. Homogeneous nanorods with a range of diameters, *e.g.*, $45 \text{ nm} < d < 200 \text{ nm}$ and a length of ca $10 \text{ }\mu\text{m}$ can be grown over large areas with a near unidirectional arrangement of the nanorods within the plane of the substrate.¹¹⁹ Polycrystalline, rather than single-crystalline, barium titanium oxide nanorods were synthesised by using an electrophoretic deposition (EPD) method. Involving the addition of a barium titanate sol to aluminium oxide (AAO) templates following by a thermal annealing process. The resultant barium titanium oxide nanorods formed using this method exhibit grain sizes ranging from 20 nm to 50 nm.¹²⁰ The preparation of ultra-long, *e.g.*, up to $45 \text{ }\mu\text{m}$, vertically aligned barium titanium oxide nanowire arrays on an oxidised titanium substrate was also investigated using a two-step hydrothermal reaction procedure. Firstly, ultra-long aligned sodium titanate arrays were developed. Secondly, these precursor sodium titanate arrays were transformed into barium titanium oxide, which retained the shape of the original nanowire templates. Such barium titanium oxide nanowires produced using this method are typically 600–630 nm in diameter and $40 \text{ }\mu\text{m}$ in length.¹²¹ Barium titanium oxide nanorods have also been synthesised using a hydrothermal method at temperature of $135 \text{ }^\circ\text{C}$, using a mixture of barium acetate, titanium isopropoxide as the starting materials and sodium hydroxide as a reagent without any surfactant or template. The resultant nanorods were short with an average diameter, $d \sim 20 \text{ nm}$.¹²² An electron-microscopy investigation was carried to prepare barium titanium oxide nanorods, by sol–gel electrophoretic deposition (EPD) into anodic aluminium oxide (AAO) membranes. The barium titanium oxide nanorods developed within the template membranes were 150 to 200 nm in diameter and $10\text{--}50 \text{ }\mu\text{m}$ in length.¹²³ A facile preparation of single-crystalline barium titanium oxide nanorods, 100 nm in diameter and $10 \text{ }\mu\text{m}$ in length, has been carried out at low temperature $50 \text{ }^\circ\text{C}$ in an ethanol solution.¹²⁴

1.5 Organic Field Effect Transistors (OFET)

1.5.1 Organic Field Effect Transistors (OFET)

Organic Field Effect Transistors (OFET) are made up of at least five functional layers, see figure 1-11: (1) a gate electrode, (2) an insulating dielectric layer (3) an organic semiconducting layer (4) a drain electrode and (5) a source electrode on top of a solid, planar substrate, for example a glass or silicon substrate, see figure 1-11.¹²⁵ The efficient functioning of an OFET

depends critically on the nature of the insulating dielectric layer, the organic semiconducting layer and the source and drain electrodes, as measured by the charge mobility of the organic semiconductor between the source and the drain electrodes, i.e., the electric current, the ON-OFF ratio (I_{on}/I_{off}) and the operating voltage of the device.¹²⁶ In order to operate in a high frequency range, a high charge carrier mobility of the device is required, while use in portable electronic devices a low operating voltage is more important. The mobility of OFETs mainly depends on semiconductor-insulator interface and contact material of the source and drain electrodes and operating voltage depends on the dielectric constant of the dielectric layer.

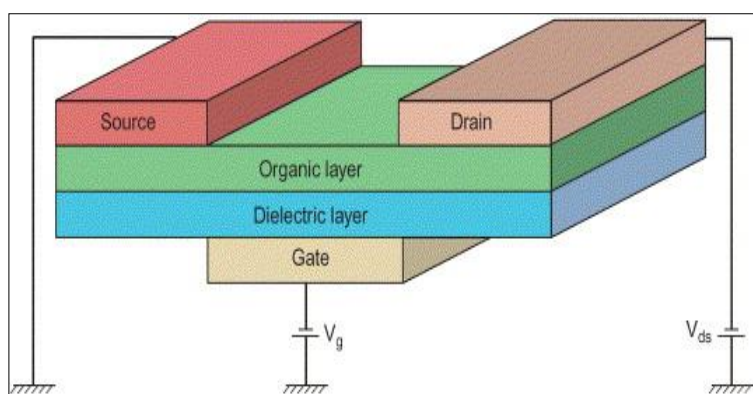


Figure 1-11: Schematic representation of the Organic Field Effect Transistor (OFET) Structure.

1.5.2 Organic Field Effect Transistors (OFET) - Challenges

In the last few years, numerous organic substances have been studied as organic semiconductors in OFETs and as potential replacements for pentacene commonly used in OFETs as the standard organic semiconductor.^{127, 128} The selection of a gate dielectric is a critical point in the fabrication of efficient OFETs as the semiconducting film grain size, for example, which has a strong influence on the field-effect charge-carrier mobility of the organic semiconductor in the OFET, is strongly influenced by the gate dielectric surface roughness. The most common gate dielectric in pentacene-based OFETs is thermally processed silicon dioxide. Unfortunately, the operating voltage of these OFETs is often relatively high, e.g., approximately 20 V. It is essential to reduce the operating voltage to less than 5 V for portable applications, principally for radio-frequency classification devices involving low power consumption. The use of high dielectric constant (k) insulators has the potential capability of reducing the operating voltage, but the surface of such high-dielectric-constant layers is often

relatively rough and, therefore, the grain size of the semiconductor films deposited on these substances is relatively small, which results in a relatively low field-effect charge-carrier mobility, *i.e.*, electric current.

Therefore, a significant amount of research has been focused on developing methods to reduce the operating voltage of pentacene-based OFETs without reducing the field-effect mobility through the use of various insulating layers.^{129, 130} For example, there was an attempt to use novel self-assembled monolayers as the dielectric layer in order to improve pentacene-based OFET performance.¹²⁹ Another example involved using HfLaO dielectric layer in a pentacene-based OFET, which reduced the operating voltage to 2 V, generated a relatively high field-effect mobility, $\mu = 0.71 \text{ cm}^2 \text{ V}^{-1} \text{ s}^{-1}$ and a moderately good on-off ratio of 10^5 .¹³¹

1.6 High-k Dielectric Materials

A wide variety of dielectric materials are commonly used in very many different applications, especially as a gate insulator for avoiding electrical conduction between the gate and the source and drain electrodes in OFETS. A dielectric material is required to have a large band gap in order to function as an insulating dielectric layer for a gate electrode in an OFET in that the large band gap prevents the electrons from the valence band being excited to the conduction band. Nevertheless, under standard OFET operating conditions there is always a voltage (the leak voltage) that will promote electrons from the valence band into the conduction band.

1.6.1 High-k Dielectric Materials for Organic Field Effect Transistors OFETs

1.6.1.1 Inorganic Dielectrics

The most common gate dielectrics used in standard OFETs based on silicon substrates are uniform, thin layers of highly pure silicon dioxide (SiO_2) with an average thickness of 200-400 nm created by physical vapour deposition at high temperature and high vacuum.¹³² However, silicon dioxide dielectric layers are often fabricated *in situ via* the oxidation of silicon with oxygen or oxygen/nitrogen in a controlled way to form gate insulator with superb mechanical, electrical, and dielectric properties. In recent times, it has been observed that the semiconductor dielectric interface in OFET devices is surrounded by a very large concentration of electron-

trapping sites, because of the presence of surface hydroxyl groups, which are formed in the form of silanols.¹³³ The problems associated with these groups have been partly resolved by using surface treatments in which a monolayer is self-assembled onto the silicon dioxide surface. High advancing aqueous contact angles ($>90^\circ$) have been measured using hexamethyldisilazane (HMDS)¹³⁴, alkanetrichlorosilanes¹³⁵, and alkanephosphonicacids¹³⁶, as the self-assembled monolayers (SAMs)¹³⁷, along with others. Some *n*-type semiconductors have been used to reduce the concentration of interfacial trap sites, which led to improved OFET performance.¹³³

The main focus in the development of novel gate dielectric substances has been primarily on the need for low-cost device production and the reduction of the operating voltages required for new flexible/printed plastic electronics applications. One of the main challenges in the improvement of OFETs has been the slightly high voltages desirable for their operation when using SiO₂ gate dielectric ($k \approx 4$), which make these devices unreasonable for inexpensive applications.

As a result, it is essential to identify and study high-*k* gate dielectrics to reach the requirements desirable for new technologies. Reduction of the device size is one of these requirements, which can be also reached by using high capacitance gate insulators. In this capacity, SiO₂ has reached its scaling limit¹³⁸, which is now leading many researchers to find alternative metal oxides, such as HfO₂, Ta₂O₅, Al₂O₃, Y₂O₃, CeO₂, TiO₂, *etc.*, as potential substitute gate insulators.

1.7 References

1. Zhang, Q.; Cao, G., Nanostructured photoelectrodes for dye-sensitized solar cells. *Nano Today* **2011**, 6, (1), 91-109.
2. Xia, Y.; Yang, P.; Sun, Y.; Wu, Y.; Mayers, B.; Gates, B.; Yin, Y.; Kim, F.; Yan, H., One-Dimensional Nanostructures: Synthesis, Characterization, and Applications. *Advanced Materials* **2003**, 15, (5), 353-389.
3. Iijima, S., Helical microtubules of graphitic carbon. *Nature* **1991**, 354, (6348), 56-58.
4. Rao, C. N. R.; Deepak, F. L.; Gundiah, G.; Govindaraj, A., Inorganic nanowires. *Progress in Solid State Chemistry* **2003**, 31, (1-2), 5-147.
5. C. Hulthen, J.; Martin, C. R., A general template-based method for the preparation of nanomaterials. *Journal of Materials Chemistry* **1997**, 7, (7), 1075-1087.
6. <http://www.mindat.org/min-213.html>. (27/02/2015).
7. <http://www.mindat.org/min-3486.html>. (27/02/2015).
8. <http://www.mindat.org/min-787.html>. (27/02/2015).
9. Barbé, C. J.; Arendse, F.; Comte, P.; Jirousek, M.; Lenzenmann, F.; Shklover, V.; Grätzel, M., Nanocrystalline Titanium Oxide Electrodes for Photovoltaic Applications. *Journal of the American Ceramic Society* **1997**, 80, (12), 3157-3171.
10. Goldberger, J.; Fan, R.; Yang, P., Inorganic Nanotubes: A Novel Platform for Nanofluidics. *Accounts of Chemical Research* **2006**, 39, (4), 239-248.
11. Jun, Y.-w.; Casula, M. F.; Sim, J.-H.; Kim, S. Y.; Cheon, J.; Alivisatos, A. P., Surfactant-Assisted Elimination of a High Energy Facet as a Means of Controlling the Shapes of TiO₂ Nanocrystals. *Journal of the American Chemical Society* **2003**, 125, (51), 15981-15985.
12. Chen, X.; Mao, S. S., Titanium dioxide nanomaterials: synthesis, properties, modifications, and applications. *Chemical reviews* **2007**, 107, (7), 2891-2959.
13. Mor, G. K.; Shankar, K.; Paulose, M.; Varghese, O. K.; Grimes, C. A., Use of Highly-Ordered TiO₂ Nanotube Arrays in Dye-Sensitized Solar Cells. *Nano Letters* **2006**, 6, (2), 215-218.

14. Saponjic, Z. V.; Dimitrijevic, N. M.; Tiede, D. M.; Goshe, A. J.; Zuo, X.; Chen, L. X.; Barnard, A. S.; Zapol, P.; Curtiss, L.; Rajh, T., Shaping Nanometer-Scale Architecture Through Surface Chemistry. *Advanced Materials* **2005**, 17, (8), 965-971.
15. Rabatic, B. M.; Dimitrijevic, N. M.; Cook, R. E.; Saponjic, Z. V.; Rajh, T., Spatially Confined Corner Defects Induce Chemical Functionality of TiO₂ Nanorods. *Advanced Materials* **2006**, 18, (8), 1033-1037.
16. Pokropivny, V. V.; Skorokhod, V. V., Classification of nanostructures by dimensionality and concept of surface forms engineering in nanomaterial science. *Materials Science and Engineering: C* **2007**, 27, (5–8), 990-993.
17. Zhai, T.; Yao, J., *One-Dimensional Nanostructures: Principles and Applications*. Wiley: 2013.
18. Hu, J.; Odom, T. W.; Lieber, C. M., Chemistry and Physics in One Dimension: Synthesis and Properties of Nanowires and Nanotubes. *Accounts of Chemical Research* **1999**, 32, (5), 435-445.
19. Manna, L.; Scher, E. C.; Li, L.-S.; Alivisatos, A. P., Epitaxial Growth and Photochemical Annealing of Graded CdS/ZnS Shells on Colloidal CdSe Nanorods. *Journal of the American Chemical Society* **2002**, 124, (24), 7136-7145.
20. Nelson, J., Organic photovoltaic films. *Current Opinion in Solid State and Materials Science* **2002**, 6, (1), 87-95.
21. Zhang, H.; Banfield, J. F., Understanding Polymorphic Phase Transformation Behavior during Growth of Nanocrystalline Aggregates: Insights from TiO₂. *The Journal of Physical Chemistry B* **2000**, 104, (15), 3481-3487.
22. Shklover, V.; Nazeeruddin, M. K.; Zakeeruddin, S. M.; Barbé, C.; Kay, A.; Haibach, T.; Steurer, W.; Hermann, R.; Nissen, H. U.; Grätzel, M., Structure of Nanocrystalline TiO₂ Powders and Precursor to Their Highly Efficient Photosensitizer. *Chemistry of Materials* **1997**, 9, (2), 430-439.
23. Burnside, S. D.; Shklover, V.; Barbé, C.; Comte, P.; Arendse, F.; Brooks, K.; Grätzel, M., Self-Organization of TiO₂ Nanoparticles in Thin Films. *Chemistry of Materials* **1998**, 10, (9), 2419-2425.

24. Bickley, R. I.; Gonzalezcarreno, T.; Lees, J. S.; Palmisano, L.; Tilley, R. J. D., A STRUCTURAL INVESTIGATION OF TITANIUM-DIOXIDE PHOTOCATALYSTS. *Journal of Solid State Chemistry* **1991**, 92, (1), 178-190.
25. Ohno, T.; Sarukawa, K.; Tokieda, K.; Matsumura, M., Morphology of a TiO₂ Photocatalyst (Degussa, P-25) Consisting of Anatase and Rutile Crystalline Phases. *Journal of Catalysis* **2001**, 203, (1), 82-86.
26. Bekbolet, M.; Ozkosemen, G., A preliminary investigation on the photocatalytic degradation of a model humic acid. *Water Science and Technology* **1996**, 33, (6), 189-194.
27. Zhang, J.; Zhou, P.; Liu, J.; Yu, J., New understanding of the difference of photocatalytic activity among anatase, rutile and brookite TiO₂. *Physical Chemistry Chemical Physics* **2014**, 16, (38), 20382-20386.
28. Cromer, D. T.; Herrington, K., The Structures of Anatase and Rutile. *Journal of the American Chemical Society* **1955**, 77, (18), 4708-4709.
29. Fujishima, A.; Zhang, X.; Tryk, D. A., TiO₂ photocatalysis and related surface phenomena. *Surface Science Reports* **2008**, 63, (12), 515-582.
30. Ramamoorthy, M.; Vanderbilt, D.; King-Smith, R. D., First-principles calculations of the energetics of stoichiometric TiO₂ surfaces. *Physical Review B* **1994**, 49, (23), 16721-16727.
31. Hengerer, R.; Bolliger, B.; Erbudak, M.; Grätzel, M., Structure and stability of the anatase TiO₂ (101) and (001) surfaces. *Surface Science* **2000**, 460, (1-3), 162-169.
32. Liang, Y.; Gan, S.; Chambers, S. A.; Altman, E. I., Surface structure of anatase TiO₂ (001): Reconstruction, atomic steps, and domains. *Physical Review B* **2001**, 63, (23), 235402.
33. Ruzycski, N.; Herman, G. S.; Boatner, L. A.; Diebold, U., Scanning tunneling microscopy study of the anatase (1 0 0) surface. *Surface Science* **2003**, 529, (1-2), L239-L244.
34. Baur, W., Atomabstände und Bindungswinkel im Brookit, TiO₂. *Acta Crystallographica* **1961**, 14, (3), 214-216.

35. Beltrán, A.; Gracia, L.; Andrés, J., Density Functional Theory Study of the Brookite Surfaces and Phase Transitions between Natural Titania Polymorphs. *The Journal of Physical Chemistry B* **2006**, 110, (46), 23417-23423.
36. Linsebigler, A. L.; Lu, G.; Yates, J. T., Photocatalysis on TiO₂ Surfaces: Principles, Mechanisms, and Selected Results. *Chemical Reviews* **1995**, 95, (3), 735-758.
37. Zhang, H.; F. Banfield, J., Thermodynamic analysis of phase stability of nanocrystalline titania. *Journal of Materials Chemistry* **1998**, 8, (9), 2073-2076.
38. Asahi, R.; Taga, Y.; Mannstadt, W.; Freeman, A. J., Electronic and optical properties of anatase TiO₂. *Journal Name: Physical Review. B, Condensed Matter and Materials Physics; Journal Volume: 61; Journal Issue: 11; Other Information: PBD: 15 Mar 2000* **2000**, Medium: X; Size: page(s) 7459-7465.
39. Sorantin, P. I.; Schwarz, K., Chemical bonding in rutile-type compounds. *Inorganic Chemistry* **1992**, 31, (4), 567-576.
40. Dette, C.; Pérez-Osorio, M. A.; Kley, C. S.; Punke, P.; Patrick, C. E.; Jacobson, P.; Giustino, F.; Jung, S. J.; Kern, K., TiO₂ Anatase with a Bandgap in the Visible Region. *Nano Letters* **2014**, 14, (11), 6533-6538.
41. Szczepankiewicz, S. H.; Colussi, A. J.; Hoffmann, M. R., Infrared Spectra of Photoinduced Species on Hydroxylated Titania Surfaces. *The Journal of Physical Chemistry B* **2000**, 104, (42), 9842-9850.
42. Ribeiro, C.; Vila, C.; Stroppa, D. B.; Mastelaro, V. R.; Bettini, J.; Longo, E.; Leite, E. R., Anisotropic Growth of Oxide Nanocrystals: Insights into the Rutile TiO₂ Phase. *The Journal of Physical Chemistry C* **2007**, 111, (16), 5871-5875.
43. Yang, S.; Gao, L., Fabrication and Characterization of Nanostructurally Flowerlike Aggregates of TiO₂ via a Surfactant-free Solution Route: Effect of Various Reaction Media. *Chemistry Letters* **2005**, 34, (7), 1044-1045.
44. Melghit, K.; Al-Rabaniah, S. S., Photodegradation of Congo red under sunlight catalysed by nanorod rutile TiO₂. *Journal of Photochemistry and Photobiology A: Chemistry* **2006**, 184, (3), 331-334.
45. Chemseddine, A.; Moritz, T., Nanostructuring Titania: Control over Nanocrystal Structure, Size, Shape, and Organization. *European Journal of Inorganic Chemistry* **1999**, 1999, (2), 235-245.

46. Cozzoli, P. D.; Kornowski, A.; Weller, H., Low-Temperature Synthesis of Soluble and Processable Organic-Capped Anatase TiO₂ Nanorods. *Journal of the American Chemical Society* **2003**, 125, (47), 14539-14548.
47. Cozzoli, P. D.; Fanizza, E.; Curri, M. L.; Laub, D.; Agostiano, A., Low-dimensional chainlike assemblies of TiO₂ nanorod-stabilized Au nanoparticles. *Chemical Communications* **2005**, (7), 942-944.
48. Casavola, M.; Grillo, V.; Carlino, E.; Giannini, C.; Gozzo, F.; Fernandez Pinel, E.; Garcia, M. A.; Manna, L.; Cingolani, R.; Cozzoli, P. D., Topologically Controlled Growth of Magnetic-Metal-Functionalized Semiconductor Oxide Nanorods. *Nano Letters* **2007**, 7, (5), 1386-1395.
49. Cozzoli, P. D.; Snoeck, E.; Garcia, M. A.; Giannini, C.; Guagliardi, A.; Cervellino, A.; Gozzo, F.; Hernando, A.; Achterhold, K.; Ciobanu, N.; Parak, F. G.; Cingolani, R.; Manna, L., Colloidal Synthesis and Characterization of Tetrapod-Shaped Magnetic Nanocrystals. *Nano Letters* **2006**, 6, (9), 1966-1972.
50. Taguchi, T.; Zhang, X.-t.; Sutanto, I.; Tokuhiko, K.-i.; Rao, T. N.; Watanabe, H.; Nakamori, T.; Uragami, M.; Fujishima, A., Improving the performance of solid-state dye-sensitized solar cell using MgO-coated TiO₂ nanoporous film. *Chemical Communications* **2003**, (19), 2480-2481.
51. Wu, J.-M.; Shih, H. C.; Wu, W.-T., Growth of TiO₂ nanorods by two-step thermal evaporation. *Journal of Vacuum Science & Technology B* **2005**, 23, (5), 2122-2126.
52. Wu, J.-M.; Shih, H. C.; Wu, W.-T.; Tseng, Y.-K.; Chen, I. C., Thermal evaporation growth and the luminescence property of TiO₂ nanowires. *Journal of Crystal Growth* **2005**, 281, (2-4), 384-390.
53. Chi, B.; Jin, T., Synthesis of Titania Nanostructure Films via TiCl₄ Evaporation-Deposition Route. *Crystal Growth & Design* **2007**, 7, (4), 815-819.
54. Wu, J.-J.; Yu, C.-C., Aligned TiO₂ Nanorods and Nanowalls. *The Journal of Physical Chemistry B* **2004**, 108, (11), 3377-3379.
55. Pradhan, S. K.; Reucroft, P. J.; Yang, F.; Dozier, A., Growth of TiO₂ nanorods by metalorganic chemical vapor deposition. *Journal of Crystal Growth* **2003**, 256, (1-2), 83-88.

56. Lakshmi, B. B.; Patrissi, C. J.; Martin, C. R., Sol–Gel Template Synthesis of Semiconductor Oxide Micro- and Nanostructures. *Chemistry of Materials* **1997**, *9*, (11), 2544-2550.
57. Takahashi, K.; Wang, Y.; Lee, K.; Cao, G., Fabrication and Li⁺-intercalation properties of V₂O₅-TiO₂ composite nanorod arrays. *Applied Physics A* **2006**, *82*, (1), 27-31.
58. Chu, S.-Z.; Wada, K.; Inoue, S.; Hishita, S.-i.; Kurashima, K., Fabrication and Structural Characteristics of Ordered TiO₂–Ru(–RuO₂) Nanorods in Porous Anodic Alumina Films on ITO/Glass Substrate. *The Journal of Physical Chemistry B* **2003**, *107*, (37), 10180-10184.
59. Kim, S.-S.; Chun, C.; Hong, J.-C.; Kim, D.-Y., Well-ordered TiO₂ nanostructures fabricated using surface relief gratings on polymer films. *Journal of Materials Chemistry* **2006**, *16*, (4), 370-375.
60. Matsui, I.; Fujimori, H., Morphology-controlled TiO₂ Nanoparticle Synthesis via Aerosol-assisted Vapor-phase Reactions. *Chemistry Letters* **2007**, *36*, (1), 80-81.
61. Mor, G. K.; Varghese, O. K.; Paulose, M.; Shankar, K.; Grimes, C. A., A review on highly ordered, vertically oriented TiO₂ nanotube arrays: Fabrication, material properties, and solar energy applications. *Solar Energy Materials and Solar Cells* **2006**, *90*, (14), 2011-2075.
62. Mor, G. K.; Varghese, O. K.; Paulose, M.; Grimes, C. A., Transparent Highly Ordered TiO₂ Nanotube Arrays via Anodization of Titanium Thin Films. *Advanced Functional Materials* **2005**, *15*, (8), 1291-1296.
63. Chu, S. Z.; Inoue, S.; Wada, K.; Hishita, S.; Kurashima, K., Self-Organized Nanoporous Anodic Titania Films and Ordered Titania Nanodots/Nanorods on Glass. *Advanced Functional Materials* **2005**, *15*, (8), 1343-1349.
64. Peng, X.; Chen, A., Aligned TiO₂ nanorod arrays synthesized by oxidizing titanium with acetone. *Journal of Materials Chemistry* **2004**, *14*, (16), 2542-2548.
65. Chen, A.; Peng, X.; Koczkur, K.; Miller, B., Super-hydrophobic tin oxide nanoflowers. *Chemical Communications* **2004**, (17), 1964-1965.

66. Peng, X.; Chen, A., Large-Scale Synthesis and Characterization of TiO₂-Based Nanostructures on Ti Substrates. *Advanced Functional Materials* **2006**, 16, (10), 1355-1362.
67. Peng, X.; Chen, A., Dense and high-hydrophobic rutile TiO₂ nanorod arrays. *Applied Physics A* **2005**, 80, (3), 473-476.
68. Bavykin, D. V.; Parmon, V. N.; Lapkin, A. A.; Walsh, F. C., The effect of hydrothermal conditions on the mesoporous structure of TiO₂ nanotubes. *Journal of Materials Chemistry* **2004**, 14, (22), 3370-3377.
69. Ding, X.; Xu, X. G.; Chen, Q.; Peng, L. M., Preparation and characterization of Fe-incorporated titanate nanotubes. *Nanotechnology* **2006**, 17, (21), 5423.
70. Xu, X. G.; Ding, X.; Chen, Q.; Peng, L. M., Electronic, optical, and magnetic properties of Fe-intercalated H₂Ti₃O₇ nanotubes: First-principles calculations and experiments. *Physical Review B* **2006**, 73, (16), 165403.
71. Wang, R. H.; Chen, Q.; Wang, B. L.; Zhang, S.; Peng, L.-M., Strain-induced formation of K₂Ti₆O₁₃ nanowires via ion exchange. *Applied Physics Letters* **2005**, 86, (13), 133101.
72. Yang, J.; Mei, S.; Ferreira, J. M. F.; Norby, P.; Quaresmâ, S., Fabrication of rutile rod-like particle by hydrothermal method: an insight into HNO₃ peptization. *Journal of Colloid and Interface Science* **2005**, 283, (1), 102-106.
73. Yang, S.; Gao, L., Fabrication and shape-evolution of nanostructured TiO₂ via a sol-solvothermal process based on benzene-water interfaces. *Materials Chemistry and Physics* **2006**, 99, (2-3), 437-440.
74. Wang, Y.; Zhang, L.; Deng, K.; Chen, X.; Zou, Z., Low Temperature Synthesis and Photocatalytic Activity of Rutile TiO₂ Nanorod Superstructures. *The Journal of Physical Chemistry C* **2007**, 111, (6), 2709-2714.
75. Sanjinés, R.; Tang, H.; Berger, H.; Gozzo, F.; Margaritondo, G.; Lévy, F., Electronic structure of anatase TiO₂ oxide. *Journal of Applied Physics* **1994**, 75, (6), 2945-2951.
76. Gratzel, M., Photoelectrochemical cells. *Nature* **2001**, 414, (6861), 338-344.
77. Hochbaum, A. I.; Yang, P., Semiconductor Nanowires for Energy Conversion. *Chemical Reviews* **2010**, 110, (1), 527-546.

78. Zhang, X.; Zhang, T.; Ng, J.; Sun, D. D., High-Performance Multifunctional TiO₂ Nanowire Ultrafiltration Membrane with a Hierarchical Layer Structure for Water Treatment. *Advanced Functional Materials* **2009**, 19, (23), 3731-3736.
79. Zhang, X.; Du, A. J.; Lee, P.; Sun, D. D.; Leckie, J. O., TiO₂ nanowire membrane for concurrent filtration and photocatalytic oxidation of humic acid in water. *Journal of Membrane Science* **2008**, 313, (1-2), 44-51.
80. Yun, H. J.; Lee, H.; Joo, J. B.; Kim, W.; Yi, J., Influence of Aspect Ratio of TiO₂ Nanorods on the Photocatalytic Decomposition of Formic Acid. *The Journal of Physical Chemistry C* **2009**, 113, (8), 3050-3055.
81. Fujishima, A.; Rao, T. N.; Tryk, D. A., Titanium dioxide photocatalysis. *Journal of Photochemistry and Photobiology C: Photochemistry Reviews* **2000**, 1, (1), 1-21.
82. Ni, M.; Leung, M. K. H.; Leung, D. Y. C.; Sumathy, K., A review and recent developments in photocatalytic water-splitting using for hydrogen production. *Renewable and Sustainable Energy Reviews* **2007**, 11, (3), 401-425.
83. Wang, X.; Li, Z.; Shi, J.; Yu, Y., One-Dimensional Titanium Dioxide Nanomaterials: Nanowires, Nanorods, and Nanobelts. *Chemical Reviews* **2014**, 114, (19), 9346-9384.
84. O'Regan, B.; Gratzel, M., A low-cost, high-efficiency solar cell based on dye-sensitized colloidal TiO₂ films. *Nature* **1991**, 353, (6346), 737-740.
85. Chen, H.-Y.; Hou, J.; Zhang, S.; Liang, Y.; Yang, G.; Yang, Y.; Yu, L.; Wu, Y.; Li, G., Polymer solar cells with enhanced open-circuit voltage and efficiency. *Nat Photon* **2009**, 3, (11), 649-653.
86. Nozik, A. J.; Beard, M. C.; Luther, J. M.; Law, M.; Ellingson, R. J.; Johnson, J. C., Semiconductor Quantum Dots and Quantum Dot Arrays and Applications of Multiple Exciton Generation to Third-Generation Photovoltaic Solar Cells. *Chemical Reviews* **2010**, 110, (11), 6873-6890.
87. Wang, Y.; Cao, G., Developments in Nanostructured Cathode Materials for High-Performance Lithium-Ion Batteries. *Advanced Materials* **2008**, 20, (12), 2251-2269.
88. Liu, R.; Duay, J.; Lee, S. B., Heterogeneous nanostructured electrode materials for electrochemical energy storage. *Chemical Communications* **2011**, 47, (5), 1384-1404.

89. Armstrong, G.; Armstrong, A. R.; Bruce, P. G.; Reale, P.; Scrosati, B., TiO₂(B) Nanowires as an Improved Anode Material for Lithium-Ion Batteries Containing LiFePO₄ or LiNi_{0.5}Mn_{1.5}O₄ Cathodes and a Polymer Electrolyte. *Advanced Materials* **2006**, 18, (19), 2597-2600.
90. Lu, X.; Yu, M.; Wang, G.; Zhai, T.; Xie, S.; Ling, Y.; Tong, Y.; Li, Y., H-TiO₂@MnO₂//H-TiO₂@C Core-Shell Nanowires for High Performance and Flexible Asymmetric Supercapacitors. *Advanced Materials* **2013**, 25, (2), 267-272.
91. Mortimer, R. J., Electrochromic Materials. *Annual Review of Materials Research* **2011**, 41, (1), 241-268.
92. Kolmakov, A.; Moskovits, M., CHEMICAL SENSING AND CATALYSIS BY ONE-DIMENSIONAL METAL-OXIDE NANOSTRUCTURES. *Annual Review of Materials Research* **2004**, 34, (1), 151-180.
93. Scanlon, D. O.; Dunnill, C. W.; Buckeridge, J.; Shevlin, S. A.; Logsdail, A. J.; Woodley, S. M.; Catlow, C. R. A.; Powell, M. J.; Palgrave, R. G.; Parkin, I. P.; Watson, G. W.; Keal, T. W.; Sherwood, P.; Walsh, A.; Sokol, A. A., Band alignment of rutile and anatase TiO₂. *Nat Mater* **2013**, 12, (9), 798-801.
94. Chen, X.; Lou, Y.; Dayal, S.; Qiu, X.; Krolicki, R.; Burda, C.; Zhao, C.; Becker, J., Doped Semiconductor Nanomaterials. *Journal of Nanoscience and Nanotechnology* **2005**, 5, (9), 1408-1420.
95. Burda, C.; Lou, Y.; Chen, X.; Samia, A. C. S.; Stout, J.; Gole, J. L., Enhanced Nitrogen Doping in TiO₂ Nanoparticles. *Nano Letters* **2003**, 3, (8), 1049-1051.
96. Chen, X.; Burda, C., Photoelectron Spectroscopic Investigation of Nitrogen-Doped Titania Nanoparticles. *The Journal of Physical Chemistry B* **2004**, 108, (40), 15446-15449.
97. Chen, X.; Lou, Y. B.; Samia, A. C. S.; Burda, C.; Gole, J. L., Formation of Oxynitride as the Photocatalytic Enhancing Site in Nitrogen-Doped Titania Nanocatalysts: Comparison to a Commercial Nanopowder. *Advanced Functional Materials* **2005**, 15, (1), 41-49.
98. Liu, J.; Zhao, X.; Duan, L.; Cao, M.; Sun, H.; Shao, J.; Chen, S.; Xie, H.; Chang, X.; Chen, C., Influence of annealing process on conductive properties of Nb-doped TiO₂

- polycrystalline films prepared by sol-gel method. *Applied Surface Science* **2011**, 257, (23), 10156-10160.
99. Furubayashi, Y.; Hitosugi, T.; Yamamoto, Y.; Inaba, K.; Kinoda, G.; Hirose, Y.; Shimada, T.; Hasegawa, T., A transparent metal: Nb-doped anatase TiO₂. *Applied Physics Letters* **2005**, 86, (25), 252101.
100. Taro, H.; Hideyuki, K.; Koichi, Y.; Hiroyuki, N.; Yutaka, F.; Shoichiro, N.; Naoomi, Y.; Akira, C.; Hiroshi, K.; Masaharu, O.; Yasushi, H.; Toshihiro, S.; Tetsuya, H., Electronic Band Structure of Transparent Conductor: Nb-Doped Anatase TiO₂. *Applied Physics Express* **2008**, 1, (11), 111203.
101. Liu, X. D.; Jiang, E. Y.; Li, Z. Q.; Song, Q. G., Electronic structure and optical properties of Nb-doped anatase TiO₂. *Applied Physics Letters* **2008**, 92, (25), 252104.
102. Singh, S.; Kaur, H.; Singh, V. N.; Jain, K.; Senguttuvan, T. D., Highly sensitive and pulse-like response toward ethanol of Nb doped TiO₂ nanorods based gas sensors. *Sensors and Actuators B: Chemical* **2012**, 171–172, 899-906.
103. Archana, P. S.; Jose, R.; Jin, T. M.; Vijila, C.; Yusoff, M. M.; Ramakrishna, S., Structural and Electrical Properties of Nb-Doped Anatase TiO₂ Nanowires by Electrospinning. *Journal of the American Ceramic Society* **2010**, 93, (12), 4096-4102.
104. Liu, Y.; Szeifert, J. M.; Feckl, J. M.; Mandlmeier, B.; Rathousky, J.; Hayden, O.; Fattakhova-Rohlfing, D.; Bein, T., Niobium-Doped Titania Nanoparticles: Synthesis and Assembly into Mesoporous Films and Electrical Conductivity. *ACS Nano* **2010**, 4, (9), 5373-5381.
105. Koninck, M. D.; Manseau, P.; Marsan, B., Preparation and characterization of Nb-doped TiO₂ nanoparticles used as a conductive support for bifunctional CuCo₂O₄ electrocatalyst. *Journal of Electroanalytical Chemistry* **2007**, 611, (1–2), 67-79.
106. Mei, B.; Sanchez, M. D.; Reinecke, T.; Kaluza, S.; Xia, W.; Muhler, M., The synthesis of Nb-doped TiO₂ nanoparticles by spray drying: an efficient and scalable method. *Journal of Materials Chemistry* **2011**, 21, (32), 11781-11790.
107. Su, H.; Huang, Y.-T.; Chang, Y.-H.; Zhai, P.; Hau, N. Y.; Cheung, P. C. H.; Yeh, W.-T.; Wei, T.-C.; Feng, S.-P., The Synthesis of Nb-doped TiO₂ Nanoparticles for Improved-Performance Dye Sensitized Solar Cells. *Electrochimica Acta* **2015**, 182, 230-237.

108. Hirano, M.; Matsushima, K., Photoactive and Adsorptive Niobium-Doped Anatase (TiO₂) Nanoparticles: Influence of Hydrothermal Conditions on their Morphology, Structure, and Properties. *Journal of the American Ceramic Society* **2006**, 89, (1), 110-117.
109. Jona, F.; Shirane, G., *Ferroelectric crystals*. Pergamon Press: 1962.
110. Popovici, D.; Akedo, J.; Okuyama, M., *Barium Titanate-Based Materials - a Window of Application Opportunities*. INTECH Open Access Publisher: 2011.
111. Vijatović, M. M.; Bobić, J. D.; Stojanović, B. D., History and Challenges of Barium Titanate: Part I. *Science of Sintering* **2008**, 40, 155-165.
112. Hench, L. L.; West, J. K., *Principles of electronic ceramics*. Wiley: 1990.
113. <http://www.azom.com/article.aspx?ArticleID=81>, (11/06/2013).
114. Urban, J. J.; Spanier, J. E.; Ouyang, L.; Yun, W. S.; Park, H., Single-Crystalline Barium Titanate Nanowires. *Advanced Materials* **2003**, 15, (5), 423-426.
115. Yun, W. S.; Urban, J. J.; Gu, Q.; Park, H., Ferroelectric Properties of Individual Barium Titanate Nanowires Investigated by Scanned Probe Microscopy. *Nano Letters* **2002**, 2, (5), 447-450.
116. Zhang, S.; Jiang, F.; Qu, G.; Lin, C., Synthesis of single-crystalline perovskite barium titanate nanorods by a combined route based on sol-gel and surfactant-templated methods. *Materials Letters* **2008**, 62, (15), 2225-2228.
117. Urban, J. J.; Yun, W. S.; Gu, Q.; Park, H., Synthesis of Single-Crystalline Perovskite Nanorods Composed of Barium Titanate and Strontium Titanate. *Journal of the American Chemical Society* **2002**, 124, (7), 1186-1187.
118. Kang, S.-O.; Jang, H.-S.; Kim, K.-B.; Park, B. H.; Jung, M.-J.; Kim, Y.-I., Synthesis of single-crystal barium titanate nanorods transformed from potassium titanate nanostructures. *Materials Research Bulletin* **2008**, 43, (4), 996-1003.
119. Limmer, S. J.; Cao, G., Sol-Gel Electrophoretic Deposition for the Growth of Oxide Nanorods. *Advanced Materials* **2003**, 15, (5), 427-431.
120. Kristina, Ž.; Francisco, H.-R.; Joan Daniel, P.; Joan Ramon, M.; Aleksander, R.; Miran, Č., Characterization of individual barium titanate nanorods and their

- assessment as building blocks of new circuit architectures. *Nanotechnology* **2011**, *22*, (38), 385501.
121. Aneesh, K.; Zhi, Z.; Haixiong, T.; Henry, A. S., Controlled synthesis of ultra-long vertically aligned BaTiO₃ nanowire arrays for sensing and energy harvesting applications. *Nanotechnology* **2014**, *25*, (37), 375603.
 122. Maxim, F.; Berger, D.; Teodorescu, F.; Hornoiu, C.; Lete, C.; Tanasescu, S., Low-Temperature Synthesis and Thermodynamic and Electrical Properties of Barium Titanate Nanorods. *Journal of Nanomaterials* **2015**, 2015, 10.
 123. Žagar, K.; Rečnik, A.; Šturm, S.; Gajović, A.; Čeh, M., Structural and chemical characterization of BaTiO₃ nanorods. *Materials Research Bulletin* **2011**, *46*, (3), 366-371.
 124. Jiang, C.; Kiyofumi, K.; Wang, Y.; Koumoto, K., Synthesis of BaTiO₃ Nanowires at Low Temperature. *Crystal Growth & Design* **2007**, *7*, (12), 2713-2715.
 125. Reese, C.; Roberts, M.; Ling, M.-m.; Bao, Z., Organic thin film transistors. *Materials Today* **2004**, *7*, (9), 20-27.
 126. Sarma, R.; Saikia, D.; Konwar, K.; Baishya, B., Pentacene thin film transistors using La₂O₃ as gate insulator. *Indian J Phys* **2010**, *84*, (5), 547-552.
 127. Lee, J.; Kim, K.; Kim, J. H.; Im, S.; Jung, D.-Y., Optimum channel thickness in pentacene-based thin-film transistors. *Applied Physics Letters* **2003**, *82*, (23), 4169-4171.
 128. Puigdollers, J.; Voz, C.; Orpella, A.; Quidant, R.; Martín, I.; Vetter, M.; Alcubilla, R., Pentacene thin-film transistors with polymeric gate dielectric. *Organic Electronics* **2004**, *5*, (1–3), 67-71.
 129. McDowell, M.; Hill, I. G.; McDermott, J. E.; Bernasek, S. L.; Schwartz, J., Improved organic thin-film transistor performance using novel self-assembled monolayers. *Applied Physics Letters* **2006**, *88*, (7), 073505-3.
 130. Sarma, R.; Saikia, D., Study of tetracene thin film transistors using La₂O₃ as gate insulator. *Indian Journal of pure and Applied Physics* **2009**, *47*, 876-879.

131. Chang, M.-F.; Lee, P.-T.; McAlister, S. P.; Chin, A., A flexible organic pentacene nonvolatile memory based on high-kappa dielectric layers. *Applied Physics Letters* **2008**, 93, (23), 233302-3.
132. Tsumura, A.; Koezuka, H.; Ando, T., Macromolecular electronic device: Field-effect transistor with a polythiophene thin film. *Applied Physics Letters* **1986**, 49, (18), 1210-1212.
133. Chua, L.-L.; Zaumseil, J.; Chang, J.-F.; Ou, E. C. W.; Ho, P. K. H.; Sirringhaus, H.; Friend, R. H., General observation of n-type field-effect behaviour in organic semiconductors. *Nature* **2005**, 434, (7030), 194-199.
134. Sirringhaus, H.; Tessler, N.; Friend, R. H., Integrated Optoelectronic Devices Based on Conjugated Polymers. *Science* **1998**, 280, (5370), 1741-1744.
135. Lin, Y. Y.; Gundlach, D. J.; Nelson, S. F.; Jackson, T. N., Stacked pentacene layer organic thin-film transistors with improved characteristics. *Electron Device Letters, IEEE* **1997**, 18, (12), 606-608.
136. Halik, M.; Klauk, H.; Zschieschang, U.; Schmid, G.; Dehm, C.; Schutz, M.; Maisch, S.; Effenberger, F.; Brunnbauer, M.; Stellacci, F., Low-voltage organic transistors with an amorphous molecular gate dielectric. *Nature* **2004**, 431, (7011), 963-966.
137. Kelley, T. W.; Boardman, L. D.; Dunbar, T. D.; Muyres, D. V.; Pellerite, M. J.; Smith, T. P., High-Performance OTFTs Using Surface-Modified Alumina Dielectrics. *The Journal of Physical Chemistry B* **2003**, 107, (24), 5877-5881.
138. Tseng, G. Y.; Ellenbogen, J. C., Toward Nanocomputers. *Science* **2001**, 294, (5545), 1293-1294.

Chapter 2

Measurement and Instruments

2.1 Measurement and Instruments

2.1.1 X-Ray Diffraction (XRD)

X-Ray diffraction (XRD) is an analytical technique for studying the structure of crystalline materials, usually at a wavelength of about 0.5 to 2.5 Å. This method is based on the diffraction of X-rays by crystal lattices. It can monitor the distance between crystal plates as well as the size and type of the unit cell ¹. In simple terms, each XRD machine has a detector, an X-ray tube and a monochromatic shutter. When an X-ray beam is incident upon the sample, the X-rays are reflected according to the Bragg condition

$$n\lambda = 2d\sin\theta \quad (2-1)$$

Where n is an integer, λ is the wavelength of the X-rays, d is the layer spacing, i.e., separation of the reflecting planes, and θ is the angle of incidence of the X-ray beam.

X-ray diffraction (XRD) is important in the estimate of the size of sub-micrometre particles or crystallites according to the Scherrer equation (2-2):

$$D = \frac{K\lambda}{\beta \cos\theta} \quad (2-2)$$

where K is a dimensional constant, 2θ is the diffraction angle, λ is the X-ray radiation wavelength, and β is the full width at half-maximum (FWHM) of the diffraction peak ².

The crystallite size can be determined by calculating the peak width in a diffraction spectrum related to a particular planar image from within the crystal unit cell. It is linked to the FWHM of a single peak in the sense that the narrower the peak, the larger the crystallite size. The periodicity of the single crystallite areas results in a large narrow peak. A broader peak is observed if the crystals are randomly organised or exhibit a low degree of periodicity, which is often the case for nanomaterials. Consequently, it is self-evident that the FWHM of the diffraction peak is directly related to the dimensions of any nanoparticles giving rise to the peak ². The X-ray powder diffraction (XRD) analysis was carried out in this thesis using a PANalytical EMPYREAN instrument.

2.1.2 Transmission Electron Microscopy (TEM)

Transmission electron microscopy (TEM) is an imaging technique with much higher resolution than optical microscopy using visible light. It is able to examine, in detail, a single column of atoms, which is 10000 times smaller than the smallest resolvable object in optical microscopy

using visible light to produce an image of the object. TEM provides important information on the size of nanoparticles and has already been widely used to determine the shape of titanium dioxide nanoparticles³. Each basic TEM instrument has five main parts: a vacuum system, a specimen stage, an electron gun, an electron lens and apertures. Transmission electron microscopy (TEM) spectra were obtained using a Jeol 2010 TEM running at 200kV. Images were obtained with a Gatan Ultrascan 4000 digital camera. Solid samples were prepared by suspension in distilled water and 5 μl aliquots of a suitable dilution dropped onto carbon coated copper grids. EDX data were obtained using an Oxford Instruments 'INCA' Energy Dispersive X-ray Spectrometer.

2.1.3 Fourier Transform Infrared Spectroscopy (FT-IR)

Infra-red (IR) spectroscopy is used to analyse the chemical composition of organic matter by absorption of infra-red radiation. In the electromagnetic spectrum, infrared radiation is divided into three parts: the far-infrared, $400\text{--}10\text{ cm}^{-1}$ ($25\text{--}1000\ \mu\text{m}$), which has low energy and is used for rotational spectroscopy; the mid-infrared, $4000\text{--}400\text{ cm}^{-1}$ ($2.5\text{--}25\ \mu\text{m}$), which is used to study associated rotational-vibrational structure and fundamental molecular vibrations and the higher-energy near-IR, $14000\text{--}4000\text{ cm}^{-1}$ ($0.8\text{--}2.5\ \mu\text{m}$ wavelength), which can excite overtone or harmonic vibrations. Each commercial IR spectrometer has a splitter, a detector, a sample tube and a reference tube. Fourier transform infrared (FT-IR) spectra were recorded on a Nicolet Magna-500 FTIR spectrometer in the work for this thesis.

2.1.4 X-ray Photoelectron Spectroscopy (XPS)

X-ray photoelectron spectroscopy is a surface-sensitive quantitative spectroscopic analytical technique for measuring the elemental composition in the parts-per-thousand range, chemical and electronic state of the elements present on the surface of a material and their empirical formula. An X-ray beam is focussed at an incidental angle on the surface of the test material and the number of electrons and their kinetic energy is measured at the time for electron escape from the first 10 nm of the material surface. Either a high vacuum, e.g., $P \sim 10\text{-}8$ millibar, or an ultra-high vacuum, e.g., UHV; $P < 10\text{-}9$ millibar, are required for this analytical technique.

2.1.5 Thermal Gravimetric Analysis (TGA)

In this analytical technique the change in sample weight is measured while the sample is heated at a constant rate, or at constant temperature, under air, *i.e.*, oxidative, or nitrogen, *i.e.*, inert, atmosphere. This analytical technique is effective for quantitative analysis of thermal reactions that are accompanied by mass changes, such as evaporation, decomposition, gas absorption, desorption and dehydration. A micro-balance used in this technique plays a significant role by measuring the change in mass of the sample, creating an imbalance, which is fed back to a force coil, which generates an additional electromagnetic force to re-establish equilibrium. The amount of additional electromagnetic force is proportional to the mass change. Thermogravimetric analyses (TGA) were performed on a Netzsch TGA TG209 thermal balance in the work for this thesis.

2.1.6 Inductively Coupled Plasma (ICP)

Inductively coupled plasma (ICP) is designed to generate plasma, which is a gas of atoms present in an ionized state, which then provide information on the chemical composition of the plasma sample. The basic set up of an ICP consists of three concentric tubes, usually made of silica, an ICP torch, a nebulizer, *i.e.*, a sample introduction system a computer interface, transfer optics, a spectrometer and a high-frequency generator. The amount of metal in the nanocomposites is determined by an inductively coupled plasma Perkin Elmer 40 emission ICP instrument in the work for this thesis.

2.1.7 Elemental Analyser (CHN Analyser)

The amount of carbon (C), hydrogen (H) and nitrogen (N) in an organic compound can be measured with this analytical technique. The analyser uses a combustion process to oxidise organic substances into simple decomposition products, which are then detected, identified and their concentration measured. The CHN analysers components are an ignition chamber, a pre-packed column, a TCD detector and spectrum analysers. A Fisons EA 1108 CHN analyser was used to provide the CHN data in the work for this thesis.

2.1.8 Nuclear Magnetic Resonance Spectroscopy (NMR)

Nuclear magnetic resonance spectroscopy is a useful, versatile technique for the determination of the molecular structure and composition that relies on measuring the interactions of nuclear magnetic fields with an applied magnetic field. NMR uses a large magnet to probe the intrinsic spin properties of atomic nuclei. Like all spectroscopic techniques, NMR uses a component of electromagnetic radiation, *i.e.*, radio frequency waves in this case, to promote and measure transitions between quantised nuclear energy levels. It can be used with samples of liquids, solids or gases, with compounds of various masses and compositions, and can be used to detect a wide range of nuclides depending on the instrumentation available. It is used in a diverse range of research areas, including organic, inorganic, and physical chemistry, medicine, biochemistry, protein science, and the food industry. Solid-state NMR (SSNMR) spectroscopy is a kind of NMR spectroscopy, characterised by the presence of anisotropic interactions. Solid-state NMR can offer information of dynamics and structure in solid materials and also for the characterisation of crystalline solids, it is often an invaluable complement to diffraction-based methods. In pharmaceutical systems, it is important to understand transformations between the different forms of a solid (polymorphs). The NMR spectroscopy in the work for this thesis was carried out using a JEOL, JNM-ECP FT NMR spectrometer (400 MHz).

2.1.9 Centrifugation

A centrifuge rotates samples at high speed driven by an electric motor. Objects are rotated very quickly about a fixed axis, thereby applying a force perpendicular to the axis. A sedimentation principle is the basis of each the many types of centrifuge. This causes more dense substances to separate out in the bottom of the tube of a liquid sample. The centrifuge in the work for this thesis was carried out using Heraeus Megafuge 8 centrifuge from Thermo Science.

2.1.10 Ultrapure Water

The ultrapure water in the work for this thesis was obtained with a specific resistivity of 18.2 M Ω .cm by using a reversed osmosis purification process followed by ion-exchange and filtration. Ultrapure water in the work for this thesis was carried out using Purelab Option and Purelab flex from Elga.

2.2 References

1. Balestrino, G.; Lagomarsino, S.; Mastrogiacomo, L.; Scarinci, F.; Tucciarone, A., Application of asymmetric reflections to the X-ray study of structural deformation of surfaces. *Thin Solid Films* **1981**, 78, (4), 327-334.
2. Lindgren, T.; Mwabora, J. M.; Avendaño, E.; Jonsson, J.; Hoel, A.; Granqvist, C.-G.; Lindquist, S.-E., Photoelectrochemical and Optical Properties of Nitrogen Doped Titanium Dioxide Films Prepared by Reactive DC Magnetron Sputtering. *The Journal of Physical Chemistry B* **2003**, 107, (24), 5709-5716.
3. Williams, D. B.; Carter, C. B., The Transmission Electron Microscope. In *Transmission Electron Microscopy*, Springer US: 2009; pp 3-22.

Chapter 3
Preparation and
Characterisation of Solution
Processable Anatase TiO₂
Nanorods

3.1 Introduction

One of the primary aims of this thesis is the synthesis of solution-processable anatase titanium dioxide nanorods (TiO_2) with a stable aliphatic surface coating, *i.e.*, TiO_2 /ligand nanocomposites, to be used as dielectric layers for low-voltage OFET applications. It was intended to deposit a thin uniform layer of the desired thickness of these TiO_2 /ligand nanocomposites on the OFET substrate surface by deposition from solution, *e.g.*, by spin coating, drop casting, *etc.* Evaporation of the solvent should produce the desired dielectric layer as a stable monodomain with a homogeneous alignment of the titanium dioxide nanorods in the plane of the substrate surface with a uniform uniaxial orientation in the azimuthal plane.

The synthesis of oleic acid-stabilised anatase titanium dioxide nanorods (TiO_2 /OA) was carried out according to modified literature methods.^{1, 2} The surface coating of the TiO_2 /OA nanocomposites was modified by replacing some of the oleic acid monolayer coating on the TiO_2 nanorods with different phosphorus ligands, such as diethyl 2-phenylethyl phosphonate (DEPPNA), octadecylphosphonic acid (ODPA) and octylphosphonic acid (OPA). It was hoped that this ligand exchange process would result in the formation of novel titanium dioxide nanorods, *i.e.*, TiO_2 /OA/DEPPNA, TiO_2 /OA/ODPA and TiO_2 /OA/OPA nanocomposites, with enhanced solubility in organic solvents. These titanium dioxide nanorods capped with different ligands, *e.g.*, DEPPNA, ODPA and OPA, may well exhibit different values of the dielectric constant. The concentration of these four ligands as a monolayer on the surface of the TiO_2 /OA, TiO_2 /OA/DEPPNA, TiO_2 /OA/ODPA and TiO_2 /OA/OPA nanocomposites was varied in order to study the correlations between the nature of the monolayer coatings and their concentration on the solubility of the nanocomposites in common organic solvents used to deposit an uniform thin layer of nanorods on a substrate surface.

3.2 Experimental

3.2.1 Materials

Titanium (IV) tetraisopropoxide (TTIP, $\geq 97.0\%$), oleic acid (OA, 90%), trimethylamine *N*-oxide (TMAO, 98%), diethyl 2-phenylethyl phosphonate (DEPPNA, 98.0%), octylphosphonic acid (OPA, 97.0%) and octadecylphosphonic acid (ODPA, 97.0%) were sourced from Sigma-Aldrich as used without further purification. Ultrapure water with a specific resistivity of 18.2

MΩ·cm was obtained by reversed osmosis followed by ion-exchange and filtration (UPQ PS system, ELGA, USA).

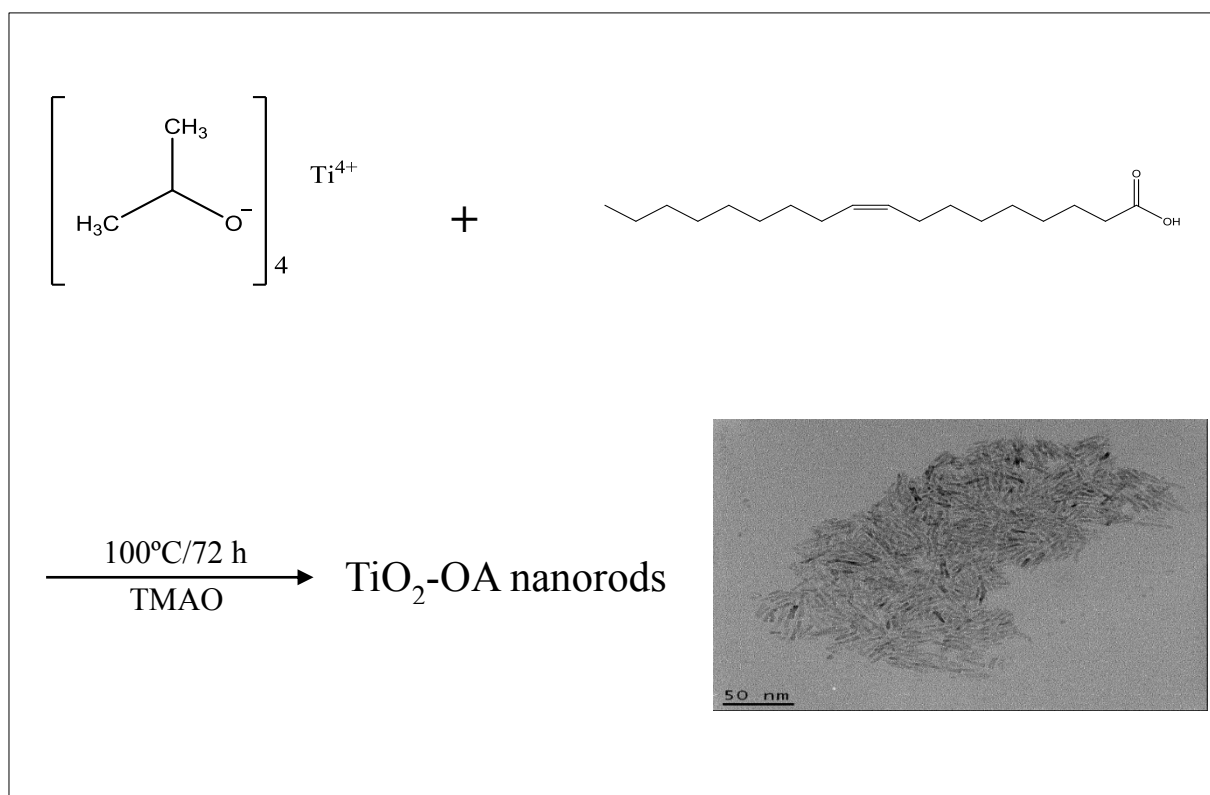
3.2.2 Synthesis of TiO₂/OA Nanocomposites Consisting of Anatase Titanium Dioxide Nanorods Coated with a Monolayer of Oleic Acid

The synthesis of oleic acid-stabilised anatase titanium dioxide nanorods (TiO₂/OA) was carried out according to modified literature methods.^{1, 2} Commercially available titanium (IV) tetraisopropoxide (TTIP) was hydrolysed in the presence of oleic acid (OA), acting as a surfactant, in presence of trimethylamine *N*-oxide (TMAO). The chemical composition, size and shape and the crystalline form of the TiO₂/OA/DEPPNA, TiO₂/OA/ODPA and TiO₂/OA/OPA nanocomposites produced by ligand exchange reactions were also determined using the combination of a range of analytical techniques, such as FT-IR, TEM, XRD, and elemental analysis, such as CHN, ICP and TGA.

Preparation of Anatase Titanium Dioxide Nanorods Capped with Oleic Acid, i.e., FA3-1 TiO₂/OA nanocomposites

Oleic acid (OA) (420 g) was dried under stirring for 1 h at 120 °C and then allowed to cool to 85 °C. Titanium (IV) isopropoxide (TTIP) (17.7 mL, 60 mmol) was added under stirring. After 5 minutes, whereby the colour of solution had changed from colourless to yellow, a solution of trimethylamine *N*-oxide (TMAO) (2 M, 60 mL) was injected quickly by syringe into the reaction mixture. After completion of this addition the temperature of the reaction mixture was increased to 100 °C. After a few minutes the solution became slightly turbid and after an hour the viscosity of the solution had increased significantly. The reaction mixture was stirred at 100 °C for a total of 72 h. Isopropanol (1.2 L) was added to the cooled reaction mixture at room temperature. The resultant precipitate was separated off by centrifugation, washed twice with isopropanol and then dried overnight in a vacuum oven overnight at 30 °C. The TiO₂/OA nanocomposite product was dissolved in toluene and then precipitated by the addition of acetone, which was separated off by centrifugation. This step was repeated twice to produce the desired FA3-1 TiO₂/OA nanocomposite, consisting of anatase titanium dioxide nanorods coated with a monolayer of oleic acid, which was dried overnight in a vacuum oven at 30 °C.

A schematic diagram of synthesis of the oleic acid-capped anatase titanium dioxide nanorods FA3-1 TiO₂/OA is shown in scheme 3-1.



Scheme 3-1: Schematic diagram of synthesis of the oleic acid-capped anatase titanium dioxide nanorods FA3-1 TiO₂/OA.

Ligand Exchange of Oleic Acid Capped Anatase Titanium Dioxide Nanorods TiO₂-OA with Phosphonate/Phosphonic Acid

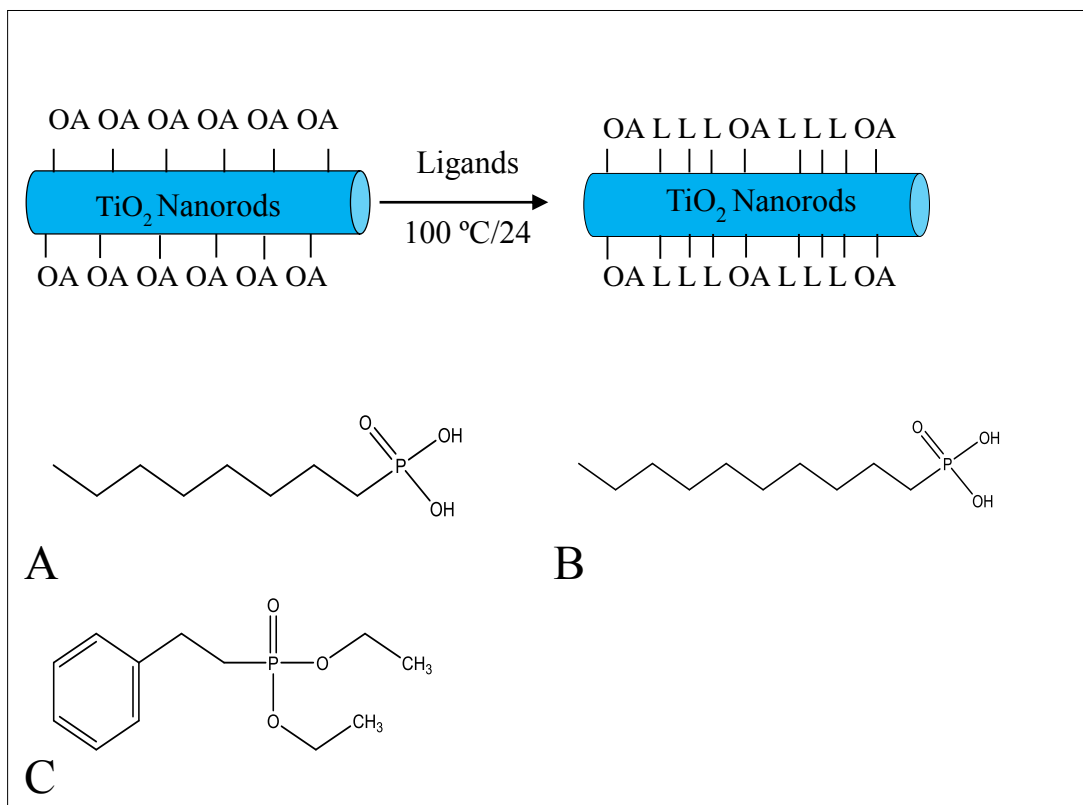
A fixed amount of ligand, *i.e.*, 25 mg of octylphosphonic acid (OPA), 25 mg of diethyl 2-phenylethyl phosphonate (DEPPNA) and 25 mg, 33 mg or 50 mg of octadecylphosphonic acid, (ODPA), was added to a solution of the FA3-1 TiO₂/OA nanocomposites (100 mg) prepared as described above in chlorobenzene (20 mL), see table 3-1 for details of these reactions. The resultant reaction mixtures were then heated at 100 °C for 24 h. The cooled reaction mixtures were evaporated down under reduced pressure to yield a solid, which was then dissolved in toluene (5 mL) and then precipitated with acetone (45 mL). The desired TiO₂/OA/DEPPNA, TiO₂/OA/ODPA and TiO₂/OA/OPA nanocomposites were washed with acetone and then dried

in a vacuum oven overnight. Scheme 3-2 shows a schematic of the reaction and the chemical structure of the phosphonate and phosphonic ligand used to create the new nanocomposites.

Table 3-1: Ligand exchange conditions of the reactions of the oleic acid-capped anatase titanium dioxide nanorods FA3-1 TiO₂/OA with the OPA, DEPPNA and ODPA ligands to produce the FA3-2 TiO₂/OA/OPA, FA3-3 TiO₂/OA/DEPPNA and FA3-4, FA3-5 and FA3-6 TiO₂/OA/ODPA nanocomposites, respectively.

Sample	Ligand	Ratio of TiO ₂ /OA:ligand
FA3-2	Octylphosphonic acid (OPA)	4:1
FA3-3	Diethyl 2-phenylethyl phosphonate (DEPPNA)	4:1
FA3-4	Octadecylphosphonic acid (ODPA)	4:1
FA3-5	Octadecylphosphonic acid (ODPA)	3:1
FA3-6	Octadecylphosphonic acid (ODPA)	2:1

A schematic diagram of the ligand exchange reactions involving the oleic acid capped anatase titanium dioxide nanorods FA3-1 TiO₂-OA with (A) octylphosphonic acid (OPA), (B) decylphosphonic acid (ODPA) and (C) 2-phenylethyl phosphonate (DEPPNA) ligands to produce the FA3-2 TiO₂/OA/OPA, FA3-3 TiO₂/OA/DEPPNA and FA3-4, FA3-5 and FA3-6 TiO₂/OA/ODPA nanocomposites, respectively., is shown in scheme 3-2.



Scheme 3-2: Diagram shows ligands exchange of oleic acid capped anatase titanium dioxide nanorods FA3-1 TiO_2 -OA with (A) octylphosphonic acid (OPA), (B) decylphosphonic acid (ODPA) and (C) 2-phenylethyl phosphonate (DEPPNA) ligands to produce the FA3-2 TiO_2 /OA/OPA, FA3-3 TiO_2 /OA/DEPPNA and FA3-4, FA3-5 and FA3-6 TiO_2 /OA/ODPA nanocomposites, respectively.

3.3 Results and Discussion

3.3.1 Characterisation of Anatase Titanium Dioxide Nanorods Capped with Oleic Acid TiO_2 /OA FA3-1

The XRD pattern of the FA3-1 titanium dioxide nanorods capped with oleic acid in the FA3-1 TiO_2 /OA nanocomposites is shown in figure 3-1. It is clear from this figure that the titanium dioxide nanorods have been produced in the anatase phase.³

The FT-IR spectrum of the FA3-1 TiO_2 /OA nanocomposites is shown in figure 3-2. The peaks at 2850, 2920 and 2955 cm^{-1} are related to the stretch absorptions of the C-H₃, C-H₂ and C-H

moieties present in the oleic acid molecules attached to the surface of the anatase titanium dioxide nanorods. The broad stretching band centred at 3465 cm^{-1} is indicative of the presence of OH^- groups attached to the surface of the anatase titanium dioxide nanorods. There are also two strong absorption peaks at 1525 and 1430 cm^{-1} , which are related to the presence of COO^- anti-symmetric as well as symmetric stretching vibrations, respectively.^{4,5}

The TEM images of the FA3-1 TiO_2/OA nanocomposites shown in figure 3-3 reveal that the TiO_2 nanorods are ca 20 in length and 3-4 nm in diameter with an aspect ratio between 5-8, with a maximum aspect ratio of 6:1. The oleic acid is not visible, as an organic coating, are not visible in the TEM images shown in figure 3-3.

Elemental analysis of the FA3-1 TiO_2/OA nanocomposites was carried out using CHN and ICP, see table 3-2. The carbon and hydrogen content of the FA3-1 TiO_2/OA nanocomposites was determined as 18.59% and 3.12%, respectively. These high values for carbon and hydrogen further provides further evidence of the presence of a significant coating of oleic acid (OA) over most of the surface of the TiO_2 nanorods. The presence of a small concentration of nitrogen (0.36%) is attributable to the presence of small residual amounts of the starting material TMAO, which could not be completely removed by the purification process, and suggests that some TMAO may have bonded to the surface of the TiO_2 nanorods. Almost exactly three quarters (74.11%) of the FA3-1 TiO_2/OA nanocomposites is made up of titanium dioxide.

The results of the TGA analyses are shown in figure 3-5. There are two observable weight losses at below $120\text{ }^\circ\text{C}$ and around $320\text{-}490\text{ }^\circ\text{C}$, which are related to the adsorption of water and decomposition of oleic acid, respectively. The results at $900\text{ }^\circ\text{C}$ is 71.57 %, close to the CHN and ICP result.

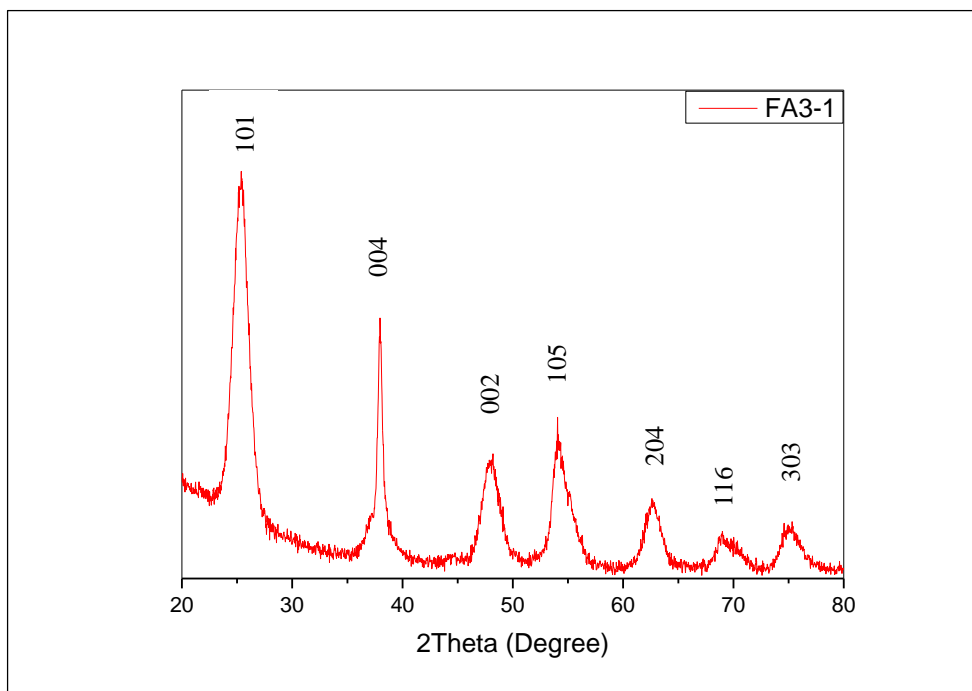


Figure 3-1: XRD pattern of FA3-1 TiO₂/OA nanocomposites consisting of anatase titanium dioxide nanorods capped with oleic acid.

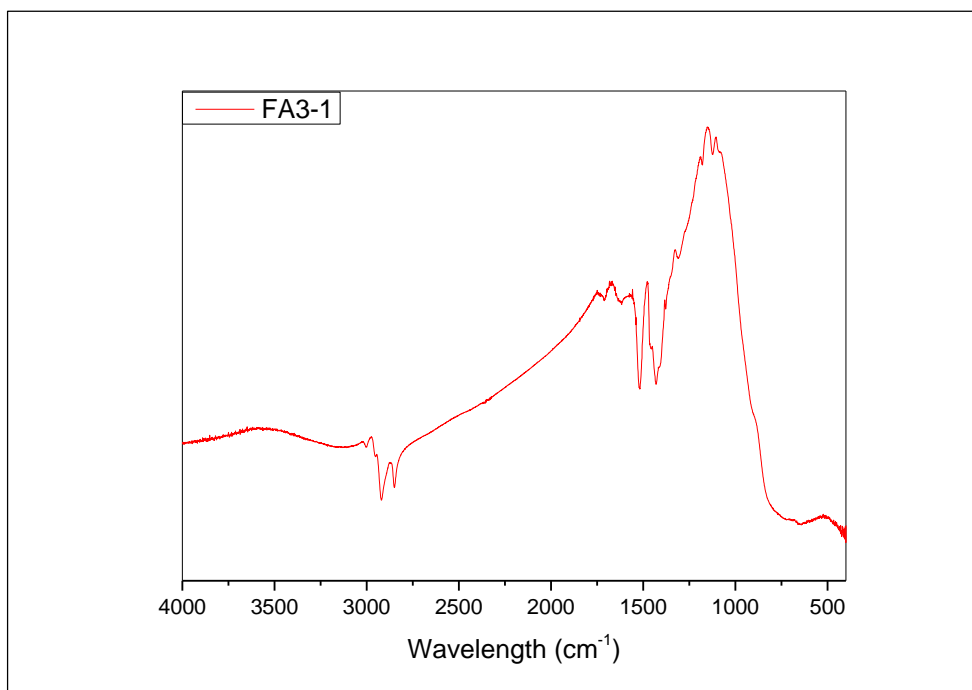


Figure 3-2: FT-IR pattern of FA3-1 TiO₂/OA nanocomposites consisting of anatase titanium dioxide nanorods capped with oleic acid.

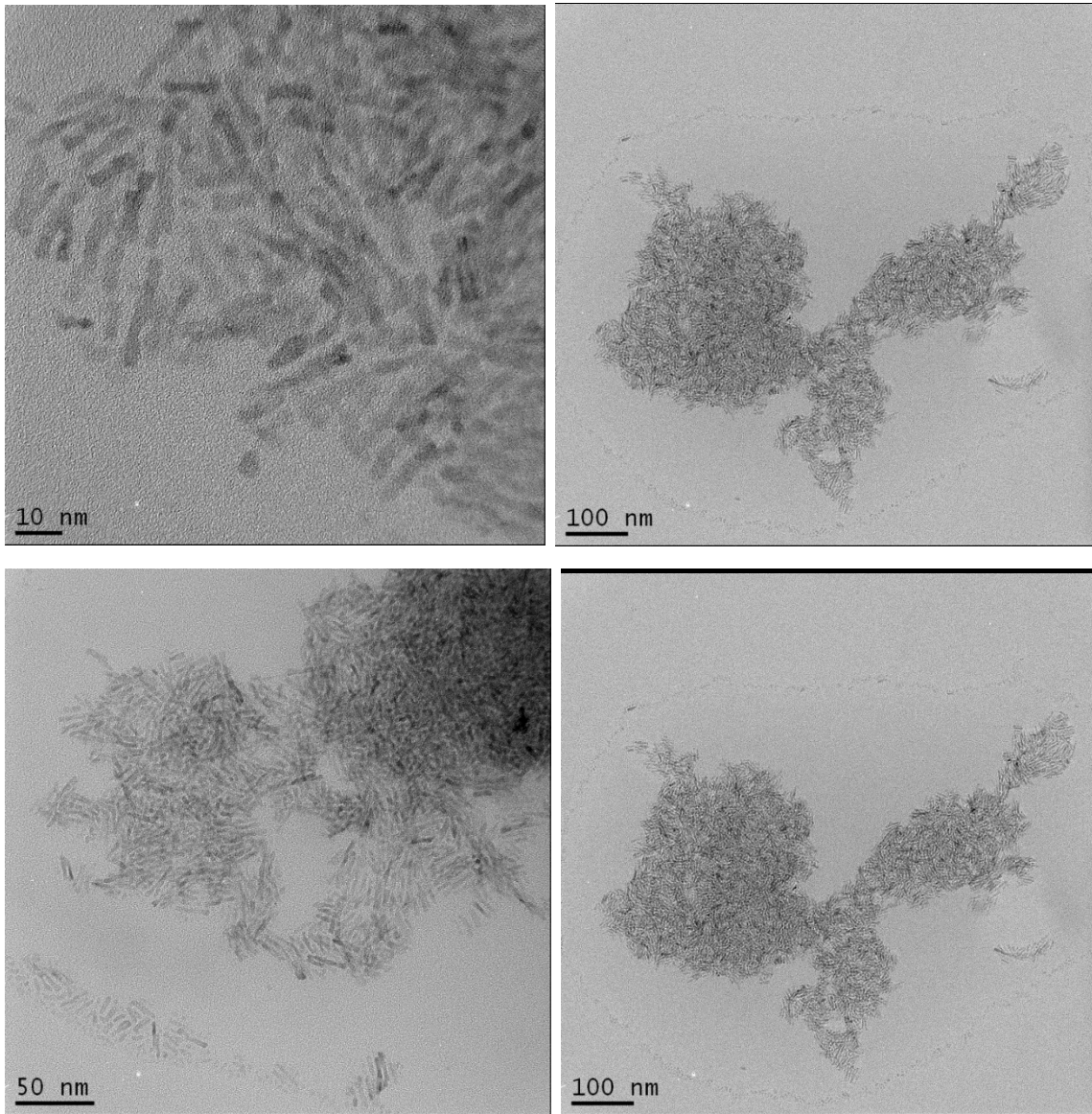


Figure 3-3: TEM images of FA3-1 TiO₂/OA nanocomposites consisting of anatase titanium dioxide nanorods capped with oleic acid.

Table 3-2: Chemical analysis of FA3-1 TiO₂/OA nanocomposites consisting of anatase titanium dioxide nanorods capped with oleic acid.

Sample	C %	H %	N %	O %	Ti %
FA3-1	18.59	3.12	0.36	31.30	42.83

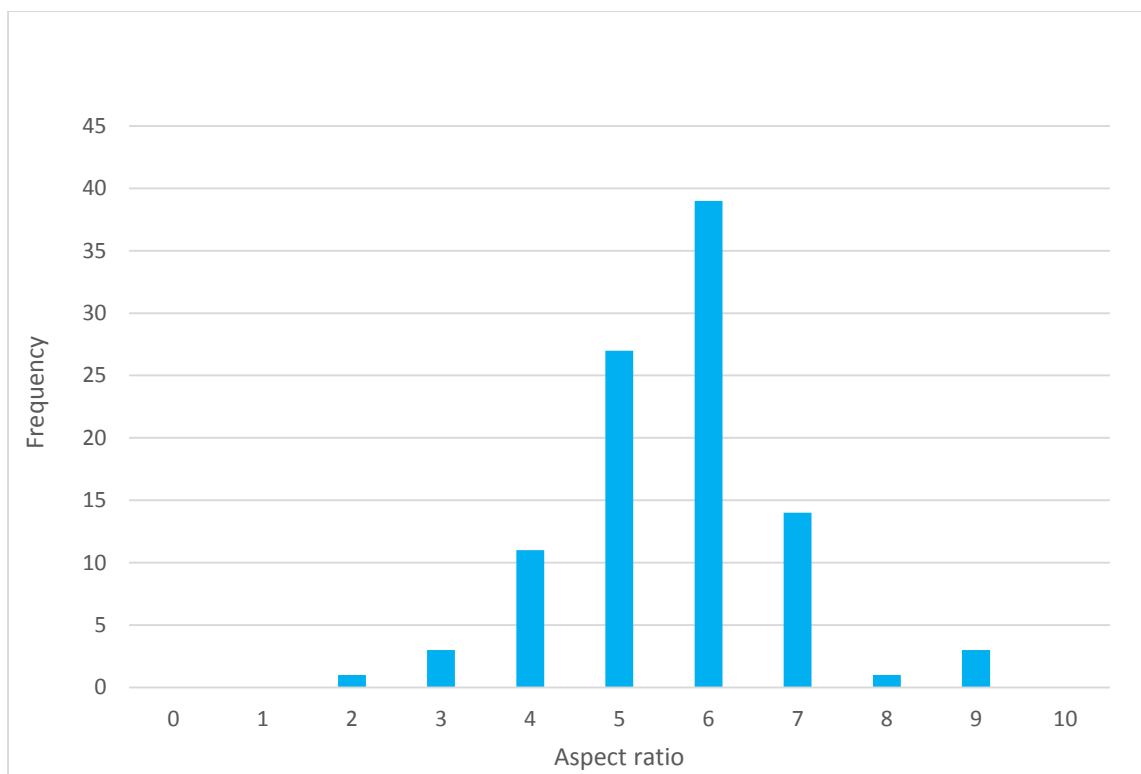


Figure 3-4: The aspect ratio distribution of FA3-1 TiO₂/OA nanocomposites consisting of anatase titanium dioxide nanorods capped with oleic acid.

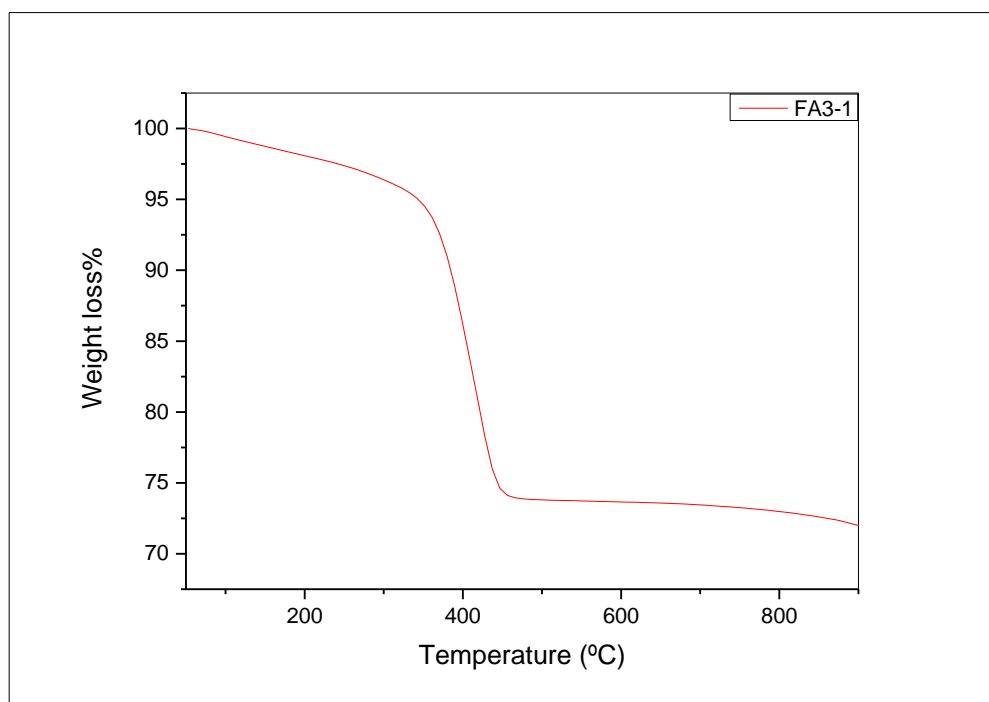


Figure 3-5: TGA analysis of FA3-1 TiO₂/OA nanocomposites consisting of anatase titanium dioxide nanorods capped with oleic acid.

Electrical Characterisation of the Oleic Acid-Stabilised Titanium Dioxide Nanorods TiO₂-OA

The hybrid insulator of the oleic acid-stabilised titanium dioxide nanorods TiO₂-OA, FA3-1 was spin coated from a 10% wt solution in chlorobenzene on prepatterned metallic electrodes. The samples were cured in a vacuum oven and finally the top metallic electrodes were evaporated to form crossbar MIM structures. The electrical characterization of these capacitors was carried out with a SII260 impedance analyser and an Agilent B2912A in air and at room temperature. The final thickness of the hybrid insulating films was ~200 nm with a RMS roughness of 2.0 nm. The estimated dielectric constant is 9-10 at 1MHz and it rapidly increases as the frequency decreases reaching the value of 30 at 1Hz, see figure 3-6. The loss tangent data show that the hybrid insulator at high frequencies behaves as an ideal capacitor (loss of the order of 10⁻²) while at low frequencies a remarkable increase in the loss tangent of our insulator is recorded.

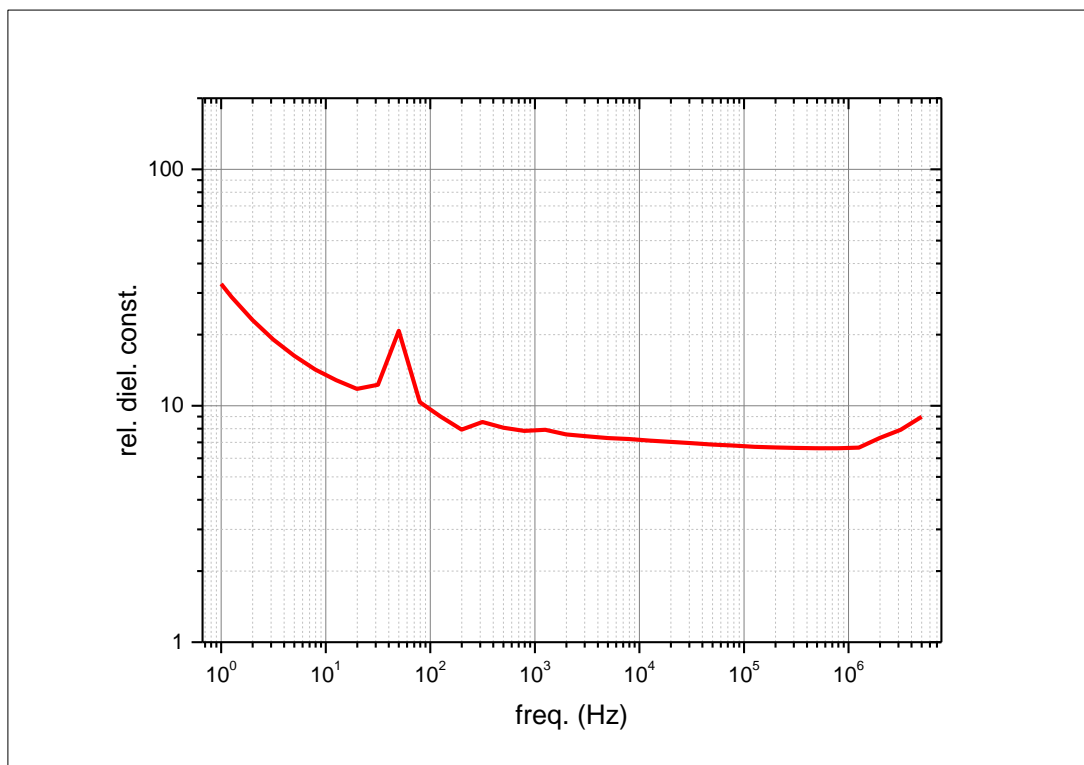


Figure 3-6: Dielectric constant k with frequency for the oleic acid-stabilised titanium dioxide nanorods TiO₂-OA, FA3-1.

3.3.2 Characterisation of the Ligand Exchanged FA3-2 TiO₂/OA/OPA, FA3-3 TiO₂/OA/DEPPNA and FA3-4, FA3-5 and FA3-6 TiO₂/OA/ODPA nanocomposites

The XRD patterns of the FA3-1 TiO₂/OA nanorods, the FA3-3 TiO₂/OA/DEPPNA nanocomposites and the FA3-5 TiO₂/OA/ODPA nanocomposites are shown in figure 3-6. As expected, no phase change in the anatase crystalline morphology of the TiO₂ nanorods can be observed.³ It is also clear from figure 3-6 that the size of the TiO₂ nanorods is also clearly not affected by the ligand exchange reactions.

The FT-IR spectra of FA3-2 TiO₂/OA/OPA, FA3-3 TiO₂/OA/DEPPNA and FA3-4, FA3-5 and FA3-6 TiO₂/OA/ODPA nanocomposites are shown in figures 3-7, 3-8 and 3-9. It can be observed that the intensities of the two peaks at 1525 and 1430 cm⁻¹ observed in the FT-IR spectrum of TiO₂/OA FA3-1 are lower in the figures 3-7, 3-8 and 3-9, which also contain a new peak appeared at 1040 cm⁻¹ related to a stretching band of P-O. The differences in these spectra indicate that part of oleic acid monolayer attached to the surface of the TiO₂ nanorods in TiO₂/OA FA3-1 has been replaced by the ligands OPA, DEPPNA and ODPA in the FA3-2 TiO₂/OA/OPA, FA3-3 TiO₂/OA/DEPPNA and FA3-4, FA3-5 and FA3-6 TiO₂/OA/ODPA nanocomposites respectively.^{6,7}

The FT-IR spectrum of the ODPA ligand contains a P=O double bond valence vibration at 1226 cm⁻¹ and a P-O-H absorption band at 940 m⁻¹. However, these two bands are not present in the FT-IR spectra of FA3-4, FA3-5 and FA3-6 TiO₂/OA/ODPA nanocomposites. These spectra also exhibit a broad absorption band, which can be attributed to the PO₃ stretching at about 1065 cm⁻¹. All these data indicate that molecules of the ODPA ligand have attached themselves onto the surface of the FA3-1 TiO₂/OA nanorods to form the FA3-4, FA3-5 and FA3-6 TiO₂/OA/ODPA nanocomposites through a tridentate bonding mode.⁸

The two absorption peaks at 1525 and 1430 cm⁻¹, indicative of the presence of oleic acid on the surface of the TiO₂ nanorods, can still be seen in the sample FA3-4 TiO₂/OA/ODPA nanocomposite prepared using a ratio 4:1 of the TiO₂/OA nanorod to the OPDA ligand. However, these peaks are quite weak, which indicates that most of oleic acid in TiO₂/OA FA3-1 has been replaced to produce the FA3-4 TiO₂/OA/ODPA nanocomposite. These two absorption peak are not present in the FT-IR spectra of the FA3-5 and FA3-6 TiO₂/OA/ODPA nanocomposites prepared using a lower ratio, i.e., 3:1 and 2:1, respectively, of the TiO₂/OA nanorod to the OPDA ligand, i.e., at a higher concentration of ligand, indicates that almost all of the oleic acid on the surface of the TiO₂ nanorods has been replaced by the ODPA ligand, as might have been expected.

These results suggest that the oleic acid on the surface of the TiO₂/OA FA3-1 nanorods can be more easily removed using the ODPa ligand than using either OPA or DEPPNA in the ligand exchange reactions.

The intensity of the two absorption peaks at 1525 and 1430 cm⁻¹ in the FT-IR spectrum of the FA3-3 TiO₂/OA/DEPPNA nanocomposite is lower than that observed in the corresponding FT-IR spectrum of the TiO₂/OA FA3-1 nanorods. A new peak at 1065 cm⁻¹ attributable to PO₃ stretching is observed in the FT-IR spectrum of the FA3-3 TiO₂/OA/DEPPNA nanocomposite due to partial replacement of oleic acid ligand in TiO₂/OA FA3-1 nanorods with DEPPNA.

The ³¹P NMR spectra of the TiO₂/OA FA3-1 nanorods, the FA3-3 TiO₂/OA/DEPPNA nanocomposite, before and after separation treatment, and the FA3-5 TiO₂/OA/ODPA nanocomposite (3:1) are shown in figure 3-10. The peak at 4.70 ppm is related to the presence of triphenylphosphine that has been added to the solution as a reference. The two peaks at 31.6 and 29.6 ppm are present in the ³¹P NMR spectra of the FA3-3 TiO₂/OA/DEPPNA nanocomposite before the separation treatment. The peak at 31.6 is related to unreacted DEPPNA that can be removed by the separation treatment, as seen in figure 3-10 (b). The ³¹P NMR spectra of the TiO₂/OA FA3-1 nanorods, the FA3-3 TiO₂/OA/DEPPNA nanocomposite, before and after separation treatment, and the FA3-5 TiO₂/OA/ODPA nanocomposite (3:1) shows only one peak at 29.6 ppm. The absence of the peak at about 38 ppm indicates that the ODPa ligand has bonded to TiO₂ nanorod surface by replacing almost all and perhaps all of the oleic acid ligand.

The TEM images of the FA3-3 TiO₂/DEPPNA and FA3-5 TiO₂/ODPA (3:1) nanocomposites, shown in figure 3-11, reveal that there is no difference in the shape and size of rods after the ligand exchange process as expected. These TEM spectra are consistent with those obtained from XRD analysis of the same samples. The aspect ratio of FA3-5 TiO₂/ODPA (3:1) nanocomposites is between 5-8, which is the same as that of the starting FA3-1 TiO₂/OA nanocomposites, as shown in figure 3-12, *i.e.*, the size and shape of the TiO₂ nanorods are not changed by the ligand exchange reaction.

The results of the CHN and ICP elemental analysis shown in table 3-3 reveal that there is a higher concentration of titanium content for the FA3-2 TiO₂/OA/OPA and FA3-3 TiO₂/OA/DEPPNA nanocomposites than that found for the FA3-4, FA3-5 and FA3-6 TiO₂/OA/ODPA nanocomposites. The carbon content is correspondingly lower for the FA3-2 TiO₂/OA/OPA and FA3-3 TiO₂/OA/DEPPNA nanocomposites than that found for the FA3-4, FA3-5 and FA3-6 TiO₂/OA/ODPA nanocomposites. There is also an increase in the

phosphorous content with increasing concentration of the ODPA ligand in the exchange reactions, *i.e.*, in FA3-4, FA3-5 and FA3-6 TiO₂/OA/ODPA nanocomposites.

The FA3-3 TiO₂/OA/DEPPNA and the FA3-5 TiO₂/OA/ODPA nanocomposite (3:1) can be dissolved in chlorobenzene up to a concentration of 40 %, see figure 3-13. These solutions can be stable for several months. On the other hand the FA3-2 TiO₂/OA/OPA nanocomposite is not soluble in chlorobenzene perhaps because the short alkyl chain is not long enough to convey an aliphatic character to the surface of the TiO₂ nanorods.

Table 3-3: Chemical analysis of the FA3-1 TiO₂/OA nanorods modified with the OPA, DEPPNA and ODPA ligands to produce the FA3-2 TiO₂/OA/OPA, FA3-3 TiO₂/OA/DEPPNA and FA3-4, FA3-5 and FA3-6 TiO₂/OA/ODPA nanocomposites.

Sample	Ligands/Ratio*	Ti%	P%	C%	H%	N%	Solubility in C ₆ H ₅ Cl
FA3-1	No ligand	42.83	---	18.59	3.12	0.36	Soluble
FA3-2	OPA/4:1	46.2	3.3	13.22	2.4	0.00	Not soluble
FA3-3	DEPPNA/4:1	46.35	0.78	17.29	2.39	0.22	Soluble
FA3-4	ODPA/4:1	41.07	2.05	20.9	3.73	0.42	Soluble
FA3-5	ODPA/3:1	37.80	2.60	22.6	4.26	0.24	Soluble
FA3-6	ODPA/2:1	34.41	3.48	26.70	4.76	0.17	Not soluble

*Ratio of TiO₂-OA: ligand

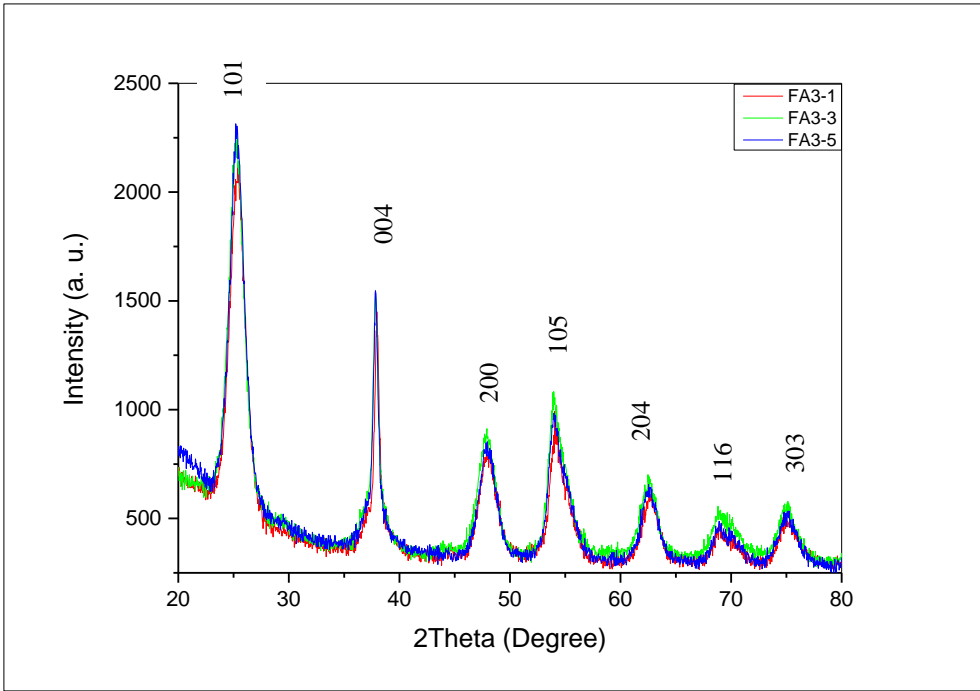


Figure 3-6: The XRD patterns of the FA3-1 TiO₂/OA nanorods, the FA3-3 TiO₂/OA/DEPPNA and FA3-5 TiO₂/OA/ODPA nanocomposites.

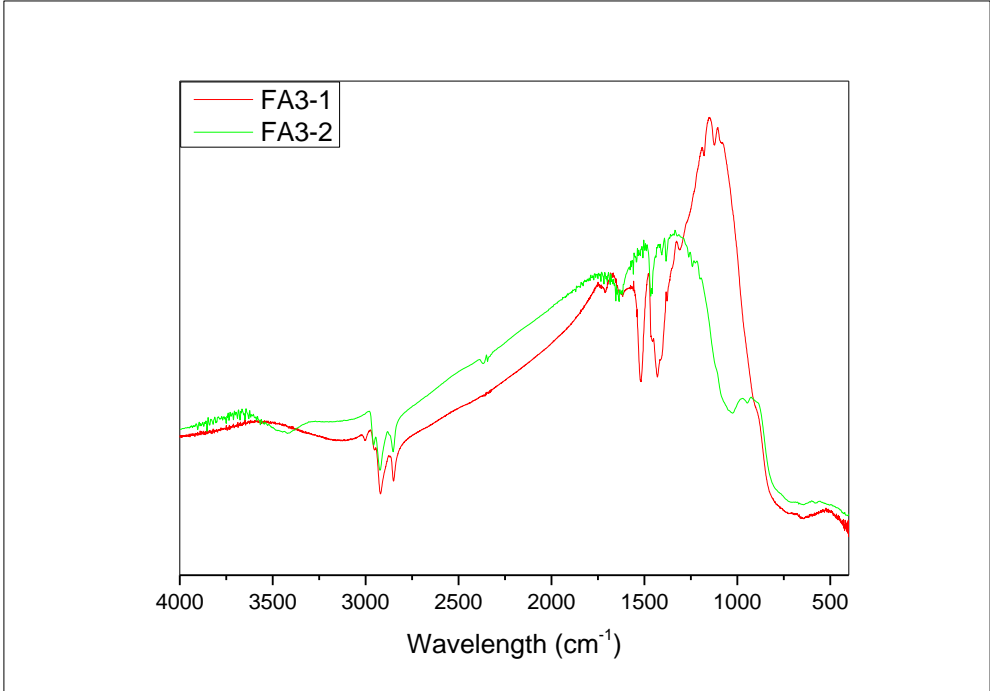


Figure 3-7: FT-IR patterns of FA3-1 TiO₂/OA nanorods and the FA3-2 TiO₂/OPA nanocomposites.

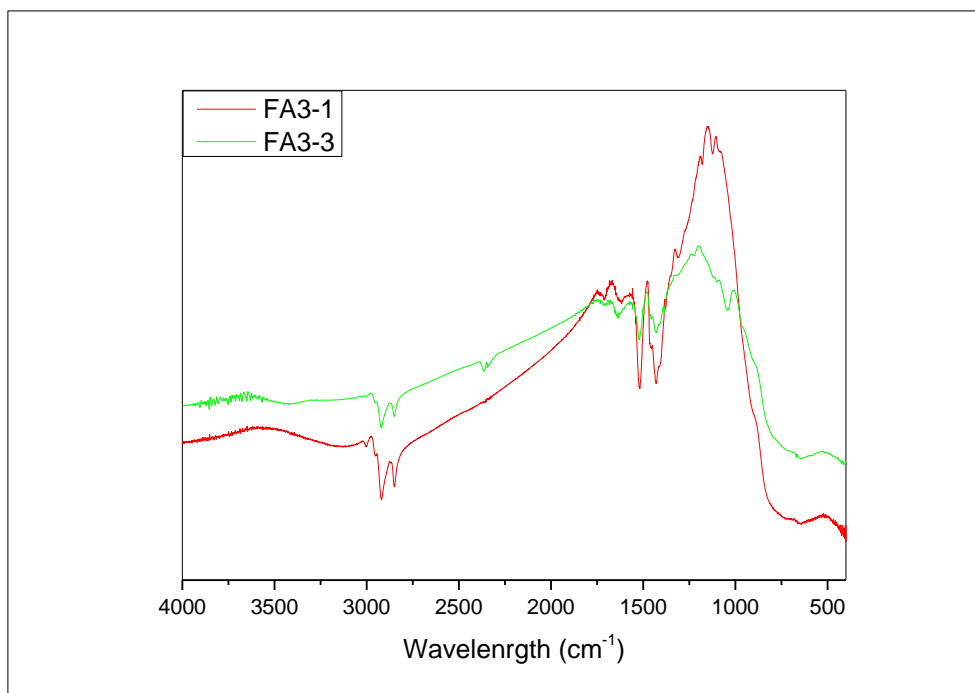


Figure 3-8: FT-IR patterns of the FA3-1 TiO₂/OA nanorods and the FA3-3 TiO₂/ DEPPNA nanocomposites.

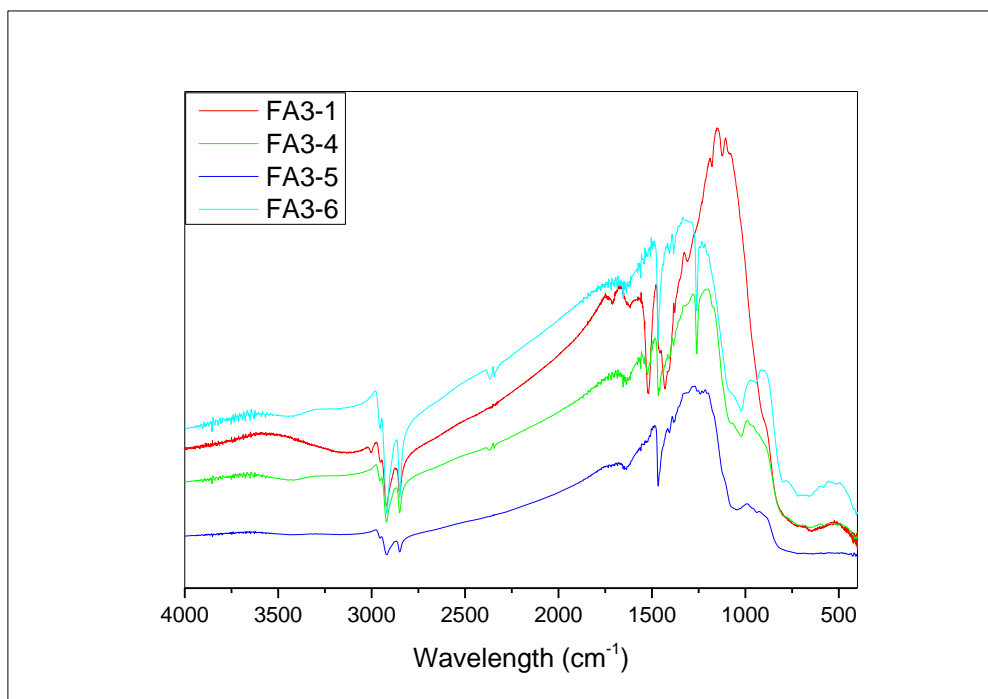


Figure 3-9: FT-IR patterns of FA3-1 TiO₂/OA nanorods and the FA3-4 (4:1), FA3-5 (3:1) and FA3-6 (2:1) TiO₂/ODPA nanocomposites.

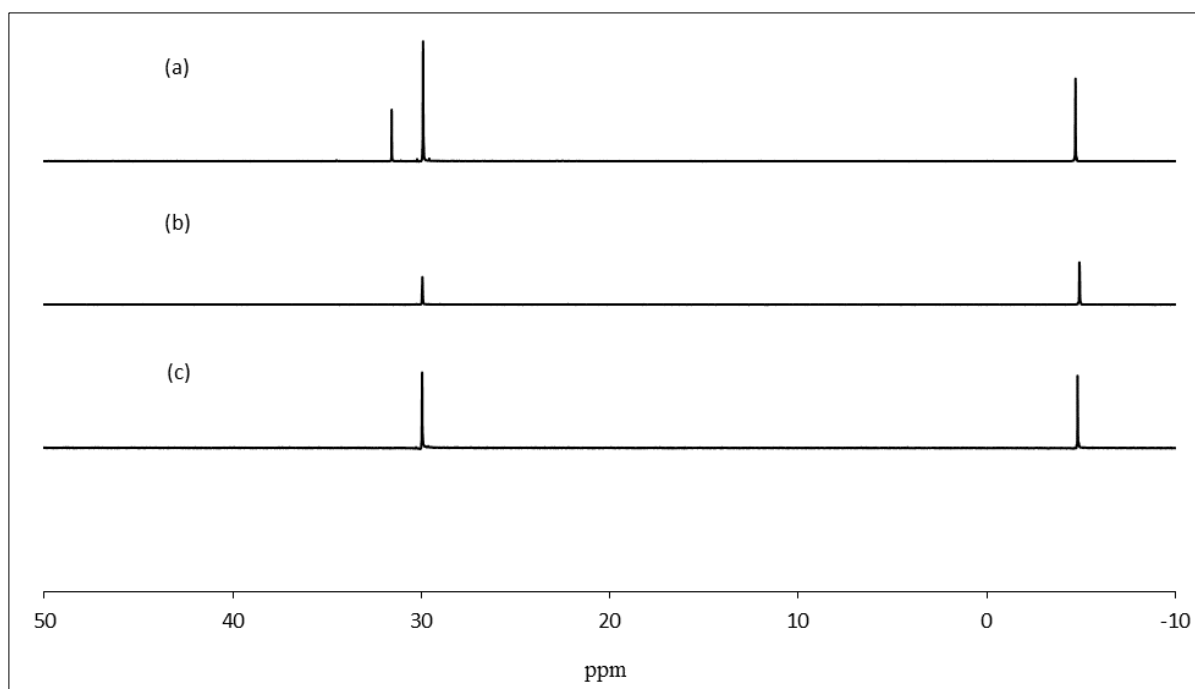


Figure 3-10: ^{31}P NMR of (a) FA3-3 $\text{TiO}_2/\text{DEPPNA}$ nanocomposites, before separation treatment (b) FA3-3 $\text{TiO}_2/\text{DEPPNA}$ nanocomposites after separation treatment, (c) FA3-5 TiO_2/ODPA nanocomposites (3:1) before separation treatment.

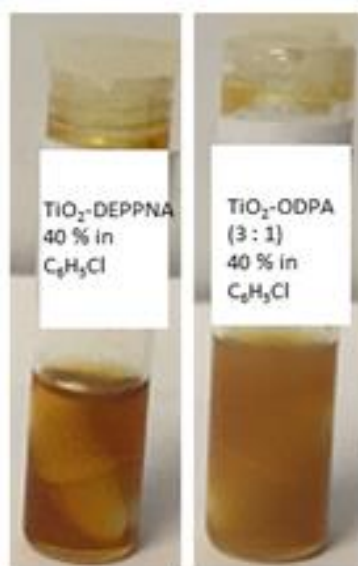
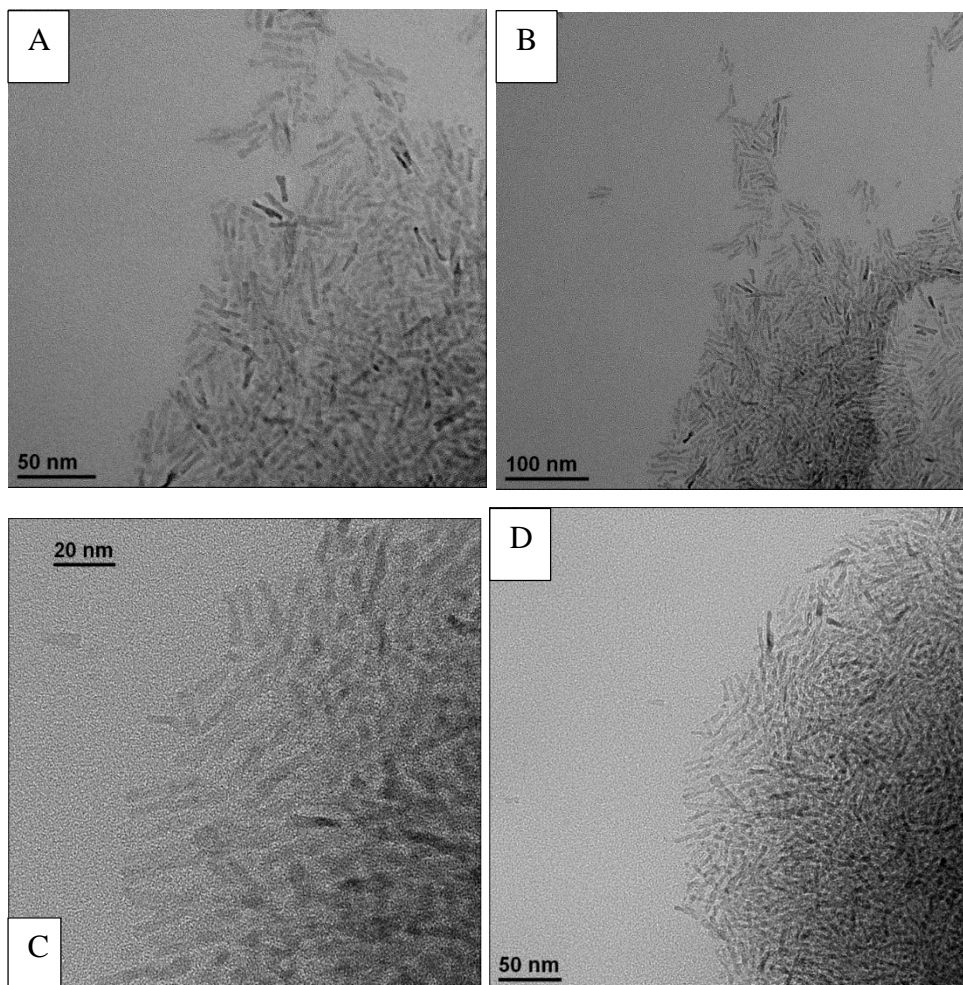


Figure 3-13: 40% Solutions of the FA3-3 $\text{TiO}_2/\text{DEPPNA}$ and FA3-5 TiO_2/ODPA (3:1) nanocomposites in chlorobenzene.



Figures 3-11: TEM images of the FA3-3 TiO₂/DEPPNA (A-B) and the FA3-5 TiO₂/ODPA nanocomposites (3:1) (C-D).

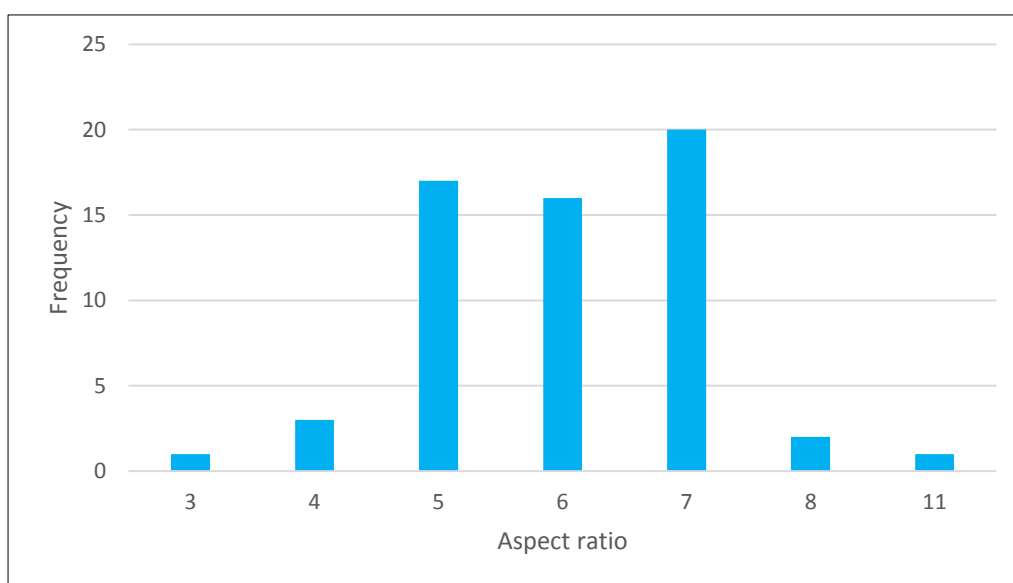


Figure 3-12: The aspect ratio distribution of the FA3-5 TiO₂/ODPA (3:1) nanocomposites.

3.3.3 Possible Mechanism for Ligand Exchange Reaction of the Anatase Titanium Dioxide Nanorods FA3-1 TiO₂/OA nanorods with OPA, DEPPNA and ODPA to produce the Ligand Exchanged FA3-2 TiO₂/OA/OPA, FA3-3 TiO₂/OA/DEPPNA and FA3-4, FA3-5 and FA3-6 TiO₂/OA/ODPA nanocomposites, respectively.

Modification of anatase titanium dioxide nanorods capped with oleic acid TiO₂-OA surface with phosphorus ligands is predicted to occur through bonding between the phosphoryl oxygen to Lewis acid sites on the titanium dioxide surface and condensation reactions between the hydroxyl groups (Ti-OH) on titanium surface and P-OX groups (where X; H, Et). Consequently, several bonding modes can occur, *e.g.*, monodentate, bidentate or tridentate bonds for the ligands with a phosphonic acid group in a terminal position. Bidentate or tridentate bonding can occur for the corresponding phosphonate ligands, see scheme 3-3^{7,9}.

The surface chemistry of titanium dioxide nanoparticles is multifaceted in that it has both acidic and basic surface hydroxyl groups (Ti-OH) as well as Lewis acid sites¹⁰.

The surface of the oleic acid-capped anatase titanium nanorods FA3-1 TiO₂/OA possesses very many hydroxyl groups (Ti-OH) as well as a high surface coverage of oleic acid molecules chemically bonded to the TiO₂ surface, as confirmed by FT-IR analysis, see figure 3-2. Thus, two kinds of reaction may occur during the ligand exchange reaction of the FA3-1 TiO₂/OA nanorods with the phosphorus ligands used in this study, *i.e.*, octylphosphonic acid (OPA), decylphosphonic acid (ODPA) and 2-phenylethyl phosphonate (DEPPNA). The phosphorus ligands may replace oleic acid via route 1 and/or by reaction of R-OX (X = H, Et) with hydroxyl groups Ti-OH via route 2.

The chemical analyses of the ligand exchange reaction of the anatase titanium dioxide FA3-1 TiO₂/OA nanorods with OPA, DEPPNA and ODPA to produce the ligand exchanged FA3-2 TiO₂/OA/OPA, FA3-3 TiO₂/OA/DEPPNA and FA3-4, FA3-5 and FA3-6 TiO₂/OA/ODPA nanocomposites, respectively, are shown in table 3-3. The ligand exchange rate (LER), *i.e.*, conversion rate, of oleic acid by DEPPNA and OPA was calculated as 18.2 % and 83.8 %, respectively, as shown in table 3-4, based on the phosphorus and carbon content of the reaction products and the carbon content of the anatase titanium dioxide FA3-1 TiO₂/OA nanorod starting materials, see index 3-1 for calculation of ligand exchange rate and analysis of the attachment of ligands on TiO₂.

On the other hand, for all the organophosphorus ligands, the molar percentage of the ligands on the TiO₂ surface is higher than that of the exchanged oleic acid, suggesting that the

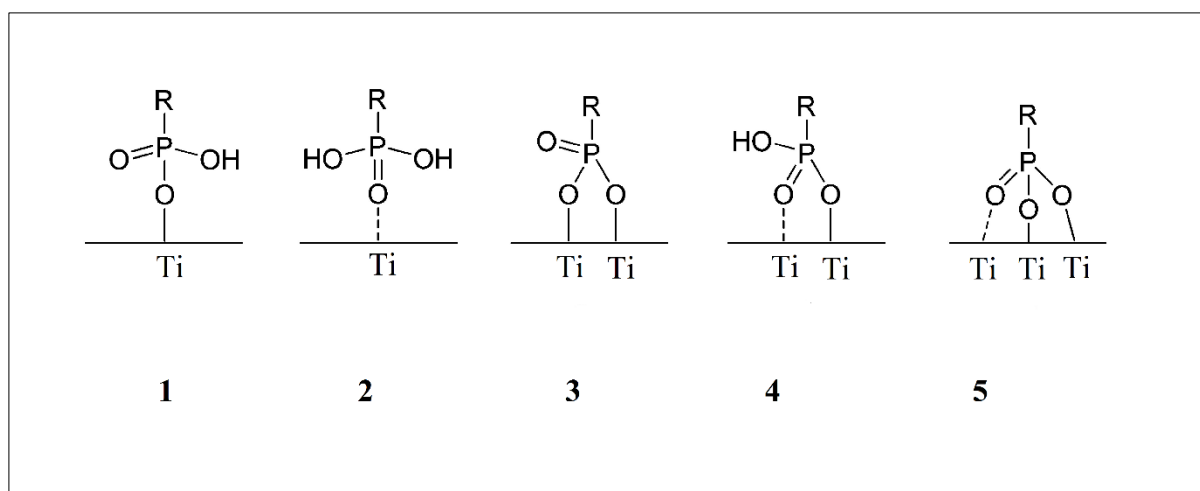
organophosphorus ligands attached themselves onto the TiO₂ surface not just *via* ligand exchange of oleic acid in the FA3-1 TiO₂/OA nanoparticles as shown in table 3-4, by route 1, see Appendix 1. The ligands may also attach themselves onto the TiO₂ surface *via* reaction of P-OH or P-OEt groups of the ligand head groups with the hydroxyl groups on the TiO₂ surface, if the TiO₂ surface has not already been fully covered with oleic acid as shown in table 3-4, see route 2¹¹. It has been calculated that for FA3-5 TiO₂/ODPA (3:1), about 77.92 % of molecules attached on TiO₂ surfaces *via* ligand exchange of oleic acid, i.e., route 1 and 22.1 % *via* reaction of P-OH groups of ODPA with the hydroxyl groups on the TiO₂ surfaces, i.e., route 2. Similar percentages of TiO₂ surface modification *via* routes 1 and 2 for other products are shown in table 3-4. A combination of these results suggests that the coverage of oleic acid on TiO₂ surfaces in the FA3-1 TiO₂/OA nanoparticles is less than 70 %.

The resonance at 29.6 ppm in the ³¹P NMR spectra of the TiO₂/OA FA3-1 nanorods, the FA3-3 TiO₂/OA/DEPPNA nanocomposite, before and after separation treatment, and the FA3-5 TiO₂/OA/ODPA nanocomposite (3:1) shown in figure 3-10, is probably ascribable to the presence of tridentate phosphonate sites, i.e., P(OTi)₃¹². Although P-OEt groups are quite stable, the same chemical shift of the purified TiO₂-DEPPNA as that of TiO₂-ODPA suggests that the ethoxy-groups have been displaced during the ligand exchange reactions and that the DEPPNA has bonded to TiO₂ surface by a tridentate mode of attachment.

Table 3-4: The rate of ligand exchange in the reactions of the anatase nanorods FA3-1 TiO₂/OA nanorods with the ligands OPA, DEPPNA and ODPA to produce the ligand exchanged FA3-2 TiO₂/OA/OPA, FA3-3 TiO₂/OA/DEPPNA and FA3-4, FA3-5 and FA3-6 TiO₂/OA/ODPA nanocomposites, respectively.

Sample	Ligands/Ratio*	Route 1 % *	Route 2 % **
FA3-2	OPA/4:1	67.77	32.23
FA3-3	DEPPNA/4:1	68.37	31.63
FA3-4	ODPA/4:1	83.87	16.13
FA3-5	ODPA/3:1	77.92	22.1
FA3-6	ODPA/2:1	66.62	33.38

* Rate 1: Ligand exchange route, LER; ** Rate 2: Reaction with hydroxyl groups.



Scheme 3-3: Some possible modes of binding between the titanium dioxide surface with phosphorus ligands, i.e., monodentate (1-2), bidentate (3-4) and tridentate bonding modes.

3.4 Conclusion and Summary

Anatase titanium nanorods, with a length of 20 nm and a width of 3-4 nm with an aspect ratio of between 5-8 with a maximum value at 6:1, capped with oleic acid have been prepared using an hydrolysis reaction using titanium (IV) tetraisopropoxide (TTIP) as the source of titanium in the presence of oleic acid as a surfactant at a relatively low temperature, i.e., 100 °C, for 72 h.

There is no difference in the shape, size and aspect ratio of the TiO₂ rods after the ligand exchange, i.e., partial or almost complete replacement of the oleic acid attached to the surface of the anatase titanium FA3-1 TiO₂/OA nanorods with phosphonic acid ligands, i.e., octylphosphonic acid (OPA) and decylphosphonic acid (ODPA) and phosphonate ligand and 2-phenylethyl phosphonate (DEPPNA).

The solubility of the TiO₂/ligand nanocomposites strongly depends on the length of aliphatic chain of the ligand attached to the surface of the nanorods, e.g., the FA3-3 TiO₂/OA/DEPPNA nanocomposite and the FA3-5 TiO₂/OA/ODPA nanocomposite (3:1) can be dissolved in chlorobenzene up to a concentration of 40% to produce solutions that can be stable for several months. On the other hand the FA3-2 TiO₂/OA/OPA nanocomposite is not soluble in chlorobenzene perhaps because the short alkyl chain is not long enough to convey an aliphatic character to the surface of the TiO₂ nanorods.

The concentration of the ligand attached to the surface of the nanorods determines the degree of solubility of the nanocomposites in organic solvents, e.g., the FA3-4 and FA3-5 TiO₂/ODPA nanocomposites (4:1 and 3:1) can be dissolved in chlorobenzene, whereas the FA3-4 and FA3-5 TiO₂/ODPA nanocomposites (2:1) cannot be dissolved in the same solvent.

The calculation of ligand exchange rate (LER) of the attachment of ligands onto the surface of the TiO₂/OA nanorods suggests that the attachment occurs *via* a combination of ligand exchange of oleic acid (route 1) and reaction of the ligand P-OH groups with the hydroxyl groups on the TiO₂ surface (route 2). These calculations suggest that the surface coverage of oleic acid on the TiO₂-OA nanorods is less than 70 %.

The binding between ODPA and TiO₂-OA should be through a tridentate attachment of phosphonic acid to the TiO₂ surface according FT-IR analysis.

3.5 References

1. Cozzoli, P. D.; Kornowski, A.; Weller, H., Low-Temperature Synthesis of Soluble and Processable Organic-Capped Anatase TiO₂ Nanorods. *Journal of the American Chemical Society* **2003**, 125, (47), 14539-14548.
2. Caputo, G.; Cingolani, R.; Cozzoli, P. D.; Athanassiou, A., Wettability conversion of colloidal TiO₂ nanocrystal thin films with UV-switchable hydrophilicity. *Physical Chemistry Chemical Physics* **2009**, 11, (19), 3692-3700.
3. Wen, B.-M.; Liu, C.-Y.; Liu, Y., Solvothermal synthesis of ultralong single-crystalline TiO₂ nanowires. *New Journal of Chemistry* **2005**, 29, (7), 969-971.
4. Thistlethwaite, P. J.; Hook, M. S., Diffuse Reflectance Fourier Transform Infrared Study of the Adsorption of Oleate/Oleic Acid onto Titania. *Langmuir* **2000**, 16, (11), 4993-4998.
5. Thistlethwaite, P. J.; Gee, M. L.; Wilson, D., Diffuse Reflectance Infrared Fourier Transform Spectroscopic Studies of the Adsorption of Oleate/Oleic Acid onto Zirconia. *Langmuir* **1996**, 12, (26), 6487-6491.
6. Gao, W.; Dickinson, L.; Grozinger, C.; Morin, F. G.; Reven, L., Self-Assembled Monolayers of Alkylphosphonic Acids on Metal Oxides. *Langmuir* **1996**, 12, (26), 6429-6435.
7. Guerrero, G.; Mutin, P. H.; Vioux, A., Anchoring of Phosphonate and Phosphinate Coupling Molecules on Titania Particles. *Chemistry of Materials* **2001**, 13, (11), 4367-4373.
8. Randon, J.; Blanc, P.; Paterson, R., Modification of ceramic membrane surfaces using phosphoric acid and alkyl phosphonic acids and its effects on ultrafiltration of BSA protein. *Journal of Membrane Science* **1995**, 98, (1-2), 119-129.
9. Hotchkiss, P. J.; Jones, S. C.; Paniagua, S. A.; Sharma, A.; Kippelen, B.; Armstrong, N. R.; Marder, S. R., The Modification of Indium Tin Oxide with Phosphonic Acids: Mechanism of Binding, Tuning of Surface Properties, and Potential for Use in Organic Electronic Applications. *Accounts of Chemical Research* **2012**, 45, (3), 337-346.

10. van Veen, J. A. R.; Veltmaat, F. T. G.; Jonkers, G., A method for the quantitative determination of the basic, acidic, and total surface hydroxy content of TiO₂. *Journal of the Chemical Society, Chemical Communications* **1985**, (23), 1656-1658.
11. Cheng, F.; Sajedin, S. M.; Kelly, S. M.; Lee, A. F.; Kornherr, A., UV-stable paper coated with APTES-modified P25 TiO₂ nanoparticles. *Carbohydrate Polymers* **2014**, 114, 246-252.
12. Maliakal, A.; Katz, H.; Cotts, P. M.; Subramoney, S.; Mirau, P., Inorganic Oxide Core, Polymer Shell Nanocomposite as a High K Gate Dielectric for Flexible Electronics Applications. *Journal of the American Chemical Society* **2005**, 127, (42), 14655-14662.

Chapter 4

Preparation and
Characterisation of Solution
Processable Metal-Doped
(Nb/In) Anatase TiO₂-M
Nanorods

4.1 Introduction

The prime aim of this chapter was to prepare solution-processable, ligand-stabilised, anatase titanium dioxide nanorods ($\text{TiO}_2\text{-L-M}$; $\text{M} = \text{Nb}$, In or Nb/In) doped with metals, which could be dissolved in typical organic solvents, *e.g.* chlorobenzene, used to deposit thin layers of functional materials on substrate surfaces from solution by standard processes, such as drop casting, spin coating, doctor blade techniques, ink-jet printing, etc. Doping titanium dioxide with *n*-type, *i.e.*, indium, and *p*-type, *i.e.*, niobium, dopants is expected to produce two kinds of ligand-stabilised, metal-doped anatase nanorods ($\text{TiO}_2\text{-L-M}$; $\text{M} = \text{Nb}$ or In) with a high dielectric constant and a low dielectric loss.¹ Ligand-stabilised, metal-doped anatase nanorods ($\text{TiO}_2\text{-L-M}$; $\text{M} = \text{Nb/In}$) containing both niobium and indium dopants were also prepared.

In order to achieve this aim, a novel method for the preparation of solution-processable, ligand-stabilised, niobium- and indium-doped, anatase nanorods ($\text{TiO}_2\text{-L-M}$; $\text{M} = \text{Nb}$, In or Nb/In) stabilised with a monolayer surface coating of oleic acid ($\text{L} = \text{OA}$) was developed.

In order to improve the solubility of the oleic acid-stabilised, niobium- and indium-doped, anatase nanorods ($\text{TiO}_2\text{-OA-M}$; $\text{M} = \text{Nb}$, In or Nb/In), a series of ligand exchange reactions were carried out, in the presence of either diethyl 2-phenylethyl phosphonate (DEPPNA) or octadecylphosphonic acid (ODPA) to replace the oleic acid coating, to identify the optimal reaction conditions to produce the surface-modified metal-doped anatase titanium dioxide nanorods ($\text{TiO}_2\text{-DEPNA-M}$; $\text{M} = \text{Nb}$, In or Nb/In and $\text{TiO}_2\text{-ODPA-M}$; $\text{M} = \text{Nb}$, In or Nb/In).

4.2 Experimental

4.2.1 Materials

Titanium (IV) tetraisopropoxide (TTIP, $\geq 97.0\%$), oleic acid (90%), trimethylamine *N*-oxide (98%), diethyl 2-phenylethyl phosphonate and octadecylphosphonic acid (97.0%), niobium (V) ethoxide (99.95%) were sourced from Sigma-Aldrich. Niobium isopropoxide (NBIO, 99%), Indium (III) isopropoxide (99.9%) and Indium (III) ethoxide (99.9%) were sourced from Alfa Aesar. Ultrapure water with a specific resistivity of $18.2\text{ M}\Omega\cdot\text{cm}$ was obtained by reversed osmosis followed by ion-exchange and filtration (UPQ PS system, ELGA, USA).

4.2.2 Solution-Processable, Metal-Doped Anatase Titanium Dioxide Nanorods Synthesis ($\text{TiO}_2\text{-M}$; $\text{M} = \text{Nb, In or Nb/In}$)

The hydrolysis reaction of titanium (IV) tetraisopropoxide (TTIP) was carried out at relatively low temperature, *e.g.* 100 °C, in presence of a source of the appropriate metal, *i.e.*, either indium or niobium, and oleic acid (OA) as a surfactant and trimethylamine N-oxide (TMAO) as a nanorod stabiliser.

$\text{TiO}_2\text{-Nb}$, niobium isopropoxide ($\text{Nb}[\text{OCH}(\text{CH}_3)_2] = \text{NBIO}$) and niobium (V) ethoxide ($\text{Nb}[\text{OC}_2\text{H}_5]_2 = \text{NBEO}$) were used as different sources of niobium in the preparation of niobium doped anatase titanium dioxide nanorods. In addition, the effect of varying the niobium concentration and the reaction time (24 h and 72 h) were investigated.

Ligand exchange reactions were carried out on the oleic acid-stabilised niobium-doped anatase titanium dioxide nanorods ($\text{TiO}_2\text{-OA-Nb}$) synthesised in these reactions under different reaction conditions. Diethyl 2-phenylethyl phosphonate (DEPPNA) and octadecylphosphonic acid (ODPA) were both used as ligands to replace the oleic acid attached to the surface of the niobium-doped anatase titanium dioxide nanorods ($\text{TiO}_2\text{-OA-Nb}$).

A series of oleic acid-stabilised, indium-doped, titanium dioxide nanorods ($\text{TiO}_2\text{-OA-In}$) were also prepared using the same method as that used to synthesise the niobium doped titanium dioxide nanorods $\text{TiO}_2\text{-Nb}$. Indium (III) isopropoxide ($\text{In}[\text{OCH}(\text{CH}_3)_2] = \text{INIO}$) and indium (III) ethoxide ($\text{In}[\text{OC}_2\text{H}_5]_2 = \text{INEO}$) were used as the source of indium.

Examples of niobium/indium-doped titanium dioxide nanorods ($\text{TiO}_2\text{-OA-Nb/In}$) were also synthesised using indium (III) isopropoxide ($\text{In}[\text{OCH}(\text{CH}_3)_2] = \text{INIO}$) and indium (III) ethoxide ($\text{In}[\text{OC}_2\text{H}_5]_2 = \text{INEO}$) as the starting materials. The synthesis of the oleic acid-stabilised, niobium/indium-doped, titanium dioxide nanorods ($\text{TiO}_2\text{-OA-Nb/In}$) was followed by ligand exchange using octadecylphosphonic acid (ODPA) as the replacement ligand to produce the corresponding octadecylphosphonic acid-stabilised, niobium/indium-doped, titanium dioxide nanorods ($\text{TiO}_2\text{-ODPA-Nb/In}$).

Synthesis of Solution-Processable, Niobium-Doped Titanium Dioxide Nanorods ($\text{TiO}_2\text{-OA-Nb}$)

Oleic acid (OA, 420 g) was dried under stirring for 1 h at 120 °C and then allowed to cool to 85 °C. Titanium (IV) isopropoxide (17.7 cm³, 60 mmol) was added under stirring until the colour of solution changed from colourless to yellow. 10 Minutes after this colour change the

required amount of niobium source was injected quickly to the reaction mixture, see Table 4-1. A 2 M solution of trimethylamine *N*-oxide (60 cm³) was then added rapidly by syringe to the reaction mixture and the reaction temperature increased to 100 °C. After a few minutes the solution became slightly turbid and after an hour the viscosity of the solution had increased significantly. The reaction mixture was stirred at 100 °C for a total reaction time of either 24 h or 72 h, see table 4-1 for details of the reaction conditions. Isopropanol (1.2 L) was added to the cooled reaction mixture and the resultant precipitate separated off by centrifugation, washed twice with isopropanol and then dried overnight under vacuum at 30 °C. This product was dissolved in toluene, precipitated by adding acetone and separated off by centrifugation. This step was repeated twice and the resultant solid product dried overnight under vacuum at 30 °C to yield the desired oleic acid-stabilised, niobium-doped titanium dioxide nanorods (TiO₂-OA-Nb) FA4-1 – FA4-8, see table 4-1.

Table 4-1: Reaction conditions for the synthesis of niobium-doped titanium dioxide nanorods (TiO₂-OA-Nb).

Sample	Niobium precursor	Ti/Nb ratio	Reaction time/h
FA4-1	Niobium isopropoxide (NBIO)	9:1	72
FA4-2	Niobium isopropoxide (NBIO)	18:1	72
FA4-3	Niobium (V) ethoxide (NBEO)	9:1	24
FA4-4	Niobium (V) ethoxide (NBEO)	9:1	72
FA4-5	Niobium (V) ethoxide (NBEO)	18:1	24
FA4-6	Niobium (V) ethoxide (NBEO)	18:1	72
FA4-7	Niobium (V) ethoxide (NBEO)	45:1	24
FA4-8	Niobium (V) ethoxide (NBEO)	45:1	72

Ligand Exchange of the Oleic Acid-Stabilised, Niobium-Doped Titanium Dioxide Nanorods (TiO₂-OA-Nb)

The required amount of either diethyl 2-phenylethyl phosphonate (DEPPNA) or octadecylphosphonic acid (ODPA), was added to a solution of oleic acid-stabilised, niobium-doped titanium dioxide nanorods (TiO₂-OA-Nb) FA4-1 – FA4-6 in chlorobenzene and the resultant reaction mixture was heated at 100 °C for 24 h, see table 4-2 for reaction condition details. At the end of reaction, the mixture was allowed to cool to room temperature. The chlorobenzene and unreacted ligands were removed under reduced pressure to yield a solid residue that was dissolved in chlorobenzene, precipitated by the addition of acetone to this solution, and then separated off by centrifugation. This purification process was repeated twice to yield either the desired 2-phenylethyl phosphonate acid-stabilised, niobium-doped titanium dioxide nanorods (TiO₂-DEPPNA-Nb) FA4-10 or the corresponding octadecylphosphonic acid acid-stabilised, niobium-doped titanium dioxide nanorods (TiO₂-ODPA-Nb) as solid products FA4-9 and FA4-11 – FA4-15, see table 4-2, that were dried under vacuum at 30 °C overnight.

Synthesis of Solution-Processable, Indium-Doped Titanium Dioxide Nanorods (TiO₂-OA-In)

The same method used to prepare oleic acid-stabilised, niobium-doped, titanium dioxide nanorods (TiO₂-OA-Nb) FA4-1 – FA4-8, see table 4-1, was used to synthesise the corresponding oleic acid-stabilised, indium-doped titanium dioxide nanorods (TiO₂-OA-In) FA4-16 and FA4-17, see table 4-3 for more details. Indium (III) isopropoxide (INIO) and indium (III) ethoxide (INEO), were used as the indium precursors, see Table 4-3 for details of the reactions conditions for the synthesis of oleic acid-stabilised, indium-doped titanium dioxide nanorods (TiO₂-OA-In) FA4-16 and FA4-17.

Table 4-2: Reaction conditions for the ligand-exchange reactions between the niobium-doped titanium dioxide nanorods (TiO₂-OA-Nb) FA4-1 – FA4-6, see table 4-1, and either octadecylphosphonic acid (ODPA) or diethyl 2-phenylethyl phosphonate (DEPPNA) to produce the ODPA-stabilised, niobium-doped titanium dioxide nanorods (TiO₂-ODPA-Nb) FA4-9 and FA4-11 – FA4-15 or the DEPPNA-stabilised, niobium-doped titanium dioxide nanorods (TiO₂-ODPA-Nb) FA4-10.

Sample	Starting Material	Ligands	Temperature/°C	Reaction Time/h
FA4-9	FA4-1	ODPA	100	24
FA4-10	FA4-1	DEPPNA	100	24
FA4-11	FA4-2	ODPA	100	24
FA4-12	FA4-6	ODPA	100	24
FA4-13	FA4-5	ODPA	100	24
FA4-14	FA4-4	ODPA	100	24
FA4-15	FA4-3	ODPA	100	24

Table 4-3: Reaction conditions for the synthesis of the oleic acid-stabilised indium-doped titanium dioxide nanorods (TiO₂-OA-In) FA4-16 and FA4-17.

Sample	Indium precursor	Ti/In ratio	Reaction time/h
FA4-16	Indium (III) isopropoxide (INIO)	9:1	72
FA4-17	Indium (III) ethoxide (INEO)	9:1	72

Synthesis of Solution-Processable Niobium/Indium Doped Titanium Dioxide Nanorods (TiO₂-OA-Nb/In)

Solution-processable, oleic acid-stabilised, titanium dioxide nanorods (TiO₂-OA-Nb/In) FA4-18 doped with both niobium and indium were prepared using the same approach as that used to synthesise solution-processable niobium-doped titanium dioxide nanorods (TiO₂-OA-Nb) FA4-1 – FA4-8, and indium-doped titanium dioxide nanorods (TiO₂-OA-In) FA416 and FA4-17.

Ligand exchange reactions of the oleic acid-stabilised, titanium dioxide nanorods (TiO₂-OA-Nb/In) FA4-18 doped with both niobium and indium were carried out at 100 °C for 24 h in chlorobenzene using either octadecylphosphonic acid (ODPA) or diethyl 2-phenylethyl phosphonate (DEPPNA) as the replacement ligands to yield the desired octadecylphosphonic acid, niobium/indium-doped titanium dioxide nanorods (TiO₂-ODPA-Nb/In) FA4-19 or the corresponding 2-phenylethyl phosphonate acid-stabilised, niobium/indium-doped titanium dioxide nanorods (TiO₂-DEPPNA-Nb/In) FA4-20.

Synthesis of Solution-Processable, Niobium/Indium-Doped Titanium Dioxide Nanorods (TiO₂-OA-Nb/In)

In the synthesis of oleic acid-stabilised titanium dioxide nanorods (TiO₂-OA-Nb/In) FA4-18 doped with niobium and indium niobium isopropoxide (NBIO) and indium (III) isopropoxide (INIO) were used as niobium and indium sources, respectively. The reaction was maintained at a temperature of 100 °C for a total reaction time of 72 h. The separation and washing treatments were carried out in a similar way to above described in sections.

Table 4-4: Reaction conditions for the synthesis of the oleic acid-stabilised, niobium/indium doped titanium dioxide nanorods (TiO₂-OA-Nb/In) FA4-18.

Sample	Niobium precursor	Indium precursor	Ti/In ratio	Ti/In ratio
FA4-18	niobium isopropoxide (NBIO)	Indium (III) isopropoxide (INIO)	9:1	9:1

Ligand Exchange of the Niobium/Indium Doped Titanium Dioxide Nanorods (TiO₂-OA-Nb/In)

The required amount of either diethyl 2-phenylethyl phosphonate (DEPPNA) or octadecylphosphonic acid (ODPA) was added to solution of oleic acid-stabilised, niobium/indium doped titanium dioxide nanorods (TiO₂-OA-Nb/In) FA4-18 in chlorobenzene and the resultant reaction mixture was heated at 100 °C for 24 h, see table 4-4 for details of the reaction condition details. The cooled reaction mixture was evaporated down under reduced pressure remove the chlorobenzene solvent and unreacted ligands. The resultant solid residue was dissolved in chlorobenzene and then precipitated by adding acetone, followed by separation by centrifugation and the standard washing treatment. This process was carried out twice. Drying the solid residue under vacuum at 30 °C for overnight yielded the desired octadecylphosphonic acid, niobium/indium-doped titanium dioxide nanorods (TiO₂-ODPA-Nb/In) FA4-19 and the corresponding 2-phenylethyl phosphonate acid-stabilised, niobium/indium-doped titanium dioxide nanorods (TiO₂-DEPPNA-Nb/In) FA4-20.

Table 4-5: Reaction conditions for the ligand-exchange reactions using the oleic acid-stabilised, niobium/indium doped titanium dioxide nanorods (TiO₂-OA-Nb/In) FA4-18 with either octadecylphosphonic acid (ODPA) or diethyl 2-phenylethyl phosphonate (DEPPNA) as the replacement ligands to yield the desired octadecylphosphonic acid, niobium/indium-doped titanium dioxide nanorods (TiO₂-ODPA-Nb/In) FA4-19 or the corresponding 2-phenylethyl phosphonate acid-stabilised, niobium/indium-doped titanium dioxide nanorods (TiO₂-DEPPNA-Nb/In) FA4-20.

Sample	Start Material	Ligands	Reaction time/h	Temp/°C
FA4-19	FA4-18	ODPA	24	100
FA4-20	FA4-18	DEPPNA	24	100

4.3 Results and Discussion

4.3.1 Characterisation of Metal-Doped Titanium Dioxide Nanorods (TiO₂-L-M)

The synthesis of solution processable ligand-stabilised, metal-doped (Nb/In), anatase titanium dioxide nanorods TiO₂-L-M (M: Nb, In or Nb/In) was carried out at low temperature (100 °C) for 24 h or 72 h. Firstly, for the oleic acid-stabilised, niobium doped titanium dioxide TiO₂-OA-Nb, niobium isopropoxide (NBIO) and Niobium (V) ethoxide (NBEO) were used as niobium sources. After that, ligand exchange of TiO₂-OA-Nb products was carried out using diethyl 2-phenylethyl phosphonate (DEPPNA) and octadecylphosphonic acid (ODPA) as ligands.

Secondly, for the oleic acid-stabilised, indium doped titanium dioxide TiO₂-OA-In, indium (III) isopropoxide (INIO) and Indium (III) ethoxide (INEO) were used as indium source.

Furthermore, for the oleic acid-stabilised, mix metals niobium/ indium doped titanium dioxide TiO₂-OA-Nb/In, niobium isopropoxide (NBIO) and indium (III) isopropoxide (INIO) were used as niobium and indium sources, respectively. The ligand exchange of TiO₂-OA-Nb/In products was carried out using diethyl 2-phenylethyl phosphonate (DEPPNA) and octadecylphosphonic acid (ODPA) as ligands.

Characterisation of the Oleic Acid-Stabilised, Niobium-Doped Titanium Dioxide Nanorods (TiO₂-OA-Nb)

The XRD patterns of the oleic acid-stabilised, niobium-doped, anatase titanium dioxide nanorods (TiO₂-OA-Nb) FA4-2 and FA4-4 and the non-doped, oleic acid-stabilised, anatase titanium dioxide nanorods (TiO₂-OA) FA3-1 are shown in figure 4-1 and those of the oleic acid-stabilised, niobium-doped, anatase titanium dioxide nanorods (TiO₂-OA-Nb) FA4-3, FA4-5 and FA4-7 are shown in figure 4-2. It is clear that the TiO₂-Nb nanorods consist of titanium dioxide in the anatase phase.² This is the same crystal structure as that shown by the reference non-doped, oleic acid-stabilised, titanium dioxide nanorods (TiO₂-OA), FA3-1, prepared without addition of niobium. No niobium peaks can be observed in the XRD spectra, which is probably due to small concentration of niobium or to the presence of amorphous niobium nanoparticles.

The FT-IR spectra for oleic acid-stabilised, niobium doped titanium dioxide nanorods ($\text{TiO}_2\text{-OA-Nb}$) FA4-1 and FA4-4 are shown in figures 4-3 and 4-4. The peaks at 2850, 2920 and 2955 cm^{-1} are related to C-H₃, C-H₂ and C-H stretch vibrations attributable to the oleic acid present on the surface of the titanium dioxide nanorods ($\text{TiO}_2\text{-OA-Nb}$). In addition, the weak broad stretching band at 3465 cm^{-1} suggests the presence of some OH⁻ groups also present on the surface of the titanium dioxide nanorods ($\text{TiO}_2\text{-OA-Nb}$). Furthermore, two strong peaks at 1525 cm^{-1} and 1430 cm^{-1} are related to COO⁻ anti-symmetric vibrations as well as symmetric stretching vibrations, respectively^{3,4}, indicating that the oleic acid has bonded on the surface of the titanium dioxide nanorods.

The TEM images of the oleic acid-stabilised, niobium-doped titanium dioxide nanorods ($\text{TiO}_2\text{-OA-Nb}$), FA4-1 (A), FA4-2 (B), FA4-3 (C) and FA4-4 (D) shown in figure 4-5 and those of FA4-5 (A), FA4-6 (B), FA4-7 (C) and FA4-8 (D) shown in figure 4-6 reveal that the size ($L = 20$ and $d = 3\text{-}4$ nm) and shape (rod-like) of the titanium dioxide nanorods are very similar to those of each other and those of the corresponding non-doped oleic acid-stabilised, anatase titanium dioxide nanorods ($\text{TiO}_2\text{-OA}$) FA3-1, prepared in a similar way in the absence of a source of niobium.

The EDX analyses for niobium-doped titanium dioxide nanorods ($\text{TiO}_2\text{-OA-Nb}$) shown in figures 4-7, there is peaks for titanium and niobium in all niobium doped anatase titanium dioxide nanorods ($\text{TiO}_2\text{-OA-Nb}$).

The elemental composition of the oleic acid-stabilised, niobium-doped, anatase titanium dioxide nanorods ($\text{TiO}_2\text{-OA-Nb}$) was investigated using CHN and ICP, see table 4-6. The concentration of titanium and carbon in the nanorods is 39.5-44.1% and 19.14-23.44%, respectively. The Ti/Nb ratio established for the niobium-doped titanium dioxide nanorods ($\text{TiO}_2\text{-OA-Nb}$) is close to that of the Ti/Nb ratio of the reagents used in the reaction to prepare the nanorods when niobium (V) ethoxide (NBEO) was used as the starting material and a reaction time of 24 h. However, when niobium isopropoxide (NNBIO) was used as starting material, the Ti/Nb ratio in the resultant FA4-1 and FA4-2 nanorods is much higher than that of the starting Ti/Nb ratio, probably due to the fact that the rate of hydrolysis of NNBIO is much lower than that of titanium isopropoxide (TTIP). The nanorods FA4-8, prepared using NBEO as niobium precursor and a reaction time of 72 h, exhibit a much higher Ti/Nb ratio (115.8:1) than that (45:1) of the starting materials, which suggests that a long reaction time reaction leads to a lower uptake of niobium in the titanium dioxide nanorods.

The XPS spectra for the 3d niobium for 3d 5/2 and 3d 3/2 and 2p titanium for 2p 5/2 and 2p 3/2 peaks taken for the oleic acid-stabilised, niobium-doped titanium dioxide nanorods ($\text{TiO}_2\text{-}$

OA-Nb) FA4-3 – FA4-6 with different niobium concentrations, as well as the non-doped, oleic acid-stabilised titanium dioxide nanorods (TiO₂-OA) FA3-1, are shown in figures 4-8 and 4-9. In addition, figure 4-10 shows the relative concentrations of niobium (V) wt% and titanium (III) wt%, determined using XPS analysis, for the oleic acid-stabilised, niobium-doped titanium dioxide nanorods (TiO₂-OA-Nb) FA4-3 – FA4-6 and the non-doped, oleic acid-stabilised titanium dioxide nanorods (TiO₂-OA) FA3-1.

The binding energy position and elemental concentration of Ti (IV), Ti (III), Nb (V) and Nb (IV), for the oleic acid-stabilised, niobium-doped, titanium dioxide nanorods (TiO₂-OA-Nb) FA4-3 – FA4-6 and the non-doped, oleic acid-stabilised, titanium dioxide nanorods (TiO₂-OA) FA3-1 are listed in table 4-7. The binding energy position and elemental concentration of O 1s, Ti 2p, C1s, Nb 3d and N 1s, for the oleic acid-stabilised, niobium-doped, titanium dioxide nanorods (TiO₂-OA-Nb) FA4-3 – FA4-6 and the non-doped, oleic acid-stabilised, titanium dioxide nanorods (TiO₂-OA) FA3-1 are listed in table 4-8.

The binding energy peak of the Ti 2p doublet with 2p_{3/2} and 2p_{1/2} are 458.43 eV and 464.14 eV, respectively, for the FA4-3 – FA4-6 oleic acid-stabilised, niobium-doped titanium dioxide nanorods (TiO₂-OA-Nb) and the FA3-1 non-doped, oleic acid-stabilised titanium dioxide nanorods (TiO₂-OA).⁵ The spin-orbit splitting of the Ti 2p_{3/2} and Ti 2p_{1/2} peaks is about 5.70 eV, suggesting that the titanium is mostly present as Ti⁴⁺, which matches with the atomic concentrations of Ti (IV), 96.36 %, and Ti (III), 3.64 %. This behaviour is very similar for the other the FA4-3 – FA4-6 oleic acid-stabilised, niobium-doped, anatase titanium dioxide nanorods (TiO₂-OA-Nb).

The Ti 2p spectra for the niobium doped TiO₂ samples displaying two peaks at 458.43 and 464.14 eV, for the FA4-3 nanorods, for example, are related to Ti⁴⁺. On the other hand, two weak peaks at 456.44 and 462.14 eV, for the FA4-3 nanorods, for example, are related to Ti³⁺. In addition, a modification of the oxidation state of TiO₂ might have occurred due to spin-orbit splitting of 2P_{1/2} and 2P_{3/2} electron bands of titanium ⁶. The shape of the Ti 2p excludes the existence of more than trace amounts of Ti²⁺ and Ti⁰, which are separated from the Ti⁴⁺ peak by about 3-4 eV ⁷. In addition, the Nb 3d spectra for the oleic acid-stabilised, niobium-doped titanium dioxide nanorods (TiO₂-OA-Nb) displaying two peaks at 206.88 and 209.58 eV, for FA4-3 as example, are related to Nb⁵⁺. On the other hand, two weak peaks at 205.88 and 208.58 eV, for FA4-3 as example, are related to Nb⁴⁺. The peaks represent the Nb 3d_{5/2} and Nb 3d_{3/2} modules ⁸, respectively. The centre of the Nb 3d_{3/2} peak matches to that of Nb⁵⁺ oxidation state ⁹.

The replacement of Ti^{4+} with Nb^{5+} changes one of the nearby Ti^{4+} ions into Ti^{3+} . The concentration of Ti^{3+} increases with the increasing of Nb^{5+} amount in the samples, as shown in figure 4-10. However, the amount of Nb^{5+} is much higher than that of Ti^{3+} , suggesting the presence of some oxygen vacancies to maintain charge equilibrium ¹⁰.

Solutions containing up to 10 % of oleic acid-stabilised, niobium-doped, anatase titanium dioxide nanorods (TiO_2 -OA-Nb) FA4-1 – FA4-8 in organic solvents, such as chlorobenzene products are shown in figure 4-11.

Table 4-6: Chemical analysis of the oleic acid-stabilised, niobium-doped titanium dioxide nanorods (TiO_2 -OA-Nb) FA4-1 – FA4-8.

Sample	Nb precursor	Ti/Nb (reaction)	Time h	Ti %	C %	H %	N %	Nb %	Ti/Nb (product)
FA4-1	NBIO	9:1	72	41.1	19.14	3.05	0.34	1.07	74.5:1
FA4-2	NBIO	18:1	72	44.1	21.24	3.3	0.49	1.1	77.8:1
FA4-3	NBEO	9:1	24	39.2	18.78	3.00	0.63	8.02	9.48:1
FA4-4	NBEO	9:1	72	37.5	19.05	2.97	0.67	7.12	10.22:1
FA4-5	NBEO	18:1	24	39.5	18.87	2.94	0.53	5.60	13.68:1
FA4-6	NBEO	18:1	72	39.7	21.2	3.35	0.60	4.20	18.33:1
FA4-7	NBEO	45:1	24	43.9	20.62	3.18	0.54	1.72	49.5:1
FA4-8	NBEO	45:1	72	40.6	23.44	3.76	0.51	0.68	115.8:1

NBIO = Niobium isopropoxide; NBEO = Niobium (V) ethoxide.

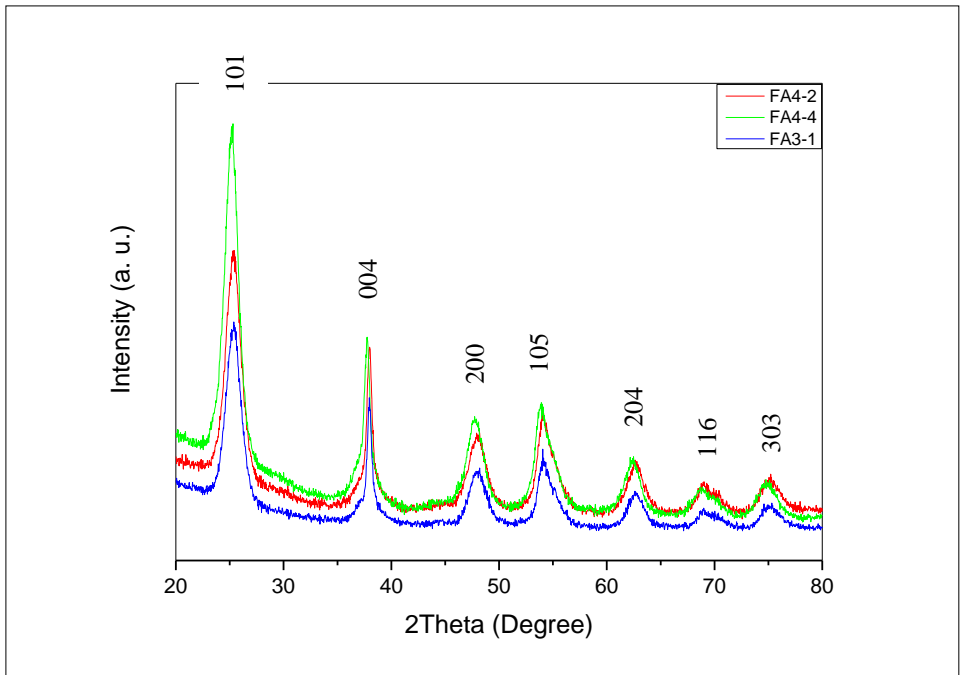


Figure 4-1: XRD patterns of the oleic acid-stabilised, niobium-doped titanium dioxide nanorods ($\text{TiO}_2\text{-OA-Nb}$) FA4-2 and FA4-4 and the non-doped, oleic acid-stabilised titanium dioxide nanorods ($\text{TiO}_2\text{-OA}$) FA3-1.

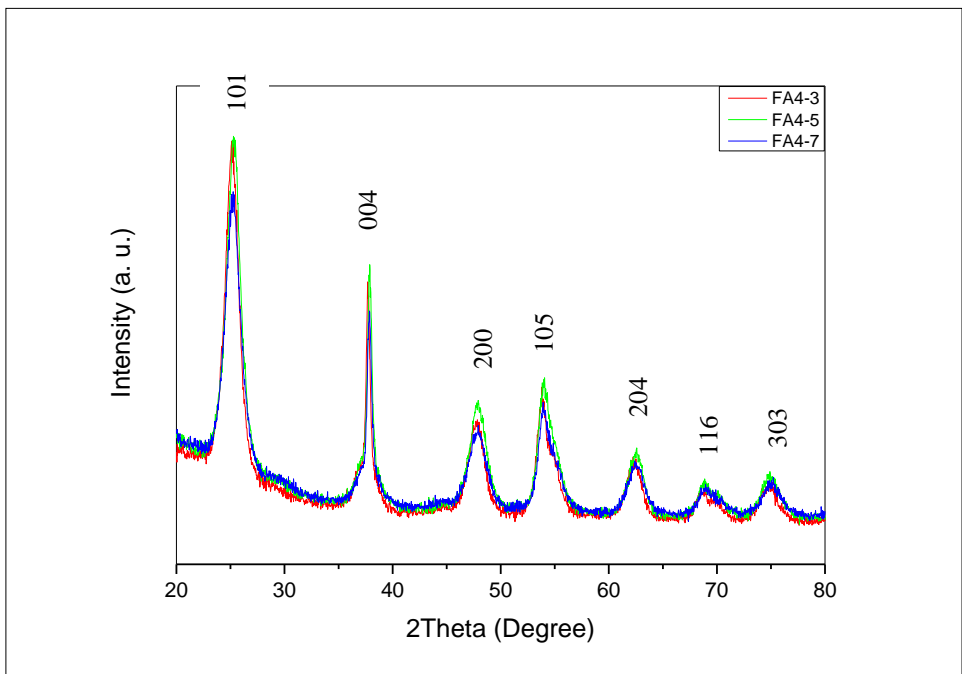


Figure 4-2: XRD patterns of the oleic acid-stabilised, niobium-doped titanium dioxide nanorods ($\text{TiO}_2\text{-OA-Nb}$) FA4-3, FA4-5 and FA4-7.

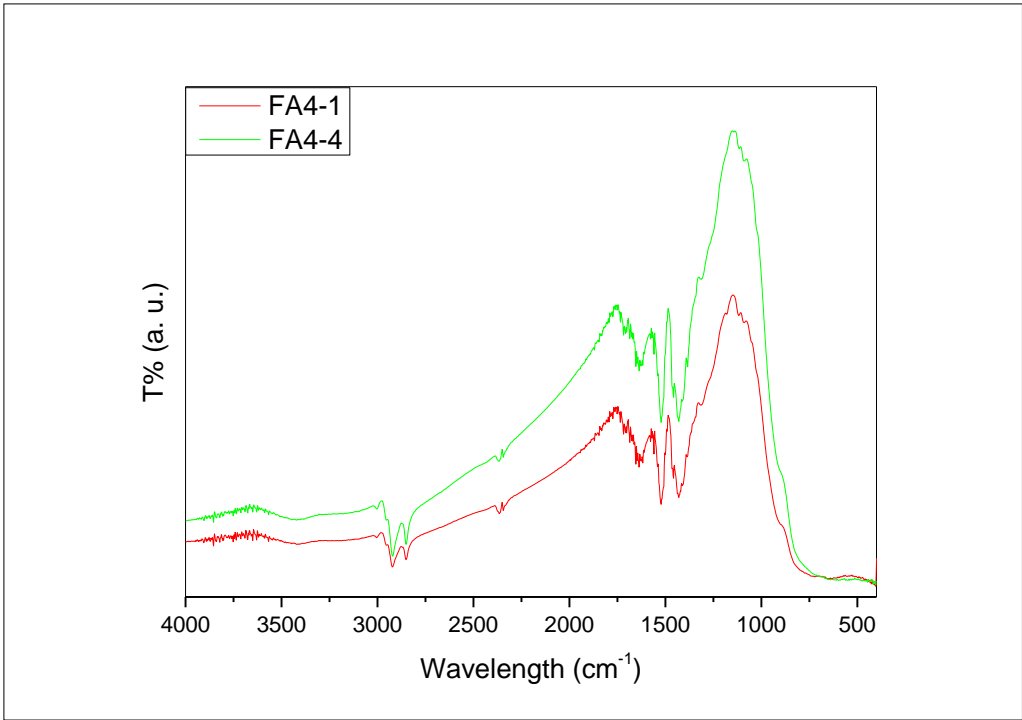


Figure 4-3: FT-IR patterns of the oleic acid-stabilised, niobium-doped titanium dioxide nanorods (TiO₂-OA-Nb) FA4-1 and FA4-4.

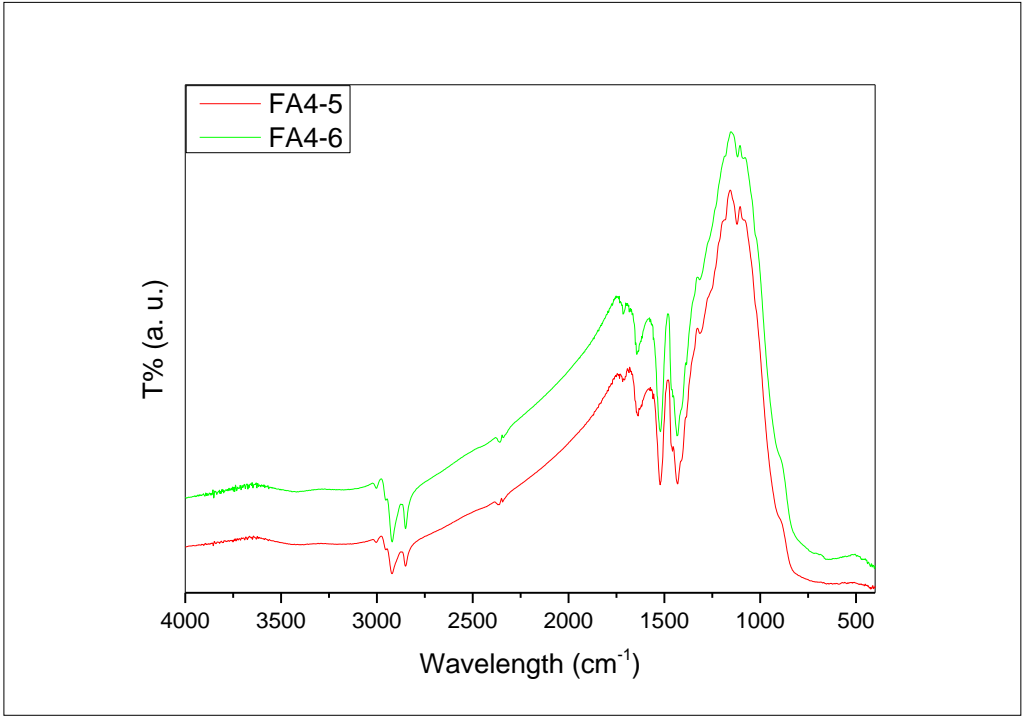


Figure 4-4: FT-IR patterns of the oleic acid-stabilised, niobium-doped titanium dioxide nanorods (TiO₂-OA-Nb) FA4-5 and FA4-6.

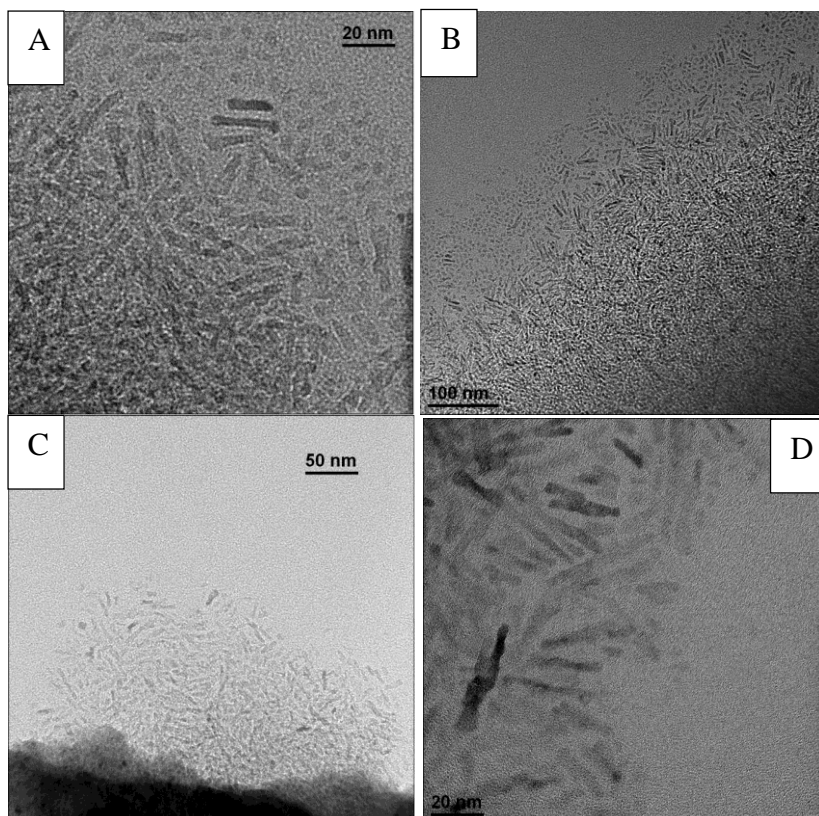


Figure 4-5: TEM images of the oleic acid-stabilised, niobium-doped titanium dioxide nanorods ($\text{TiO}_2\text{-OA-Nb}$), FA4-1 (A), FA4-2 (B), FA4-3 (C) and FA4-4 (D).

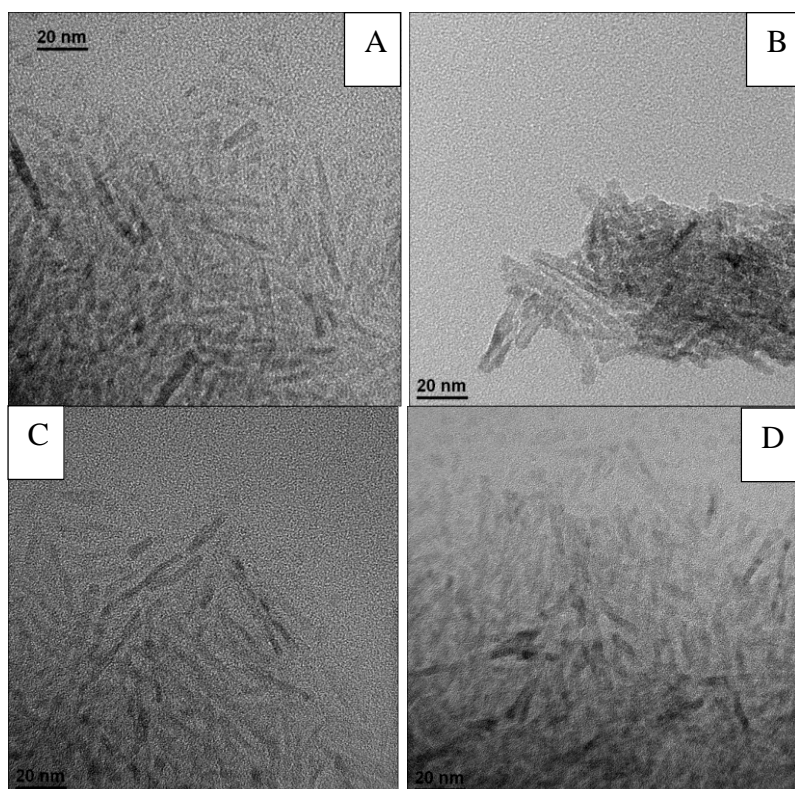


Figure 4-6: TEM images of the oleic acid-stabilised, niobium-doped titanium dioxide nanorods ($\text{TiO}_2\text{-OA-Nb}$) FA4-5 (A), FA4-6 (B), FA4-7 (C) and FA4-8 (D).

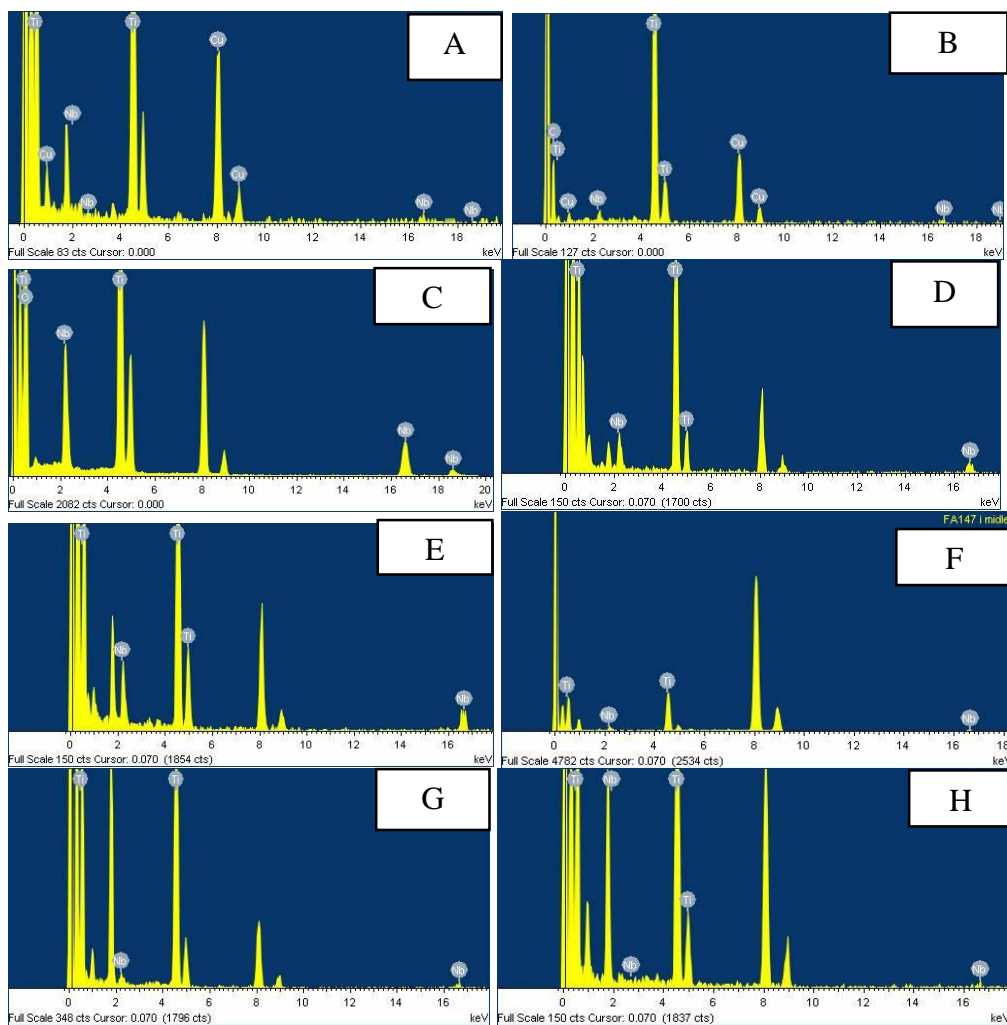


Figure 4-7: EDX results of the oleic acid-stabilised, niobium-doped titanium dioxide nanorods ($\text{TiO}_2\text{-OA-Nb}$) FA4-1 (A), FA4-2 (B), FA4-3 (C), FA4-4 (D), FA4-5 (E), FA4-6 (F), FA4-7 (G) and FA4-8 (H).

Table 4-7: The binding energy position (eV) and elemental concentration (%) for Ti (IV), Ti (III), Nb (V) and Nb (IV) ions present in the non-doped, oleic acid-stabilised titanium dioxide nanorods (TiO₂-OA) FA3-1 and the oleic acid-stabilised, niobium-doped titanium dioxide nanorods (TiO₂-OA-Nb) FA4-3 – FA4-6.

Sample	Ti (IV)		Ti (III)		Nb (V)		Nb (IV)	
	eV	%	eV	%	eV	%	eV	%
FA3-1	458.35	65.35	456.35	1.33	---	---	---	---
	464.05	32.66	462.05	0.66	---	---	---	---
FA4-3	458.43	64.25	456.44	2.43	206.88	53.02	205.88	7.02
	464.14	32.11	462.14	1.21	209.58	35.29	208.58	4.67
FA4-4	458.43	64.33	456.43	2.35	206.90	53.49	205.88	6.55
	464.13	32.15	462.13	1.17	209.60	35.6	208.58	4.36
FA4-5	458.48	64.68	462.17	3.00	206.88	54.8	205.88	5.24
	464.18	36.86	456.48	1.00	209.58	36.47	208.58	3.49
FA4-6	458.40	54.80	456.40	1.80	206.88	55.38	205.88	4.66
	464.10	36.47	462.10	0.90	209.58	36.86	208.58	3.10

Table 4-8: The binding energy position (eV) and elemental concentration (%) for O 1s, Ti 2p, C 1s, Nb 3d and N 1s of the non-doped, oleic acid-stabilised titanium dioxide nanorods (TiO₂-OA) FA3-1 and the oleic acid-stabilised, niobium-doped titanium dioxide nanorods (TiO₂-OA-Nb) FA4-3 – FA4-6.

Sample	O 1s		Ti 2p		C 1s		Nb 3d		N 1s	
	eV*	%**	eV	%	eV	%	eV	%	eV	%
FA3-1	529.6	27.84	458.4	11.83	284.6	58.5	---	---	398.2	1.82
FA4-3	529.8	30.75	458.5	11.64	284.6	54.89	206.9	1.84	400.8	0.88
FA4-4	529.8	30.15	458.5	10.85	284.6	56.26	207.0	1.74	401.4	1.01
FA4-5	529.7	32.46	458.4	12.26	284.6	52.62	207.0	1.42	339.6	1.23
FA4-6	529.7	29.32	458.4	11.14	284.6	57.34	206.8	0.94	402.0	1.25

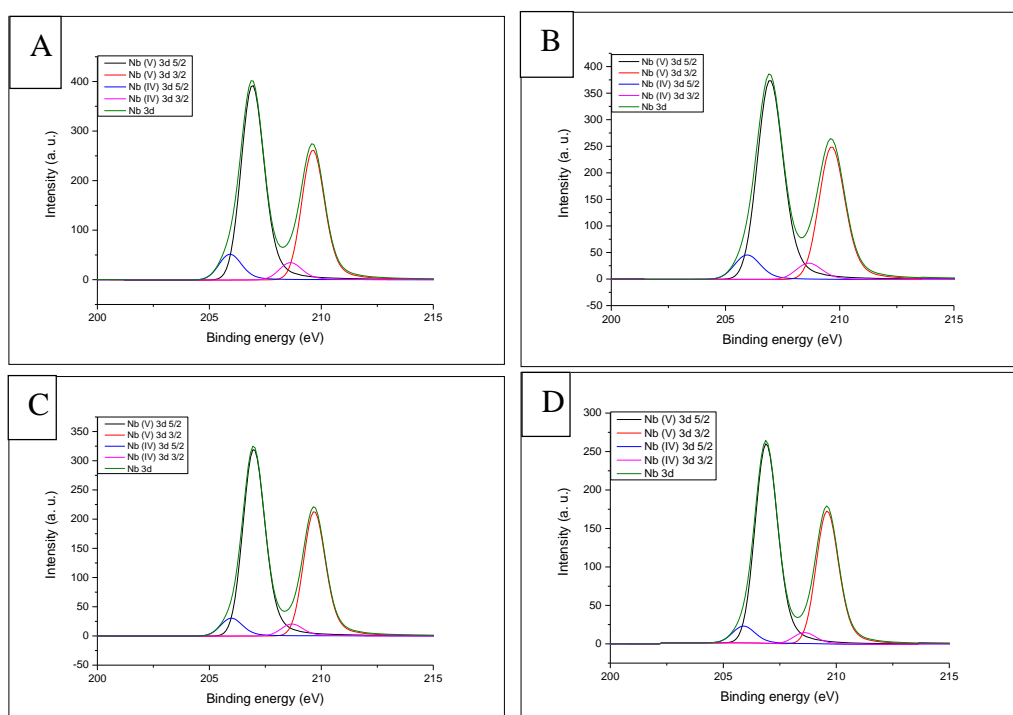


Figure 4-8: XPS data for Nb 3d spectra (3d_{5/2} and 3d_{3/2}) of the oleic acid-stabilised, niobium-doped, anatase titanium dioxide nanorods (TiO₂-OA-Nb), (A) FA4-3, (B) FA4-4, (C) FA4-5 and (D) FA4-6.

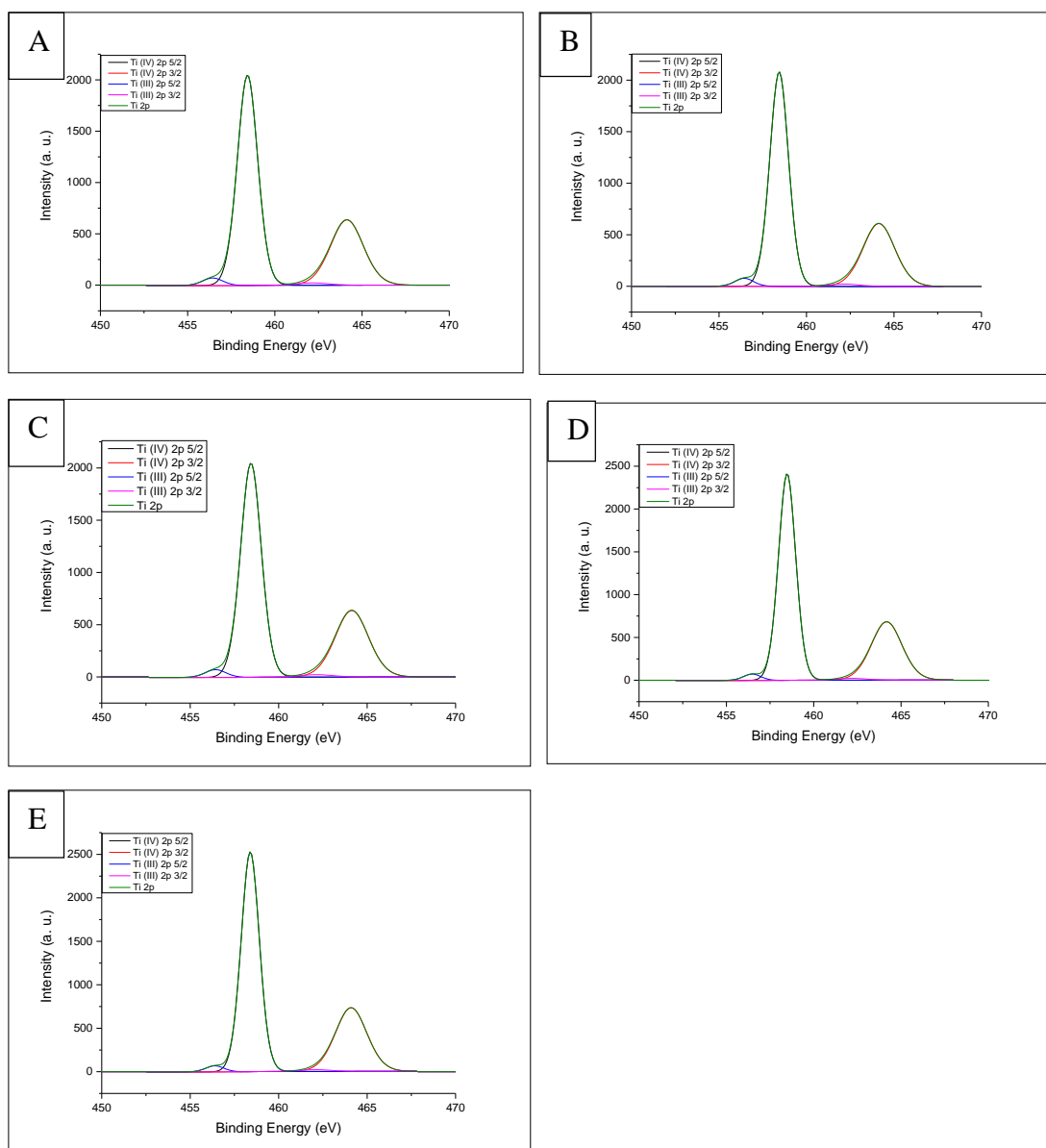


Figure 4-9: XPS data for Ti 2p spectra (2p 5/2 and 2p 3/2) of the oleic acid-stabilised, niobium-doped, anatase titanium dioxide nanorods (TiO₂-OA-Nb), (A) FA3-1 (B) FA4-3, (C) FA4-4, (D) FA4-5 and (E) FA4-6.

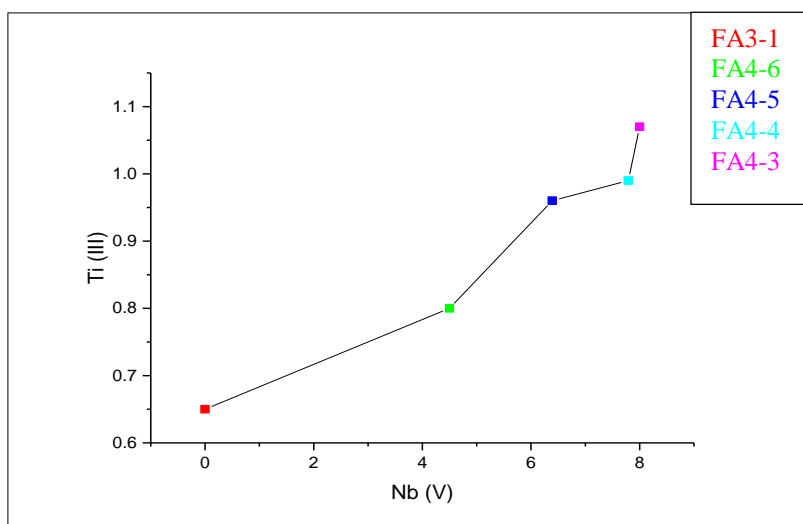


Figure 4-10: Proportion between Nb (IV) wt. % (XPS) and Ti (III) wt. % (XPS) for non-doped, oleic acid-stabilised titanium dioxide nanorods ($\text{TiO}_2\text{-OA}$) FA3-1 and the oleic acid-stabilised, niobium-doped titanium dioxide nanorods ($\text{TiO}_2\text{-OA-Nb}$) FA4-3 – FA4-6.

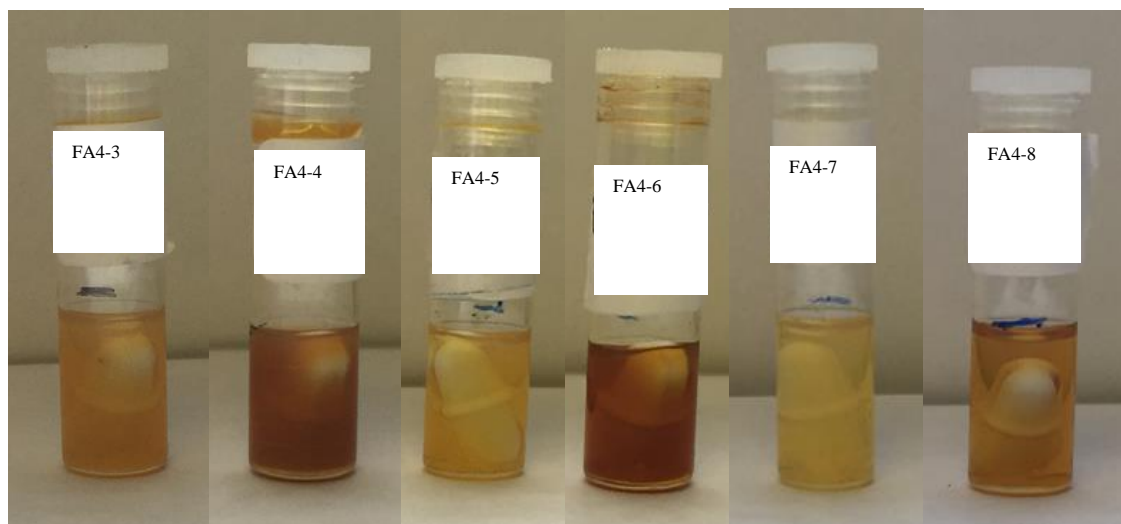


Figure 4-11: Solutions of the oleic acid-stabilised, niobium-doped titanium dioxide nanorods ($\text{TiO}_2\text{-OA-Nb}$) FA4-3, (NBEO, 9:1, 24 h), FA4-4, (NBEO, 9:1, 72 h), FA4-5, (NBEO, 18:1, 24 h), FA4-6, (NBEO, 18:1, 72 h) FA4-7, (NBEO, 45:1, 24 h), and FA4-8, (NBEO, 45:1, 72 h).

Characterisation of the Ligand Exchanged Products the Niobium Doped Anatase Titanium Dioxide Nanorods TiO₂-Nb

The ligand-exchanged products of the ligand-stabilised, niobium-doped, titanium dioxide nanorods (TiO₂-DEPPNA-Nb) FA4-10 and (TiO₂-ODPA-Nb) FA4-9 and FA4-11 - FA4-15 derived from ligand exchange reactions between oleic acid-stabilised, niobium-doped anatase titanium dioxide nanorods (TiO₂-OA-Nb) FA4-1 - FA4-6 and diethyl 2-phenylethyl phosphonate (DEPPNA) and octadecylphosphonic acid (ODPA), respectively, are collated in table 4-9.

The XRD patterns of the OPDA-stabilised, niobium-doped titanium dioxide nanorods (TiO₂-ODPA-Nb) FA4-11 and FA4-13 – FA4-15 are shown in figure 4-12. The anatase phase has been retained in the OPDA-stabilised products FA4-11 and FA4-13 – FA4-15 after the ligand exchange process.¹¹ No niobium peaks can be observed probably due to the low concentration of niobium or the presence of amorphous niobium metal nanoclusters.

The FT-IR patterns of the ligand exchanged products of the ligand-stabilised, niobium-doped, titanium dioxide nanorods (TiO₂-DEPPNA-Nb) FA4-10 and (TiO₂-ODPA-Nb) FA4-9 and FA4-11 - FA4-15 derived from ligand exchange reactions between oleic acid-stabilised niobium doped anatase titanium dioxide nanorods (TiO₂-OA-Nb) FA4-1 - FA4-6 and diethyl 2-phenylethyl phosphonate (DEPPNA) and octadecylphosphonic acid (ODPA), respectively, are shown in figures 4-13 and 4-14.

The intensities of the two peaks at 1525 and 1430 cm⁻¹ for the ligand-stabilised, niobium-doped, titanium dioxide nanorods (TiO₂-DEPPNA-Nb) FA4-10, shown in figure 4-13, have decreased and there is a new peak appeared at 1040 cm⁻¹ compared to the FT-IR spectrum of the corresponding oleic acid-stabilised, niobium-doped, titanium dioxide nanorods (TiO₂-OA-Nb) FA4-10. The peak at 1040 cm⁻¹ can be related to stretching band of P-O, which indicates that part of the monolayer of oleic acid in oleic acid-stabilised, niobium-doped, titanium dioxide nanorods (TiO₂-OA-Nb) FA4-10 has been replaced by the DEPPNA ligand.^{12, 13}

The FT-IR spectra of ODPA-stabilised, niobium-doped titanium dioxide (TiO₂-ODPA-Nb) FA4-9 and FA4-11 - FA4-15, shown in figures 4-13 and 4-14, exhibit a P=O double bond vibration at 1226 cm⁻¹ and a P-O-H absorption peak at 940 m⁻¹. However, these two bands are not present in all the ODPA-exchanged products. A broad band attributable to the PO₃ stretching vibration is observed at about 1065 cm⁻¹ for the ODPA-stabilised, niobium-doped, titanium dioxide (TiO₂-ODPA-Nb) FA4-9 and FA4-11 - FA4-15. These FT-IR absorption

spectra indicate that the ODPa ligand has indeed been attached to surface of the TiO₂ nanorods through tridentate bonding mode in the ligand exchange reactions.¹⁴

The TEM images of the ODPa-stabilised, niobium-doped titanium dioxide nanorods (TiO₂-ODPa-Nb) FA4-13 (A-B) prepared by a ligand exchange reaction using the oleic acid-stabilised, niobium-doped titanium dioxide nanorods (TiO₂-OA-Nb) FA4-5 (C-D) are shown in figure 4-15. It is clear to see that there is no difference in the size and shape of the oleic acid-stabilised starting materials FA4-5 and the resultant ODPa-stabilised products FA4-13.

The chemical analysis of the ligand-stabilised, niobium-doped titanium dioxide nanorods (TiO₂-DEPPNA-Nb) FA4-10 and (TiO₂-ODPa-Nb) FA4-9 and FA4-11 - FA4-15 derived from ligand exchange reactions between oleic acid-stabilised niobium doped titanium dioxide nanorods (TiO₂-OA-Nb) FA4-1 - FA4-6 and diethyl 2-phenylethyl phosphonate (DEPPNA) and octadecylphosphonic acid (ODPa), respectively, are collated in table 4-9. The titanium content in all the ligand-exchanged samples FA4-11 - FA4-15 is lower than that of the oleic acid-stabilised starting (TiO₂-OA-Nb) materials FA4-1 - FA4-6. The carbon content is also lower in the ligand-exchanged samples FA4-11 - FA4-15 is lower than that of the oleic acid-stabilised starting (TiO₂-OA-Nb) materials FA4-1 - FA4-6 as the DEPPNA and ODPa ligands contain less carbon atoms than oleic acid. There is a slight change in Ti/Nb ratios when using NBIO as niobium source. On the other hand, there is a big change in Ti/Nb ratios when using NBEO as the source of niobium. The phosphorous content of the ligand-stabilised, niobium-doped titanium dioxide nanorods (TiO₂-DEPPNA-Nb) FA4-10 is lower than that of the ODPa-stabilised, niobium-doped titanium dioxide nanorods (TiO₂-ODPa-Nb) FA4-9 and FA4-11 - FA4-15 due to the almost complete replacement of the oleic acid monolayer by a corresponding layer of ODPa.

Up to 10 % of the ODPa-stabilised, niobium-doped titanium dioxide nanorods (TiO₂-ODPa-Nb) FA4-9 and FA4-11 - FA4-15 can be dissolved in organic solvents, *e.g.*, chlorobenzene, as shown in figure 4-18 for FA4-9, FA4-12 and FA4-13.

Table 4-9: Chemical analysis of the ligand-stabilised, niobium-doped, anatase titanium dioxide nanorods (TiO₂-DEPPNA-Nb) FA4-10 and (TiO₂-ODPA-Nb) FA4-9 and FA4-11 - FA4-15 derived from ligand exchange reactions between oleic acid-stabilised niobium doped anatase titanium dioxide nanorods (TiO₂-OA-Nb) FA4-1 - FA4-6 and diethyl 2-phenylethyl phosphonate (DEPPNA) and octadecylphosphonic acid (ODPA), respectively.

Sample	Starting material Ti/Nb ratio	Ligands	Ti %	C %	H %	Nb %	P %	Ti/Nb ratio
FA4-9	FA4-1/74.5:1	ODPA	40.71	23.46	4.1	1.02	2.41	77.41:1
FA4-10	FA4-1/74.5:1	DEPPNA	43.36	18.7	2.66	1.14	0.5	73.77:1
FA4-11	FA4-2/77.8:1	ODPA	37.4	23.34	3.95	1.35	2.37	53.73:1
FA4-12	FA4-6/18.33:1	ODPA	34.1	23.33	4.04	8.8	2.17	7.52:1
FA4-13	FA4-5/13.68:1	ODPA	32.34	21.56	3.72	6.78	2.53	9.25:1
FA4-14	FA4-4/10.22:1	ODPA	34.9	25.38	4.44	3.4	3.1	19.91:1
FA4-15	FA4-3/9.48:1	ODPA	35.8	21.99	3.79	4.6	2.6	15.10:1

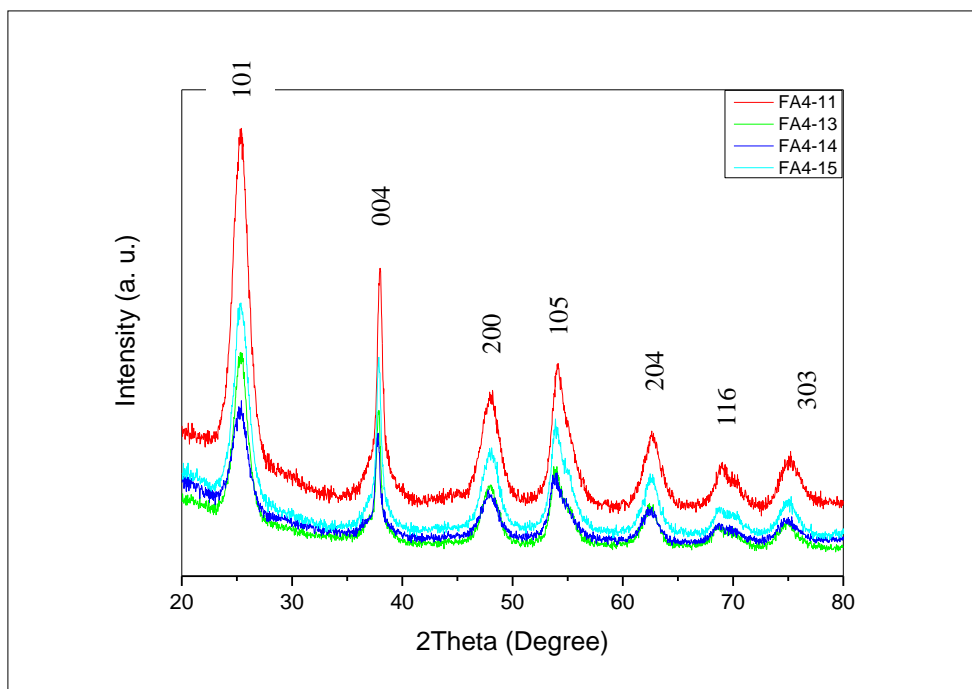


Figure 4-12: XRD patterns of the ODPA-stabilised, niobium-doped titanium dioxide nanorods ($\text{TiO}_2\text{-ODPA-Nb}$) FA4-11 and FA4-13 - FA4-15.

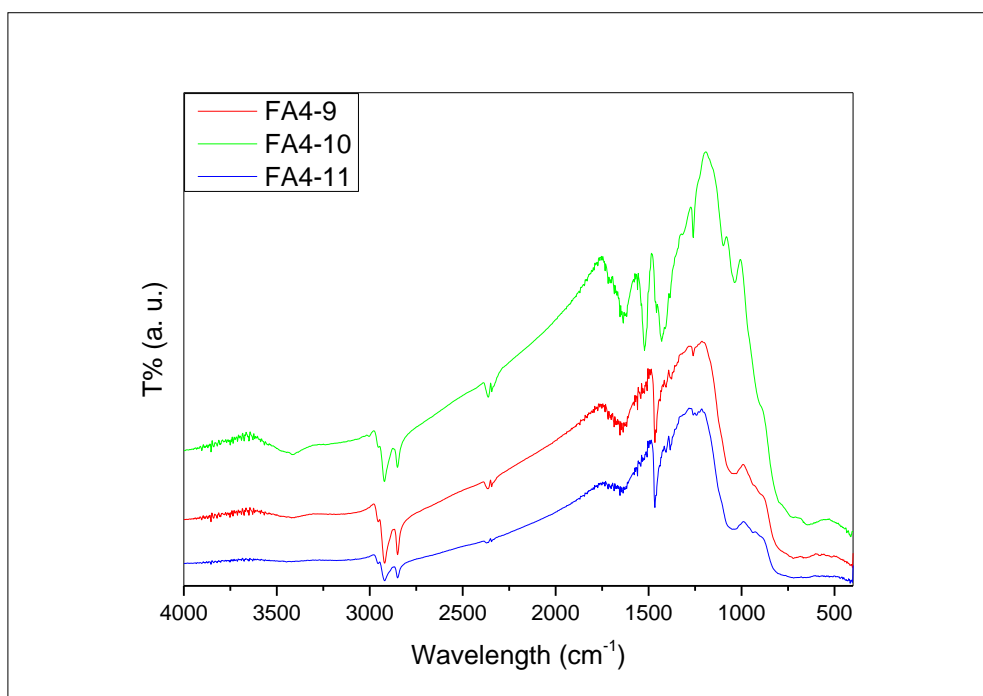


Figure 4-13: FT-IR patterns of the DEPPNA-stabilised, niobium-doped titanium dioxide nanorods ($\text{TiO}_2\text{-DEPPNA-Nb}$) FA4-10 and the ODPA-stabilised, niobium-doped titanium dioxide nanorods ($\text{TiO}_2\text{-ODPA-Nb}$) FA4-9 and FA4-11.

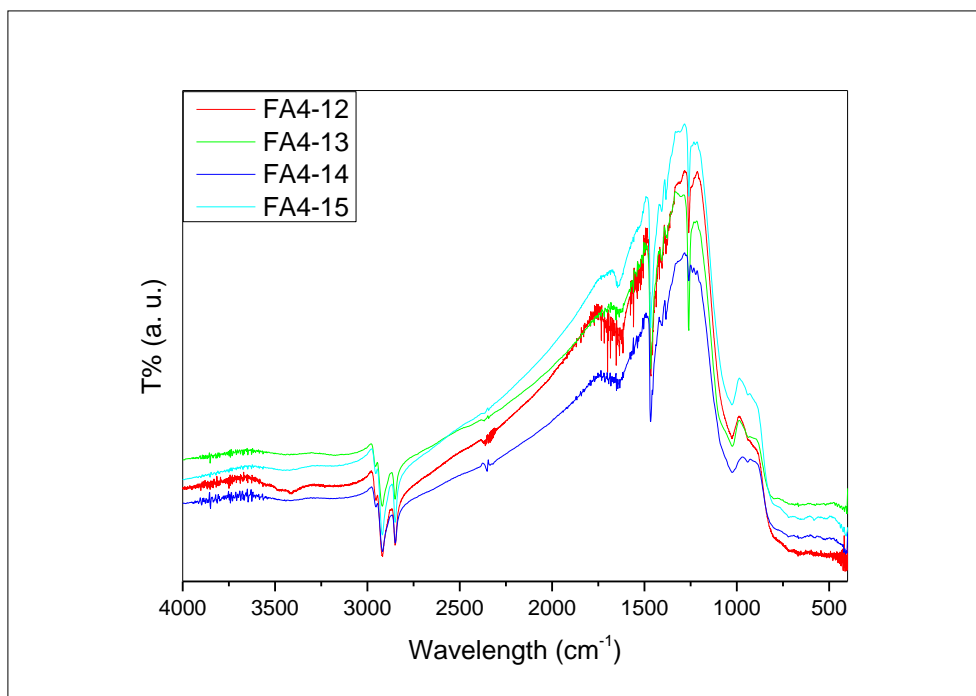


Figure 4-14: FT-IR patterns of the OPDA-stabilised, niobium-doped titanium dioxide nanorods ($\text{TiO}_2\text{-OPDA-Nb}$) FA4-12 - FA4-15.

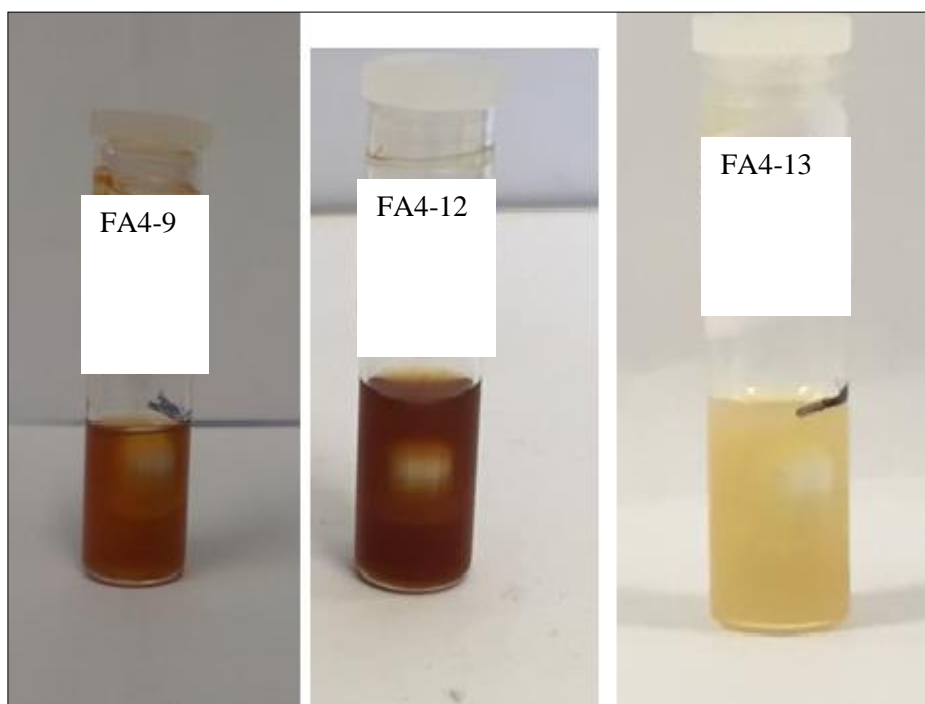


Figure 4-16: Solutions of the ligand exchanged products of the ODPA-stabilised, niobium-doped titanium dioxide nanorods ($\text{TiO}_2\text{-ODPA-Nb}$) FA4-9, FA4-12 and FA4-13 in chlorobenzene.

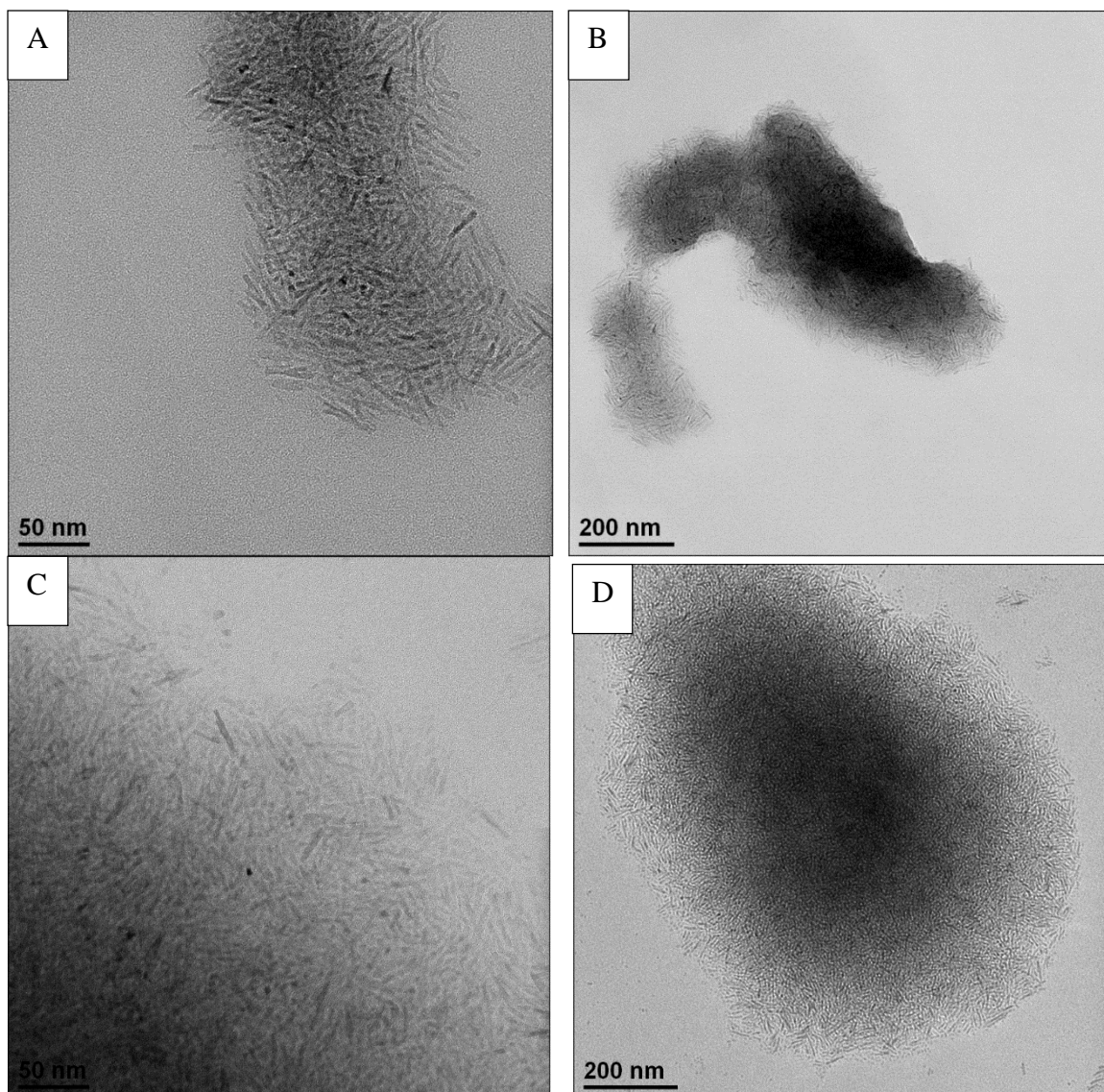


Figure 4-15: TEM images of the ODPA-stabilised, niobium-doped titanium dioxide nanorods ($\text{TiO}_2\text{-ODPA-Nb}$) FA4-13 (A-B) prepared by a ligand exchange reaction using the oleic acid-stabilised, niobium-doped titanium dioxide nanorods ($\text{TiO}_2\text{-OA-Nb}$) FA4-5 (C-D).

Characterisation of Solution-Processable, Oleic Acid-Stabilised, Indium-Doped, Anatase Titanium Dioxide Nanorods (TiO₂-In)

The reaction conditions for the synthesis of the oleic acid-stabilised, indium-doped titanium dioxide nanorods (TiO₂-OA-In) FA4-16 and FA4-17 are shown in table 4-10.

The XRD patterns of the oleic acid-stabilised, indium-doped titanium dioxide nanorods (TiO₂-OA-In) FA4-16 and FA4-17 are shown in figure 4-17. It can be noticed that only anatase phase can be observed in all samples.¹¹ No indium peaks can be observed probably due to small amount of niobium contents or presence of amorphous indium nanoclusters.

The FT-IR patterns of the oleic acid-stabilised, indium-doped titanium dioxide nanorods (TiO₂-OA-In) FA4-16 and FA4-17 are shown in figure 4-18. The peaks at 2850, 2920 and 2955 cm⁻¹ are associated with the stretch vibrations of C-H₃, C-H₂ and C-H attributable to the oleic acid bonded on the surface of the nanorods (TiO₂-OA-In) FA4-16 and FA4-17. In addition, the broad stretching vibration at 3465 cm⁻¹ suggests the presence of some hydroxyl groups (OH⁻) attached to the surface of the titanium dioxide nanorods (TiO₂-OA-In) FA4-16 and FA4-17. Furthermore, the two strong peaks at 1525 and 1430 cm⁻¹ are related to COO⁻ anti-symmetric and symmetric stretching vibrations bonded on the surface, respectively, of the (TiO₂-OA-In) FA4-16 and FA4-17^{3,4}, suggesting that oleic acid has bonded on the surface of the nanorods (TiO₂-OA-In) FA4-16 and FA4-17.

The TEM images of the oleic acid-stabilised, indium-doped titanium dioxide nanorods (TiO₂-OA-In) FA4-16 and FA4-17 shown in figure 4-19 reveal that the TiO₂ nanorods (TiO₂-OA-In) FA4-16 and FA4-17 are ca 20 nm in length and 3-4 nm in diameter.

The results of elemental analyses of the oleic acid-stabilised, indium-doped titanium dioxide nanorods (TiO₂-OA-In) FA4-16 and FA4-17 are shown in table 4-10. It can be seen that the titanium content is about 39% in both samples. In addition, the carbon content is 22.3% and 26.04% for FA4-16 and FA4-17, respectively. Furthermore, the Ti/In ratio in the nanorods (TiO₂-OA-In) FA4-16 and FA4-17 is very high (136:1 and 82:1) compared to that of the starting material Ti/In ratio (9:1) in the reactions to prepare both samples suggesting that some indium may have been lost during the reaction or the purification process.

The oleic acid-stabilised, indium-doped, anatase titanium dioxide nanorods (TiO₂-OA-In) FA4-16 and FA4-17 can be dissolved in organic solvents, *e.g.* chlorobenzene, up to a concentration of 10 %, as shown in figure 4-20.

Table 4-10: Chemical analysis of the oleic acid-stabilised, indium-doped titanium dioxide nanorods (TiO₂-OA-In) FA4-16 and FA4-17.

Sample	In precursor	Ti/Nb (start)	Ti%	C%	H%	N%	In%	Ti/In
FA4-16	INIO	9:1	39.5	22.3	3.47	0.4	0.7	136:1
FA4-17	INEO	9:1	38.9	26.04	3.95	0.63	1.18	82:1

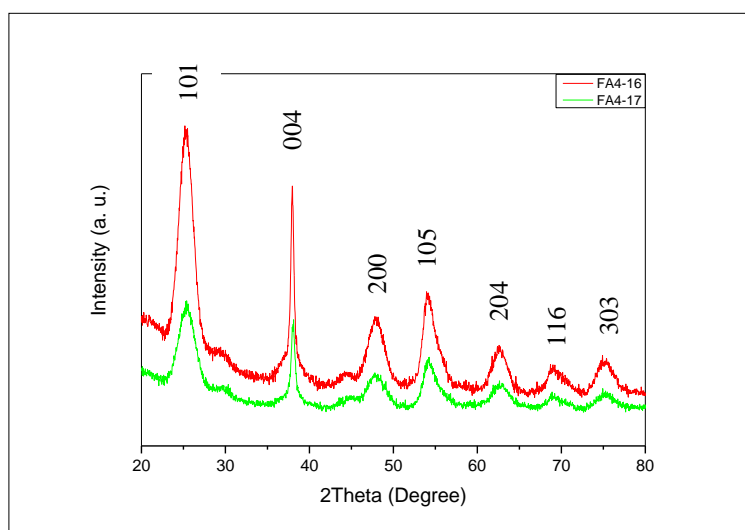


Figure 4-17: XRD patterns of the oleic acid-stabilised, indium-doped titanium dioxide nanorods (TiO₂-OA-In) FA4-16 and FA4-17.

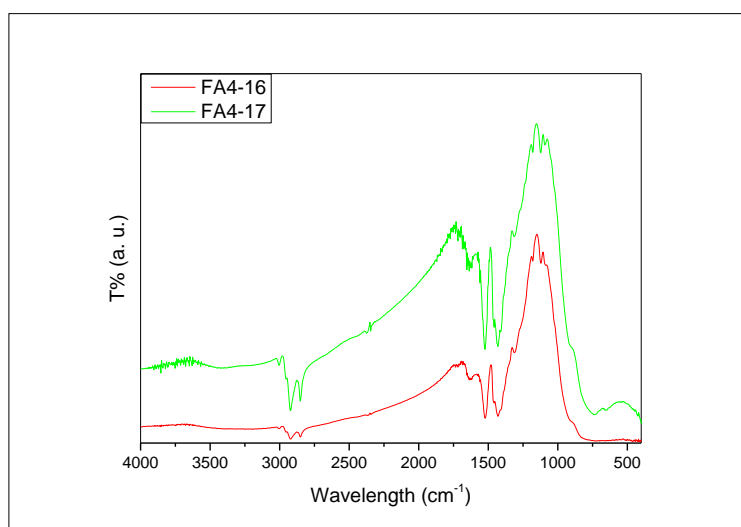


Figure 4-18: FT-IR patterns of the oleic acid-stabilised, indium-doped titanium dioxide nanorods (TiO₂-OA-In) FA4-16 and FA4-17.

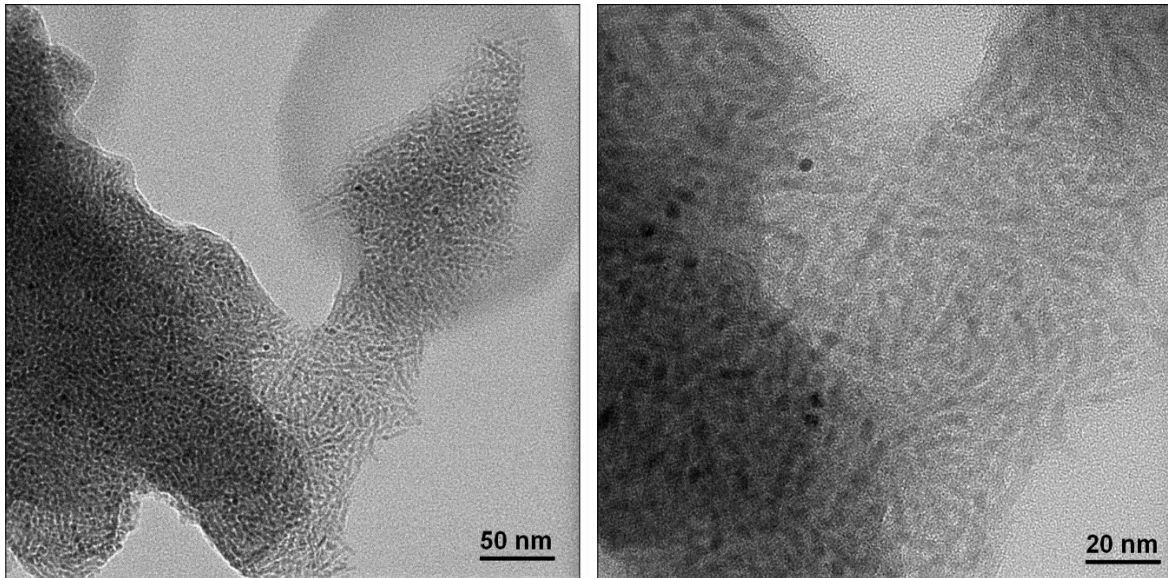


Figure 4-19: TEM images of the oleic acid-stabilised, indium-doped titanium dioxide nanorods ($\text{TiO}_2\text{-OA-In}$) FA4-16.

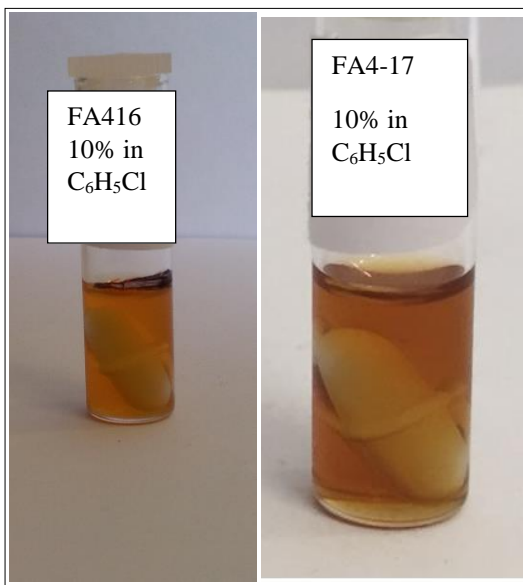


Figure 4-20: Solutions of the oleic acid-stabilised, indium-doped titanium dioxide nanorods ($\text{TiO}_2\text{-OA-In}$) FA4-16 and FA4-17.

Characterisation of the Oleic Acid-Stabilised, Niobium/Indium-Doped Anatase Titanium Dioxide Nanorods (TiO₂-OA-Nb/In)

The reaction conditions for the synthesis of the oleic acid-stabilised, niobium/indium-doped titanium dioxide nanorods (TiO₂-OA-Nb/In) FA4-18 are shown in table 4-11.

The XRD pattern of the oleic acid-stabilised, niobium/indium-doped titanium dioxide nanorods (TiO₂-OA-Nb/In) FA4-18 is shown in figure 4-21. Only anatase phase can be observed in the XRD pattern of the TiO₂-Nb/In sample.¹¹ No niobium peaks can be observed probably due to small amount of niobium/indium contents or presence of amorphous niobium/indium.

The FT-IR pattern of the oleic acid-stabilised, niobium/indium-doped titanium dioxide nanorods (TiO₂-OA-Nb/In) FA4-18 is shown in figure 4-22. Two strong absorption peaks at 1525 and 1430 cm⁻¹ are related to COO⁻ anti-symmetric and symmetric stretching vibrations, respectively, of carboxyl-groups bonded to the surface of the oleic acid-stabilised, niobium/indium-doped titanium dioxide nanorods (TiO₂-OA-Nb/In) FA4-18.^{3,4} The peaks at 2850, 2920 and 2955 cm⁻¹ are associated with stretch vibrations of C-H₃, C-H₂ and C-H groups of the oleic acid attached to the surface of the oleic acid-stabilised, niobium/indium-doped titanium dioxide nanorods (TiO₂-OA-Nb/In) FA4-18. The broad stretching absorption band at 3465 cm⁻¹ suggests that some hydroxyl (OH) groups are also attached to the surface of the oleic acid-stabilised, niobium/indium-doped titanium dioxide nanorods (TiO₂-OA-Nb/In) FA4-18.

The TEM images of the oleic acid-stabilised, niobium/indium-doped titanium dioxide nanorods (TiO₂-OA-Nb/In) FA4-18, shown in figure 4-23, reveal nanorods of 20 nm in length and 3-4 nm in diameter.

The chemical composition of the oleic acid-stabilised, niobium/indium-doped titanium dioxide nanorods (TiO₂-OA-Nb/In) FA4-18 is shown in table 4-11. The Ti/Nb and Ti/In ratios in the oleic acid-stabilised, niobium/indium-doped titanium dioxide nanorods (TiO₂-OA-Nb/In) FA4-18 are 90:1 and 150:1, respectively, much lower than the Ti/Nb and Ti/In (9:1) ratios of the starting materials.

Up to 10 % of the oleic acid-stabilised, niobium/indium-doped titanium dioxide nanorods (TiO₂-OA-Nb/In) FA4-18 can dissolved in organic solvents, *e.g.* chlorobenzene, as shown in figure 4-24.

Table 4-11: Chemical analysis of the oleic acid-stabilised, niobium/indium-doped titanium dioxide nanorods (TiO₂-OA-Nb/In) FA4-18.

Sample	Starting product Ti/In*	Ti %	C %	H %	N %	Nb %	In %	Product Ti/Nb	Ti/In
FA4-18	9:1	42.9	20.8	3.26	0.37	0.9	0.71	90:1	150:1

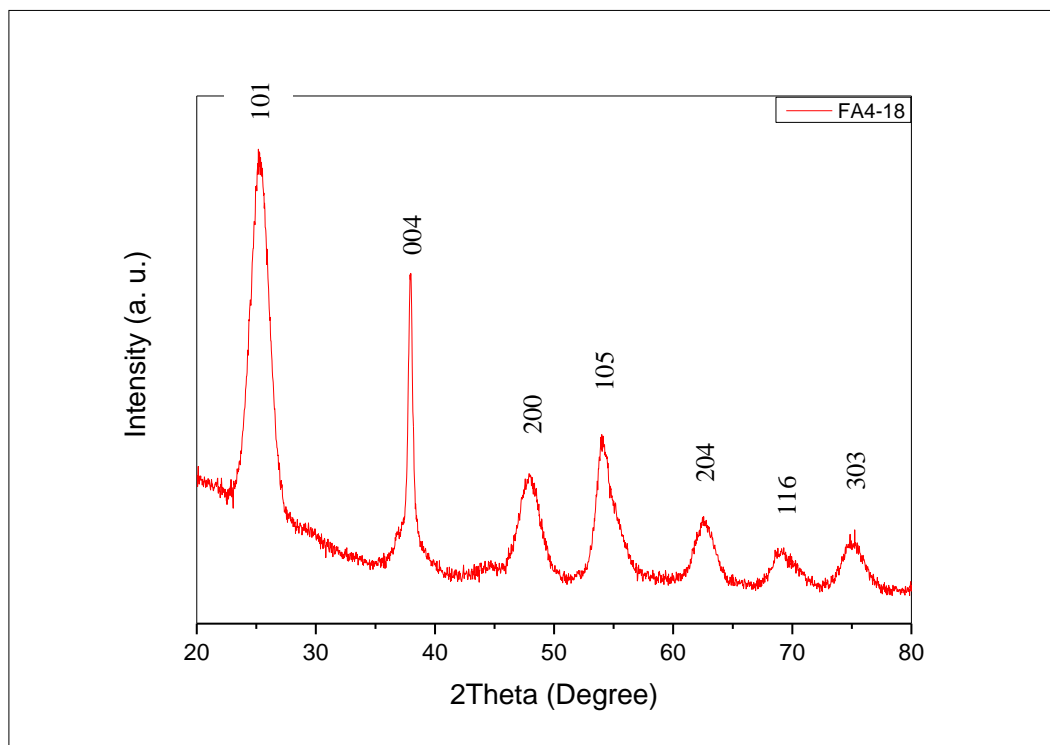


Figure 4-21: XRD pattern of the oleic acid-stabilised, niobium/indium-doped titanium dioxide nanorods (TiO₂-OA-Nb/In) FA4-18.

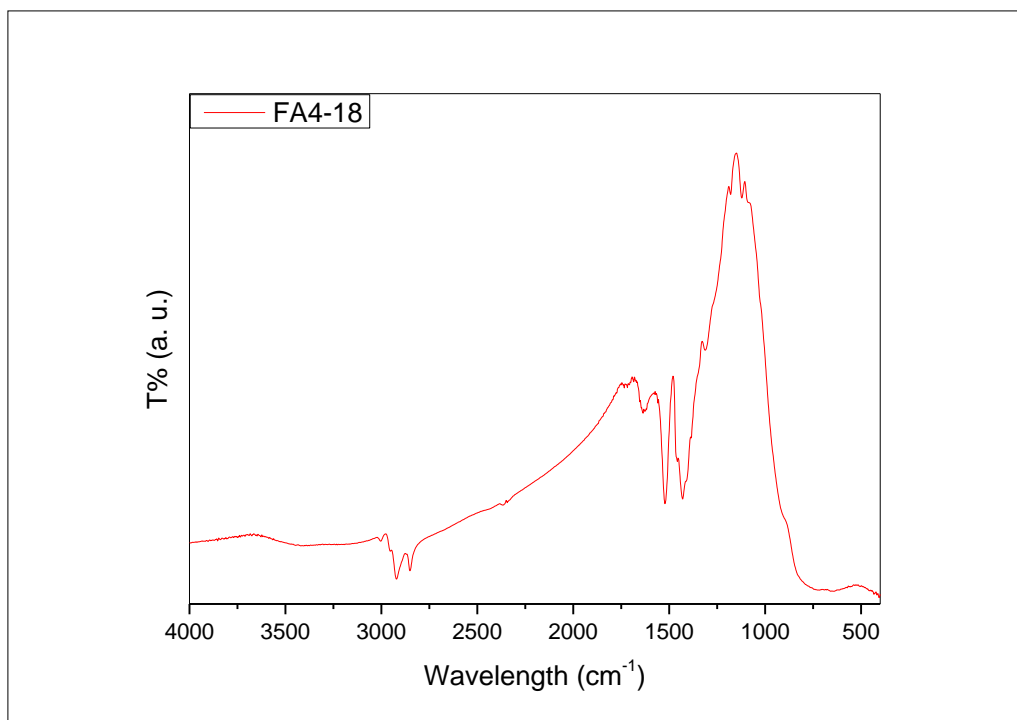


Figure 4-22: FT-IR pattern of the oleic acid-stabilised, niobium/indium-doped titanium dioxide nanorods (TiO₂-OA-Nb/In) FA4-18.

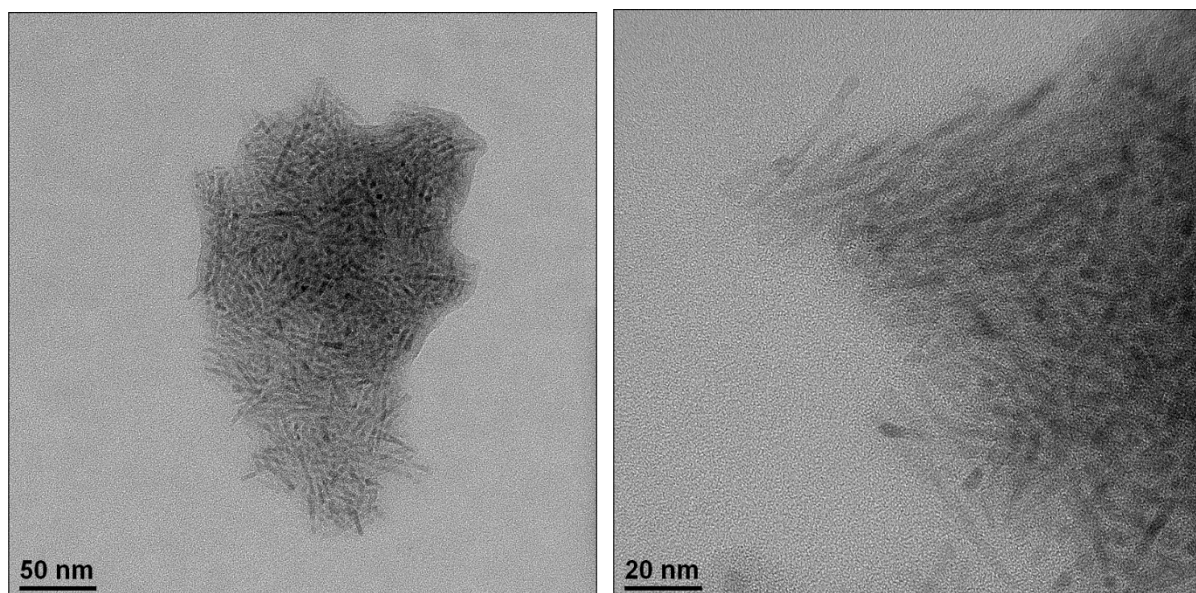


Figure 4-23: TEM images of the oleic acid-stabilised, niobium/indium-doped titanium dioxide nanorods (TiO₂-OA-Nb/In) FA4-18.

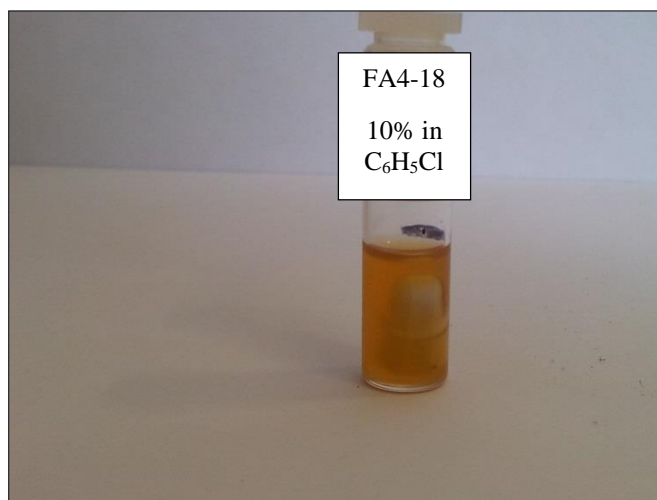


Figure 4-24: Solution of the oleic acid-stabilised, niobium/indium-doped titanium dioxide nanorods ($\text{TiO}_2\text{-OA-Nb/In}$) FA4-18 in chlorobenzene.

Characterisation of the Ligand-Exchanged Niobium/Indium-Doped Anatase Titanium Dioxide Nanorods ($\text{TiO}_2\text{-L-Nb/In}$)

The reaction conditions for the synthesis of the ODPA-stabilised, niobium/indium-doped titanium dioxide nanorods ($\text{TiO}_2\text{-ODPA-Nb/In}$) FA4-19 and the DEPPNA-stabilised, niobium/indium-doped titanium dioxide nanorods ($\text{TiO}_2\text{-DEPPNA-Nb/In}$) FA4-20, prepared by ligand exchange reactions of the oleic acid-stabilised, niobium/indium doped titanium dioxide nanorods ($\text{TiO}_2\text{-OA-Nb/In}$) FA4-18 using octadecylphosphonic acid (ODPA) and diethyl 2-phenylethyl phosphonate (DEPPNA) used as ligands, respectively, are shown in table 4-12.

The XRD patterns of the ODPA-stabilised, niobium/indium-doped titanium dioxide nanorods ($\text{TiO}_2\text{-ODPA-Nb/In}$) FA4-19 and the DEPPNA-stabilised, niobium/indium-doped titanium dioxide nanorods ($\text{TiO}_2\text{-DEPPNA-Nb/In}$) FA4-20 are shown in figure 4-25. No niobium and indium peaks can be observed probably due to small amount of niobium/indium contents or the presence of amorphous niobium/indium nanoclusters.

The FT-IR patterns of the ODPA-stabilised, niobium/indium-doped titanium dioxide nanorods ($\text{TiO}_2\text{-ODPA-Nb/In}$) FA4-19 and the DEPPNA-stabilised, niobium/indium-doped titanium dioxide nanorods ($\text{TiO}_2\text{-DEPPNA-Nb/In}$) FA4-20 are shown in figure 4-26. The FT-IR spectrum of the ODPA-stabilised, niobium/indium-doped titanium dioxide nanorods ($\text{TiO}_2\text{-ODPA-Nb/In}$) FA4-19 shows a P=O double bond valence vibration at 1226 cm^{-1} and a P-O-H absorption band at 940 m^{-1} . A broad band attributable to a PO_3 stretching vibration is

observed at about 1065 cm^{-1} . The FT-IR spectrum suggests that the ODPa ligand has been attached on TiO_2 surface through a tridentate bonding mode.¹⁴ The two peaks at 1525 and 1430 cm^{-1} present in the FT-IR spectrum of the oleic acid-stabilised, niobium/indium doped titanium dioxide nanorods ($\text{TiO}_2\text{-OA-Nb/In}$) FA4-18 are not observed in the corresponding FT-IR spectrum of the ODPa-stabilised, niobium/indium-doped titanium dioxide nanorods ($\text{TiO}_2\text{-ODPA-Nb/In}$) FA4-19, which indicates that all of the oleic acid monolayer has been replaced by ODPa in the ligand-exchange reaction.

The DEPPNA-stabilised, niobium/indium-doped titanium dioxide nanorods ($\text{TiO}_2\text{-DEPPNA-Nb/In}$) FA4-20 exhibit two peaks at 1525 and 1430 cm^{-1} with a lower intensity than that of the starting material, i.e., oleic acid-stabilised, niobium/indium doped titanium dioxide nanorods ($\text{TiO}_2\text{-OA-Nb/In}$) FA4-18. The new peak at 1040 cm^{-1} can be related to a stretching vibration of P-O, which indicates that part of the oleic acid in oleic acid-stabilised, niobium/indium doped titanium dioxide nanorods ($\text{TiO}_2\text{-OA-Nb/In}$) FA4-18 has been replaced by the DEPPNA ligand.^{12, 13}

The results of elemental analysis of ligand exchange products of the ODPa-stabilised, niobium/indium-doped titanium dioxide nanorods ($\text{TiO}_2\text{-ODPA-Nb/In}$) FA4-19 and the DEPPNA-stabilised, niobium/indium-doped titanium dioxide nanorods ($\text{TiO}_2\text{-DEPPNA-Nb/In}$) FA4-20 are shown in table 4-12. The titanium content for ligand-stabilised nanorods FA4-19 and FA4-20, are lower (35.6% and 39.9%, respectively) than that (42.9%) of the starting material, i.e., the oleic acid-stabilised, niobium/indium doped titanium dioxide nanorods ($\text{TiO}_2\text{-OA-Nb/In}$) FA4-18. The niobium and indium content is also lower. The phosphorous concentration of the ODPa-stabilised, niobium/indium-doped titanium dioxide nanorods ($\text{TiO}_2\text{-ODPA-Nb/In}$) FA4-19 is higher than that of the DEPPNA-stabilised, niobium/indium-doped titanium dioxide nanorods ($\text{TiO}_2\text{-DEPPNA-Nb/In}$) FA4-20 due to the fact that ODPa has completely replaced the oleic acid monolayer on the surface of the nanorods ($\text{TiO}_2\text{-OA-Nb/In}$) FA4-18.

Up to 10 % of the ligand exchanged products of niobium/indium doped anatase titanium dioxide nanorods $\text{TiO}_2\text{-Nb/In}$ with octadecylphosphonic acid (ODPA), FA4-19, and diethyl 2-phenylethyl phosphonate (DEPPNA), FA4-20, can dissolve in organic solvents, e.g. chlorobenzene, as shown in figure 4-27.

Table 4-12: Chemical analysis of the ODP A-stabilised, niobium/indium-doped titanium dioxide nanorods (TiO₂-ODPA-Nb/In) FA4-19 and the DEPPNA-stabilised, niobium/indium-doped titanium dioxide nanorods (TiO₂-DEPPNA-Nb/In) FA4-20, prepared by ligand-exchange reactions of the oleic acid-stabilised, niobium/indium doped titanium dioxide nanorods (TiO₂-OA-Nb/In) FA4-18 using octadecylphosphonic acid (ODPA) and diethyl 2-phenylethyl phosphonate (DEPPNA) used as ligands, respectively.

Sample	Start Material	Ligands	Ti%	C%	H%	N%	Nb%	In%	P%
FA4-19	FA4-18	ODPA	35.6	23.4	4.03	0.33	0.75	0.41	1.98
FA4-20	FA4-18	DEPPNA	39.9	19.7	2.82	0.34	0.82	0.61	0.5

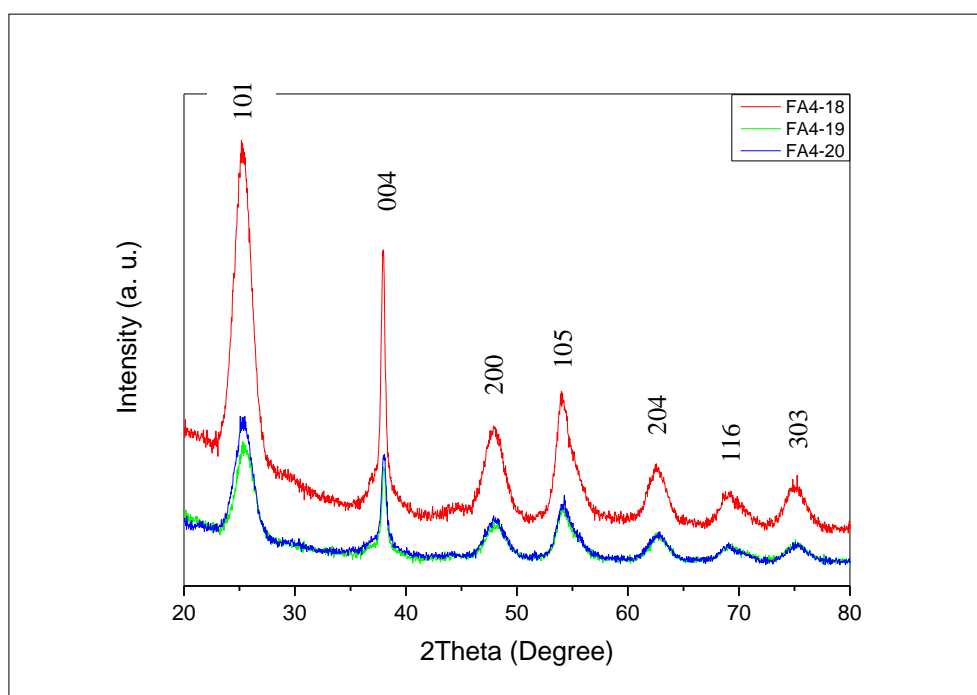


Figure 4-25: XRD patterns of the oleic acid-stabilised, niobium/indium-doped titanium dioxide nanorods (TiO₂-OA-Nb/In) FA4-18, the ODP A-stabilised, niobium/indium-doped titanium dioxide nanorods (TiO₂-ODPA-Nb/In) FA4-19 and the DEPPNA-stabilised, niobium/indium-doped titanium dioxide nanorods (TiO₂-DEPPNA-Nb/In) FA4-20.

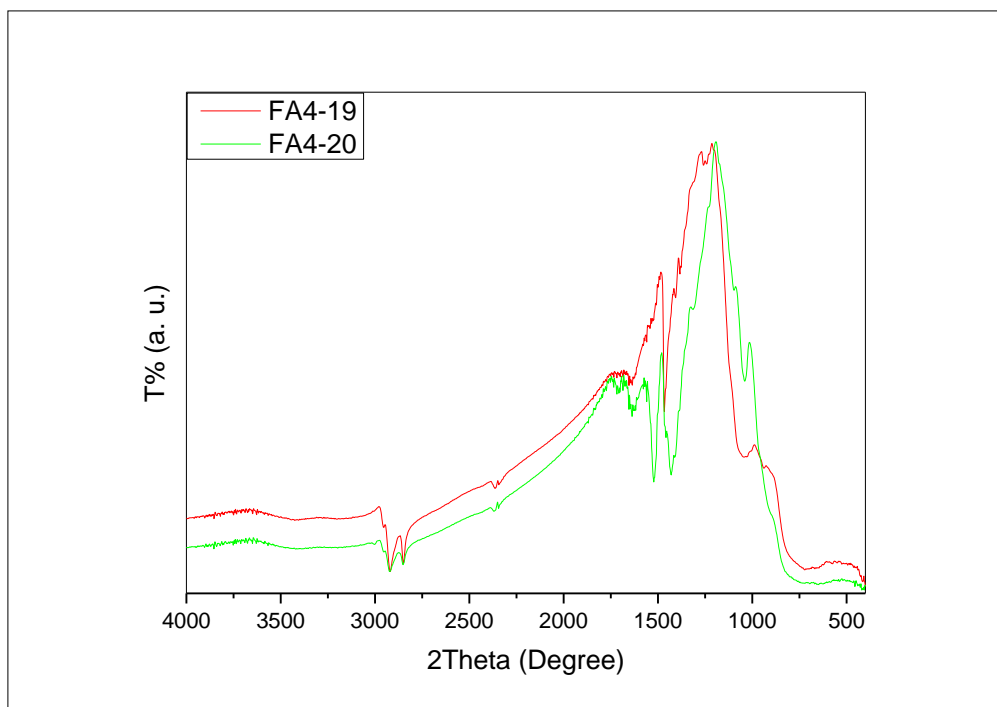


Figure 4-26: FT-IR patterns of the ODPA-stabilised, niobium/indium-doped titanium dioxide nanorods ($\text{TiO}_2\text{-ODPA-Nb/In}$) FA4-19 and the DEPPNA-stabilised, niobium/indium-doped titanium dioxide nanorods ($\text{TiO}_2\text{-DEPPNA-Nb/In}$) FA4-20.

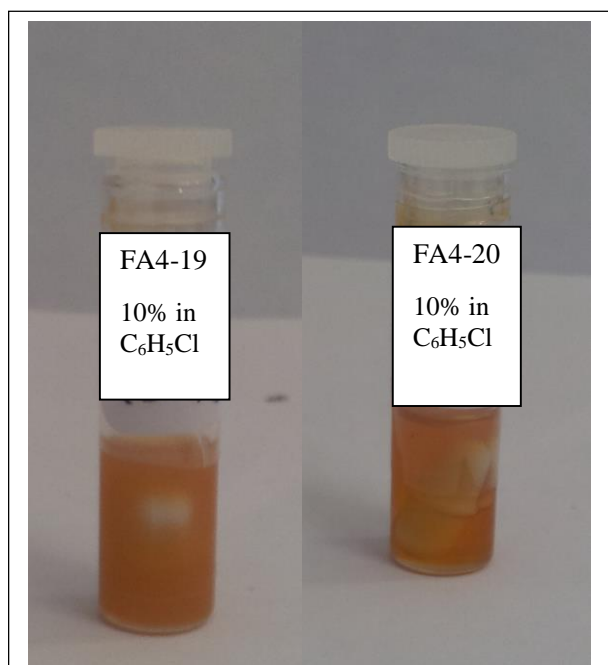


Figure 4-27: Solution of the ODPA-stabilised, niobium/indium-doped titanium dioxide nanorods ($\text{TiO}_2\text{-ODPA-Nb/In}$) FA4-19 and the DEPPNA-stabilised, niobium/indium-doped titanium dioxide nanorods ($\text{TiO}_2\text{-DEPPNA-Nb/In}$) FA4-20 in chlorobenzene.

4.4 Conclusion and Summary

Novel methods for the preparation of solution-processable, ligand-stabilised, metal-doped anatase nanorods ($\text{TiO}_2\text{-L-M}$; L = OA, ODPA or DEPPNA; M = Nb, In or Nb/In) have been developed.

Niobium isopropoxide (NBIO) and niobium (V) ethoxide (NBEO) were used as niobium sources for the preparation of oleic acid-stabilised, niobium-doped nanorods ($\text{TiO}_2\text{-L-M}$; L = OA; M = Nb). The Ti/Nb ratios are close to the starting ratios when using niobium (V) ethoxide (NBEO) as the niobium source. XPS analysis shows that the titanium and niobium anions are present mainly as Ti^{4+} and Nb^{+5} in the oleic acid-stabilised, niobium-doped nanorods ($\text{TiO}_2\text{-OA-Nb}$).

The Ti/In ratios are much higher than that of the starting materials when using indium (III) isopropoxide (INIO) and indium (III) ethoxide (INEO) as an indium source in the synthesis of oleic acid-stabilised, indium-doped nanorods ($\text{TiO}_2\text{-OA-In}$).

XRD analysis shows the formation of anatase TiO_2 phase for all of the oleic acid-stabilised, metal-doped nanorods ($\text{TiO}_2\text{-OA-M}$; M = Nb or In). TEM analysis indicates that the oleic acid-stabilised, metal-doped nanorods ($\text{TiO}_2\text{-OA-M}$; M = Nb or In) are about 20 and 3-4 nm in length and diameter, respectively.

Up to 10% of these oleic acid-stabilised, niobium-doped nanorods ($\text{TiO}_2\text{-OA-M}$; M = Nb or In) can be dissolved in organic solvents, *e.g.* chlorobenzene, commonly used to deposit thin layers of functional materials on substrate surfaces from solution by standard processes, such as drop casting, spin coating, doctor blade techniques, ink-jet printing, *etc.*

Ligand exchange reactions involving the oleic acid-stabilised, metal-doped nanorods ($\text{TiO}_2\text{-L-M}$; L = OA; M = Nb or In) with diethyl 2-phenylethyl phosphonate (DEPPNA) and octadecylphosphonic acid (ODPA) to produce the corresponding ODPA- or DEPPNA-stabilised, metal-doped nanorods ($\text{TiO}_2\text{-L-M}$; L = ODPA or DEPPNA; M = Nb or In) does not lead to a change in the type of phase or the size and shape of the starting nanorods ($\text{TiO}_2\text{-OA-M}$; M = Nb or In). All of the oleic acid on the surface of the oleic acid-stabilised, niobium-doped nanorods ($\text{TiO}_2\text{-OA-Nb}$) has been replaced by ODPA in the ligand-exchange reactions to yield the corresponding ODPA-stabilised, niobium-doped nanorods ($\text{TiO}_2\text{-ODPA-Nb}$). Up to 10% of these ODPA- or DEPPNA-stabilised, metal-doped nanorods ($\text{TiO}_2\text{-L-M}$; L = ODPA or DEPPNA; M = Nb or In) can be dissolved in common organic solvents, such as chlorobenzene, for example.

A mixture of niobium isopropoxide (NBIO) and indium (III) isopropoxide (INIO) were used as niobium and indium sources for the preparation of oleic acid-stabilised, niobium/indium-doped nanorods ($\text{TiO}_2\text{-L-M}$; L = OA; M = Nb/In) in the anatase phase as confirmed by XRD analysis. The concentration of Ti/Nb or Ti/In is much higher in the oleic acid-stabilised, niobium/indium-doped nanorods ($\text{TiO}_2\text{-L-M}$; L = OA; M = Nb/In) compared to those of the starting materials used in the reactions. Up to 10% of these oleic acid-stabilised, niobium/indium-doped nanorods ($\text{TiO}_2\text{-L-M}$; L = OA; M = Nb/In) can be dissolved in organic solvents, such as chlorobenzene.

Ligand exchange reactions of oleic acid-stabilised, niobium/indium-doped nanorods ($\text{TiO}_2\text{-L-M}$; L = OA; M = Nb/In) were carried out using diethyl 2-phenylethyl phosphonate (DEPPNA) and octadecylphosphonic acid (ODPA) as ligands to prepare the corresponding ODPA- or DEPPNA-stabilised, niobium/indium-doped nanorods ($\text{TiO}_2\text{-L-M}$; L = ODPA or DEPPNA; M = Nb/In). There was no change in phase, shape or size of the nanorods as a result of the ligand exchange reactions. All the oleic acid on $\text{TiO}_2\text{-Nb/In}$ surface has been replaced by ODPA in the ODPA-stabilised, niobium/indium-doped nanorods ($\text{TiO}_2\text{-L-M}$; L = ODPA; M = Nb/In). Up to 10% of these ligand-exchanged ODPA- or DEPPNA-stabilised, niobium/indium-doped nanorods ($\text{TiO}_2\text{-L-M}$; L = ODPA or DEPPNA; M = Nb/In) can be readily dissolved in chlorobenzene, for example.

4.5 References

1. Hu, W.; Liu, Y.; Withers, R. L.; Frankcombe, T. J.; Norén, L.; Snashall, A.; Kitchin, M.; Smith, P.; Gong, B.; Chen, H.; Schiemer, J.; Brink, F.; Wong-Leung, J., Electron-pinned defect-dipoles for high-performance colossal permittivity materials. *Nat Mater* **2013**, 12, (9), 821-826.
2. Wei, X.; Zhu, G.; Fang, J.; Chen, J., Synthesis, Characterization, and Photocatalysis of Well-Dispersible Phase-Pure Anatase TiO₂ Nanoparticles. *International Journal of Photoenergy* **2013**, 2013, 6.
3. Thistlethwaite, P. J.; Hook, M. S., Diffuse Reflectance Fourier Transform Infrared Study of the Adsorption of Oleate/Oleic Acid onto Titania. *Langmuir* **2000**, 16, (11), 4993-4998.
4. Thistlethwaite, P. J.; Gee, M. L.; Wilson, D., Diffuse Reflectance Infrared Fourier Transform Spectroscopic Studies of the Adsorption of Oleate/Oleic Acid onto Zirconia. *Langmuir* **1996**, 12, (26), 6487-6491.
5. Ganesh, I.; Gupta, A. K.; Kumar, P. P.; Chandra Sekhar, P. S.; Radha, K.; Padmanabham, G.; Sundararajan, G., Preparation and characterization of Co-doped TiO₂ materials for solar light induced current and photocatalytic applications. *Materials Chemistry and Physics* **2012**, 135, (1), 220-234.
6. Sharma, R. K.; Bhatnagar, M. C.; Sharma, G. L., Mechanism in Nb doped titania oxygen gas sensor. *Sensors and Actuators B: Chemical* **1998**, 46, (3), 194-201.
7. Atashbar, M. Z.; Sun, H. T.; Gong, B.; Wlodarski, W.; Lamb, R., XPS study of Nb-doped oxygen sensing TiO₂ thin films prepared by sol-gel method. *Thin Solid Films* **1998**, 326, (1-2), 238-244.
8. Xu, Z.; Li, Q.; Gao, S.; Shang, J., Synthesis and Characterization of Niobium-doped TiO₂ Nanotube Arrays by Anodization of Ti-20Nb Alloys. *Journal of Materials Science & Technology* **2012**, 28, (10), 865-870.
9. Morris, D.; Dou, Y.; Rebane, J.; Mitchell, C. E. J.; Egdell, R. G.; Law, D. S. L.; Vittadini, A.; Casarin, M., Photoemission and STM study of the electronic structure of Nb-doped TiO₂. *Physical Review B* **2000**, 61, (20), 13445-13457.

10. Gai, Z.; Cheng, Z.; Wang, X.; Zhao, L.; Yin, N.; Abah, R.; Zhao, M.; Hong, F.; Yu, Z.; Dou, S., A colossal dielectric constant of an amorphous TiO₂:(Nb, In) film with low loss fabrication at room temperature. *Journal of Materials Chemistry C* **2014**, 2, (33), 6790-6795.
11. Chen, D.; Huang, F.; Cheng, Y.-B.; Caruso, R. A., Mesoporous Anatase TiO₂ Beads with High Surface Areas and Controllable Pore Sizes: A Superior Candidate for High-Performance Dye-Sensitized Solar Cells. *Advanced Materials* **2009**, 21, (21), 2206-2210.
12. Gao, W.; Dickinson, L.; Grozinger, C.; Morin, F. G.; Reven, L., Self-Assembled Monolayers of Alkylphosphonic Acids on Metal Oxides. *Langmuir* **1996**, 12, (26), 6429-6435.
13. Guerrero, G.; Mutin, P. H.; Vioux, A., Anchoring of Phosphonate and Phosphinate Coupling Molecules on Titania Particles. *Chemistry of Materials* **2001**, 13, (11), 4367-4373.
14. Randon, J.; Blanc, P.; Paterson, R., Modification of ceramic membrane surfaces using phosphoric acid and alkyl phosphonic acids and its effects on ultrafiltration of BSA protein. *Journal of Membrane Science* **1995**, 98, (1-2), 119-129.

Chapter 5
Preparation and
Characterisation of Solution
Processable Rutile TiO₂
Nanorods

5.1 Introduction

In this chapter, three different methods have been developed to prepare nanorods of TiO₂ in the rutile phase. Firstly, a homogenous white precipitate of nanorods of TiO₂ was obtained by using a hydrolysis of TiOCl₂ in presence of water at different temperatures. The second method, a hydrothermal treatment of TiOCl₂ in an acidic medium was investigated. Third method, titanium (IV) chloride (TiCl₄) in aqueous solution was used as a start material in hydrothermal method in presence of amine. All the final products have been characterised and their structure and composition confirmed by a combination of XRD, FT-IR and TEM.

In order to prepare solution-processable nanorods of TiO₂, different surface-modification methods have been investigated to cover and cap the surface of the rutile TiO₂ nanorods with a coating of various organic ligands. Firstly, a modification of dry TiO₂ nanorods with oleic acid (OA) in chlorobenzene was investigated. Secondly, a two-stage treatment of TiO₂ in an acidic medium was studied, using a selection of oleic acid, diethyl 2-phenylethyl phosphonate (DEPPNA), octylphosphonic acid (OPA) and decylphosphonic acid (ODPA). Thirdly, the surface of wet TiO₂ nanorods was modified with a range of oleic acid and a range of amine ligands, *e.g.*, octylamine, dodecylamine and hexadecylamine. A combination of analytical techniques, *i.e.*, XRD, FT-IR, TEM, CHN, TGA and ICP, was used to characterise the resultant products.

In this chapter, each method of synthesis of the nanorods of TiO₂ will be described followed by their subsequent surface modification.

5.2 Experimental

5.2.1 Materials

Titanium (IV) chloride (TiCl₄, %), oleic acid (OA, 90 %), diethyl 2-phenylethyl phosphonate (DEPPNA, 98.0 %), octylphosphonic acid (OPA, 97.0 %), octadecylphosphonic acid (ODPA, 97.0 %), dodecylamine (*n*-C₁₂H₂₃NH₂, 98.0 %), octylamine (*n*-C₈H₁₇NH₂, 70.0 %), hexadecylamine (*n*-C₁₆H₃₃NH₂, 98.0 %) and sodium carbonate (Na₂CO₃, ≥ 99%) were sourced from Sigma-Aldrich. Chlorobenzene, toluene, methanol, ethanol, *N,N*-dimethylformamide, hydrochloric acid, nitric acid were sourced from Fisher. Decylphosphonic acid was synthesised

in cooperation with Dr Fei Cheng. Ultrapure water with a specific resistivity of 18.2 MΩ·cm was obtained by reverse osmosis followed by ion-exchange and filtration (UPQ PS system, ELGA, USA).

5.2.2 Synthesis of Rutile TiO₂ Nanorods

Preparation of Stable Solution of Titanium Oxy Chloride (TiOCl₂)

Titanium (IV) chloride was used as the starting material in all three methods used in this thesis for the preparation of rutile TiO₂ nanorods. TiCl₄ is highly sensitive ¹ to air and water, with which it reacts very rapidly to form a white fumes. Thus, it was converted into a stable solution of TiOCl₂, which is much more stable, shown in equation (5-1). ²



In a typical process, displayed in figure 5-1, TiCl₄ (17.1 g) under an anhydrous atmosphere of nitrogen was slowly transferred by Teflon tube to 35 ml of cooled, distilled-water in an ice bath under constant stirring. Some yellow blocks of the unstable intermediate product TiO(OH)₂ were formed throughout the process. ² After all TiCl₄ had been transferred, more cooled distilled water (79 mL) was added to the reaction mixture, which was stirred at room temperature for several hours to produce a clear solution (0.79 M, 114 mL).

This TiOCl₂ solution was kept in a plastic bottle in the fridge for further use. It can be stable in this state without precipitation even for more than one year.

On the other hand, if a large volume of water is added directly to the TiCl₄, a turbid white suspension is formed by creation of Ti(OH)₄ due to the hydrolysis of the TiCl₄. ^{3,4}



Figure 5-1: A photo of process of transferring titanium (IV) chloride (TiCl₄) to a stable solution of titanium oxychloride (TiOCl₂).

Approach 1: Synthesis of Rutile TiO₂ Nanorods from TiOCl₂ and H₂O (NRs-Rutile-1)

Rutile TiO₂ nanorods (NRs-Rutile-1) were first prepared by elimination of hydrochloric acid from the reaction of titanium oxychloride (TiOCl₂) and water at different temperature, *i.e.*, 50 °C, 70 °C and 90 °C, according to a modified literature method.⁸ Three separate reactions were then carried out in attempts to modify the surface of the TiO₂ nanorods FA5-2 (NRs-Rutile-1), prepared according to Approach 1.

Rutile TiO₂ Nanorods Preparation (NRs-Rutile-1)

In order to prepare nanorods of rutile TiO₂, a pre-prepared TiOCl₂ solution (0.79 M, 5.4 ml) was added to distilled-water (8 ml) under stirring at different temperatures, *i.e.*, 50°C, 70°C and 90°C for 24h. The solution turned cloudy after around 3 h in each case. After the reaction was complete, the reaction mixture was allowed to cool to room temperature. The white precipitate obtained after separation by centrifugation was washed twice with water and then dried overnight in a vacuum oven at 30 °C to yield the rutile TiO₂ nanorods FA5-1, FA5-2 and FA5-3, prepared at 50°C, 70°C or 90°C, respectively.

Surface Modification of Rutile TiO₂ Nanorods (NRs-Rutile-1) with Oleic Acid or Alkyl Amines

Three different, but related surface treatment methods 1-3, were carried out in an attempt to improve the solubility of the rutile TiO₂ nanorods FA5-2 (NRs-Rutile-1) prepared using Approach 1. Each of these treatments involved reactions to coat the surface of the rutile TiO₂ nanorods with as much as possible of an aliphatic coating of oleic acid, various straight-chain, primary *n*-alkyl amines (C_nH_{2n+1}NH₂; n = 8, 12 and 16), see section 5.2.1 Materials and the following sections. The different function groups were chosen to react with the surface of the TiO₂ nanorods, especially in chemical reactions with the free hydroxyl groups (-OH) present on the titanium dioxide surface, in order to produce TiO₂/ligand nanocomposites in the rutile phase.

In surface treatment method 1, the rutile TiO₂ nanorods FA5-2 (NRs-Rutile-1) prepared using Approach 1 with oleic acid in chlorobenzene at either 50 °C or 100 °C, using different quantities of oleic acid and using different reaction times. The main purpose of these reactions is to facilitate the bonding of oleic acid onto the surface of the TiO₂ nanorods to serve two main

purposes: firstly to stabilise the surface of the TiO₂ nanorods FA5-2 (NRs-Rutile-1) and thereby prevent aggregation of the nanorods in the solid state and in solution and secondly to lower the surface polarity and tension and thereby produce soluble rutile TiO₂/OA nanocomposites FA5-4 – FA5-6, which can be dissolved in common organic solvents, such as chlorobenzene.

In surface treatment methods 2 and 3, the rutile TiO₂ nanorods FA5-2 (NRs-Rutile-1) prepared using Approach 1 with ligand, oleic acid or primary *n*-alkyl amines (C_nH_{2n+1}NH₂; n = 8, 12 and 16), in either ethanol or DMF at either 78°C or 120°C for several days. Some of the TiO₂/ligand nanocomposites prepared using surface treatment 2 were then treated again using surface treatment methods 3 in attempts to increase the degree of surface coverage of the TiO₂/ligand nanocomposites. These additional surface treatments served to increase the amount of these TiO₂/ligand nanocomposites that could then be dissolved in organic solvents, such as chlorobenzene, to produce solutions with a concentration high enough, *e.g.*, 10 % to facilitate the deposition of thin uniform layers of the TiO₂/ligand nanocomposites on a substrate surface from solution using methods, such as drop casting, spin casting or even inkjet printing, for example.

Synthesis of Rutile TiO₂/OA Nanocomposites – Surface Treatment Method 1

The required amount of oleic acid was dissolved in a volume of chlorobenzene and the resultant solution was then added to a suspension of the dried powder rutile TiO₂ nanorods FA5-2 (NRs-Rutile-1) of (0.1 g) in chlorobenzene. The reaction mixture was sonicated for 30 min before being heated at either 50 °C or 100 °C under stirring for 3 or 5 days, see table 5-1 for details of the individual reaction conditions. After separation by centrifugation, the resultant solid was washed twice with acetone, centrifuged again to remove any residues of oleic acid and then dried overnight in a vacuum oven at 30°C to yield the desired oleic acid-capped TiO₂/OA nanocomposites FA5-4 - FA5-6 as a white powder.

Table 5-1: Reaction conditions for the surface modification of the rutile TiO₂ nanorods (NRS-Rutile 1) FA5-2, prepared using Approach 1 to yield the desired oleic acid-capped TiO₂/OA nanocomposites FA5-4 - FA5-6 prepared using surface treatment method 1.

Reaction Product	Starting Material	Ligand/g	Reaction Time/days	Solvent /ml	Reaction Temperature/°C
FA5-4	FA5-2	OA/2.5	3	Chlorobenzene/10	50
FA5-5	FA5-2	OA/5.0	5	Chlorobenzene/10	100
FA5-6	FA5-2	OA/15.0	3	Chlorobenzene/20	100

Synthesis of Rutile TiO₂/ligand Nanocomposites – Surface Treatment Method 2

A solution of the desired amounts of oleic acid or primary *n*-alkyl amine ($n\text{-C}_n\text{H}_{2n+1}\text{NH}_2$; $n = 8, 12$ and 16) in ethanol was added to a solution of freshly prepared rutile TiO₂ nanorods FA5-2 (NRs-Rutile-1) but before drying, in ethanol (10 ml). The resultant reaction mixture was heated at either 78 °C or 120 °C for either 6 or 7 days, see table 5-2 for details of the individual reactions. The oleic acid-capped TiO₂/OA nanocomposites FA5-7 - FA5-12 prepared at different reaction times (6 – 10 days) and for different amounts of solvents (20 ml and 35 ml) and the primary *n*-alkyl amine-capped TiO₂/AA nanocomposites FA5-13 – FA5-16, obtained after centrifuge, were washed twice with ethanol and then dried overnight in a vacuum oven at 30 °C, see table 5-2 for details of the reaction conditions for the individual reactions carried out.

Table 5-2: Reaction conditions for the surface modification of the rutile TiO₂ nanorods FA5-2 (NRs-Rutile-1), prepared as described in section 5.2.2.2.1, to yield the desired oleic acid-capped TiO₂/OA nanocomposites FA5-7 - FA5-12 and the primary *n*-alkyl amine-capped TiO₂/AA(12, 12, 8 and 16) nanocomposites FA5-13 – FA5-16, respectively, prepared using surface treatment method 2 under identical reaction conditions.

Reaction Product	Starting Material	Ligand/g	Reaction Time/days	Solvent /ml	Reaction Temperature/°C
FA5-7	FA5-2	OA/8	6	Ethanol/20	78
FA5-8	FA5-2	OA/16	7	Ethanol/20	78
FA5-9	FA5-2	OA/32	7	Ethanol/35	78
FA5-10	FA5-2	OA/32	10	Ethanol/35	78
FA5-11	FA5-2	OA/16	7	DMF/35	120
FA5-12	FA5-2	OA/32	7	DMF/35	120
FA5-13	FA5-2	<i>n</i> -C ₁₂ H ₂₅ NH ₂ /5	7	Ethanol/20	78
FA5-14	FA5-2	<i>n</i> -C ₁₂ H ₂₅ NH ₂ /10	7	Ethanol/20	78
FA5-15	FA5-2	<i>n</i> -C ₈ H ₁₇ NH ₂ /8	7	Ethanol/20	78
FA5-16	FA5-2	<i>n</i> -C ₁₆ H ₃₃ NH ₂ /8	7	Ethanol/20	78

Synthesis of Rutile TiO₂/ligand Nanocomposites – Surface Treatment Method 3

Either rutile TiO₂/OA nanocomposites FA5-8 (dry) and FA5-9 (dry), prepared using surface treatment method 2, or freshly prepared TiO₂/OA nanocomposites FA5-10 (wet) and FA5-14 (dry), prepared using surface treatment method 2, were added a solution of oleic acid or dodecyl amine dissolved in either ethanol or toluene. The resultant reaction mixture was heated at either

78 °C or 125 °C for 3 or 4 days, see table 5-3 for details of the individual reactions. At the end of the reaction, the mixture was cooled to room temperature, centrifuged and then washed twice with ethanol and dried overnight in a vacuum oven at 30 °C to yield the desired doubly oleic acid-capped TiO₂/OAx2 nanocomposites FA5-17, FA5-18 and FA5-20 or the oleic acid- and dodecyl amine-capped TiO₂/OA/AA(12) nanocomposite FA5-19, as a white powder.

Table 5-3: Reaction conditions for the surface modification of the rutile TiO₂/OA nanocomposites FA5-8 (dry) and FA5-9 (dry), prepared using surface treatment method 2, or TiO₂/OA nanocomposites FA5-10 (wet) and FA5-14 (dry), prepared using surface treatment method 2, to yield the doubly oleic acid-capped TiO₂/OAx2 nanocomposites FA5-18, FA5-20 and FA5-17, respectively, or the oleic acid- and dodecyl amine-capped TiO₂/OA/AA(12) nanocomposite FA5-19, respectively, prepared using surface treatment method 3.

Reaction Product	Starting Material	Ligand/g	Reaction Time/days	Solvent /ml	Reaction Temperature/°C
FA5-17	FA5-7/wet	OA/16	3	Ethanol/25	78
FA5-18	FA5-5/dry	OA/16	4	Toluene/30	125
FA5-19	FA5-11/dry	<i>n</i> -C ₁₂ H ₂₅ NH ₂ /5	4	Toluene/35	125
FA5-20	FA5-6/dry	OA/5	4	Toluene/35	125

Approach 2: Hydrothermal Synthesis of Rutile TiO₂ Nanorods from TiOCl₂ (NRs-Rutile-2)

The aim of this reaction, which involves hydrothermal treatment of TiOCl₂ at 220 °C for 2 h, see section 5.2.2.3.1, is to produce TiO₂ nanorods (NRs-Rutile-2) with a more advantageous, i.e., greater, aspect ratio from that achieved using the Approach 1, used to prepare rutile TiO₂ nanorods (NRs-Rutile-1). Surface modification reactions were then carried out in attempts to modify the surface of the TiO₂ nanorods FA5-21 (NRs-Rutile-2), prepared according to Approach 2.

Rutile TiO₂ Nanorods Preparation (NRs-Rutile-2)

In a typical reaction, a hydrothermal treatment of TiOCl₂ was carried out using a slightly modified procedure from a literature synthesis.⁵ A stock solution (60 mL) of TiOCl₂ (0.44 M) was placed in a 100 ml autoclave and heated at 220 °C for two hours. After the autoclave vessel was cooled to room temperature, the product was separated by centrifugation, washed twice with a buffer of ammonium acetate-acetic acid as well as methanol and then dried overnight in a vacuum oven at 30 °C to yield the desired rutile FA5-21 TiO₂ nanorods (NRs-Rutile-2).

Surface Modification of Rutile TiO₂ Nanorods (NRs-Rutile-2) with Oleic Acid

Surface modification reactions were then carried out in attempts to modify the surface of the TiO₂ nanorods FA5-21 (NRs-Rutile-2), prepared according to Approach 2 with oleic acid in ethanol or DMF at either 78 °C or 110 °C, using different quantities of oleic acid and using different reaction times. The main purpose of these reactions is to facilitate the bonding of oleic acid onto the surface of the rutile TiO₂ nanorods FA5-21 (NRs-Rutile-2) to serve two main purposes: firstly to stabilise the surface of the rutile TiO₂ nanorods FA5-21 (NRs-Rutile-2) and thereby prevent aggregation of the nanorods in the solid state and in solution and secondly to lower the surface polarity and tension and thereby produce soluble rutile TiO₂/OA nanocomposites FA22 – FA5-25, which can be dissolved in common organic solvents, such as chlorobenzene.

Synthesis of Rutile TiO₂/OA Nanocomposites – Surface Treatment Method 1

This reaction was designed to improve the solubility of the rutile FA5-21 TiO₂ nanorods (NRs-Rutile-2) prepared using Approach 2. Wet FA5-21 TiO₂ nanorods (NRs-Rutile-2) were added to a solution of the requisite amount of oleic acid dissolved in either ethanol or *N,N*-dimethylformamide, see table 5-4 for details of the individual reactions. The resultant reaction mixture was heated at either 78°C or 110°C for several days, see table 5-4 for details of the individual reactions. At the end of the reaction, the mixture was allowed to cool to room temperature, centrifuged and then washed twice with ethanol and finally dried overnight in a vacuum oven at 30 °C to yield the desired oleic acid-capped TiO₂/OA nanocomposites FA5-22 - FA5-25 as a white powder.

Table 5-4: Reaction conditions for the surface modification of the rutile TiO₂ nanorods FA5-21 (NRs-Rutile-2) to yield the desired oleic acid-capped TiO₂/OA nanocomposites FA5-22 - FA5-25 prepared using surface treatment method 1 under identical reaction conditions.

Reaction Product	Starting Material	Ligand/g	Reaction Time/days	Solvent /ml	Reaction Temperature/°C
FA5-22	NRs-Rutile-2	OA/8	6	Ethanol/20	78
FA5-23	NRs-Rutile-2	OA/16	6	Ethanol/20	78
FA5-24	NRs-Rutile-2	OA/8	3	DMF/20	110
FA5-25	NRs-Rutile-2	OA/16	3	DMF/20	110

Approach 3: Hydrothermal Synthesis of Rutile TiO₂ Nanorods in the Presence of 3-Hydroxytyramine Hydrogen Chloride (NRs-Rutile-3)

A hydrothermal treatment for TiOCl₂ in the presence of 3-hydroxytyramine hydrogen chloride was carried out using a modified process from a literature method ⁶ to yield the FA5-26 TiO₂ nanorods (Rutile-NRs-3). Two separate reactions were then carried out in attempts to modify the surface of the TiO₂ nanorods FA5-26 (NRs-Rutile-3), prepared according to Approach 3 with n-alkyl phosphonic acids, oleic acid or diethyl 2-phenylethyl phosphonate.

Rutile TiO₂ Nanorods Preparation (NRs-Rutile-3)

In typical reaction, an aqueous solution (89.4 ml, 2.1 M) of sodium carbonate (Na₂CO₃) was added drop-wise to a 3.3 M solution of TiOCl₂ (39.5 ml) to form a white suspension (pH = 10). 3-Hydroxytyramine hydrogen chloride (299.3 mg) was then added to the reaction mixture under stirring and the resultant mixture heated for an hour at 60 °C. Subsequently, in order to remove residual amounts of 3-hydroxytyramine hydrogen chloride and sodium carbonate, the reaction mixture was washed several times with water and then centrifuged. Water (19.8 ml) was added to the resultant precipitate and the pH adjusted (pH = 0.5) by the drop-wise addition of 15% nitric acid. The suspension was aged for three hours at room temperature before being placed in a Teflon-lined autoclave and heated for 13 h at 150 °C. After completion of the hydrothermal treatment, the resultant reaction product was washed with water several times and then dried in a vacuum oven at 30 °C overnight to yield the desired FA5-26 TiO₂ nanorods (Rutile-NRs-3) as a white powder.

Surface Modification of Rutile TiO₂ Nanorods (NRs-Rutile-3) with n-Alkyl Phosphonic Acids, Oleic Acid or Diethyl 2-Phenylethyl Phosphonate

Surface treatment of the rutile FA5-26 TiO₂ nanorods (Rutile-NRs-3), prepared using Approach 3, and was carried out in two stages, i.e., surface treatment methods 1 and 2. The main purpose of these reactions is to facilitate the bonding of the aliphatic ligands onto the surface of the TiO₂ nanorods to serve two main purposes: firstly to stabilise the surface of the TiO₂ nanorods FA5-26 (NRs-Rutile-3) and thereby prevent aggregation of the nanorods in the solid state and in solution and secondly to lower the surface polarity and tension and thereby

produce soluble rutile TiO₂/ligand nanocomposites FA27 – FA5-41, which can be dissolved in common organic solvents, such as chlorobenzene.

Synthesis of Rutile TiO₂/ligand Nanocomposites – Surface Treatment Method 1

The surface of either the FA5-2 TiO₂ nanorods (NRs-Rutile-1) or the FA5-26 TiO₂ nanorods (Rutile-NRs-3) was modified using either octyl phosphonic acid (OPA) or decylphosphonic acid (ODPA) as ligands in a modified literature process ⁷ to produce the TiO₂/OPA nanocomposites FA5-27 – FA5-31 & FA5-33 and the TiO₂/ODPA nanocomposite FA5-32, respectively, under the same reaction conditions.

Surface Treatment Method 1: the required amount of octyl/decyl or octadecylphosphonic acid, see table 5-5 for details of the individual reactions, was added to a solution of DMF (100 mL) and 37% hydrochloric acid (1 mL). This solution was then added drop-wise under stirring to a dispersion of either the FA5-2 TiO₂ nanorods (NRs-Rutile-1), prepared using Approach 1 or FA5-26 TiO₂ nanorods (NRs-Rutile-3), prepared using Approach 3 (1.536 g), prepared using Approach 3, in distilled-water (10.18 mL). The resultant white turbid suspension during the addition was then heated at 120 °C for 4 h. Methanol (150 mL) was added to the reaction mixture under stirring and the clear liquid was decanted off from the solid precipitate formed. Methanol (150 mL) was added again to the reaction mixture and the process was repeated twice. The suspension was then centrifuged (30 min/4000 rpm). The resultant solid in each centrifuge tube was suspended in toluene (5 mL) and stirred for 30 min. Methanol (15 mL) was added to each tube and the resultant suspensions centrifuged (30 min/4000 rpm). This process was repeated twice and the resultant TiO₂/OPA nanocomposites FA5-27 – FA5-31 and FA5-33 and the TiO₂/ODPA nanocomposite FA5-32 dried in a vacuum oven at 30 °C overnight.

Table 5-5: Conditions for the surface modification of rutile TiO₂ nanorods FA5-2 (NRs-Rutile-1), prepared using Approach 1 described in section 5.2.2.2.1, and FA5-26 TiO₂ nanorods (NRs-Rutile-3) prepared using Approach 3 described in section 5.2.2.4.1 with either octylphosphonic acid or decylphosphonic acid to yield the TiO₂/OPA nanocomposites FA5-27 – FA5-31 and FA5-33 and the TiO₂/ODPA nanocomposite FA5-32 using surface treatment method 1.

Reaction Product	Starting Material	Ligand	Reaction Time/h	Solvent /ml	Reaction Temperature/°C
FA5-27	FA5-26	OPA	4	DMF/100	120
FA5-28	FA5-26	OPA	4	DMF/100	120
FA5-29	FA5-26	ODPA	4	DMF/100	120
FA5-30	FA5-26	OPA	4	DMF/100	120
FA5-31	FA5-26	OPA	4	DMF/100	120
FA5-32	FA5-26	ODPA	4	DMF/100	120
FA5-33	FA5-2 (NRs-Rutile-1)	OPA	4	DMF/100	120

Synthesis of Rutile TiO₂/ligand Nanocomposites – Surface Treatment Method 2

The surface of the rutile TiO₂ nanorods TiO₂/OPA nanocomposites FA5-27 – FA5-31 & FA5-33 and the TiO₂/ODPA nanocomposite FA5-32, prepared using method 1, was modified again, but this time using oleic acid or diethyl 2-phenylethyl phosphonate (DEPPNA), as ligands in a modified literature process ⁷ to produce the TiO₂/OPA/OA nanocomposites FA5-34, FA5-36 – FA5-39 and FA5-41, the TiO₂/OPA/DEPPNA nanocomposite FA5-35 and the TiO₂/ODPA/OA nanocomposite FA5-40, respectively, under the same reaction conditions.

Surface Treatment Method 2: A required amount of either oleic acid or diethyl 2-phenylethyl phosphonate (DEPPNA), see table 5-6 for details of the individual reactions carried out in the

second stage of this surface treatment process, was added to a suspension in toluene (50 ml) of the TiO₂/OPA nanocomposites FA5-27 – FA5-31 and FA5-33 and the TiO₂/ODPA nanocomposite FA5-32 as a powder, prepared from either the FA5-2 TiO₂ nanorods (NRs-Rutile-1), prepared using Approach 1 or FA5-26 TiO₂ nanorods (NRs-Rutile-3), prepared using Approach 3 in the first stage of these surface treatment reactions using surface treatment method 1. 37% Hydrochloric acid (5 drops) was added to the reaction mixture and the resultant mixture heated at 125 °C for 72 h. At the end of reaction, the washing treatment described in the surface treatment method 1 was repeated. The reaction products, *i.e.*, the TiO₂/OPA/OA nanocomposites FA5-34, FA5-36 – FA5-39 and FA5-41, the TiO₂/OPA/DEPPNA nanocomposite FA5-35 and the TiO₂/ODPA/OA nanocomposite FA5-40, were dried overnight in a vacuum oven at 30 °C.

Table 5-6: Conditions for the surface modification of the TiO₂/OPA nanocomposites FA5-27 – FA5-31 and FA5-33 and the TiO₂/ODPA nanocomposite FA5-32 using oleic acid to yield the TiO₂/OPA/OA nanocomposites FA5-34, FA5-36 – FA5-39 and the FA5-41 and for the surface modification of the TiO₂/OPA nanocomposite FA5-27 with diethyl 2-phenylethyl phosphonate to yield the TiO₂/ODPA/OA nanocomposite FA5-40, respectively, using surface treatment method 2.

Reaction Product	Starting Material	Ligand	Reaction Time/h	Solvent /ml	Reaction Temperature/°C
FA5-34	FA5-27	OA	72	Toluene/50	125
FA5-35	FA5-27	DEPPNA	72	Toluene/50	125
FA5-36	FA5-28	OA	72	Toluene/50	125
FA5-37	FA5-29	OA	72	Toluene/50	125
FA5-38	FA5-30	OA	72	Toluene/50	125
FA5-39	FA5-31	OA	72	Toluene/50	125
FA5-40	FA5-32	OA	72	Toluene/50	125
FA5-41	FA5-33	OA	72	Toluene/50	125

5.3 Results and Discussion

5.3.1 Approach 1: Synthesis of Rutile TiO₂ Nanorods from TiOCl₂ and H₂O (NRs-Rutile-1)

In this method, rutile TiO₂ nanorods were prepared by elimination of hydrochloric acid from the reaction of titanium oxychloride (TiOCl₂) and water at different temperature, *i.e.*, 50 °C, 70 °C and 90 °C, as shown in equation 5-2. ⁸



Characterisation of Rutile TiO₂ Nanorods Preparation (NRs-Rutile-1)

The XRD patterns of the FA5-1 - FA5-3 TiO₂ nanorods (NRs-Rutile-1) are shown in figure 5-2. It is noticed that all the diffraction peaks are related to TiO₂ rutile phase ⁹. It is also notable that the intensity of the peaks and the degree of crystallisation increase with the reaction temperature. The full width at half maximum (FWHM) of peaks of TiO₂ becomes narrower with the increase of reaction temperature, indicating that the mean size of the crystalline nanoparticles increases with the increase in reaction temperature. ¹⁰

Figure 5-3 shows the FT-IR patterns of the FA5-1 - FA5-3 rutile TiO₂ nanorods (NRs-Rutile-1). It can be observed that there are several peaks associated with TiO₂. A broad peak at 500-600 cm⁻¹ is attributable to the vibration of the O-Ti-O bonds in the structure of TiO₂. The peak at 1625cm⁻¹ and the broad peaks at 3100-3600 cm⁻¹ can be ascribed to hydroxyl group vibrations due to the adsorption of water. ¹¹

The TEM images of the FA5-1 - FA5-3 rutile TiO₂ nanorods (NRs-Rutile-1) are shown in figure 5-3. The images clearly show the presence of hair-like nanorods of TiO₂ in the samples FA5-1 and FA5-2. Nanorods of TiO₂ with a larger diameter are apparent in the TEM image of the FA5-3 sample. These TEM results are in good agreement with the XRD observations, *i.e.*, the size of the nanorods is greater in reactions carried out at higher temperatures.

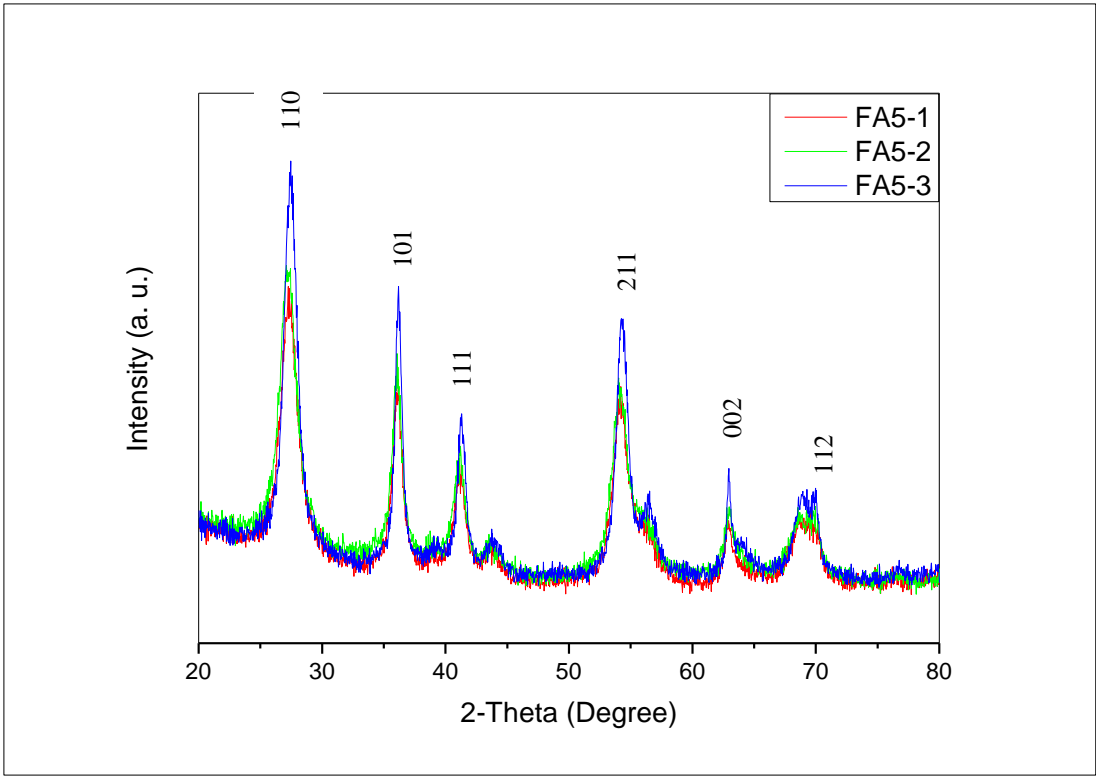


Figure 5-2: XRD patterns of the rutile TiO₂ nanorods FA5-1 - FA5-3 (NRs-Rutile-1).

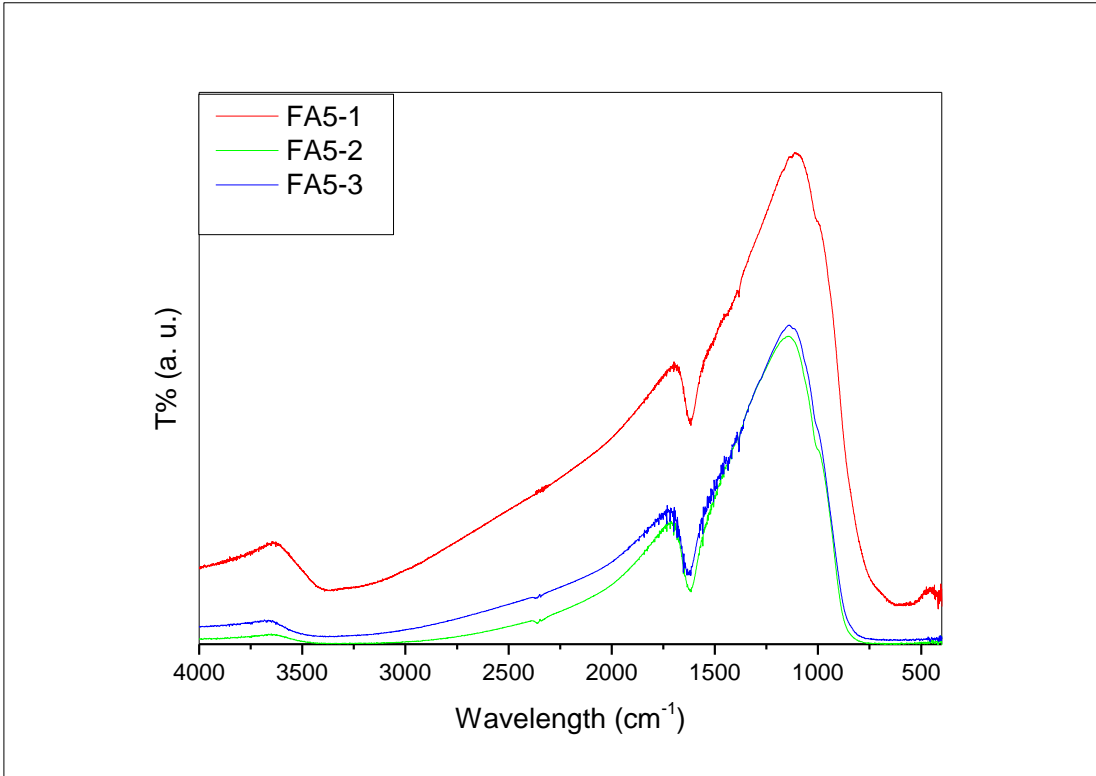


Figure 5-3: FT-IR patterns of the rutile TiO₂ nanorods FA5-1 - FA5-3(NRs-Rutile-1).

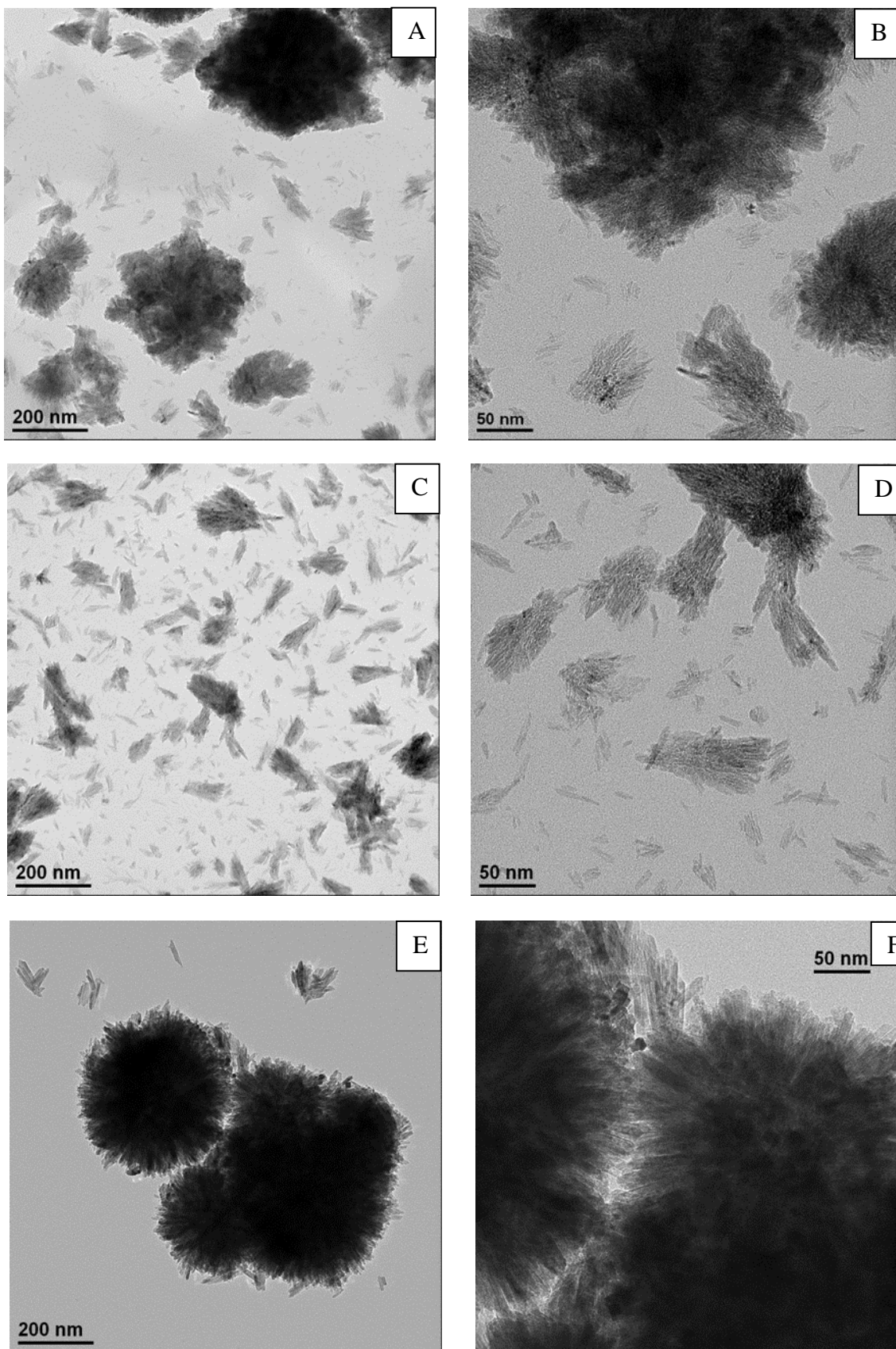
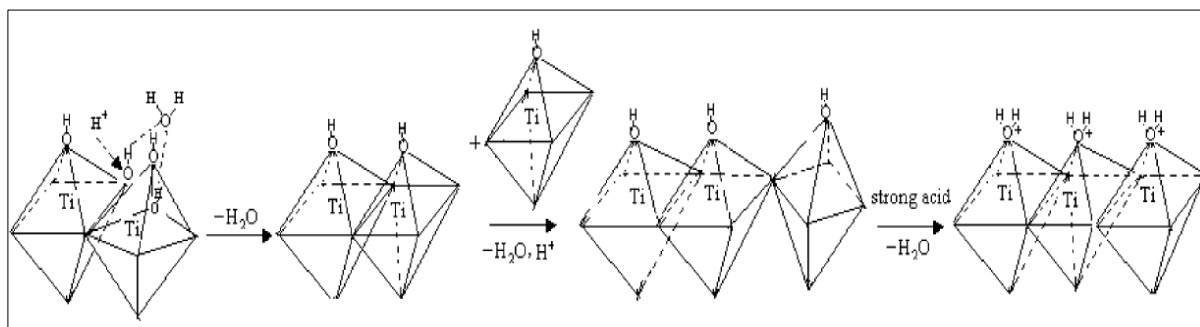


Figure 5-4: TEM images of the rutile TiO₂ nanorods FA5-1 (A-B), FA5-2 (C-D) and FA5-3 (E-F) (Rutile-NRs-1).

Possible Mechanism of Rutile TiO₂ Nanorods Formation (NRs-Rutile-1)

It is well acknowledged that TiO₂ in both phases, anatase and rutile, can form beginning from TiO₆ octahedral and that the phase conversion proceeds by the reorganisation of the octahedral. Organisation of octahedral through sharing of face will lead to form the anatase phase while the sharing of edge to form the rutile phase. In aqueous medium, surfaces of TiO₆ octahedral easily protonated to chain with hydroxyl groups of other TiO₆ octahedral forming Ti–O–Ti oxygen link bonds by removing of water particle. The protonation treatment followed by the imaginable sharing of face of TiO₆ octahedral will lead to form of anatase phase although sharing of edge indications to rutile phase. In the present reaction, sharing of edge is preferred to form rutile phase¹². The formation of TiO₂ rutile phase is schemed in scheme 5-1.¹³

It was approved in theory that the formation of the nanorods (hair-like) rutile of TiO₂ is due to high HCl acid circumstances in which the creation of nanorods (hair-like) titanium oxide through a suitable ratio of length and diameter is favoured in thermodynamic.¹⁴



Scheme 5-1: The formation of TiO₂ rutile phase.

Surface Modification of Rutile TiO₂ Nanorods (NRs-Rutile-1) with Oleic Acid or Primary n-Alkyl Amines

Three TiO₂/OA nanocomposites FA5-4 – FA5-6 were produced by surface modification of the rutile TiO₂ nanorods FA5-2 (NRs-Rutile-1) with oleic acid. The TiO₂/OA nanocomposites FA5-4 – FA5-6 were then characterised in terms of crystal morphology, nanorods dimensions and aspect ratio, degree of aggregation and solubility in chlorobenzene.

Synthesis of Rutile TiO₂/OA Nanocomposites– Surface Treatment Method 1

Three separate reactions were carried out in attempts to modify the surface of the rutile TiO₂ nanorods FA5-2 (NRs-Rutile-1), prepared according to Approach 1 with oleic acid in chlorobenzene at either 50 °C or 100 °C, using different quantities of oleic acid and using different reaction times. The main purpose of these reactions is to facilitate the bonding of oleic acid onto the surface of the rutile TiO₂ nanorods to serve two main purposes: firstly to stabilise the surface of the rutile TiO₂ nanorods FA5-2 (NRs-Rutile-1) and thereby prevent aggregation of the nanorods in the solid state and in solution and secondly to lower the surface polarity and tension and thereby produce soluble rutile TiO₂/OA nanocomposites FA5-4 – FA5-6, which can be dissolved in common organic solvents, such as chlorobenzene.

Characterisation of Rutile TiO₂/OA Nanocomposites Preparation – Surface Treatment Method 1

It is clear from the XRD patterns of the reaction products shown in figure 5-5 that the rutile phase present in the TiO₂ nanorods FA5-2 (NRs-Rutile-1) used as the starting material in the surface treatment reaction has been maintained in the TiO₂/OA nanocomposites FA5-4 – FA5-6 after reaction with oleic acid.

The FT-IR of the rutile TiO₂ nanorods FA5-2 (NRs-Rutile-1) used as the starting material and the TiO₂/OA nanocomposites FA5-4 – FA5-6, made from them by coating them with oleic acid using surface treatment method 1, are shown in figure 5-6. Some new peaks are apparent in the FT-IR spectra of the TiO₂/OA nanocomposites FA5-4 – FA5-6 that are not apparent in the corresponding FT-IR spectrum of the rutile TiO₂ nanorods FA5-2 (NRs-Rutile-1). The peaks around 1500 cm⁻¹ and 1435 cm⁻¹ are related to asymmetric and symmetric of COO⁻, respectively. The peaks round 2850-3000 cm⁻¹ are linked to the stretch vibrations of C-H₃, C-H₂ and C-H.^{15 16} These results are indicative of a significant degree of surface coverage of the TiO₂ nanorods in the TiO₂/OA nanocomposites FA5-4 – FA5-6 with oleic acid.

The results of the TGA analysis of the TiO₂/OA nanocomposites FA5-4 and FA5-6 compared with that of the rutile TiO₂ nanorods FA5-2 (NRs-Rutile-1), are shown in figure 5-7. It can be seen that for rutile TiO₂ nanorods FA5-2 (NRs-Rutile-1) one weight loss (10.8%) occurs at <120 °C due to desorption of physically adsorbed of water. On the other hand, two weight losses (17.1 % and 17.9 %) are exhibited for the TiO₂/OA nanocomposites FA5-4 and FA5-6, firstly due to adsorbed water at <120 °C and secondly due to decomposition of surface-bound

oleic acid at around 320-490 °C. The results are consistent with the results of the corresponding CHN analyses of the TiO₂/OA nanocomposites FA5-4 - FA5-6, see table 5-7, which also provide further evidence of the presence of an organic coating, *i.e.*, oleic acid, on the surface of the TiO₂/OA nanocomposites FA5-4 - FA5-6.

The TEM images of rutile the TiO₂ nanorods FA5-2 (NRs-Rutile-1) and the TiO₂/OA nanocomposites FA5-6, respectively, are shown in figure 5-8. No difference in length and diameter of the TiO₂ nanorods can be observed before and after the surface modification using surface treatment method 1. The TiO₂/OA nanocomposites FA5-4 – FA5-6 still aggregate even though the TiO₂ nanorods are now covered, at least to some degree, with a flexible, aliphatic coating of oleic acid.

The degree of modification of the surface of the rutile TiO₂ nanorods FA5-2 (NRs-Rutile-1) using different amounts of oleic acid was analysed using a combination of combustion analysis CHN and ICP, see table 5-7. The carbon content determined for the TiO₂/OA nanocomposites FA5-4 – FA5-6 after reaction with oleic acid using surface treatment method 1 is greater at higher concentration of oleic acid used in the reaction. However, the degree of carbon content does not increase linearly with increasing amounts of oleic acid used in the reaction, *i.e.*, the amount of oleic acid used in the reaction to produce the TiO₂/OA nanocomposite FA5-6 was a factor of six higher than that used in the reaction to produce the TiO₂/OA nanocomposite FA5-4. There is no significant change in the carbon content with the increasing reaction temperature.

Table 5-7: chemical analyses for the oleic acid-capped TiO₂/OA nanocomposites FA5-4 - FA5-6 prepared using surface treatment method 1.

Sample	Temperature /°C	OA/g	C%	H%	N%	Solubility in C ₆ H ₅ Cl
FA5-4	50	2.5	7.42	1.35	0.00	Not soluble
FA5-5	100	5	8.07	1.04	0.00	Not soluble
FA5-6	100	15	9.06	1.37	0.00	Not soluble

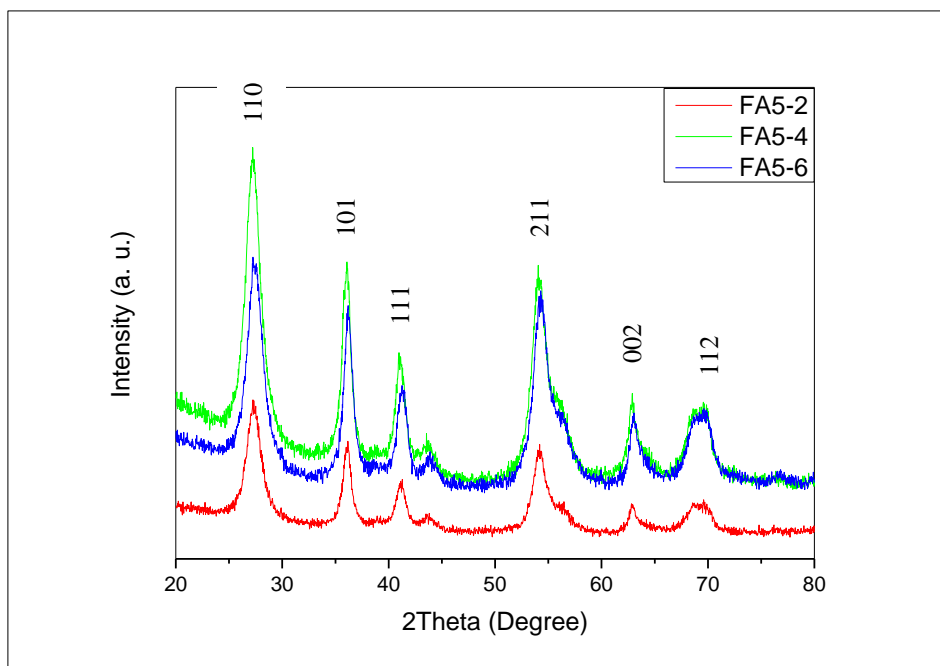


Figure 5-5: XRD patterns of the surface modification of the rutile TiO_2 nanorods FA5-2 (NRS-Rutile 1) and the oleic acid-capped TiO_2/OA nanocomposites FA5-4 and FA5-6 prepared using surface treatment method 1.

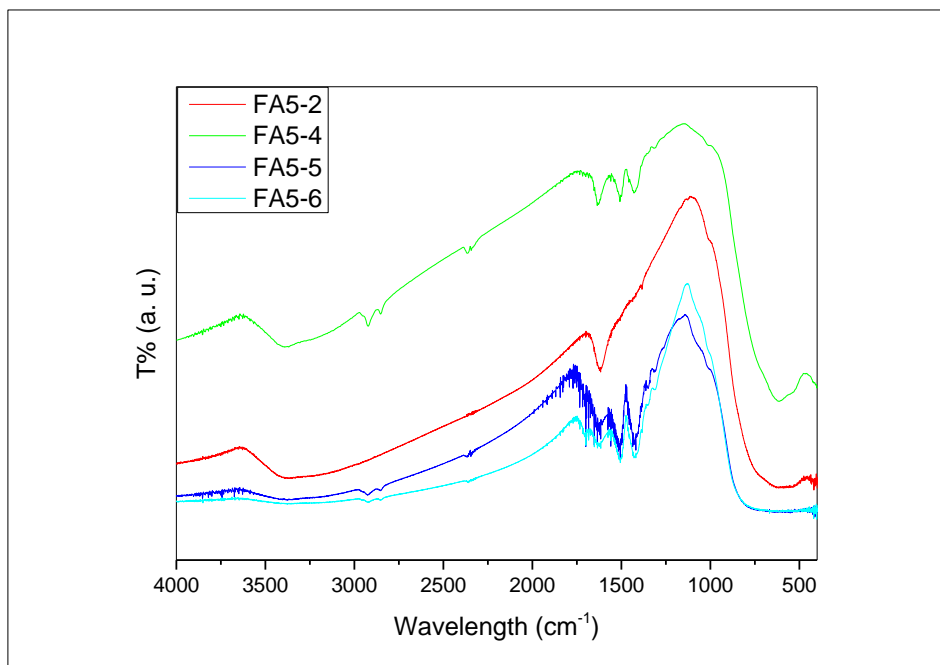


Figure 5-6: FT-IR patterns of the surface modification of the rutile TiO_2 nanorods FA5-2 (NRS-Rutile 1) and the oleic acid-capped TiO_2/OA nanocomposites FA5-4 - FA5-6 prepared using surface treatment method 1.

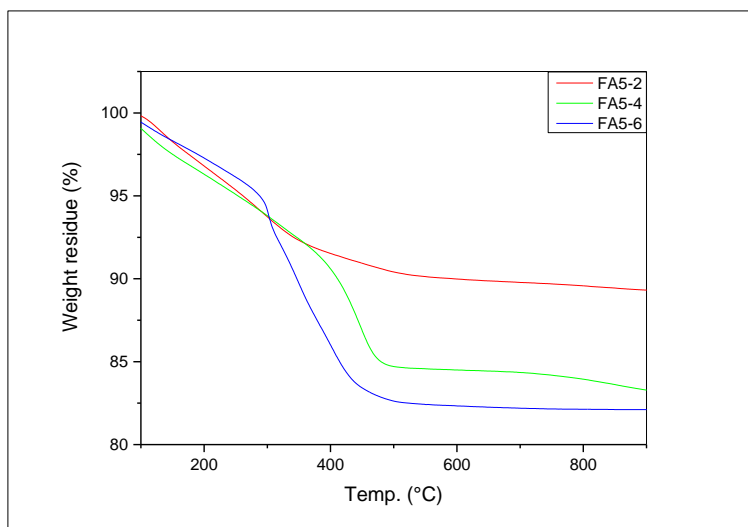


Figure 5-7: TGA of the surface modification of the rutile TiO_2 nanorods FA5-2 (NRS-Rutile 1) and the oleic acid-capped TiO_2/OA nanocomposites FA5-4 and FA5-6 prepared using surface treatment method 1.

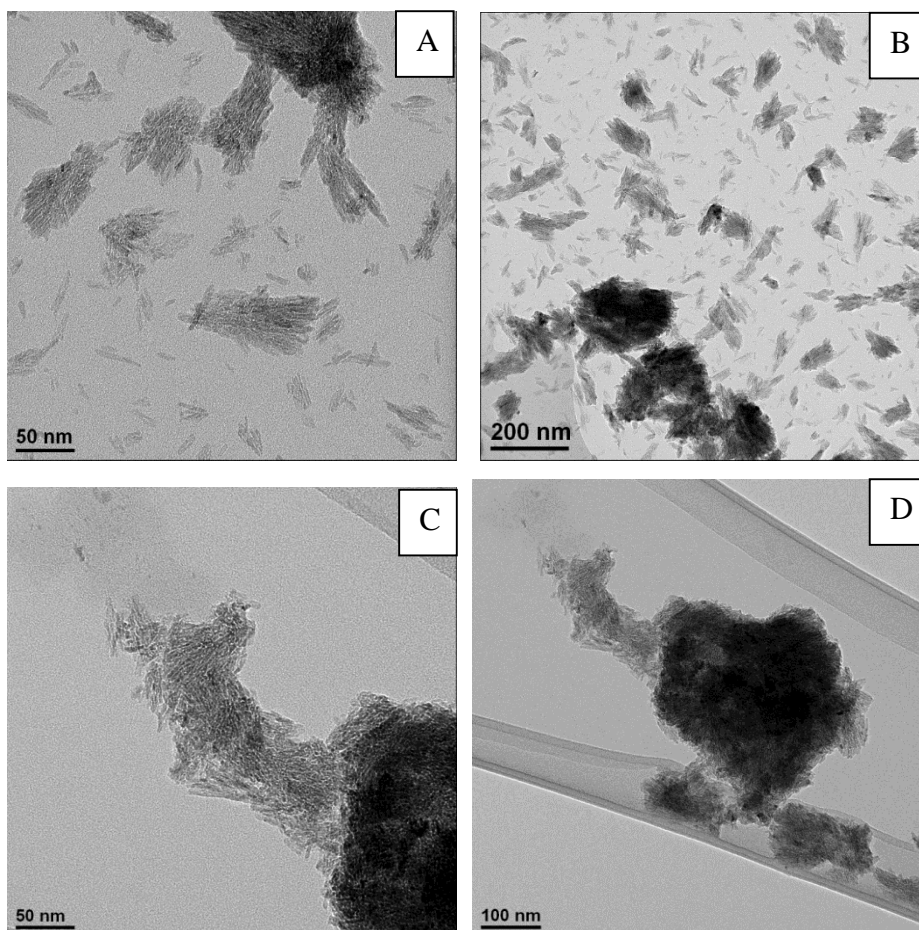
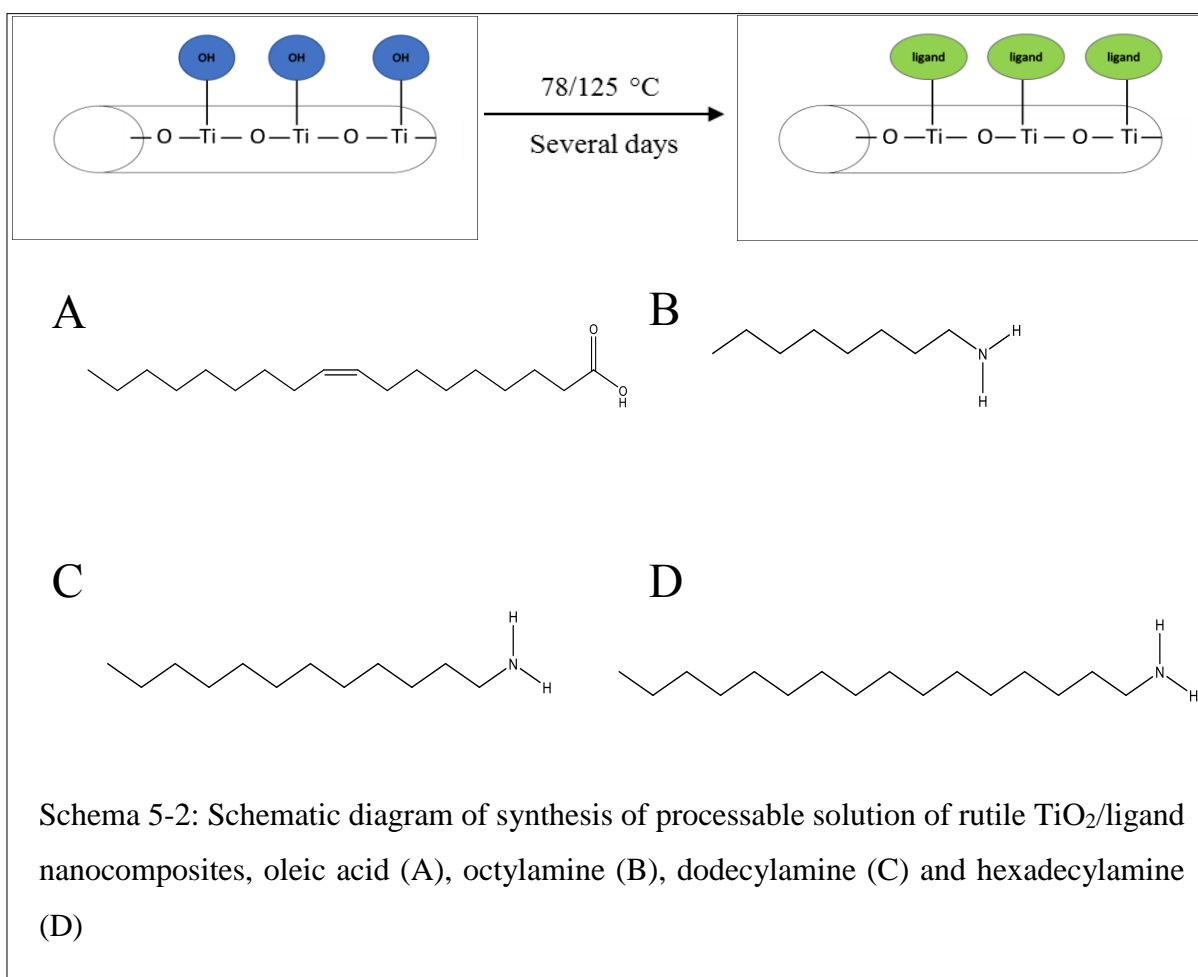


Figure 5-8: TEM images of the surface modification of the rutile TiO_2 nanorods FA5-2 (NRS-Rutile 1) (A-B) and the oleic acid-capped TiO_2/OA nanocomposites FA5-4 (C-D) prepared using surface treatment method 1.

Synthesis of Rutile TiO₂/Ligand Nanocomposites – Surface Treatment Methods 2

Since the TiO₂/OA nanocomposites FA5-4 - FA5-6, prepared using surface treatment 1, are not soluble enough in the required organic solvents, e.g., chlorobenzene, see table 5-7, to be sufficiently solution-processable in common organic solvents for deposition from solution, e.g., by drop casting. Doctor blade techniques, spin coating or inkjet printing, to enable fabrication of prototype, test devices, two additional surface treatment methods 2 and 3, see below, for the nanorods-surface modification were investigated in order to attach a larger concentration of aliphatic ligands onto the surface of the TiO₂ nanorods, i.e., a more uniform, higher surface coverage, in order to produce the desired solution-processable TiO₂/ligand nanocomposites.



Characterisation of Rutile TiO₂/ligand Nanocomposites Preparation – Surface Treatment Method 2

In the first method, *i.e.*, the surface treatment method 2 the synthesis of solution-processable rutile TiO₂/ligand nanocomposites was carried out using wet rutile TiO₂ nanorods FA5-2 (NRs-Rutile-1) as the starting material. The wet rutile TiO₂ nanorods were reacted with different amounts of ligands, *i.e.*, oleic acid, used in surface treatment method 1, and three primary straight-chain alkyl amines ($n\text{-C}_n\text{H}_{2n+1}\text{NH}_2$; $n = 12, 8$ and 16), in different solvents at different reaction temperatures for different times to produce the desired oleic acid-capped TiO₂/OA nanocomposites FA5-7 - FA5-12 and the primary n -alkyl amine-capped TiO₂/AA nanocomposites FA5-13 – FA5-16, respectively, see table 5-8.

The XRD patterns of the rutile TiO₂ nanorods FA5-2 (NRs-Rutile-1), the oleic acid-capped TiO₂/OA nanocomposites FA5-7, FA5-9 and FA5-11 and the primary n -alkyl amine-capped TiO₂/AA(12, 8 and 16) nanocomposites FA5-13, FA5-15 and FA5-16, respectively, are shown in figures 5-10 and 5-11, respectively. It can be seen that all of the rutile TiO₂ nanorods possess a rutile phase.⁹ Compared with the XRD patterns of the rutile TiO₂ nanorods FA5-2 (NRs-Rutile-1), see figure 5-2, the diffraction peaks shown in figures 5-10 and 5-11 are slightly shifted due to the TiO₂ nanorods surface modification of the oleic acid-capped TiO₂/OA nanocomposites FA5-7, FA5-9 and FA5-11 and the primary n -alkyl amine-capped TiO₂/AA nanocomposites FA5-13, FA5-15 and FA5-16.

The FT-IR spectra of the rutile TiO₂ nanorods FA5-2 (NRs-Rutile-1) and the oleic acid-capped TiO₂/OA nanocomposites FA5-7, FA5-9 and FA5-11 are shown in figure 5-12 in order to facilitate comparisons between TiO₂ nanorods FA5-2 (NRs-Rutile-1) and oleic acid-capped TiO₂/OA nanocomposites. It can be seen that some new peaks are apparent in the FT-IR spectra of the TiO₂/OA nanocomposites FA5-7, FA5-9 and FA5-11 than are not observed in the corresponding FT-IR spectrum of the TiO₂ nanorods FA5-2 (NRs-Rutile-1), see figure 5-3. The peak observed at 1735 cm^{-1} (stretching of C=O) in conjunction with the two peaks at 1500 and 1435 cm^{-1} associated to asymmetric and symmetric of COO⁻, is indicative of the carboxyl-group being bonded to the TiO₂ surface *via* reaction with the hydroxyl groups on the TiO₂ surface. The peak at 1735 cm^{-1} is probably due to the presence of oleates, which may be produced during the reaction. Peaks around $2850\text{-}3000\text{ cm}^{-1}$ are related to the stretch vibrations of CH₃, CH₂ and CH groups present in the oleic acid coating.^{15,16}

These spectra are confirm the presence of a significant aliphatic coating on the surface of the TiO₂ nanorods.

The FT-IR spectra for the rutile TiO₂ nanorods FA5-2 (NRs-Rutile-1) and the alkyl amine-modified TiO₂/AA(12, 12, 8 and 16) nanocomposites FA5-13 - FA5-16, respectively, shown in figure 5-13, reveal some additional absorption peaks in the FT-IR spectra of the TiO₂/AA(12, 12, 8 and 16) nanocomposites. The peaks at 1390 and 1480 cm⁻¹ are related to CH₃ deformation vibrations.¹⁷ With respect to the vibrations of amine (NH₂) and ammonium (NH₂⁺) groups, it may be supposed that additional peaks will be observable at 1580-1650 cm⁻¹ and 1560-1620 cm⁻¹, respectively. However, these absorption areas are close to each other, overlap and cannot be individually resolved. Thus, it is difficult to know, with any degree of certainty, which types of amino groups, (NH₂) or (NH₂⁺), are present¹⁵. Peaks around 2850-3000 cm⁻¹ are related to stretch vibrations of CH₃ and CH₂ groups from the alkyl amine¹⁵. These spectra are strongly indicative of a significant presence of an aliphatic coating on the surface of the TiO₂ nanorods. The TGA analysis of some of the oleic acid-capped TiO₂/OA nanocomposites FA5-9 - FA5-12 and the primary *n*-alkyl amine-capped TiO₂/AA(12, 12, 8 and 16) nanocomposites FA5-13 - FA5-16 with oleic acid and primary *n*-alkyl amine surface coatings, prepared using surface treatment 2, are shown in figure 5-14 and 5-15, respectively. It can be seen that there is a weight loss at <120 °C due to adsorbed water. Also, there is another weight loss around 320-490 °C reasonably related to desorption of chemically bound oleic acid and amines on the TiO₂ nanorod surface. The percentage weight loss of the TiO₂/OA nanocomposites FA5-9 - FA5-12 modified with oleic acid, see figure 5-14, is higher than that observed for the TiO₂/AA(12, 12, 8 and 16) nanocomposites FA5-13 - FA5-16 modified with primary *n*-amines, see figure 5-15, which is consistent with the results of the CHN analysis, see table 5-8.

The TEM images of the TiO₂/OA nanocomposites FA5-7 and FA5-9 and the TiO₂/AA(12) nanocomposite FA5-14, after surface-modification with oleic acid and dodecylamine, respectively, are shown in figure 5-16. Compared with the corresponding TEM images of the FA5-2 (NRs-Rutile-1) TiO₂ nanorods shown in figure 5-4, it is apparent that the degree of aggregation of the TiO₂ nanorods in the TiO₂/OA nanocomposites FA5-7 and FA5-9 and the TiO₂/AA(12) nanocomposite FA5-14, after surface-modification with oleic acid and dodecylamine, respectively, has been very significantly reduced as intended initially.

The degree of modification of the surface of the TiO₂ nanorods FA5-2 (NRs-Rutile-1) to produce the oleic acid-capped TiO₂/OA nanocomposites FA5-7 - FA5-12 and the primary *n*-alkyl amine-capped TiO₂/AA(12, 12, 8 and 10) FA5-13 - FA5-16, respectively, was measured using CHN and ICP chemical analysis as shown in table 5-8.

The highest carbon content for all the TiO₂/OA nanocomposites prepared is 16.64%. The carbon content of the TiO₂/OA nanocomposites FA5-7 - FA5-12, prepared using the surface

treatment method 2, is higher than that observed for the corresponding TiO₂/OA nanocomposites FA5-4 - FA5-6, prepared using the surface treatment method 1, see table 5-7. However, the carbon content is lower at longer reaction times as shown in table 5-8 for the TiO₂/OA nanocomposites FA5-9 and FA5-10, prepared under identical reaction conditions apart from the reaction time, *i.e.*, 7 days and 10 days, respectively. This difference in carbon content might be due to detachment of oleic acid from the surface of the TiO₂ nanorods occurring over time during the reaction.

The carbon content is lower for the TiO₂/OA nanocomposites FA5-7 - FA5-10, prepared using ethanol as solvent than that determined for the TiO₂/OA nanocomposites FA5-11 and FA5-12, prepared using DMF as solvent. There is no significant difference in the carbon, hydrogen and titanium content of the TiO₂/OA nanocomposites FA5-11 and FA5-12, prepared under identical reaction conditions using DMF as the solvent, even when doubling the oleic acid concentration from that used to prepared FA5-11 to that used to prepared FA5-12. The presence of 0.5% of nitrogen indicates that a reaction has occurred between the TiO₂ nanorods and the DMF solvent. The carbon content in the primary *n*-alkyl amine-capped TiO₂/AA(12, 12, 8 and 10) FA5-13 – FA5-16, respectively, is also higher with the increasing length of the alkyl chain of the alkyl amines (*n*-C_nH_{2n+1}NH₂; *n* = 8, 12 and 16), as might have been reasonably expected. A stable colloidal solution of the TiO₂/OA nanocomposites FA5-7 and FA5-9 with an oleic acid coating, respectively, each prepared in ethanol, see table 5.8, can be made up to a concentration of 10% in chlorobenzene for FA5-9, see figure 5-9. On the other hand, colloidal solutions of the TiO₂/OA nanocomposites FA5-11 and FA5-12, prepared using DMF as the solvent and the TiO₂/AA(12, 12, 8 and 10) FA5-13 – FA5-16, respectively, with an primary *n*-alkyl amine coating (*n*-C_nH_{2n+1}NH₂; *n* = 8, 12 and 16) are only stable for several hours, see figure 5-9 for an image of a fairly concentrated (6%) colloidal solution of the TiO₂/AA nanocomposite FA5-13 with a dodecyl amine (*n*-C_nH_{2n+1}NH₂; *n* = 12) coating.

Table 5-8: Chemical analyses for the oleic acid-capped TiO₂/OA nanocomposites FA5-7 - FA5-12 and the primary *n*-alkyl amine-capped TiO₂/AA(12, 12, 8 and 10) nanocomposites FA5-13 – FA5-16, respectively, using surface treatment method 2.

Sample	ligand/g	Solvent	T/d	Ti%	C%	H%	N%	Solubility
FA5-7	OA/8	Ethanol	6	64.0	12.9	1.8	0.0	2 % colloidal solution
FA5-8	OA/16	Ethanol	7	69.2	10.6	1.9	0.0	5 % colloidal solution
FA5-9	OA/32	Ethanol	7	41.1	16.7	2.6	0.0	10 % colloidal solution
FA5-10	OA/32	Ethanol	10	50.0	9.6	1.5	0.0	5 % colloidal solution
FA5-11	OA/16	DMF	7	57.2	20.3	3.5	0.4	Not soluble
FA5-12	OA/32	DMF	7	56.9	20.5	3.5	0.5	Not soluble
FA5-13	<i>n</i> -C ₁₂ H ₂₅ NH ₂ /5	Ethanol	7	50.8	9.5	2.0	0.7	Not soluble
FA5-14	<i>n</i> -C ₁₂ H ₂₅ NH ₂ /10	Ethanol	7	49.3	11.9	2.3	1.0	Not soluble
FA5-15	<i>n</i> -C ₈ H ₁₇ NH ₂ /8	Ethanol	7	51.4	9.9	2.2	1.2	Not soluble
FA5-16	<i>n</i> -C ₁₆ H ₃₃ NH ₂ /8	Ethanol	7	45.7	16.5	3.4	1.2	Not soluble

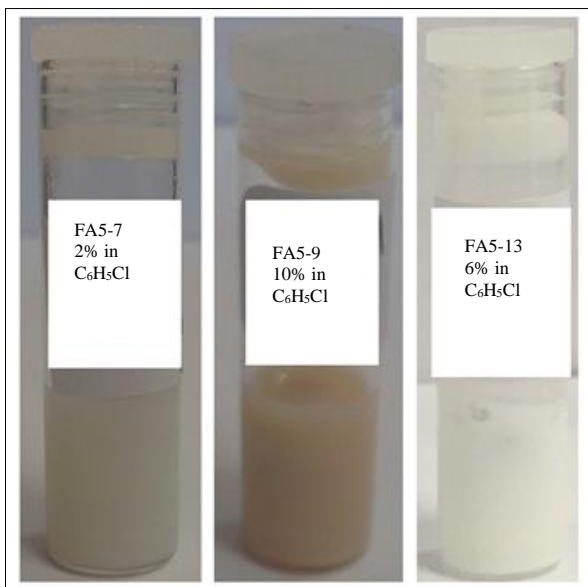


Figure 5-9: colloidal solution of the oleic acid-capped TiO_2/OA nanocomposites FA5-7 and FA5-9 and the dodecyl amine-capped $\text{TiO}_2/\text{AA}(12)$ nanocomposite FA5-13 ($n\text{-C}_n\text{H}_{2n+1}\text{NH}_2$; $n = 12$) in chlorobenzene ($\text{C}_6\text{H}_5\text{Cl}$).

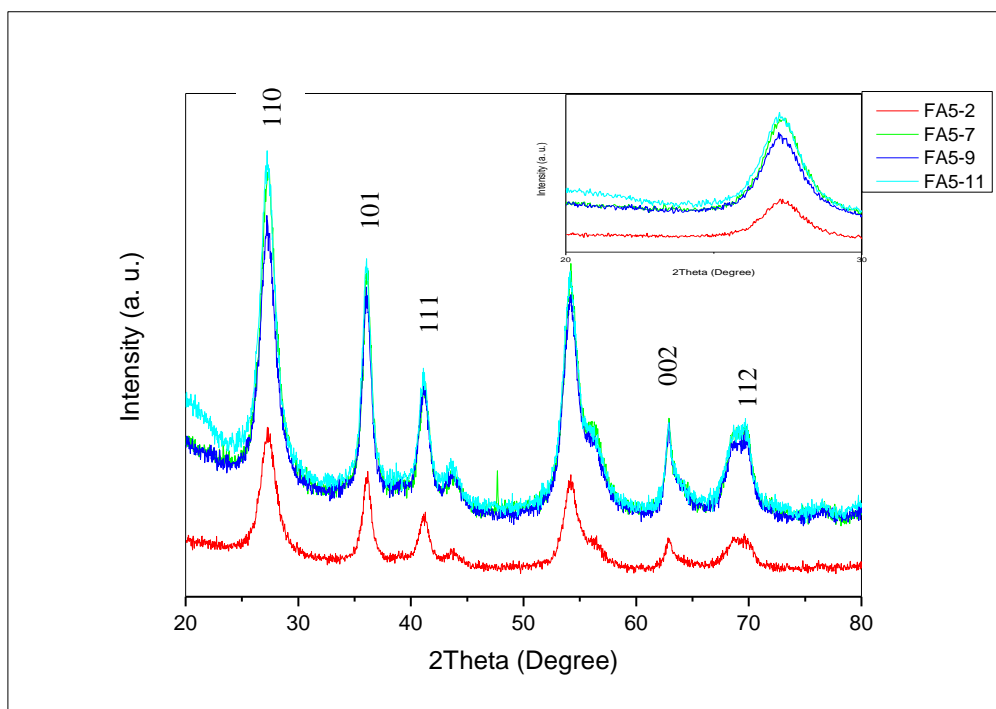


Figure 5-10: XRD patterns of the surface modification of the rutile TiO_2 nanorods FA5-2 (NRS-Rutile 1) and the oleic acid-capped TiO_2/OA nanocomposites FA5-7, FA5-9 and FA5-11 prepared using surface treatment method 2.

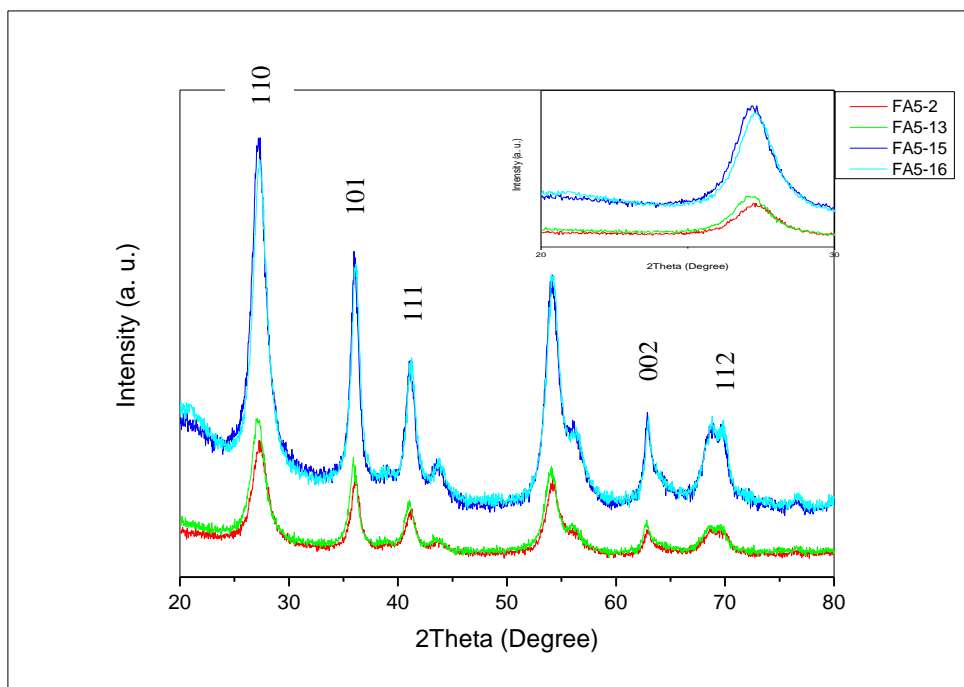


Figure 5-11: XRD patterns of the rutile TiO₂ nanorods FA5-2 (NRs-Rutile-1) and the primary *n*-alkyl amines-capped TiO₂/AA(12, 8 and 16) nanocomposites FA5-13, FA5-15 and FA5-16 modified with primary *n*-alkyl amines (C_nH_{2n+1}NH₂; n = 12, 8 and 16, respectively) using surface treatment method 2.

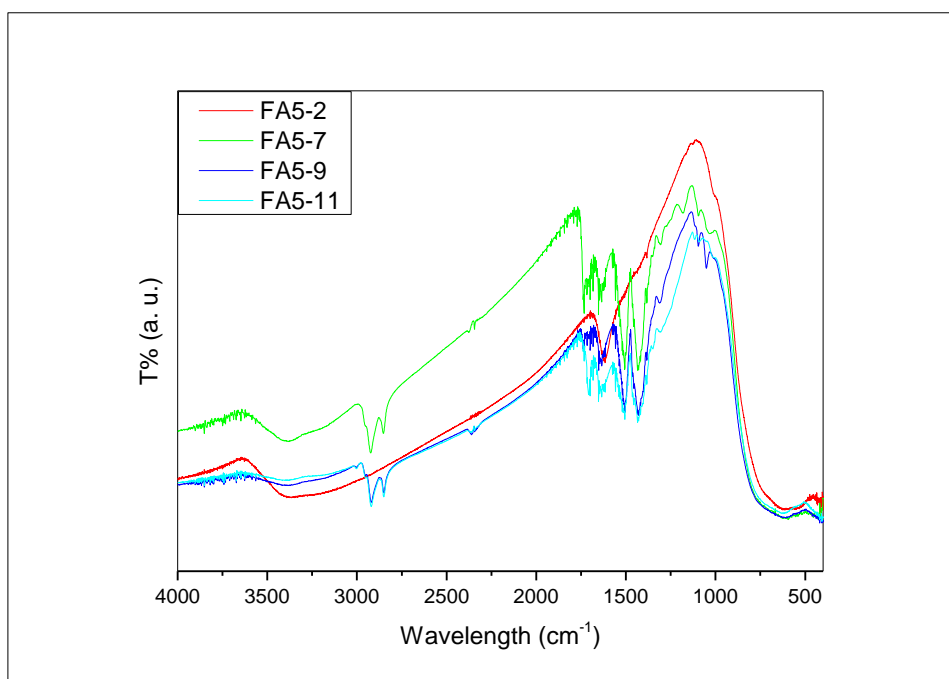


Figure 5-12: FT-IR patterns of the rutile TiO₂ nanorods FA5-2 (NRs-Rutile-1) and the oleic acid-capped TiO₂/OA nanocomposites FA5-7, FA5-9 and FA5-11 using surface treatment method 2.

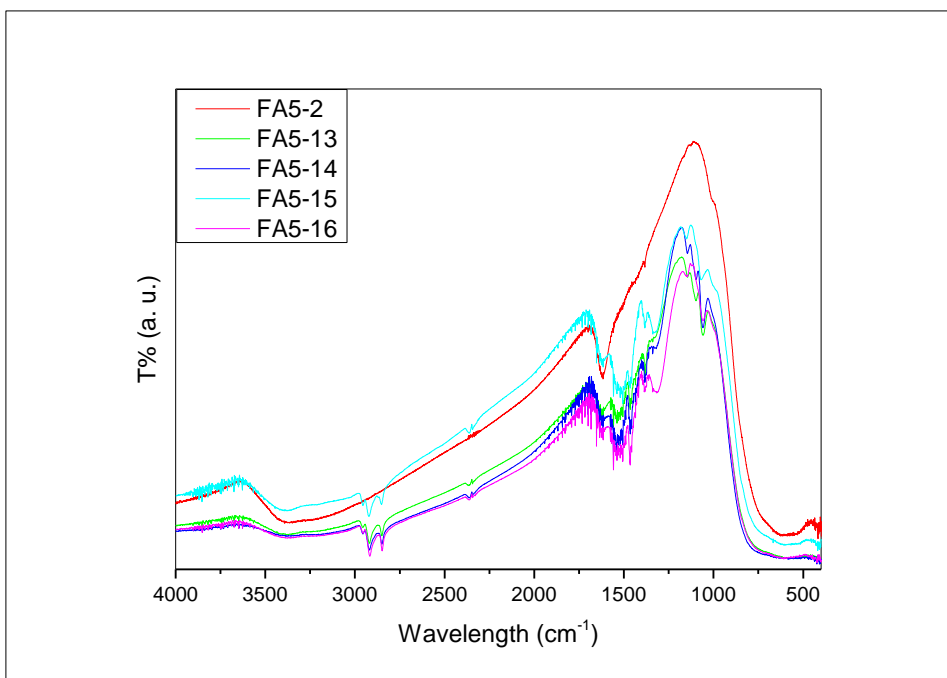


Figure 5-13: FT-IR patterns of the rutile TiO₂ nanorods FA5-2 (NRs-Rutile-1) and the primary *n*-alkyl amines-capped TiO₂/AA(12, 12, 8 and 16) nanocomposites FA5-13 - FA5-16, respectively, modified with primary *n*-alkyl amines (C_nH_{2n+1}NH₂; n = 12, 12, 8 and 16, respectively) using surface treatment method 2.

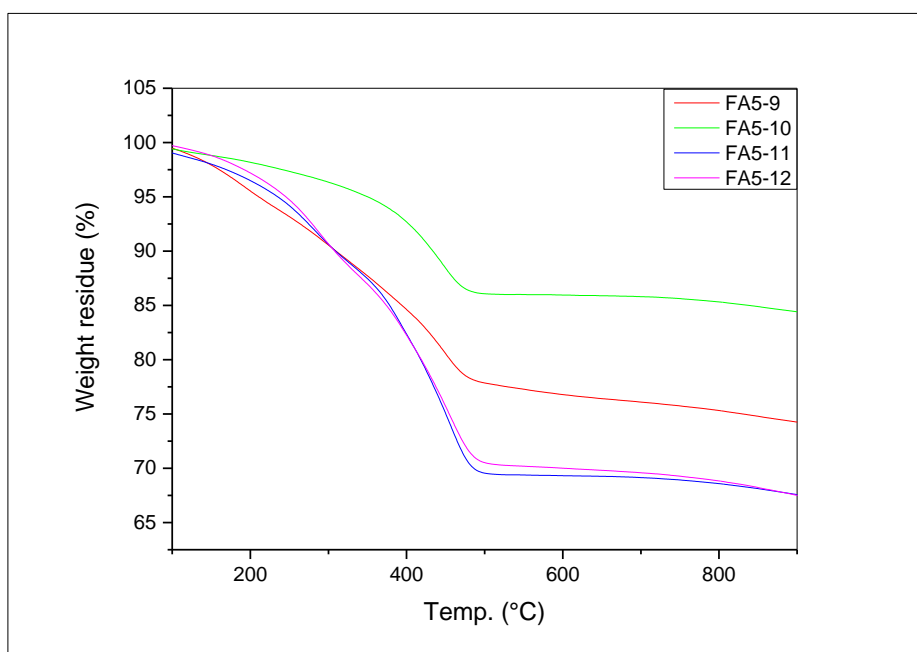


Figure 5-14: TGA of the oleic acid-capped TiO₂/OA nanocomposites FA5-7, FA5-9 and FA5-11 modified with oleic acid using surface treatment method 2.

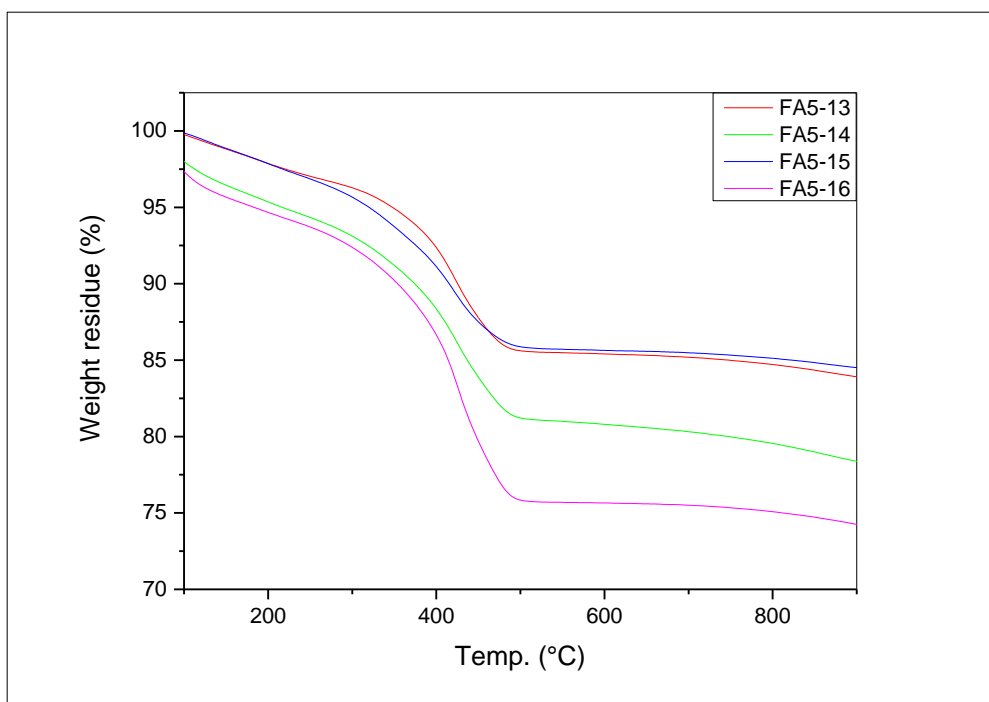


Figure 5-15: TGA of the primary *n*-alkyl amines-capped TiO₂/AA(12, 12, 8 and 16) nanocomposites FA5-13 - FA5-16, respectively, modified with primary *n*-alkyl amines (C_nH_{2n+1}NH₂; n = 12, 12, 8 and 16) using surface treatment method 2.

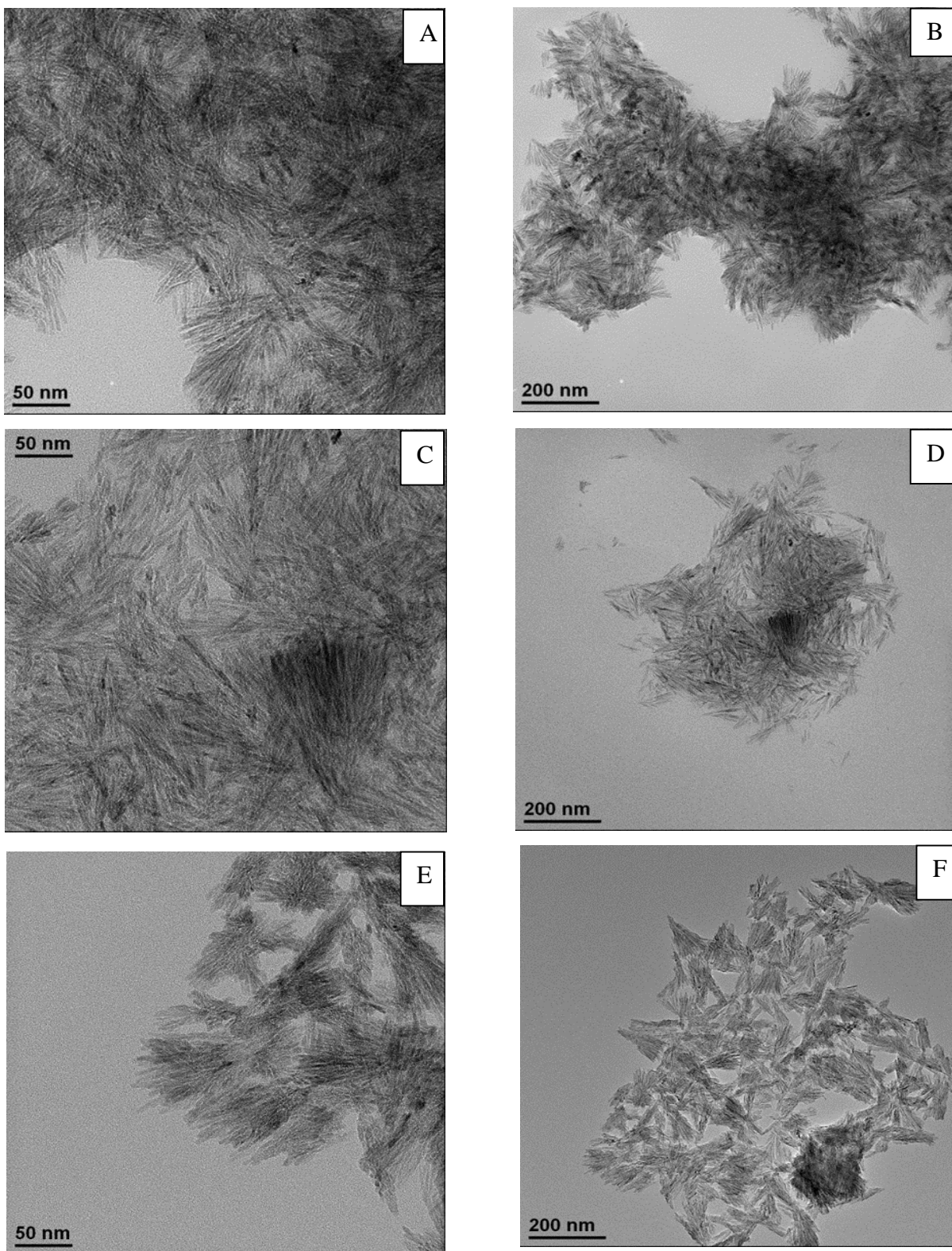
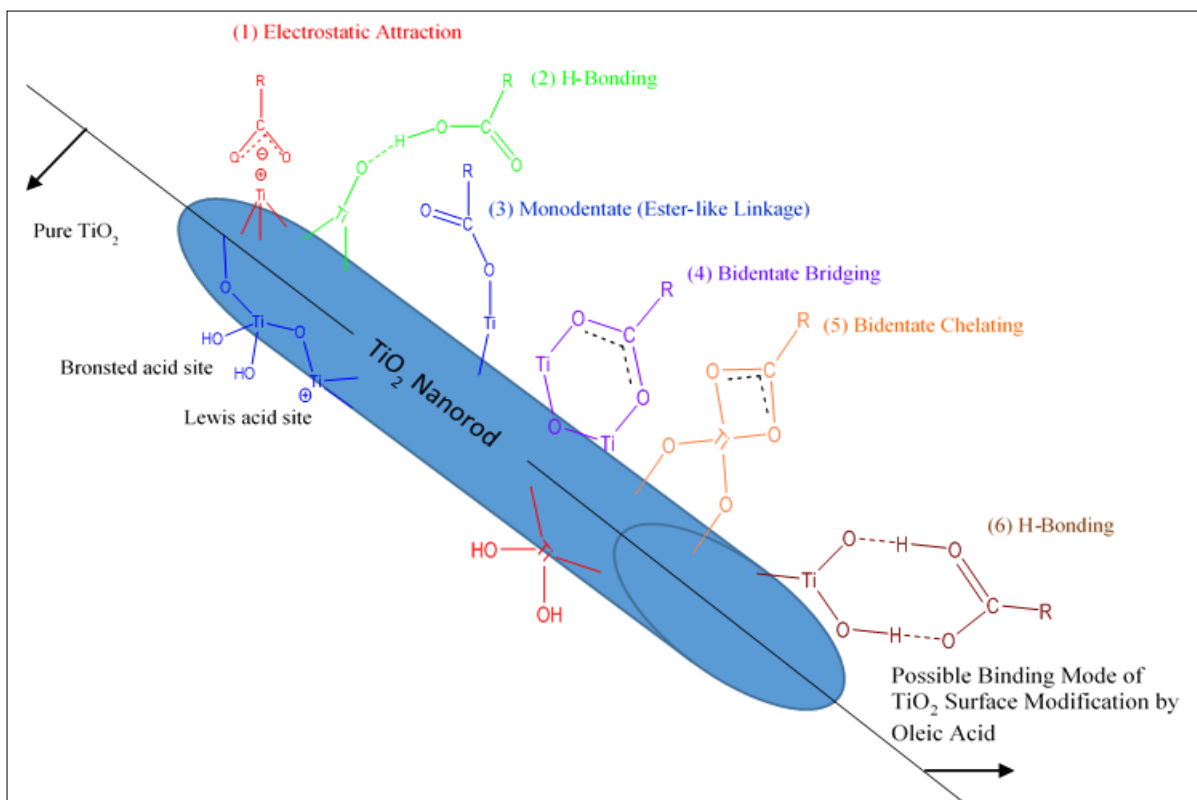


Figure 5-16: TEM images of the oleic acid-capped TiO_2/OA nanocomposites FA5-7 (A-B), TiO_2/OA nanocomposites FA5-9 (C-D) using surface treatment method 2 and the dodecylamine-capped $\text{TiO}_2/\text{AA}(12)$ nanocomposite FA5-14 (E-F) also using surface treatment method 2.

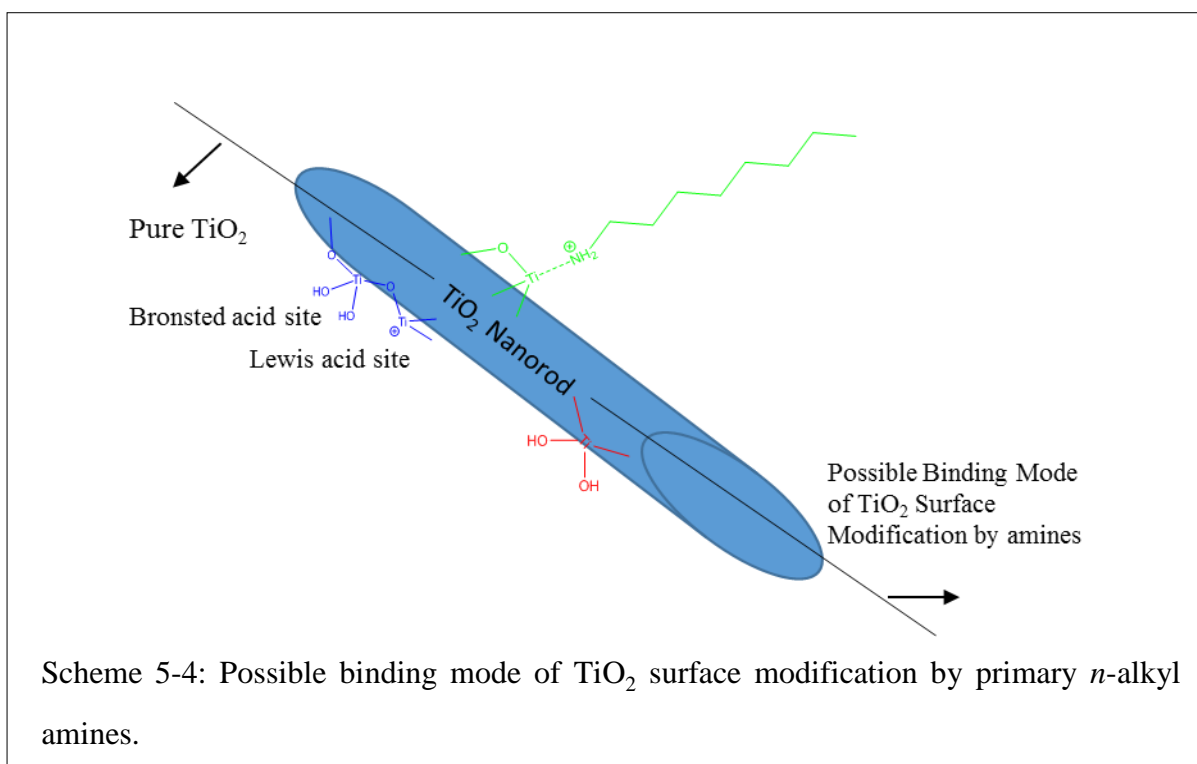
Possible Mechanism for Rutile TiO₂/ligand Nanocomposites Formation – Surface Treatment Method 2

Scheme 5-3 demonstrates the possible bonding forms of a carboxylic group to the surface of the TiO₂/OA nanocomposites, such as simple adsorption, *e.g.*, hydrogen bonding and electrostatic attraction and chemical adsorptions, *e.g.*, a bridging- or chelating-ester linkage.

The presence of the peaks at 1500 and 1435 cm⁻¹ in the FT-IR spectra shown in figure 5-11 confirms the presence of chemical bonds between the Bronsted acid site (Ti-OH) and the carboxylic group (COO).^{18, 19} The peaks at 1735 cm⁻¹ are suggestive of some chemical adsorption of oleic acid onto the surface of the nanorods with no chemical bonding taking place.¹⁸ Chemical bonds between the amino-groups of the primary *n*-alkyl amines and Lewis acid sites, such as Ti⁺, on the surface of the TiO₂/AA nanocomposites can be reasonably be assumed, see Scheme 5-4.¹⁵



Scheme 5-3: Possible binding mode of TiO_2 surface modification by carboxylic acid; (1) electrostatic attraction, (2 and 6) H-Bonding, (3) monodentate (ester-like linkage) (4) bidentate bridging (5) bidentate chelating.



Scheme 5-4: Possible binding mode of TiO_2 surface modification by primary *n*-alkyl amines.

Electrical Characterisation of Rutile TiO₂/ligand Nanocomposites Preparation – Surface Treatment Method 2:

The hybrid insulator of rutile TiO₂/ligand nanocomposites preparation – surface treatment method 2 product FA5-9 was spin coated from a 10% wt solution in chlorobenzene on prepatterned metallic electrodes. The samples were cured in a vacuum oven and finally the top metallic electrodes were evaporated to form crossbar MIM structures. The electrical characterization of these capacitors was carried out with a SII260 impedance analyser and an Agilent B2912A in air and at room temperature. The final thickness of the hybrid insulating films was ~200 nm with a RMS roughness of 1.0 nm. The estimated dielectric constant is 9-10 at 1 MHz and it rapidly increases as the frequency decreases reaching the value of 30 at 1 Hz, see figure 5-17. The loss tangent data show that the hybrid insulator at high frequencies behaves as an ideal capacitor (loss of the order of 10⁻²) while at low frequencies a remarkable increase in the loss tangent of our insulator is recorded.

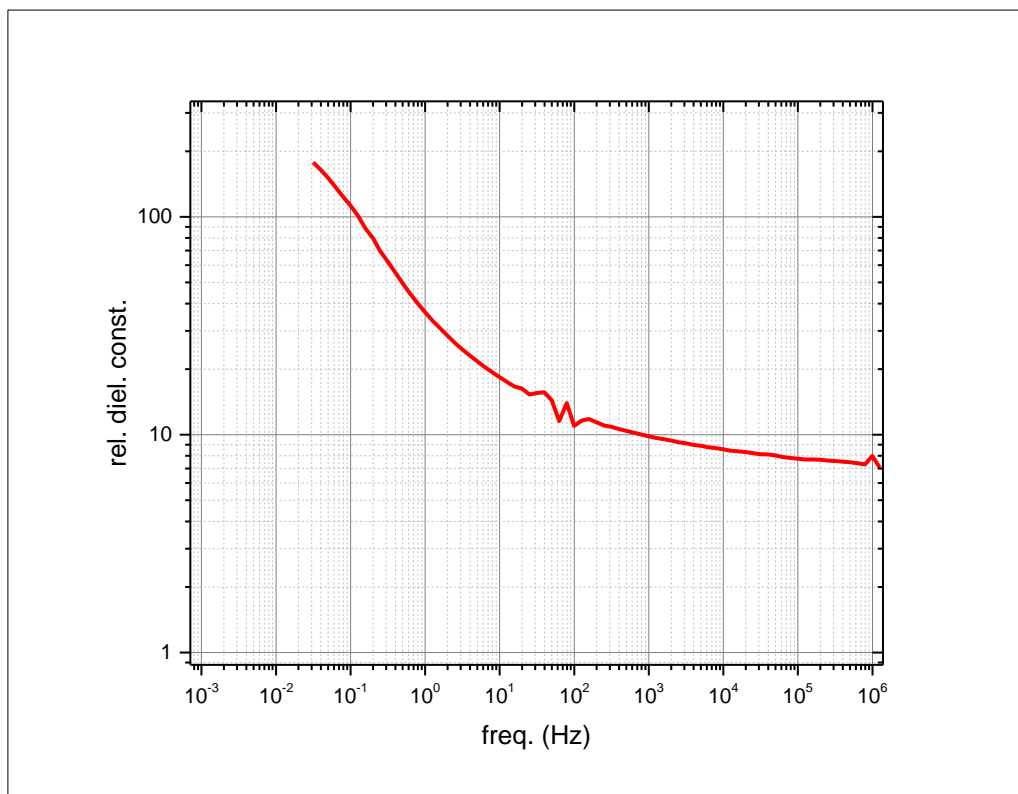


Figure 5-17: Dielectric constant k with frequency for rutile TiO₂/ligand nanocomposites preparation – surface treatment method 2 product FA5-9.

Synthesis of Rutile TiO₂/Ligand Nanocomposites – Surface Treatment Methods 3

In order to further to improve the solubility of the rutile TiO₂/OA nanocomposites FA5-8 (dry) and FA5-9 (dry), both prepared using surface treatment method 2 or freshly prepared TiO₂/OA nanocomposites FA5-10 (wet) and FA5-14 (dry), both prepared using surface treatment method 2 a further surface modification, *i.e.*, using surface treatment method 2 of these nanocomposites using oleic acid or dodecyl amine as the ligand, was carried out in ethanol and toluene as solvents at 78 °C or 110 °C for 6-10 days in attempts to increase the degree and homogeneity of the coverage of the nanorod surface of the resultant doubly oleic acid-capped TiO₂/OAx₂ nanocomposites FA5-17, FA5-18 and FA5-20 or the oleic acid- and dodecyl amine-capped TiO₂/OA/AA(12) nanocomposite FA5-19, see table 5-9.

Characterisation of Rutile TiO₂/ligand Nanocomposites Preparation – Surface Treatment Method 3

The XRD patterns of the rutile TiO₂ nanorods FA5-2 (NRs-Rutile-1) and the oleic acid/dodecyl amine-capped TiO₂/OA/AA(12) nanocomposite FA5-19 as well as that of the twice oleic acid-capped TiO₂/OAx₂ nanocomposite FA5-20, after the additional surface modification using surface treatment method 3, shown in figure 5-18 reveal that the rutile phase is retained in the all TiO₂/ligand nanocomposites FA5-19 and FA5-20, prepared using this third surface treatment method. The slight shift in the peaks compared to those observed for FA5-2 (NRs-Rutile-1) indicate that the oleic acid or dodecyl amine ligand, respectively, has chemically bonded to the surface of the rutile TiO₂ nanorods FA5-2 (NRs-Rutile-1), see table 5-9.

The FT-IR spectra presented in figures 5-19 of the rutile TiO₂ nanorods FA5-2 (NRs-Rutile-1) and the TiO₂/OAx₂ nanocomposites FA5-17, FA5-18 and FA5-20, prepared using oleic acid as the ligand in successive surface treatments using methods 2 and 3, reveal that there is no significant difference in the nanorod morphology between that of the TiO₂/OA nanocomposites FA5-10, FA5-8 and FA5-9 used to prepare the TiO₂/OAx₂ nanocomposites FA5-17, FA5-18 and FA5-20, respectively. Two peaks associated with asymmetric and symmetric of COO⁻ can be observed at 1500 and 1435 cm⁻¹, respectively. The peak at 1735 cm⁻¹ is related to oleates produced during the reaction. The peaks observed between 2850-3000 cm⁻¹ are related to stretch vibrations of CH₃, CH₂ and CH from oleic acid attached to the surface of the TiO₂ nanocomposites.^{15, 16} The FT-IR spectrum, shown in figure 5-20, of the oleic acid/dodecyl

amine-capped TiO₂/OA/AA(12) nanocomposite FA5-19, prepared from the TiO₂/OA nanocomposite FA5-14 using dodecylamine as the ligand in surface treatment 3, reveals no significant differences from the FT-IR spectrum of the TiO₂/OA nanocomposite FA5-14, modified with oleic acid using surface treatment method 2 shown in figure 5-12, apart from some additional amine peaks, and that of the dodecyl amine-capped TiO₂/AA(12) nanocomposite FA5-14, shown in figure 5-12, also prepared using surface treatment method 2. The peaks observed at 1390 cm⁻¹ and 1480 are related to CH₃ deformation vibrations.¹⁷ The peaks observed at 1510 and 1615 cm⁻¹ could be attributable to vibrations of (NH₂) and (NH₂⁺).¹⁵ The peaks observed at 2850-3000 cm⁻¹ are related to stretch vibrations of CH₃ and CH₂.¹⁵ These spectra are a good indication for a high degree of surface coverage, of the TiO₂/OAx2 nanocomposites FA5-17, FA5-18 and FA5-20, prepared using oleic acid, and the TiO₂/OA nanocomposite FA5-14 using dodecylamine as the ligand in surface treatment 3.

The TEM images shown in figure 5-22 for the doubly oleic acid-capped TiO₂/OAx2 nanocomposites FA5-17 (A-B), FA5-18 (C-D) and the oleic acid/dodecyl amine-capped TiO₂/OA/AA(12) nanocomposite FA5-19 (E-F), modified again using surface treatment method 3, reveal that the degree of aggregation of the TiO₂ nanorods is higher than that observed in figure 5-16 for the corresponding TiO₂/OA nanocomposites FA5-7 and FA5-9 and the TiO₂/AA(12) nanocomposite FA5-14, respectively, just prepared using the surface treatment method 2. There is no difference in diameter or length in the TiO₂ nanorods after the second surface treatment, compare figures 5-16 and 5-22. The degree of aggregation is more apparent for the oleic acid/dodecyl amine-capped TiO₂/OA/AA(12) nanocomposite FA5-19.

The degree of modification of rutile TiO₂ nanorods was measured using CHN and ICP chemical analysis, see table 5-9. Compared with the data (64.0%), for the oleic acid-capped TiO₂/OA nanocomposite FA5-7, see table 5-8, prepared just using surface treatment method 2, there is an observable lower titanium content (46.7%), see table 5-9, for the TiO₂/OAx2 nanocomposites FA5-17, prepared in two steps from the rutile TiO₂ nanorods FA5-2 (NRs-Rutile-1) and the TiO₂/OA nanocomposite FA5-7 using oleic acid as the ligand in two successive surface treatments using methods 2 and 3, respectively.

However, the titanium content (53.7%) determined for the oleic acid/dodecyl amine-capped TiO₂/OA/AA(12) nanocomposite FA5-19, prepared using dodecyl amine as the ligand in the additional surface treatment method 3 is higher than those (50.8% and 49.3%) of the primary *n*-alkyl amine-capped TiO₂/AA nanocomposites FA5-13 and FA5-14, respectively, produced from the rutile TiO₂ nanorods FA5-2 (NRs-Rutile-1) by modification with either octyl amine, dodecyl amine or hexadecylamine using surface treatment method 2 alone, see table 5-9.

The carbon content (21.8%) is higher for the TiO₂/OAx₂ nanocomposites FA5-17, coated twice with oleic acid using a combination of surface treatment methods 2 and 3 compared with that (12.9%) of the corresponding TiO₂/OA nanocomposites FA5-7 coated just once with oleic acid using method 2. On the other hand, the carbon content (8.4%) for the oleic acid/dodecyl amine-capped TiO₂/OA/AA(12) nanocomposite FA5-19, prepared using dodecyl amine as the ligand in the additional surface treatment method 3, is lower than those (9.5% and 11.9%) that of the corresponding dodecyl amine-capped TiO₂/AA nanocomposites FA5-13 and FA5-14 produced from the rutile TiO₂ nanorods FA5-2 (NRs-Rutile-1) by modification with dodecyl amine using surface treatment method 2 alone, see tables 5-8 and 5-9. The carbon content (21.8%) of the TiO₂/OAx₂ nanocomposite FA5-17 is almost double that (12.9%) of the TiO₂/OA nanocomposite FA5-7, from which it was prepared in ethanol using surface treatment method 3. The carbon content determined for the TiO₂/OAx₂ nanocomposite FA5-17 is the highest of any of the nanocomposites prepared using the surface treatments 2 and 3, see tables 5-8 and 5-9. The carbon content (13.7%) determined for the TiO₂/OAx₂ nanocomposite FA5-18 using toluene instead of ethanol, as the reaction solvent is much lower than that (21.8%) of the TiO₂/OAx₂ nanocomposite FA5-17. The low nitrogen (0.6%) and carbon content (8.35%) observed for the oleic acid/dodecyl amine-capped TiO₂/OA/AA(12) nanocomposite FA5-19 is indicative of a low surface coverage attributable, perhaps, to weak bonds between the dodecyl amine ligand and the TiO₂ nanorod surface.

TGA analysis of the oleic acid/dodecyl amine-capped TiO₂/OA/AA(12) nanocomposite FA5-19 and the twice oleic acid-capped TiO₂/OAx₂ nanocomposites FA5-17 and FA5-20, modified again using surface treatment method 3, shown in figure 5-21, reveal a weight loss at <120 °C and between 320-490 °C related to adsorbed water and carbon decomposition, respectively. FA5-17 exhibits the highest weight loss compatible with the CHN analysis.

Table 5-9: Chemical analyses for the doubly oleic acid-capped TiO₂/OAx₂ nanocomposites FA5-17, FA5-18 and FA5-20 and the oleic acid/dodecyl amine-capped TiO₂/OA/AA(12) nanocomposite FA5-19, prepared using surface treatment method 3.

Sample	Ligand/g	Solvent	Ti%	C%	H%	N%	Solubility
FA5-17	OA/16	Ethanol	46.7	21.82	3.32	0	10 %
FA5-18	OA/16	Toluene	47	13.7	1.74	0	Not soluble
FA5-19	Dodecylamine/5	Toluene	53.7	8.35	1.81	0.6	Not soluble
FA5-20	OA/5	Toluene	49.4	14.32	1.78	0	Not soluble

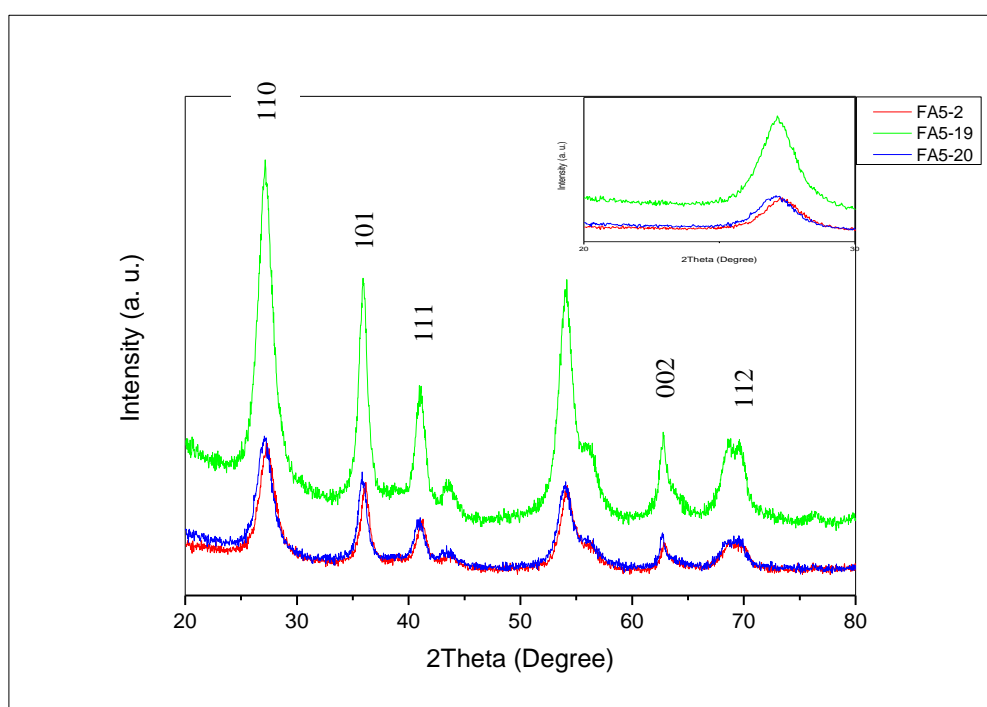


Figure 5-18: XRD patterns of the rutile TiO₂ nanorods FA5-2 (NRs-Rutile-1) and the oleic acid/dodecyl amine-capped TiO₂/OA/AA(12) nanocomposite FA5-19 as well as that of the doubly oleic acid-capped TiO₂/OAx₂ nanocomposite FA5-20 prepared using surface treatment method 3.

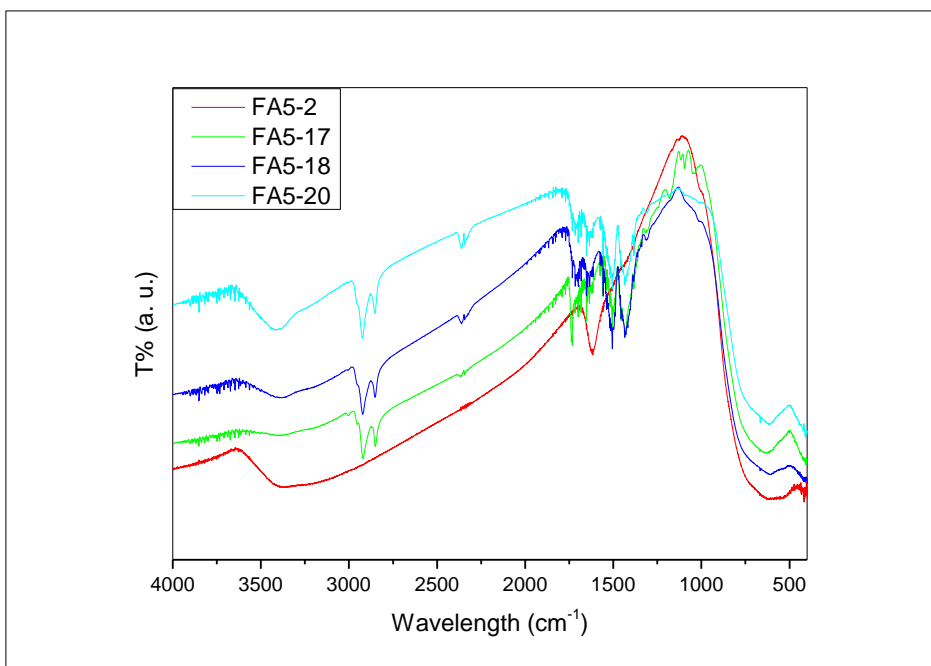


Figure 5-19: FT-IR patterns of the rutile TiO₂ nanorods FA5-2 (NRs-Rutile-1) and the doubly oleic acid-capped TiO₂/OAx2 nanocomposites FA5-17, FA5-18 and FA5-20, prepared using surface treatments using methods 3.

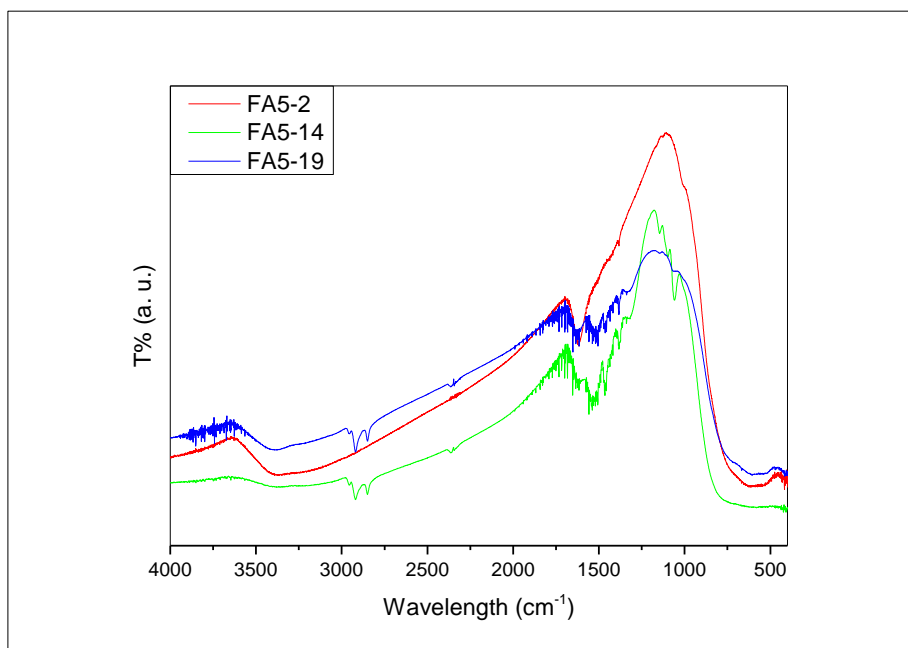


Figure 5-20: FT-IR patterns of the rutile TiO₂ nanorods FA5-2 (NRs-Rutile-1), the dodecyl amine-capped TiO₂/AA(12) nanocomposite FA5-14, prepared using surface treatment method 2, and oleic acid/dodecylamine-capped TiO₂/OA/AA(12) nanocomposite FA5-19 prepared using surface treatment method 3.

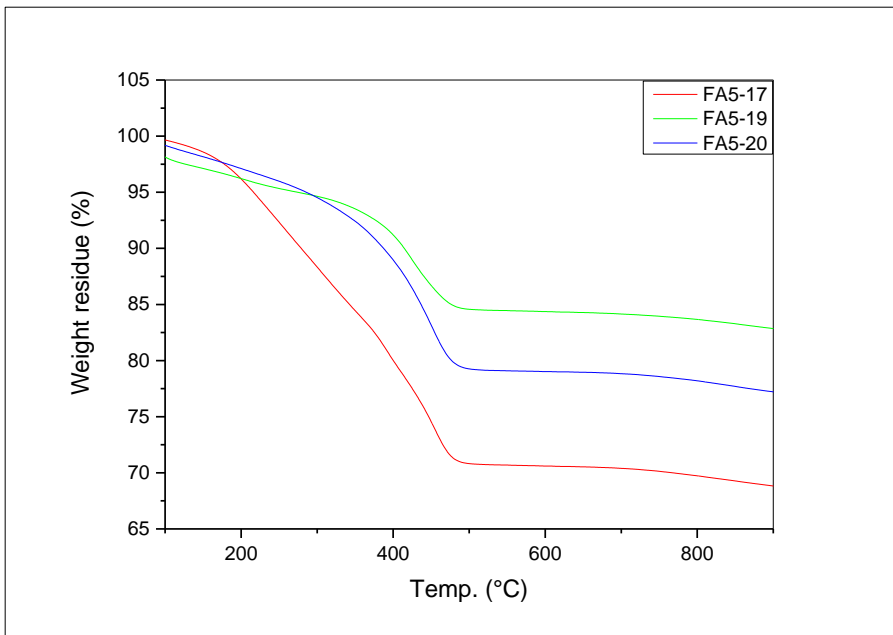


Figure 5-21: TGA of the oleic acid/dodecylamine-capped $\text{TiO}_2/\text{OA}/\text{AA}(12)$ nanocomposite FA5-19 as well as that of the doubly oleic acid-capped $\text{TiO}_2/\text{OAx}2$ nanocomposites FA5-17 and FA5-20 prepared using surface treatment method 3.

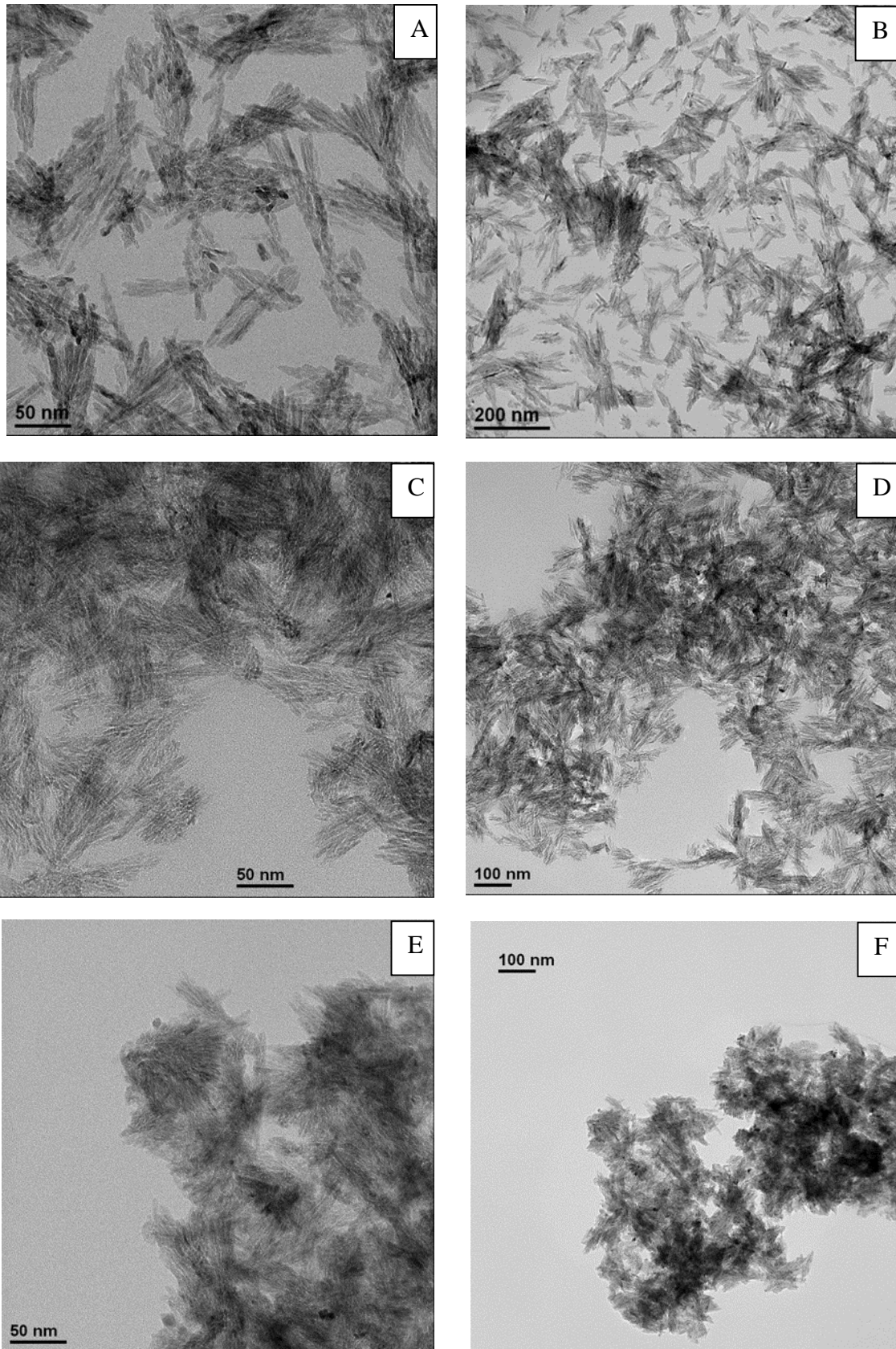


Figure 5-22: TEM images of doubly oleic acid-capped $\text{TiO}_2/\text{OA} \times 2$ nanocomposites FA5-17(A-B), FA5-18 (C-D) and the oleic acid/dodecylamine-capped $\text{TiO}_2/\text{OA}/\text{DA}$ nanocomposite FA5-19 (E-F) prepared using surface treatment method 3.

5.3.2 Approach 2: Hydrothermal Synthesis of Rutile TiO₂ Nanorods from TiOCl₂ (NRs-Rutile-2)

The aim of this reaction, which involves hydrothermal treatment of TiOCl₂ at 220 °C for 2 h, see section 5.2.2.3.1, is to produce rutile TiO₂ nanorods (NRs-Rutile-2) with a more advantageous, i.e., greater, aspect ratio from that achieved using the Approach 1, used to prepare rutile TiO₂ nanorods (NRs-Rutile-1), see section 5.2.2.2.1.

Characterisation of Rutile TiO₂ Nanorods Preparation (NRs-Rutile-2)

The XRD pattern shown in figure 5-23, indicates clearly that the rutile phase has been obtained in the preparation of the rutile TiO₂ nanorods FA5-21 (NRs-Rutile-2) using Approach 2.⁹ However, there is also a small peak at 26°, which is related to the anatase phase.² The full width at half maximum (FWHM) of the peaks of the rutile TiO₂ nanorods FA5-21 is narrower than that observed for the rutile TiO₂ nanorods (NRs-Rutile-1) FA5-1 – FA5-3 prepared using Approach 1 which indicates that the length-to-breadth (aspect) ratio of the rutile TiO₂ nanorods is greater using Approach 2 rather than Approach 1.

Figure 5-24 shows the FT-IR spectrum of rutile TiO₂ nanorods FA5-21 (NRs-Rutile-2). The weak peaks around 1600 cm⁻¹ are suggestive of the presence of a small amount of adsorbed water on the TiO₂ surface. There are also broad peaks at 3100–3600 cm⁻¹ associated with the presence of hydroxyl groups on the surface of the TiO₂ nanorods.¹¹

The TEM images of rutile TiO₂ nanorods FA5-21 (NRs-Rutile-2), shown in figure 5-25, are consistent with XRD results and reveal the presence of long (150-200 nm), narrow (25-40 nm) TiO₂ nanorods. The rutile TiO₂ nanorods FA5-21 (NRs-Rutile-2), prepared using Approach 2, are much bigger than those the rutile TiO₂ nanorods (NRs-Rutile-1) FA5-1 – FA5-3 prepared using Approach 1, see figure 5-4.

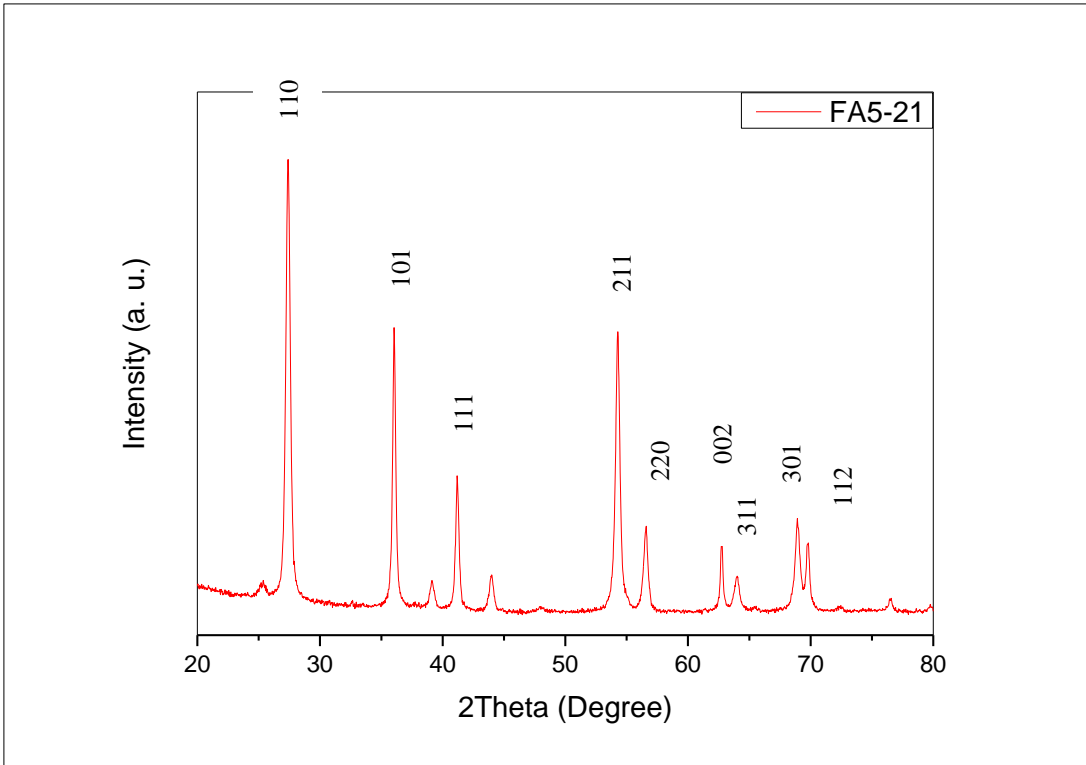


Figure 5-23: XRD pattern of the rutile TiO₂ nanorods FA5-21 (NRs-Rutile-2).

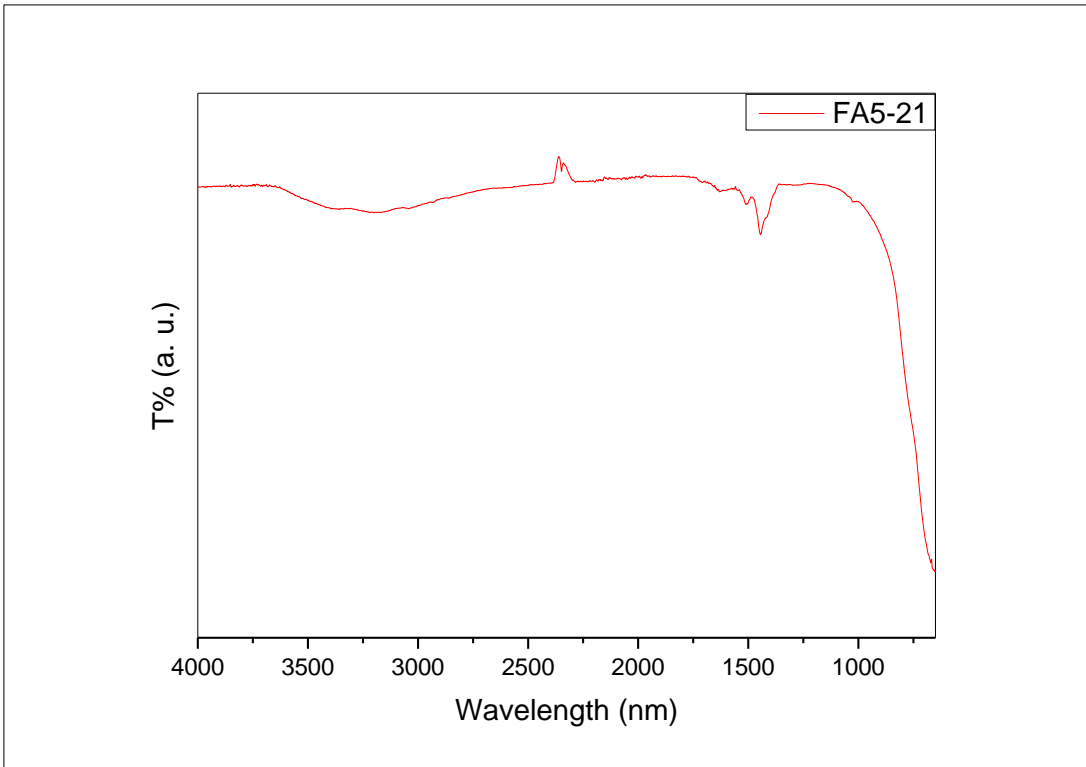


Figure 5-24: FT-IR pattern of the rutile TiO₂ nanorods FA5-21 (NRs-Rutile-2).

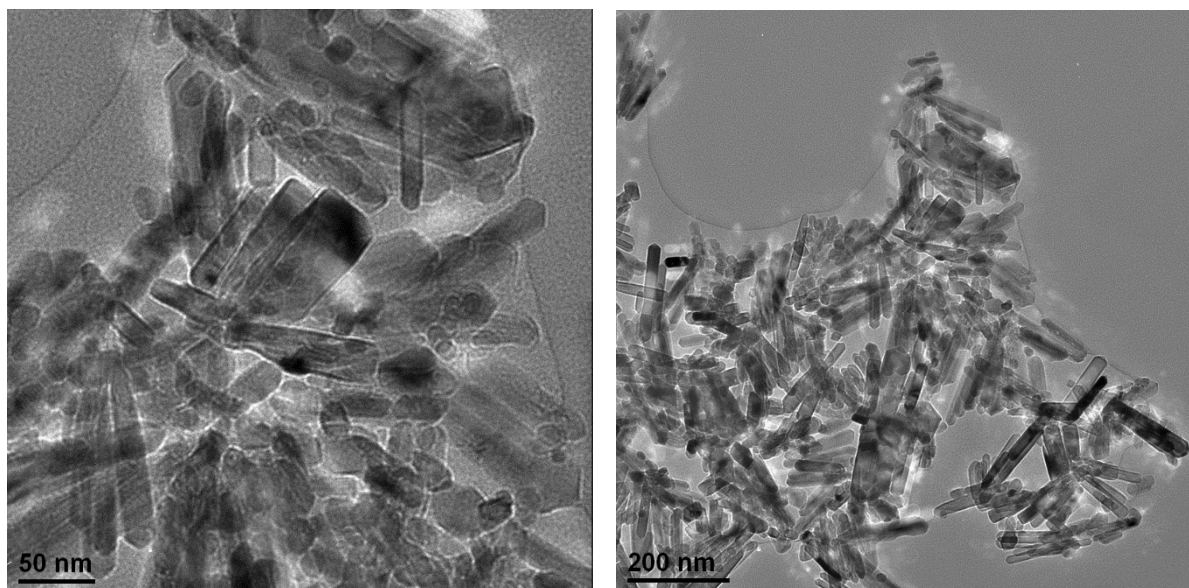


Figure 5-25: TEM images of the rutile TiO₂ nanorods FA5-21 (NRs-Rutile-2).

Surface Modification of Rutile TiO₂ Nanorods (NRs-Rutile-2) with Oleic Acid

The surface of the rutile TiO₂ nanorods FA5-21 (NRs-Rutile-2), synthesised using Approach 2 was coated with a monolayer of oleic acid to produce the TiO₂/OA nanocomposites FA5-22 – FA5-25. The surface modification using wet rutile TiO₂ nanorods FA5-21 (NRs-Rutile-2) as the starting material and two concentration (8 g and 16 g) of oleic acid was carried out at different temperatures, i.e., 78 °C or 110 °C, for several days (3 and 6 days) using either ethanol or dichloromethane as the solvent in a range of reactions designed to optimise the morphology, size and shape (aspect ratio) of the TiO₂/OA nanocomposites FA5-22 – FA5-25 prepared.

Characterisation of Surface Modification of Rutile TiO₂/OA Nanocomposites Preparation – Surface Treatment Method 1

The XRD patterns of the rutile TiO₂ nanorods FA5-21 (Rutile-NRs-2) and the TiO₂/OA nanocomposites FA5-22 – FA5-25 prepared from the rutile TiO₂ nanorods FA5-21 (Rutile-NRs-2) by surface modification with oleic acid, shown in figure 5-26, reveal that all of TiO₂/OA nanocomposites FA5-22 – FA5-25 exhibit the rutile phase for the TiO₂ nanorods. The minor peak at 26°, related to the presence of small concentration of the anatase phase, is still present in the TiO₂/OA nanocomposites FA5-22 and FA5-23, prepared using ethanol as the reaction solvent. However, this small peak cannot be observed in those samples of the

TiO₂/OA nanocomposites FA5-24 and FA5-25, prepared using DMF as the reaction solvent, perhaps due to the higher reaction temperature used in these reactions.

The FT-IR patterns of the rutile TiO₂ nanorods FA5-21 (Rutile-NRs-2) and the TiO₂/OA nanocomposites FA5-22 – FA5-25, shown in figure 5-27, contain two peaks at 1500 and 1435 cm⁻¹ related to asymmetric and symmetric of COO⁻, respectively. An expected carbonyl stretching peak (C=O) at 1711 cm⁻¹ cannot be observed. The peak at 1740 cm⁻¹ is indicative of the fact that some oleates may have been produced during the reaction. The peaks observed at 2850-3000 cm⁻¹ are related to stretch vibrations of CH₃, CH₂ and CH.^{15, 16}

These spectra are indicative of a significant degree of surface coverage of the TiO₂ nanorods (Rutile-NRs-2) of the TiO₂/OA nanocomposites FA5-22 – FA5-25 with oleic acid.

The dimensions of the TiO₂/OA nanocomposites FA5-22 – FA5-25, prepared from the FA5-21 TiO₂ nanorods (Rutile-NRs-2) by surface modification with oleic acid, shown as TEM images in figure 5-29, reveal that they are the same as those of the FA5-21 TiO₂ nanorods (Rutile-NRs-2) before the surface modification with oleic acid.

The degree of modification of the surface of the rutile TiO₂ nanorods FA5-21 (Rutile-NRs-2), prepared using Approach 2 with a coating of oleic acid to produce the TiO₂/OA nanocomposites FA5-22 - FA5-25 was analysed using CHN and ICP chemical analysis, see table 5-10. The concentration of titanium in these the TiO₂/OA nanocomposites (FA5-22 - FA5-25), prepared using Approach 2 lies in the range of 77.3 – 79.0 %, which is higher those (41.1 - 69.2% and 46.7 - 53.7%) observed for the TiO₂/OA nanocomposites FA5-9 – FA5-12 and the TiO₂/OAx2 nanocomposites FA5-17, FA5-18 and FA5-20, see tables 5-8 and 5-9, respectively, prepared using the surface treatment methods 2 and 3, respectively, of the FA5-2 TiO₂ nanorods (Rutile-NRs-1), prepared by Approach 1. This can be explained by the geometric relationship between the size of the nanorods and their surface area. Larger, bulkier nanorods have a lower surface area and so, logically, less oleic acid can be bonded onto the rutile TiO₂ nanorod surface in relative terms. The nature of the reaction solvent, temperatures and times appears to have little effect on the chemical compositions of the surface-modified TiO₂/OA nanocomposites FA5-22 - FA5-25.

The TGA analysis of the TiO₂/OA nanocomposites FA5-24 and FA5-25, prepared from the rutile TiO₂ nanorods FA5-21 (Rutile-NRs-2) by surface modification with oleic acid using DMF as the reaction solvent shown in figure 5-28, reveals that two weight loss events occur, i.e., at <120 °C, due to desorption of adsorbed water, and between 320-490 °C due to slow decomposition of the oleic acid surface coating. The weight losses (9 % and 12 %) for the

TiO₂/OA nanocomposites FA5-24 and FA5-25, respectively, are consistent with those determined using CHN analysis.

Table 5-10: Chemical analyses of the oleic acid-capped TiO₂/OA nanocomposites FA5-22 – FA5-25, prepared using surface treatment method 1.

Sample	OA/g	Solvent	Temp./°C	Ti%	C%	H%	N%	Solubility
FA5-22	8	Ethanol	78	77.7	3.88	0.00	0.00	Not soluble
FA5-23	16	Ethanol	78	79.0	4.46	0.46	0.00	Not soluble
FA5-24	8	DMF	110	78.2	4.17	0.55	0.00	Not soluble
FA5-25	16	DMF	110	77.3	6.86	0.86	0.00	Not soluble

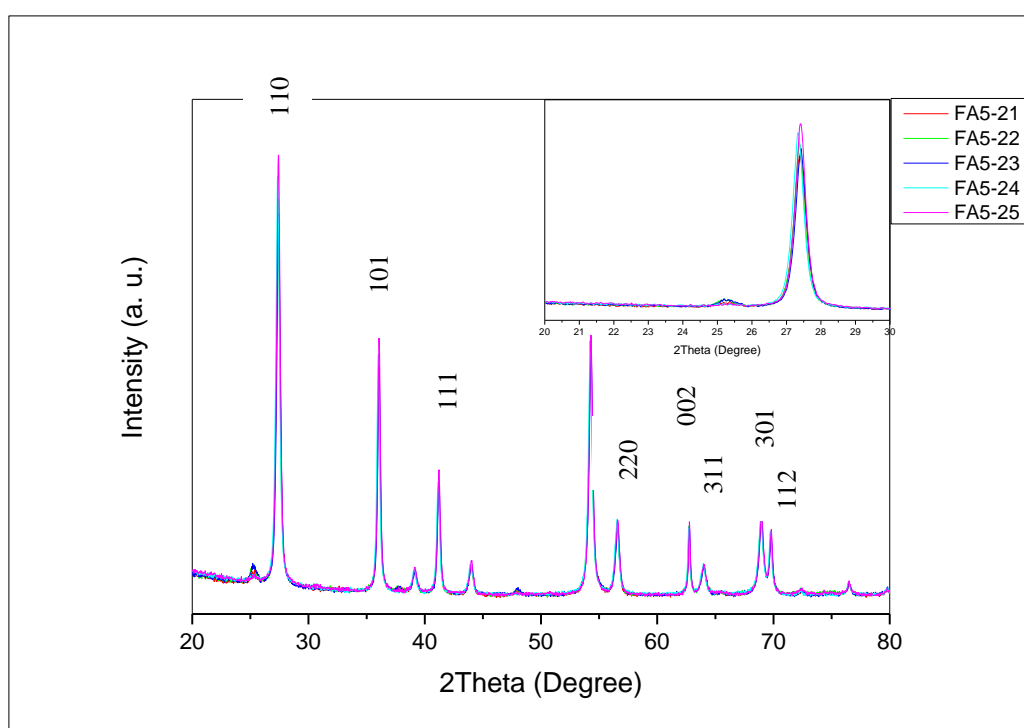


Figure 5-26: XRD patterns of the rutile TiO₂ FA5-21 nanorods (Rutile-NRs-2) and the oleic acid-capped TiO₂/OA nanocomposites FA5-22 – FA5-25 prepared using surface treatment method 1.

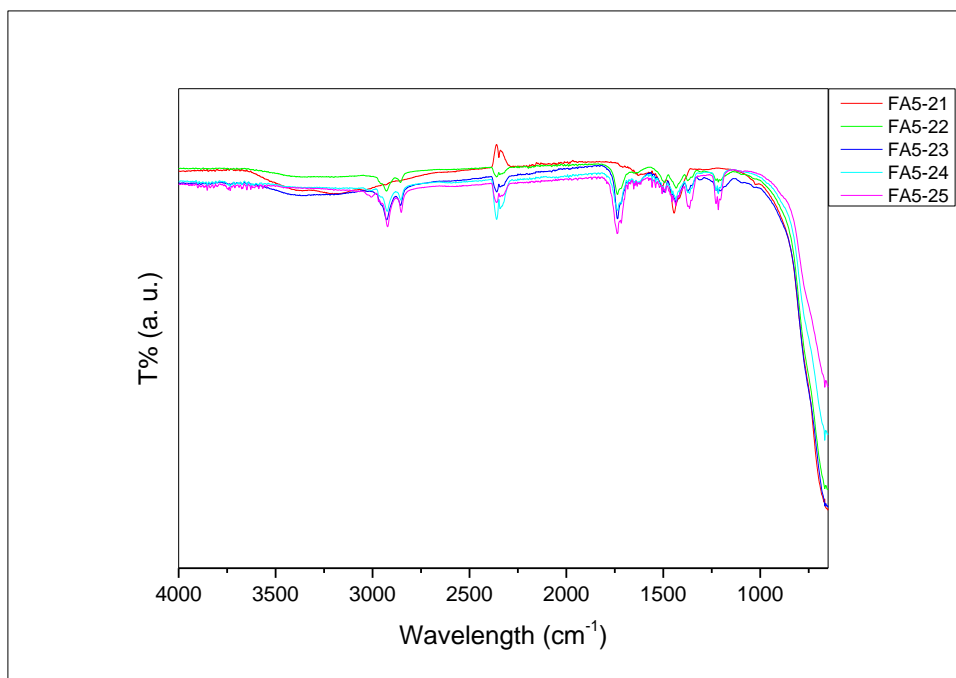


Figure 5-27: FT-IR patterns of the rutile TiO₂ FA5-21 nanorods (Rutile-NRs-2) and the oleic acid-capped TiO₂/OA nanocomposites FA5-22 – FA5-25 prepared using surface treatment method 1.

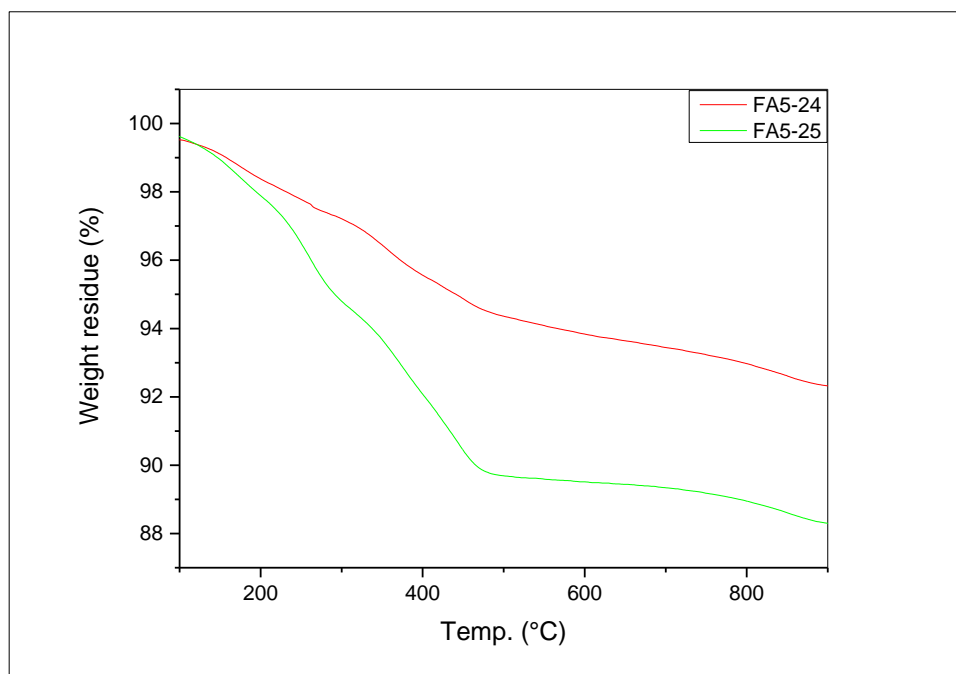


Figure 5-28: TGA of the oleic acid-capped TiO₂/OA nanocomposites FA5-24 and FA5-25, prepared using surface treatment method 1.

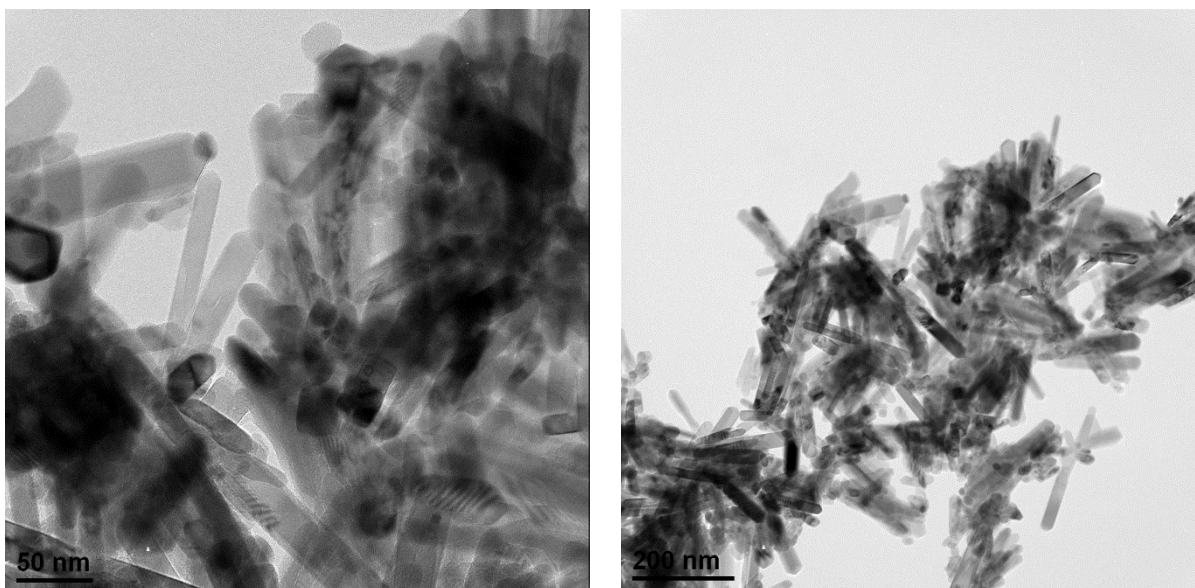


Figure 5-29: TEM images of the oleic acid-capped TiO₂/OA nanocomposites FA5-22, prepared using surface treatment method 1.

Approach 3: Hydrothermal Synthesis of Nanorods of Rutile TiO₂ in Presence of Amine (NRs-Rutile-3)

Since the rutile TiO₂ nanorods, i.e., rutile TiO₂ FA5-21 nanorods (Rutile-NRs-2), prepared using Approach 2 appear to be too large to serve as the basis of solution-processable nanocomposites, e.g., TiO₂/OA nanocomposites FA5-22 – FA5-25 prepared from the rutile TiO₂ FA5-21 nanorods (Rutile-NRs-2) by surface modification with oleic acid, a similar reaction to that used in Approach 2 using TiOCl₂ as the starting material, but carried out in Approach 3 in the presence of 3-hydroxytyramine hydrogen chloride [(HO)₂C₆H₃CH₂CH₂NH₂·HCl], was investigated as a means of achieving the aim of synthesising nanorods of rutile TiO₂ i.e., rutile TiO₂ FA5-26 nanorods (Rutile-NRs-3), with a lower aspect ratio than that for the TiO₂ nanorods prepared using Approach 2, i.e., rutile TiO₂ FA5-21 nanorods (Rutile-NRs-2), see figure 5-24.

Characterisation of Rutile TiO₂ Nanorods Preparation (NRs-Rutile-3)

The XRD pattern of the TiO₂ FA5-26 nanorods (Rutile-NRs-3), shown in figure 5-30, reveals the formation of rutile TiO₂⁹ with a minor peak at 26° related to the presence of some TiO₂ nanorods in the anatase phase². The full width at half maximum (FWHM) of peaks of TiO₂ is bigger than that observed for the TiO₂ nanorods (NRs-Rutile-2) in the rutile phase prepared using the Approach 2 suggesting that the dimensions of nanorods are greater using the Approach 2 than using this modified method incorporating the use of 3-hydroxytyramine hydrogen chloride.

The FT-IR spectrum of the rutile TiO₂ FA5-26 nanorods (Rutile-NRs-3), presented in figure 5-31, reveals the expected broad peak at 500-600 cm⁻¹ attributable to the vibration of the O–Ti–O bonds in the framework of TiO₂. Also, adsorption of water is figured in the peak at 1625 cm⁻¹. A broad peaks at 3100–3600 cm⁻¹ is associated to the hydroxyl group's vibrations.¹¹

The TEM image of the rutile TiO₂ FA5-26 nanorods (Rutile-NRs-3), shown in figure 5-32, reveals the presence of TiO₂ nanorods in the rutile phase with an average length of 80 nm (around 50-100 nm) and a smaller diameter (ca 20 nm). However, some FA5-26 TiO₂ nanoparticles with length of ca 25 nm can also be observed.

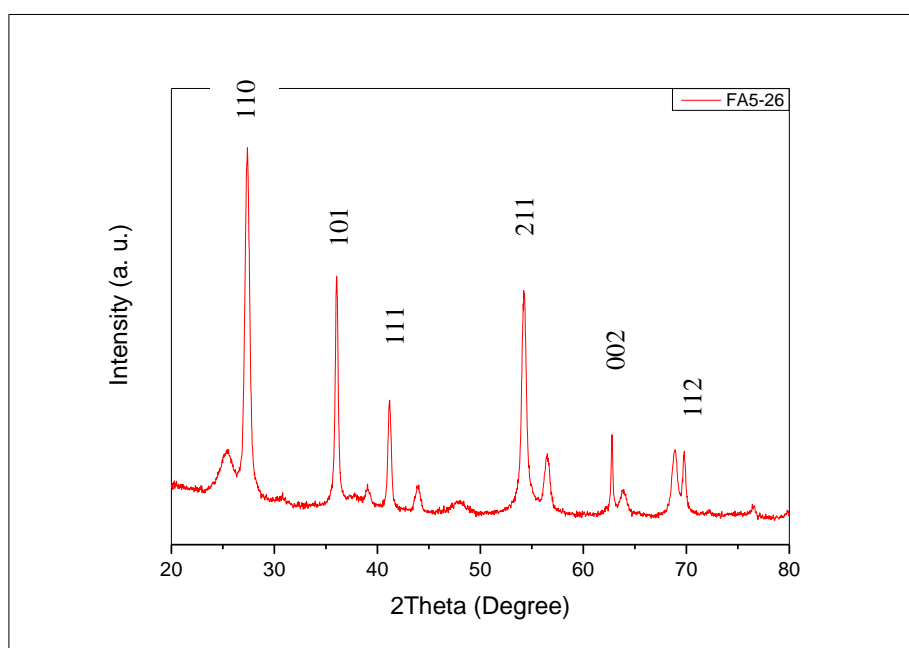


Figure 5-30: XRD patterns of the rutile TiO₂ FA5-26 nanorods (Rutile-NRs-3).

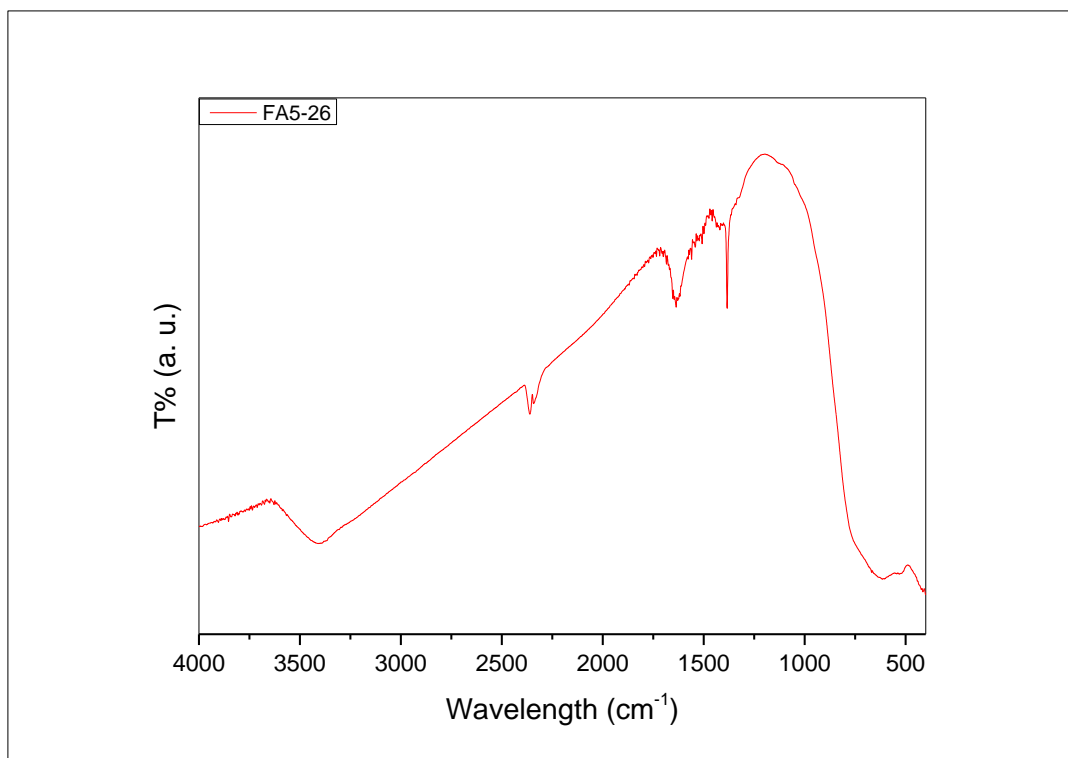


Figure 5-31: FT-IR patterns of the rutile TiO₂ FA5-26 nanorods (Rutile-NRs-3).

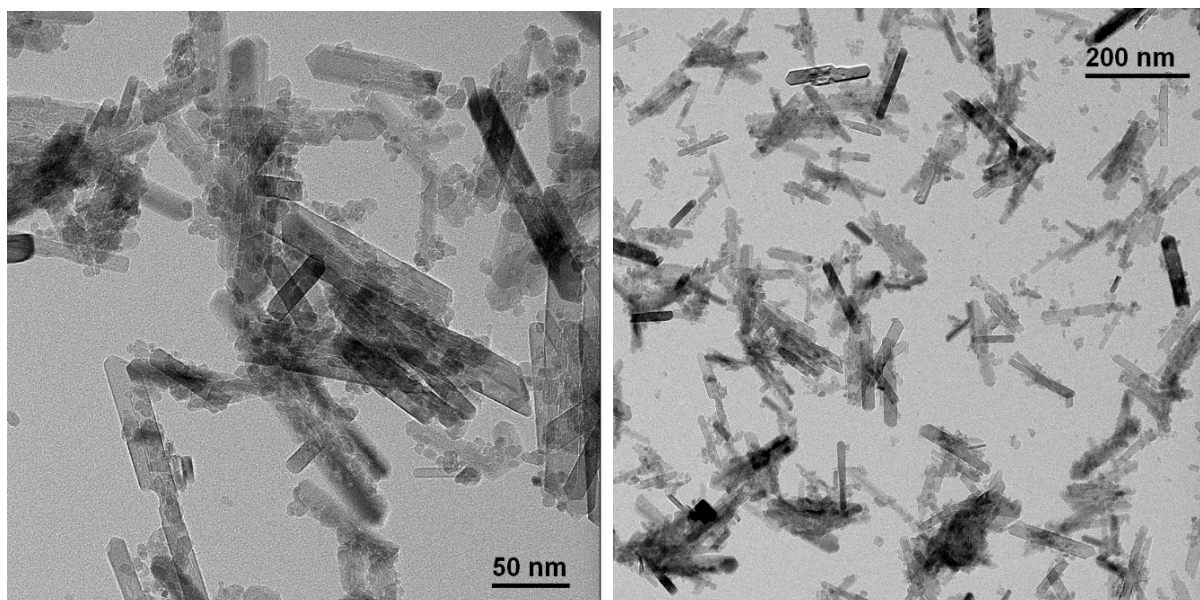


Figure 5-32: TEM images of the rutile TiO₂ FA5-26 nanorods (Rutile-NRs-3).

Surface Modification of Rutile TiO₂ Nanorods (NRs-Rutile-3) with n-Alkyl Phosphonic Acids, Oleic Acid or Diethyl 2-Phenylethyl Phosphonate

The surface modification of the rutile TiO₂ FA5-26 nanorods (Rutile-NRs-3), prepared using Approach 3, was also investigated in two sequential surface treatment processes.

In the first surface treatment method 1, the rutile TiO₂ FA5-26 nanorods (Rutile-NRs-3) and rutile FA5-2 TiO₂ nanorods (Rutile-NRs-1), respectively, were reacted with either octylphosphonic acid (OPA) or decylphosphonic acid (ODPA) at 120 °C for 4 h in DMF in the presence of several drops of hydrochloric acid to yield the TiO₂/OPA nanocomposites FA5-27, FA5-28, FA5-30 And FA5-31, the TiO₂/ODPA nanocomposites FA5-29 and FA5-32 and the TiO₂/OPA nanocomposite FA5-33, respectively, see table 5-11.

In the second surface treatment method the TiO₂/OPA nanocomposites FA5-27, FA5-28, FA5-30, FA5-31 and FA5-33 and the TiO₂/ODPA nanocomposites FA5-29 and FA5-32, prepared using surface treatment method 1 were reacted with either oleic acid or diethyl 2-phenylethyl phosphonate (DEPPNA) at 125 °C for 72 h in DMF in the presence of several drops of hydrochloric acid to yield the TiO₂/OPA/OA nanocomposites FA5-34, FA5-36, FA5-38, FA5-39 and FA5-41, the TiO₂/OPA/DEPPNA nanocomposite FA5-35 and the TiO₂/ODPA/OA nanocomposites FA5-37 and FA5-40, respectively, using surface treatment method 2, see table 5-12.

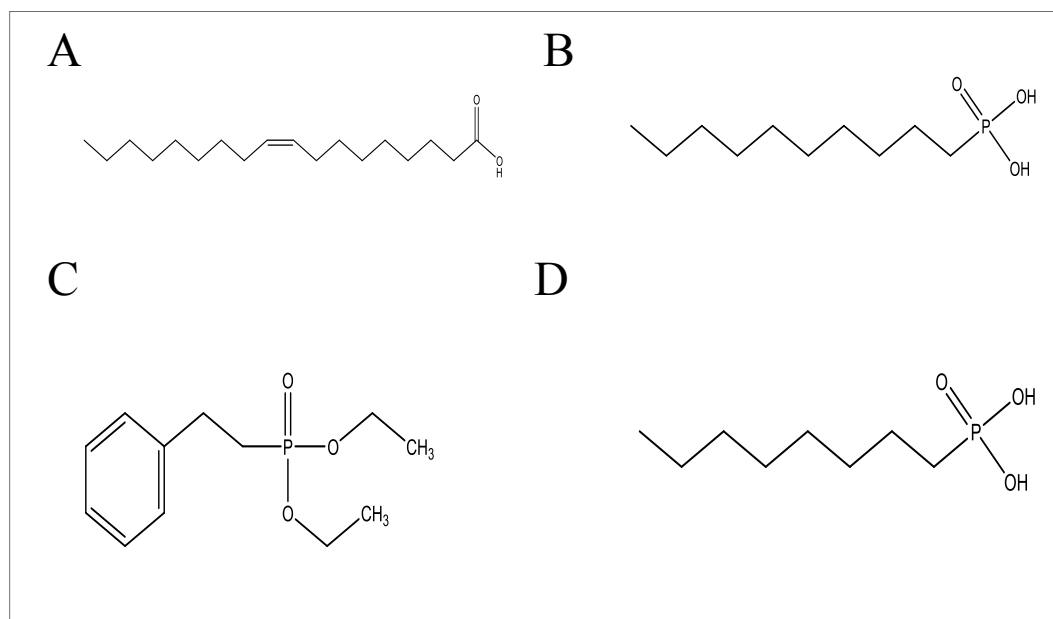
Table 5-11: Chemical analyses for the octylphosphonic acid-capped TiO₂/OPA nanocomposites FA5-27, FA5-28, FA5-31 and FA5-33, the decylphosphonic acid-capped TiO₂/ODPA nanocomposites FA5-29 and FA5-32, prepared using surface treatment method 1.

Sample	Ligand	Starting Material	Ti %	C %	H %	P %
FA5-27	OPA	NRs-Rutile-3/FA5-26	68.28	3.28	0.12	0.67
FA5-28	OPA	NRs-Rutile-3/FA5-26	54.57	3.45	0.00	0.92
FA5-29	ODPA	NRs-Rutile-3/FA5-26	58.12	4.14	0.00	0.95
FA5-30	OPA	NRs-Rutile-3/FA5-26				
FA5-31	OPA	NRs-Rutile-3/FA5-26	56.90	4.53	0.00	---
FA5-32	ODPA	NRs-Rutile-3/FA5-26	---	5.09	0.66	---
FA5-33	OPA	NRs-Rutile-1/FA5-2	51.28	9.43	1.67	2.73

Table 5-12: Chemical analyses for the TiO₂/OPA/OA nanocomposites FA5-34, FA5-36, FA5-38, FA5-39 and FA5-41, the TiO₂/OPA/DEPPNA nanocomposite FA5-35, the TiO₂/ODPA/OA nanocomposites FA5-37 and FA5-40, prepared using surface treatment method 2.

Sample	Ligand	Starting Material	Ti%	C %	H %	P %
FA5-34	OA	FA5-27	52.85	6.99	0.92	0.65
FA5-35	DEPPNA	FA5-27	57.10	3.69	0.54	1.11
FA5-36	OA	FA5-28	59.05	3.54	0.00	0.84
FA5-37	OA	FA5-29	56.91	5.06	0.00	0.73
FA5-38	OA	FA5-30	---	21.58	2.12	---
FA5-39	OA	FA5-31	---	5.31	0.31	---
FA5-40	OA	FA5-32	---	5.54	0.62	---
FA5-41	OA	FA5-33	50.24	8.17	1.40	2.59

The ligands used in these two reactions are shown in scheme 5-5.



Scheme 5-5: Structures of ligands that used in acid-stabilisation of the FA5-26 TiO₂ nanorods (Rutile-NRs-3); (A) oleic acid (OA), (B) decylphosphonic acid (ODPA), (C) 2-(phenyl)ethyl phosphonate (DEPPNA) and (D) octylphosphonic acid (OPA).

Synthesis of Rutile TiO₂/Ligand Nanocomposites – Surface Treatment Methods 1 and 2

The XRD patterns of the TiO₂/OPA nanocomposites FA5-27 and FA5-28, the TiO₂/ODPA nanocomposites FA5-29 and FA5-32 and the TiO₂/OPA nanocomposite FA5-33, prepared from either the rutile TiO₂ FA5-26 nanorods (Rutile-NRs-3) or the rutile TiO₂ nanorods FA5-2 (NRs-Rutile-1), respectively using surface treatment method 1, are shown in figure 5-33. The XRD patterns of the TiO₂/OPA/OA nanocomposites FA5-34, FA5-37 and FA5-41 and the TiO₂/OPA/DEPPNA nanocomposite FA5-35, prepared from the TiO₂/OPA nanocomposites FA5-27, FA5-29, FA5-33 and FA5-27, respectively, using the subsequent surface treatment method 2, are shown in figure 5-34. These XRD patterns reveal that the rutile phase of all of TiO₂ nanorods has been retained in all the surface-modified products, i.e., the TiO₂/OPA nanocomposites FA5-27 and FA5-28 and the TiO₂/ODPA nanocomposites FA5-29 and FA5-32 and the TiO₂/OPA/OA nanocomposites FA5-34, FA5-37 and FA5-41 and the TiO₂/OPA/DEPPNA nanocomposite FA5-35, along with a peak at 26° related to anatase phase

for the original starting material, i.e., the rutile TiO₂ FA5-26 nanorods (Rutile-NRs-3) prepared in Approach 3, see figure 5-19. The TiO₂/OPA nanocomposite FA5-33 exhibits a rutile phase, but no anatase phase, as it was prepared from the rutile TiO₂ FA5-2 nanorods (Rutile-NRs-1), see figure 5-2.

There is no difference in the intensity of the XRD peaks compared with those observed for any of the starting materials, i.e., rutile TiO₂ FA5-26 nanorods (Rutile-NRs-3) and the TiO₂/OPA nanocomposites FA5-27, FA5-29, FA5-33 and FA5-27.

The FT-IR spectra of the TiO₂/OPA nanocomposites FA5-27 and FA5-28 and the TiO₂/ODPA nanocomposite FA5-29, prepared from the rutile TiO₂ FA5-26 nanorods (Rutile-NRs-3) using surface treatment method 1, are shown in figure 5-35. The FT-IR spectra of the TiO₂/OPA/OA nanocomposites FA5-34, FA5-36 and FA5-41, the TiO₂/OPA/DEPPNA nanocomposite FA5-35 and the TiO₂/ODPA/OA nanocomposite FA5-40, prepared from the TiO₂/OPA nanocomposites FA5-27, FA5-28 and FA5-33, TiO₂/OPA nanocomposites FA5-27 and the TiO₂/ODPA nanocomposite FA5-32, respectively, using surface treatment method 2, are shown in figure 5-36. These FT-IR spectra reveal the presence of some new peaks compared to those of the FT-IR spectra of the unmodified rutile TiO₂ FA5-26 nanorods (Rutile-NRs-3) and rutile TiO₂ FA5-2 nanorods (Rutile-NRs-1), shown in figure 5-30 and figure 5-3, respectively. The peak at 1040 cm⁻¹ is evidence for P-O stretching vibration and the peak at 970 cm⁻¹ is characteristic of a P-O-C stretching vibration.^{20, 21} The stretch vibrations of CH₃, CH₂ and CH can be observed as peaks at 2850-3000 cm⁻¹.^{15, 16}

There is no difference in the shape and size of the TiO₂ nanorods of the TiO₂/OPA nanocomposites FA5-27 and FA5-28 and the TiO₂/ODPA nanocomposite FA5-29, prepared from the rutile TiO₂ FA5-26 nanorods (Rutile-NRs-3), see figure 5-31, prepared using surface treatment method 1 as revealed in the TEM images shown in figure 5-37. There is also no difference in the shape and size of the TiO₂ nanorods of the TiO₂/OPA/OA nanocomposite FA5-36 shown in figure 5-38. However, there is still some degree of aggregation for the TiO₂/ligands nanocomposites after the surface modification.

The degree of modification of TiO₂ nanorods prepared using the two sequential surface treatment methods 1 and was analysed using CHN and ICP chemical analysis, see tables 5-11 and 5-12, respectively. The carbon and phosphor contents obtained for the TiO₂/OPA nanocomposites FA5-27, FA5-28 and FA5-31 and the TiO₂/ODPA nanocomposites FA5-29 and FA5-32, prepared from the rutile TiO₂ FA5-26 nanorods (Rutile-NRs-3) using surface treatment method 1, lie within the ranges 3.3-4.1% and 0.6-0.95%, respectively. These values are much lower than those determined for the TiO₂/OPA nanocomposite FA5-33, prepared

from the rutile TiO₂ FA5-2 nanorods (Rutile-NRs-1), respectively, using surface treatment method 1.

Table 5-12 collates the results for the chemical analyses obtained for the TiO₂/OPA/OA nanocomposites FA5-34, FA5-36, FA5-38, FA5-39 and FA5-41, the TiO₂/OPA/DEPPNA nanocomposite FA5-35 and the TiO₂/ODPA/OA nanocomposites FA5-37 and FA5-40, prepared from the TiO₂/OPA nanocomposites FA5-27, FA5-28, FA5-31 and FA5-33 and the TiO₂/ODPA nanocomposites FA29 and FA5-32, respectively, using surface treatment method 2.

A much higher phosphorous content is observed for the TiO₂/OPA/DEPPNA nanocomposite FA5-35 with the phosphorous-containing DEPPNA ligand as a part of the surface coating. However, the phosphorous content of the TiO₂/OPA/OA nanocomposites FA5-34, FA5-36, FA5-38, FA5-39 and FA5-41 and the TiO₂/ODPA/OA nanocomposites FA5-37 and FA5-40 is lower than those determined for the corresponding TiO₂/OPA nanocomposites FA5-27, FA5-28, FA5-31 and FA5-33 and the TiO₂/ODPA nanocomposites FA29 and FA5-32, respectively, with only oleic acid as a surface coating as a result of the surface treatment method 1.

The highest carbon content (21.58%) by far is observed for the TiO₂/OPA/OA nanocomposite FA5-38.

The titanium content determined for the TiO₂/OPA/OA nanocomposites FA5-34, FA5-36, FA5-38, FA5-39 and FA5-41, the TiO₂/OPA/DEPPNA nanocomposite FA5-35 and the TiO₂/ODPA/OA nanocomposites FA5-37 and FA5-40, prepared using surface treatment method 2, is lower than that observed for the corresponding TiO₂/OPA nanocomposites FA5-27, FA5-28 and FA5-31, the TiO₂/ODPA nanocomposites FA29 and FA5-32 and the TiO₂/OPA nanocomposite FA5-33, prepared from the rutile TiO₂ FA5-26 nanorods (Rutile-NRs-3) and rutile TiO₂ nanorods FA5-2 (Rutile-NRs-1), respectively, surface treatment method 1, used to prepare them.

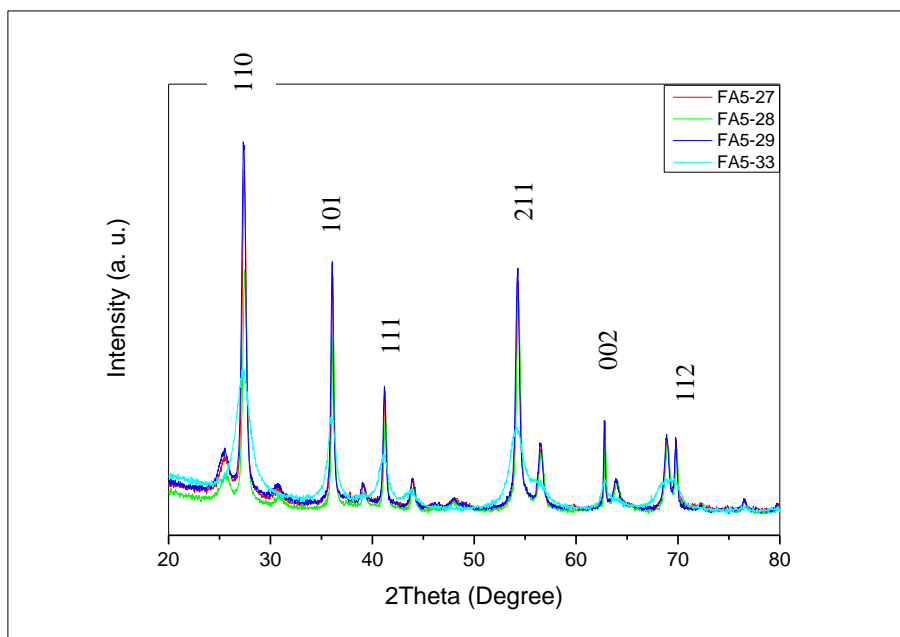


Figure 5-33: XRD patterns of the octylphosphonic acid-capped TiO_2/OPA nanocomposites FA5-27, FA5-28 and FA5-33 and the decylphosphonic acid-capped TiO_2/ODPA nanocomposites FA5-29 and FA5-32 prepared using surface treatment method 1.

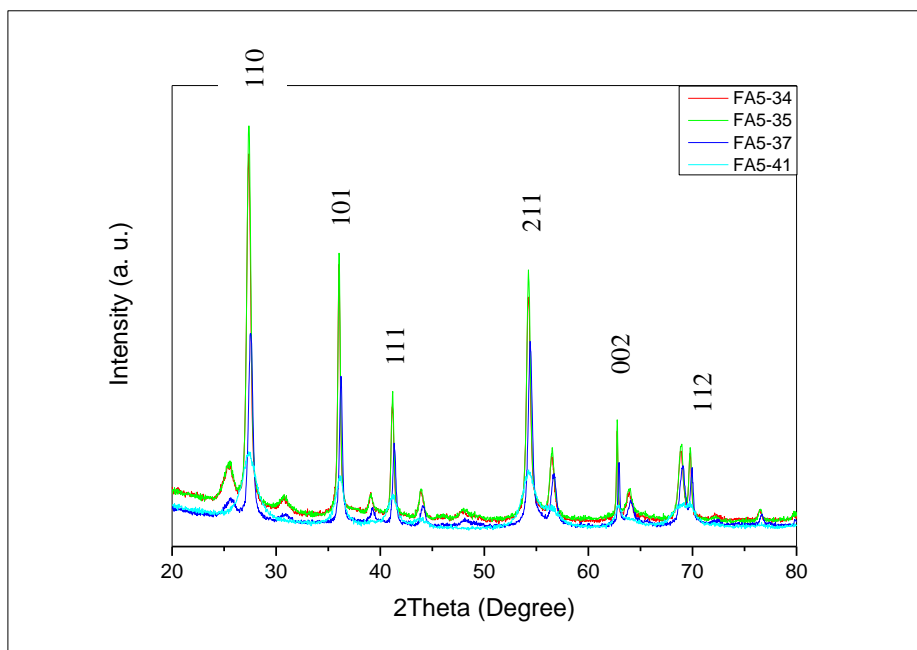


Figure 5-34: XRD pattern of the octylphosphonic acid and oleic acid-capped $\text{TiO}_2/\text{OPA}/\text{OA}$ nanocomposites FA5-34, FA5-37 and FA5-41 and the octylphosphonic acid and 2-(phenyl)ethyl phosphonate $\text{TiO}_2/\text{OPA}/\text{DEPPNA}$ nanocomposite FA5-35, prepared using surface treatment method 2.

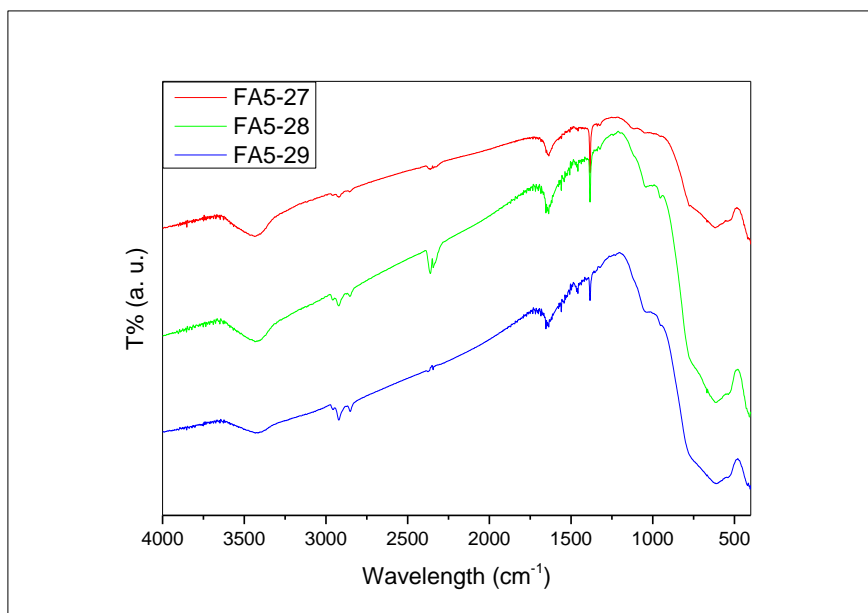


Figure 5-35: FT-IR pattern of the octylphosphonic acid-capped TiO₂/OPA nanocomposites FA5-27 and FA5-28 and the decylphosphonic acid-capped TiO₂/ODPA nanocomposite FA5-29, prepared using surface treatment method 1.

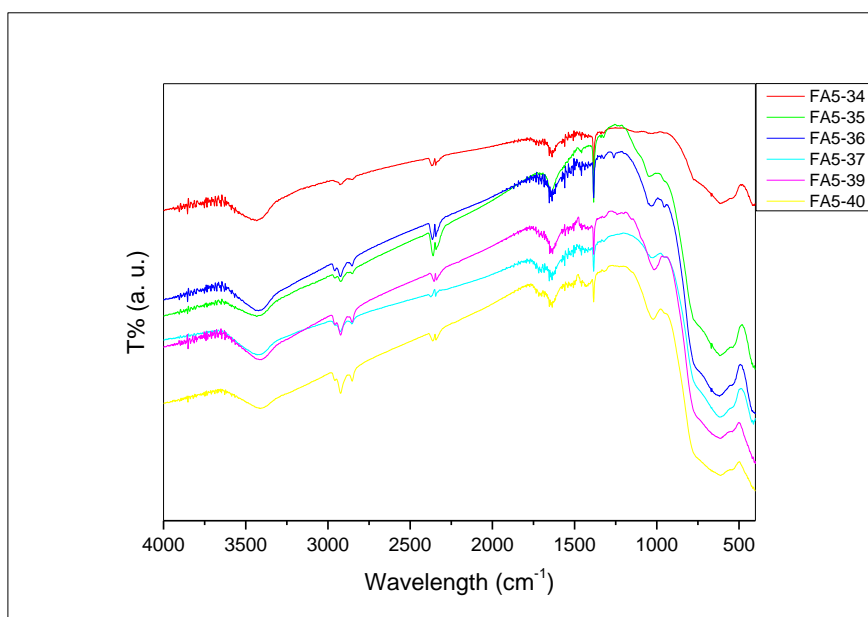


Figure 5-36: the octylphosphonic acid and oleic acid-capped TiO₂/OPA/OA nanocomposites FA5-34, FA5-36 and FA5-41, the octylphosphonic acid and 2-(phenyl) ethyl phosphonate-capped TiO₂/OPA/DEPPNA nanocomposite FA5-35 and the octylphosphonic acid and decylphosphonic acid-capped TiO₂/ODPA/OA nanocomposite FA5-40, prepared using surface treatment method 2.

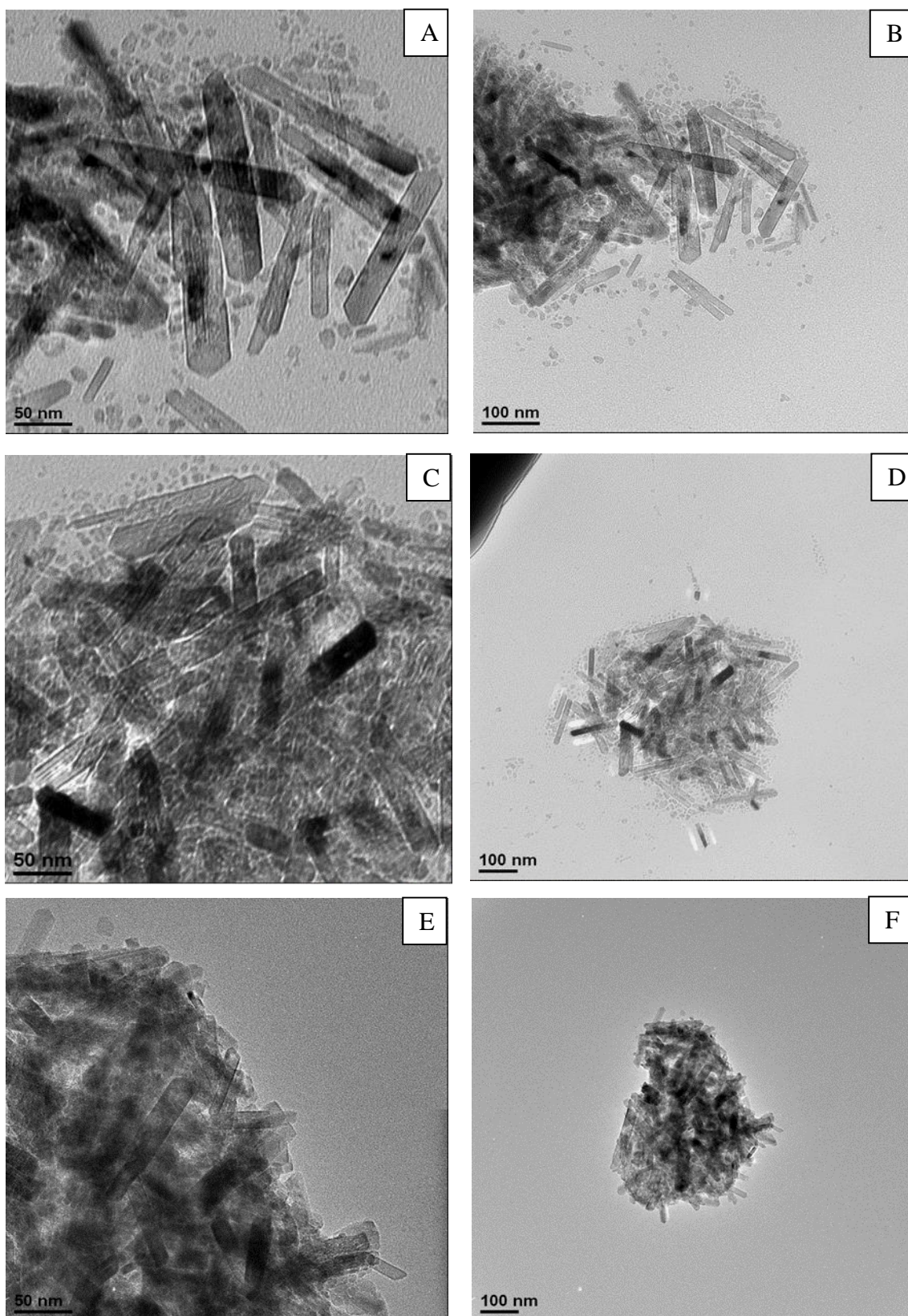


Figure 5-37: TEM images of the octylphosphonic acid-capped TiO₂/OPA nanocomposites FA5-27 (A-B), FA5-28 (C-D) and the decylphosphonic acid-capped TiO₂/ODPA nanocomposite FA5-29 (E-F) prepared using surface treatment method 1.

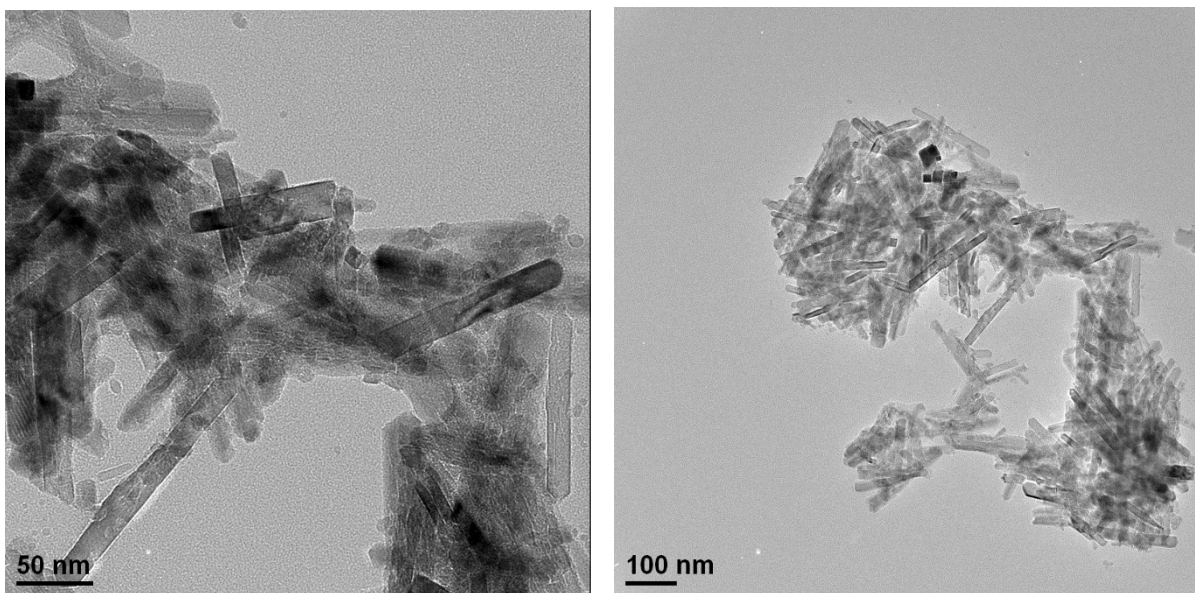


Figure 5-38: TEM images of the octylphosphonic acid and oleic acid-capped TiO_2 /OPA/OA nanocomposites FA5-36 prepared using surface treatment method 2.

5.4 Conclusion and Summary

Rutile TiO₂ nanorods have been synthesised using three different approaches and the surface modification of these nanorods has been investigated. In the first method hair-like, rutile TiO₂ nanorods (Rutile-NRs-1) were prepared using an hydrolysis reaction involving TiOCl₂ and water at 50 °C, 70 °C and 90 °C for 24 h. Surface modification of the rutile TiO₂ nanorods (Rutile-NRs-1) prepared using this method was carried out using wet TiO₂ nanorods with ligands, such as oleic acid and alkyl amines i.e., octyl amine, dodecyl amine and hexadecyl amine, either in ethanol at 78 °C or in DMF at 110 °C as the solvent for several days. The carbon content of the resultant TiO₂/ligand nanocomposites can be relatively high, e.g., 21 %, which is indicative of a high surface coverage with the ligand. The aliphatic surface coating of the TiO₂/ligand nanocomposites leads to a relatively high degree of solubility in organic solvents, so some of them can be suspended up to a concentration of 10 % in chlorobenzene. These colloidal solutions are stable for several months. The hybrid insulator of rutile TiO₂/ligand nanocomposites preparation – surface treatment method 2 product FA5-9 was spin coated from a 10% wt solution in chlorobenzene on prepatterned metallic electrodes, with final thickness of the hybrid insulating films was ~200 nm and the dielectric constant is 9-10 at 1 MHz

The second approach to produce rutile TiO₂ nanorods involved using a hydrothermal treatment of TiOCl₂ at 220 °C for 2 h. These rutile TiO₂ nanorods (Rutile-NRs-2) are relatively long, i.e., 150-200 nm and broad, i.e., 25-40 nm. Such large nanorods have a lower effective surface area than those prepared using approach 1 and so less oleic acid is attached in relative terms to the TiO₂/ligand nanocomposite surface, i.e., the carbon content for the resultant TiO₂/ligand nanocomposites is low, e.g., 6 %. The combination of the relatively low surface coverage and the large dimensions of these TiO₂/ligand nanocomposites leads to a limited degree of solubility in organic solvents.

The third approach involved the hydrothermal reaction of TiOCl₂ in the presence of 3-hydroxytyramine hydrogen chloride, [(HO)₂C₆H₃CH₂CH₂NH₂·HCl] for 13 h at 150°C to prepare smaller rutile TiO₂ nanorods (Rutile-NRs-3), e.g., 80 nm and 20 nm in length and diameter, respectively. However, the presence of some smaller TiO₂ nanoparticles, e.g., 25 nm long, is also observed. Surface modification was carried out using either oleic acid or phosphonate/phosphonic acid as ligands. Unfortunately, the solubility of TiO₂/ligand

nanocomposites, is limited due to a lower surface coverage of the ligands bonded onto the nanorod surface.

5.5 References

1. Collins, A. M., *Nanotechnology Cookbook: Practical, Reliable and Jargon-free Experimental Procedures*. Elsevier: 2012.
2. Kim, S.-J.; Park, S.-D.; Jeong, Y. H.; Park, S., Homogeneous Precipitation of TiO₂ Ultrafine Powders from Aqueous TiOCl₂ Solution. *Journal of the American Ceramic Society* **1999**, 82, (4), 927-932.
3. Sekar, M. M. A.; Patil, K. C., Combustion synthesis and properties of fine-particle dielectric oxide materials. *Journal of Materials Chemistry* **1992**, 2, (7), 739-743.
4. Kudaka, K.; Iizumi, K.; Sasaki, K., Preparation of Stoichiometric Barium Titanyl Oxalate Tetrahydrate. *American Ceramic Society Bulletin* **1982**, 61, 1236.
5. Cheng, H.; Ma, J.; Zhao, Z.; Qi, L., Hydrothermal Preparation of Uniform Nanosize Rutile and Anatase Particles. *Chemistry of Materials* **1995**, 7, (4), 663-671.
6. Tahir, M. N.; Theato, P.; Oberle, P.; Melnyk, G.; Faiss, S.; Kolb, U.; Janshoff, A.; Stepputat, M.; Tremel, W., Facile Synthesis and Characterization of Functionalized, Monocrystalline Rutile TiO₂ Nanorods. *Langmuir* **2006**, 22, (12), 5209-5212.
7. Ruiterkamp, G. J.; Hempenius, M. A.; Wormeester, H.; Vancso, G. J., Surface functionalization of titanium dioxide nanoparticles with alkanephosphonic acids for transparent nanocomposites. *Journal of Nanoparticle Research* **2011**, 13, (7), 2779-2790.
8. Wang, T.-H.; Navarrete-López, A. M.; Li, S.; Dixon, D. A.; Gole, J. L., Hydrolysis of TiCl₄: Initial Steps in the Production of TiO₂. *The Journal of Physical Chemistry A* **2010**, 114, (28), 7561-7570.
9. Chen, H.-S.; Su, C.; Chen, J.-L.; Yang, T.-Y.; Hsu, N.-M.; Li, W.-R., Preparation and Characterization of Pure Rutile TiO₂ Nanoparticles for Photocatalytic Study and Thin Films for Dye-Sensitized Solar Cells. *Journal of Nanomaterials* **2011**, 2011, 8.
10. Zhang, Y. F.; Su, C. W.; Xia, H.; Xiao, P. F., *Advanced Materials and Processing 2010 - Proceedings of the 6th International Conference on Icamp*. World Scientific Publishing Company: 2014.

11. Nakamoto, K., *Infrared and Raman Spectra of Inorganic and Coordination Compounds, Theory and Applications in Inorganic Chemistry*. Wiley: 2008.
12. Samuel, V.; Pasricha, R.; Ravi, V., Synthesis of nanocrystalline rutile. *Ceramics International* **2005**, 31, (4), 555-557.
13. Li, Y.; Lee, N.-H.; Hwang, D.-S.; Song, J. S.; Lee, E. G.; Kim, S.-J., Synthesis and Characterization of Nano Titania Powder with High Photoactivity for Gas-Phase Photooxidation of Benzene from TiOCl_2 Aqueous Solution at Low Temperatures. *Langmuir* **2004**, 20, (25), 10838-10844.
14. Zheng, Y. Q.; Shi, E. W.; Yuan, R. L., *Science in China Series E* **1999**, 1999, (29), 206.15. Nakayama, N.; Hayashi, T., Preparation and characterization of poly(l-lactic acid)/ TiO_2 nanoparticle nanocomposite films with high transparency and efficient photodegradability. *Polymer Degradation and Stability* **2007**, 92, (7), 1255-1264.
16. Gao, Y.; Chen, G.; Oli, Y.; Zhang, Z.; Xue, Q., Study on tribological properties of oleic acid-modified TiO_2 nanoparticle in water. *Wear* **2002**, 252, (5-6), 454-458.
17. Stuart, B. H., *Infrared Spectroscopy: Fundamentals and Applications*. Wiley: 2004.
18. Qu, Q.; Geng, H.; Peng, R.; Cui, Q.; Gu, X.; Li, F.; Wang, M., Chemically Binding Carboxylic Acids onto TiO_2 Nanoparticles with Adjustable Coverage by Solvothermal Strategy. *Langmuir* **2010**, 26, (12), 9539-9546.
19. Mallakpour, S.; Aalizadeh, R., A simple and convenient method for the surface coating of TiO_2 nanoparticles with bioactive chiral diacids containing different amino acids as the coupling agent. *Progress in Organic Coatings* **2013**, 76, (4), 648-653.
20. Gao, W.; Dickinson, L.; Grozinger, C.; Morin, F. G.; Reven, L., Self-Assembled Monolayers of Alkylphosphonic Acids on Metal Oxides. *Langmuir* **1996**, 12, (26), 6429-6435.
21. Guerrero, G.; Mutin, P. H.; Vioux, A., Anchoring of Phosphonate and Phosphinate Coupling Molecules on Titania Particles. *Chemistry of Materials* **2001**, 13, (11), 4367-4373.

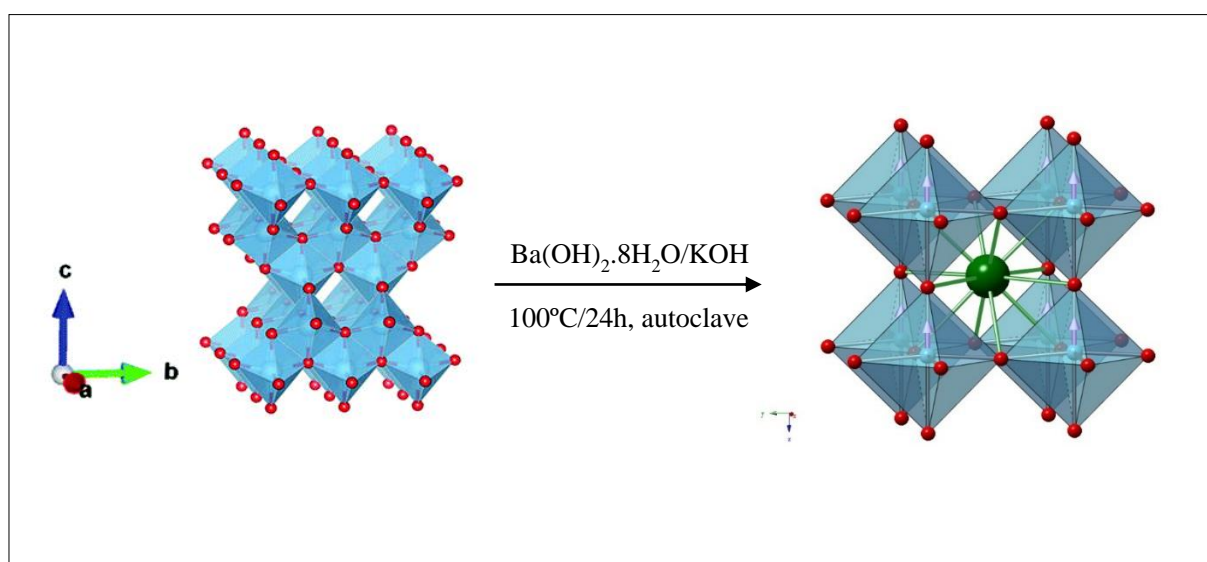
Chapter 6

Preparation and
Characterisation of Barium
Titanium Oxide Nanorods
 BaTiO_3

6.1 Introduction

A major aim of this thesis was an investigation on the best methods of preparation of nanorods of barium titanium oxide (BaTiO_3) of a given shape, size and dispersity. The incentive for this work is the fact that barium titanium oxide is widely used in numerous electronic and electro-optic applications due to a favourable combination of mechanical and physical properties, including its very high dielectric constant, k .¹⁻³ Therefore, improved methods of synthesis are required in order to prepare solution-processable barium titanium oxide nanorods, which could be deposited from solution as a thin uniform film of a controlled thickness onto a substrate surface, e.g., using doctor blade, inkjet printing, spin coating drop-casting techniques, etc., and patterned, for example, as the dielectric layer in Organic Field-Effect Transistors (OFETs) with improved performance. Three main approaches to prepare solution-processable barium titanium oxide nanorods described in this chapter represent a major part of the work carried out for this thesis.

Approach 1 involves using a hydrothermal reaction involving barium hydroxide octahydrate ($\text{Ba}(\text{OH})_2 \cdot 8\text{H}_2\text{O}$) as the source of barium in an autoclave at low temperature to convert titanium dioxide (TiO_2) nanorods of a given shape and size into the corresponding barium titanium oxide (BaTiO_3) nanorods with retention of the original dimensions of the starting precursor nanorods see schema 6-1.^{8,9}



Schema 6-1: Schematic diagram of synthesis of barium titanium oxide from the oleic acid-stabilised titanium dioxide nanorods TiO_2 -OA.

Titanium dioxide nanorods, in either the anatase or the rutile phase, of different shapes, sizes and polydispersity, see subsections 1-1, 1-2 and 1-3 below, are used as starting materials in this approach.

Anatase oleic acid-stabilised titanium dioxide nanorods (TiO₂-OA), see chapter 3, will be used as the starting material in the first reactions using approach 1-1. Then the conversion of hair-like rutile titanium dioxide nanorods, see chapter 5, section 5.3.2, and larger rutile titanium dioxide nanorods, see chapter 5, section 5.3.3, to barium titanium oxide nanorods will be investigated using the same method in approaches 1-2 and 1-3, respectively.

The influence of the reaction temperature, the concentration of titanium dioxide nanorods, different molar ratios of Ba/Ti as well as the value of pH will be studied in attempts to achieve complete conversion of the precursor titanium dioxide (TiO₂) nanorods into the corresponding barium titanium oxide (BaTiO₃) nanorods with retention of the original dimensions in high overall yield.

In Approach 1-1 short ($l = \sim 20$ nm and $d = \sim 3-4$ nm) oleic acid-stabilised titanium dioxide nanorods (TiO₂-OA) are converted into the analogous barium titanium oxide (BaTiO₃) nanorods using a modified literature method.^{6, 7} Since these TiO₂-OA nanorods can be dissolved in organic solvents, e.g., chlorobenzene, see chapter 3, one objective of this approach is to determine whether these solution-processable, oleic acid-stabilised titanium dioxide nanorods (TiO₂-OA) can be converted into analogous oleic acid-stabilised barium titanium oxide (BaTiO₃) nanorods, which could then also be dissolved in common organic solvents for deposition from solution on device substrates.

In Approach 1-2 small hair-like, rutile titanium dioxide nanorods (TiO₂), see chapter 5, will be used as the starting material in order to determine whether the nature of the phase of the titanium dioxide nanorods can be retained in the analogous barium titanium oxide nanorods using this kind of hydrothermal reaction.

In Approach 1-3 large ($l = \sim 80$ nm and $d = \sim 20$ nm) titanium dioxide (TiO₂) nanorods also in the rutile phase, see chapter 5, will be used as the starting material in order to determine whether large titanium dioxide nanorods could also be converted efficiently into the analogous barium titanium oxide nanorods with retention of shape, size, dispersity and crystallite form.

Approach 2 involves a hydrothermal reaction and a single source of Ba/Ti, i.e., barium titanium ethylhexano-isopropoxide [BaTi(O₂CC₇H₁₅)(OC₃H₇)₅], in water and tetramethyl ammonium hydroxide (TMAH) (30% in water) to prepare barium titanium oxide nanorods directly. The idea behind this reaction is that the single source precursor will possibly lead to the formation of homogenous barium titanium oxide nanorods with a Ba/Ti ration equal to 1.0. In a typical

reaction, an hydrothermal treatment of barium titanium ethylhexano-isopropoxide $[\text{BaTi}(\text{O}_2\text{CC}_7\text{H}_{15})(\text{OC}_3\text{H}_7)_5]$ will be carried out using a slightly modified procedure from a literature synthesis.⁴

Approach 3 involves the preparation of barium titanium oxide nanorods in the presence of ethylene glycol using a modification of a literature method.⁵ Barium chloride (BaCl_2) and titanium oxy chloride (TiOCl_2) are used as the source of barium and titanium, respectively. Sodium hydroxide is used to increase the pH values during the reaction. The aim of this reaction is to prepare barium titanium oxide nanorods, which might be dissolved in organic solvent, directly.

6.2 Experimental

6.2.1 Materials

Oleic acid (OA, 90 %), barium hydroxide octahydrate ($\text{Ba}(\text{OH})_2 \cdot 8\text{H}_2\text{O}$, $\geq 98\%$), barium chloride (BaCl_2), ethylene glycol ($\text{HOCH}_2\text{CH}_2\text{OH}$) and tetramethyl ammonium hydroxide (TMAH) (30% in water) were obtained from Sigma-Aldrich. Potassium hydroxide (KOH), sodium hydroxide (NaOH) and chlorobenzene were purchased from Fisher. Formic acid ($> 96\%$) was obtained from Sigma-Aldrich. Barium titanium ethylhexano-isopropoxide ($\text{BaTi}(\text{O}_2\text{CC}_7\text{H}_{15})(\text{OC}_3\text{H}_7)_5$, 99.5%) was supplied by Alfa-Aesar. Ultrapure water with a specific resistivity of $18.2 \text{ M}\Omega \cdot \text{cm}$ was obtained by reversed osmosis followed by ion-exchange and filtration (UPQ PS system, ELGA, USA).

6.2.2 Synthesis of Barium Titanium Oxide (BaTiO_3) Nanorods

Three general approaches, as described below, were used to prepare barium titanium oxide nanorods.

Approach 1: Synthesis of Barium Titanium Oxide Nanorods BaTiO_3 from Nanorods of Titanium Dioxide TiO_2

Approach 1-1: Synthesis of Barium Titanium Oxide Nanorods BaTiO_3 from Oleic Acid-Stabilised Titanium Dioxide Nanorods ($\text{TiO}_2\text{-OA}$)

Oleic acid-stabilised titanium dioxide ($\text{TiO}_2\text{-OA}$) nanorods, see chapter 3, and barium hydroxide octahydrate were used as sources of titanium and barium, respectively. In typical reaction barium titanium oxide (3.78 g, 0.2 M) was added to a suspension of the TiO_2 nanorods (1.89 g, 0.2 M) in distilled water (60 mL). An aqueous solution (3 %) of potassium hydroxide (30 mL) was added to the reaction mixture to increase the value of pH to 12.3. After sonication of the resultant mixture for 30 min, it was transferred to a Teflon autoclave (100 mL) and heated at 100 °C for 24 h. The resultant suspension was then allowed to cool to room temperature and then washed twice with distilled water and then (1 M) formic acid in order to remove residues of barium carbonate (BaCO_3). The resultant solid was dried at 30°C in a vacuum oven overnight for further analysis. This reaction was carried out using different concentrations of the titanium dioxide nanorods and barium hydroxide octahydrate, the temperature and pH and reaction times were varied, see table 6-1, in order to produce the barium titanium oxide (BaTiO_3) nanorods FA6-1 - FA6-11.

Approach 1-2: Synthesis of Barium Titanium Oxide (BaTiO_3) Nanorods from Small, Hair-like Rutile Titanium Dioxide (TiO_2) Nanorods

A mixture of hair-like rutile titanium dioxide (TiO_2) nanorods, FA5-2, see chapter 5, barium hydroxide and water was heated in an autoclave for 24 h at 100 °C and worked up as described in section 6.2.2.1.1 Only the concentration of barium hydroxide was varied in the two reactions carried out, see table 6-2, in order to produce the barium titanium oxide (BaTiO_3) nanorods FA6-12 and FA6-13.

Table 6-1: Reaction conditions for the preparation of the barium titanium oxide (BaTiO₃) nanorods FA6-1 - FA6-11.

Sample	TiO ₂ -OA/g	Ba(OH) ₂ /g	H ₂ O/mL	T/°C	pH	Time/h
FA6-1	0.96	3.78	60	100	12.3	24
FA6-2	0.96	3.78	60	80	12.3	24
FA6-3	0.96	3.78	60	125	12.3	24
FA6-4	0.48	1.89	60	100	12.3	24
FA6-5	0.28	1.134	60	100	12.3	24
FA6-6	0.28	1.134	60	125	12.3	24
FA6-7	0.28	1.134	60	80	12.3	24
FA6-8	0.96	3.78	60	100	7.8	24
FA6-9	0.96	3.78	60	100	12.3	6
FA6-10	0.96	3.78	60	100	12.3	12
FA6-11	0.96	5.67	60	100	12.3	24

Table 6-2: Reaction conditions for the preparation of the barium titanium oxide (BaTiO₃) nanorods FA6-12 and FA6-13.

Sample	TiO ₂ /g	Ba(OH) ₂ /g	H ₂ O/mL	T/°C	Time/h
FA6-12	0.96	3.78	60	100	24
FA6-13	0.96	5.67	60	100	24

Approach 1-3: Synthesis of Barium Titanium Oxide (BaTiO₃) Nanorods from Large Rutile Titanium Dioxide (TiO₂) Nanorods

A mixture of large ($l = \sim 80$ nm and $d = \sim 20$ nm), rutile titanium dioxide (TiO₂) nanorods, see chapter 5, section 5.2.2.4.1, barium hydroxide and water was heated in an autoclave for 24 h at 100 °C. The reaction time (24/48 h) and the Ba/Ti molar ratio were varied, see table 6-3, and in order produce the barium titanium oxide (BaTiO₃) nanorods FA6-14 and FA6-17.

Table 6-3: Reaction conditions for the preparation of the barium titanium oxide (BaTiO₃) nanorods FA6-14 and FA6-17.

Sample	TiO ₂ /g	Ba(OH) ₂ /g	H ₂ O/mL	T/°C	Time/h
FA6-14	0.96	3.78	60	100	24
FA6-15	0.96	3.78	60	100	48
FA6-16	0.96	5.67	60	100	24
FA6-17	0.96	5.67	60	100	48

Approach 2: Synthesis of Barium Titanium Oxide (BaTiO₃) Nanorods from a Single-source Ba/Ti Precursor

In a typical reaction, an aqueous (25%) tetramethyl ammonium hydroxide solution (30 mL) and distilled water (30 mL) were added to barium titanium ethylhexano-isopropoxide [BaTi(O₂CC₇H₁₅)(OC₃H₇)₅] (0.94 g, 1.5 mmol) under constant stirring for 30 min. The resultant reaction mixture was transferred to a Teflon-autoclave and stirred at room temperature for 30 min. A stream of nitrogen was bubbled through the reaction mixture for 15 min to remove CO₂ to avoid the formation of barium carbonate (BaCO₃). The Teflon-autoclave was sealed quickly, put in a furnace and then heated at 120 °C for 24 h. After being allowed to cool to room temperature, the resultant white precipitate was filtered off, washed twice with water and then twice with methanol, before being dried overnight in a vacuum oven at 30 °C.

Approach 3: Synthesis of Barium Titanium Oxide (BaTiO₃) Nanorods in the Presence of Ethylene glycol

In a typical reaction an aqueous solution of barium chloride (15 mL, 0.3 M) were mixed with titanium oxy chloride (TiOCl₂, 5 mL, 0.2 M) at room temperature. The pH value was adjusted to pH = 14 by adding 10 M sodium hydroxide (10 mL). Ethylene glycol (5 mL) and distilled water (15 mL) were added to the reaction mixture to reduce the pH value to 13.8. The resultant reaction mixture was then transferred to a Teflon-autoclave and heated at 200 °C for 24 h. The reaction mixture was allowed to cool to room temperature, separated by centrifugation and the resultant solid was then washed twice with water and then twice with (1 M) formic acid, before being dried overnight in a vacuum oven at 30 °C.

6.3 Results and Discussion

6.3.1 Approach 1: Characterisation of Barium Titanium Oxide Nanorods BaTiO₃ Transferred from Titanium Dioxide Nanorods TiO₂

Approach 1-1: Characterisation of Barium Titanium Oxide Nanorods (BaTiO₃) from Conversion of Oleic Acid-Stabilised Titanium Dioxide (TiO₂-OA) Nanorods

The XRD spectra of the oleic acid-stabilised titanium dioxide nanorods (TiO₂-OA) FA3-1, and the barium titanium oxide (BaTiO₃) nanorods FA6-1 - FA6-11, as well as that of FA6-11 AW after washing with formic acid, respectively, produced using FA3-1 as the starting material in approach 1-1 are shown in figures 6-1 - 6-4.

Figures 6-1, 6-2 and 6-4 show that only individual reflection is obtainable at an angle of $2\theta \approx 45^\circ$. Characteristically, the cubic form of barium titanium oxide should have only an individual reflection (200) at about a 2θ of 45° in its X-ray diffraction pattern. Two reflections corresponding to (200) and (020) in this area should be observed for a tetragonal form of the barium titanium phase. Therefore, the XRD spectra shown in figures 6-1 and 6-2 indicate that all samples of the barium titanium oxide (BaTiO₃) nanorods FA6-1 - FA6-7, produced from FA3-1 as the starting material, exhibit the cubic phase of barium titanium oxide.¹⁰ The XRD peaks are sharp and strong, indicating a relatively high degree of crystallinity of these powder products.¹¹ Figure 6-1 reveals the presence of barium carbonate impurities in the FA6-1 crude

product, which are removed by washing with formic acid as shown in the XRD spectrum of FA6-1 AW.

The XRD spectra of the barium titanium oxide nanorods FA6-1 - FA6-7 and FA6-9 - FA6-11 recorded in the figures 6-1, 6-2 and 6-4 reveal the anatase titanium dioxide in the FA3-1 nanorods, used as the starting material in the reactions carried out at pH = 12.3, has been completely converted to the corresponding barium titanium oxide nanorods. On the other hand only small amount of the titanium dioxide nanorods in the FA3-1 used as the starting material in a reaction carried out at pH = 7.8, has been converted into barium titanium oxide nanorods in the sample FA6-8, see figure 6-3. These contrasting results show clearly that pH value of the reaction solution has a great effect on the conversion of titanium dioxide to barium titanium oxide in these hydrothermal reactions.

The FT-IR spectra of the barium titanium oxide nanorods FA6-1 - FA6-11 are presented in figures 6-5 - 6-8. The FT-IR spectrum of the oleic acid-stabilised titanium dioxide (TiO₂-OA) nanorods FA3-1 is also included in the figures in order to facilitate comparisons between the FT-IR spectra of the starting materials and the reaction products created using the synthetic approach 1-1. It is noteworthy that a new peak is apparent at 550 cm⁻¹ in all the FT-IR spectra of the barium titanium oxide nanorods FA6-1 - FA6-11, which can be attributed to the presence of O₆ in the barium titanium oxide structure¹². In addition, the presence of peaks at 1500 and 1435 cm⁻¹ which is related to asymmetric and symmetric of COO⁻, respectively and peaks around 2850-3000 cm⁻¹ relate to stretching of CH₃, CH₂ and CH, indicating that some oleic acid has indeed attached on the barium titanium oxide surface.^{13,14}

The TEM images of the barium titanium oxide nanorods FA6-1 - FA6-11, shown in figures 6-9 - 6-12, reveal that the shape of titanium dioxide nanorods has not been entirely retained in the barium titanium oxide nanorods produced and that some damage to the integrity of these rods is apparent for all of the samples prepared at pH = 12.3. Indeed barium titanium oxide nanoparticles with variable sizes can be observed. For the sample FA6-8, prepared in a reaction carried out at pH = 7.8, most of the rods remain, indicating that most the oleic acid-stabilised titanium dioxide nanorods (TiO₂-OA) have not been converted to barium titanium oxide as suggested by interpretation of the XRD spectrum shown in figure 6-3.

The elemental composition of the products was determined using a combination of ICP and CHN analysis, see table 6-4. Generally, the barium content lies in the range of 36% - 52 % except that of FA6-8, whose atomic ratio of Ti/Ba = 16.15, which is consistent with the XRD and TEM results. The Ti/Ba atomic ratio is higher for the products FA6-1, FA6-4 and FA6-6 prepared with a lower concentration of starting material, which suggests that the efficiency of

the conversion of the titanium dioxide nanorods to the analogous barium titanium oxide nanorods increases with increasing concentration of the starting materials. The Ti/Ba atomic ratio is also lower at higher reaction temperatures, *i.e.*, for the samples FA6-1 - FA6-3. The Ti/Ba atomic ratio = 1.56 for the sample FA6-2 prepared at 80 °C, in contrast to the Ti/Ba atomic ratio = 1.14 observed for the sample FA6-3 prepared at 125 °C. There is no significant difference in Ti/Ba atomic ratio for the samples FA6-1, FA6-9 and FA6-10 prepared at different reaction times, *i.e.*, for 24, 12 or 6 hours, which implies that the conversion reaction occurs quickly and readily. A higher concentration of the Ba(OH)₂ starting material, *e.g.*, 5.67 g instead of 3.78 g in the reaction to prepare the sample FA6-11 compared to that used to prepare the sample FA6-1 leads to a reduction in the Ti/Ba ratio, *i.e.*, from 1.14 to 1.03, which is consistent with the fact that the barium titanium oxide nanorods in sample FA6-11 are present in a very pure cubic phase.

It should be noted that although about 10% of carbon is present in the barium titanium oxide nanorods samples FA6-1 - FA6-7 and FA6-9 - FA6-11, *i.e.*, with the exception of FA6-8, none of these samples can be dissolved in chlorobenzene.

Table 6-4: Chemical analysis of the barium titanium oxide nanorods FA6-1 - FA6-11 prepared from the oleic acid-stabilised titanium dioxide (TiO₂-OA) nanorods FA3-1.

Sample	Ti%	C%	H%	Ba%	Atom ratio of Ti/Ba
FA6-1	19.82	10.38	1.58	43.77	1.30
FA6-2	22.94	12.4	1.61	42.14	1.56
FA6-3	19.21	10.48	1.31	48.34	1.14
FA6-4	25.74	12.74	1.77	37.97	1.94
FA6-5	25.03	13.06	1.65	35.03	2.05
FA6-6	22.22	12.03	1.46	36.69	1.74
FA6-7	22.75	11.66	1.51	41.26	1.58
FA6-8	37.18	20.12	2.84	6.6	16.15
FA6-9	20.74	10.99	1.68	47.89	1.24
FA6-10	21.22	10.90	1.68	46.65	1.30
FA6-11	18.84	9.45	1.14	52.43	1.03

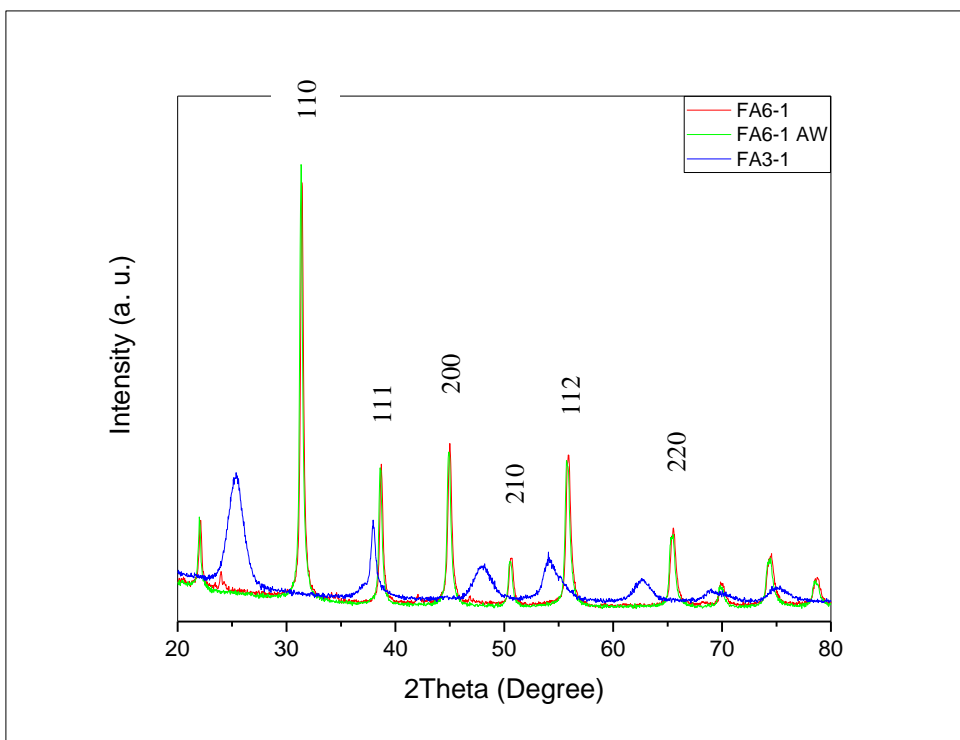


Figure 6-1: XRD spectra of the oleic acid-stabilised titanium dioxide nanorods ($\text{TiO}_2\text{-OA}$) FA3-1 and the barium titanium oxide (BaTiO_3) nanorods FA6-1 and FA6-1 AW, before and after washing with formic acid, respectively, produced using FA3-1 as the starting material.

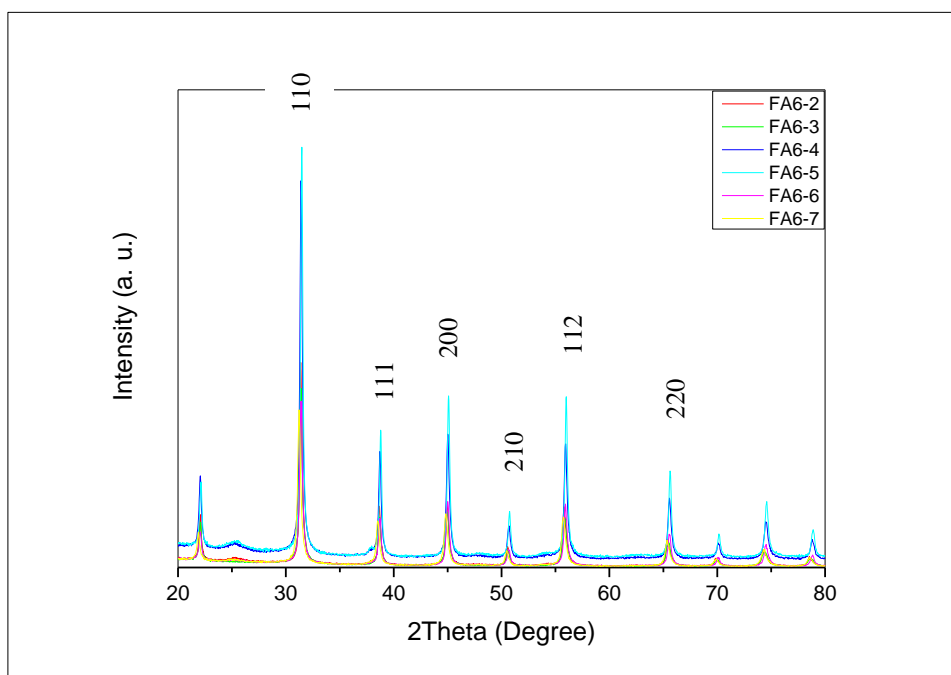


Figure 6-2: XRD spectra for the barium titanium oxide nanorods FA6-2 - FA6-7 produced from FA3-1 as the starting material.

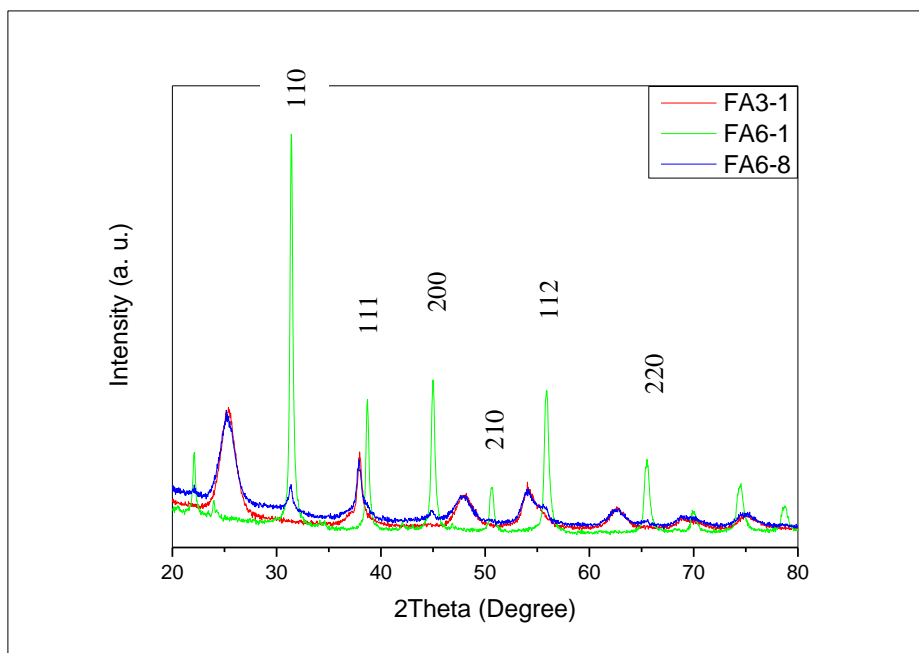


Figure 6-3: XRD spectra of the oleic acid-stabilised titanium dioxide nanorods (TiO₂-OA) FA3-1 and the barium titanium oxide nanorods FA6-1 and FA6-8 produced from FA3-1 at different pH values, i.e., pH = 12.3 and pH = 7.8, respectively, produced using FA3-1 as the starting material.

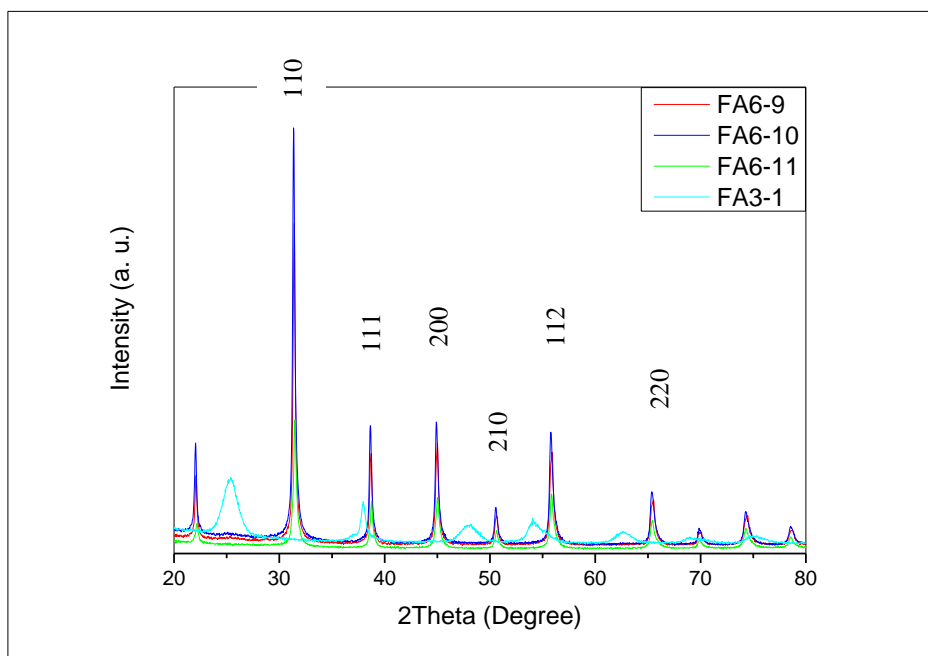


Figure 6-4: XRD spectra of the oleic acid-stabilised titanium dioxide nanorods (TiO₂-OA) FA3-1 and the barium titanium oxide nanorods FA6-9 - FA6-11 produced from FA3-1 as the starting material.

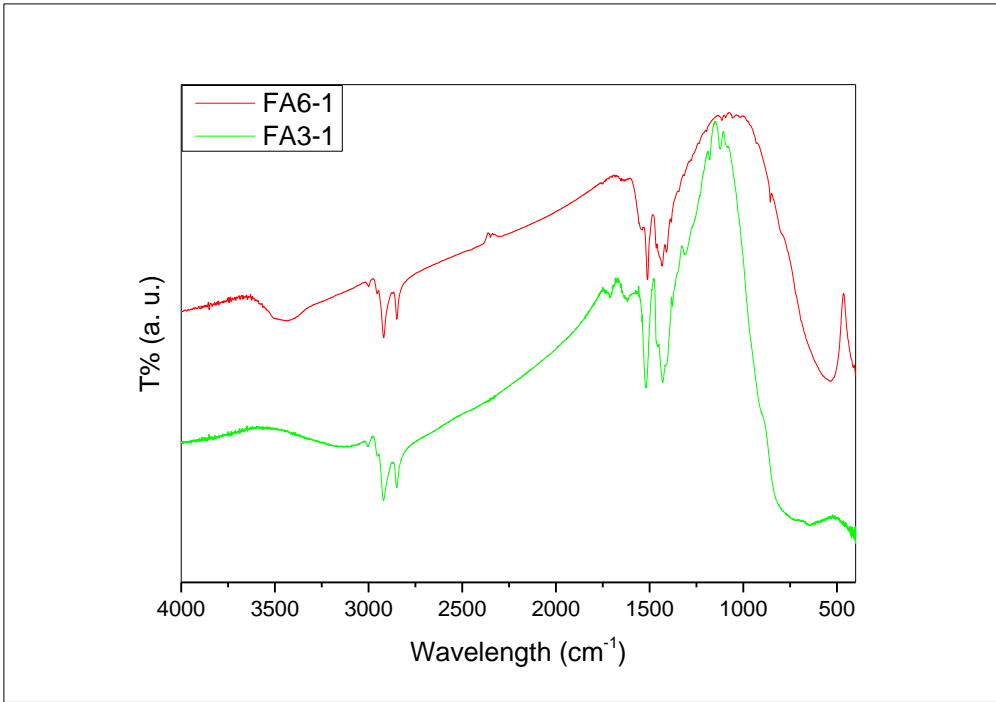


Figure 6-5: FT-IR spectra of the barium titanium oxide nanorods sample FA6-1 and the oleic acid-stabilised titanium dioxide (TiO₂-OA) nanorods sample FA3-1 used as the starting material.

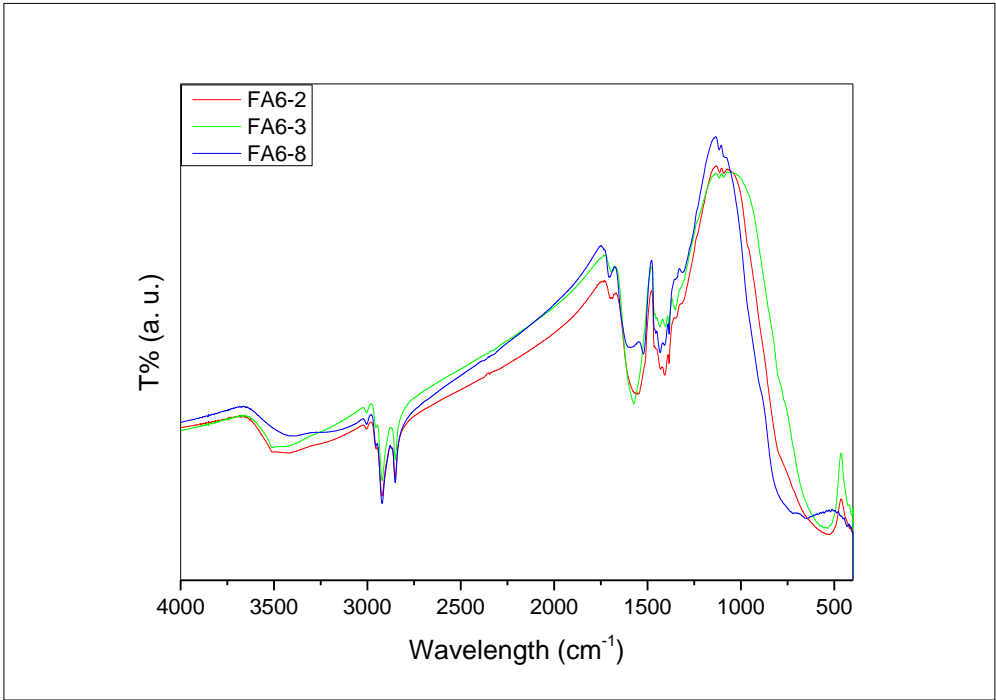


Figure 6-6: FT-IR spectra of the barium titanium oxide nanorods samples FA6-2, FA6-3 and FA6-8, produced using FA3-1 as the starting material.

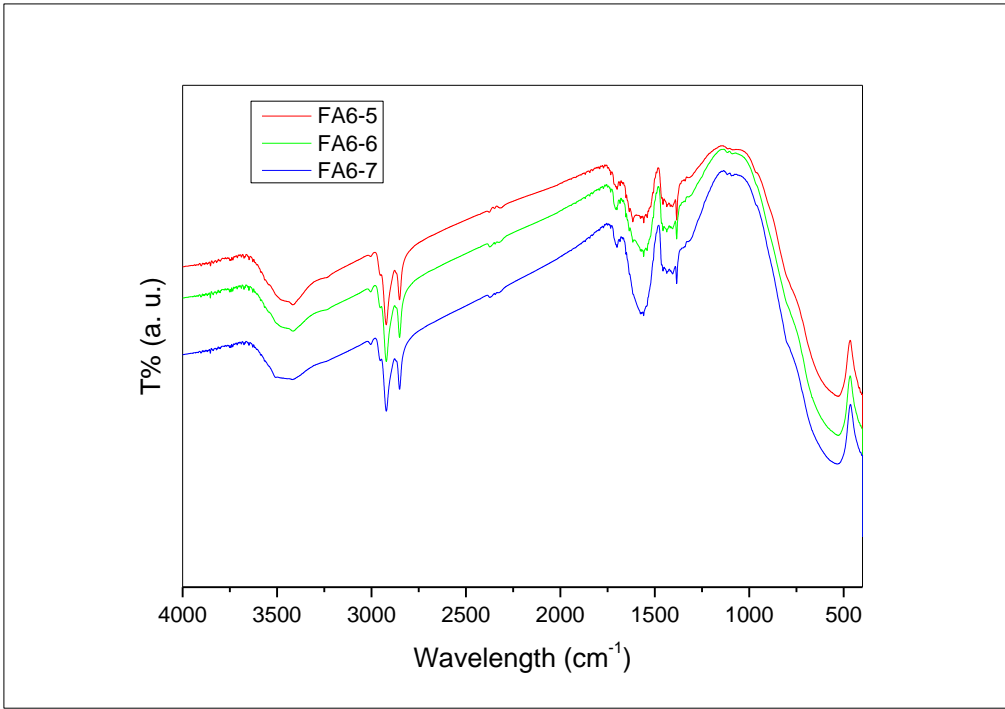


Figure 6-7: FT-IR spectra of the barium titanium oxide nanorods samples FA6-5 - FA6-7, produced using FA3-1 as the starting material.

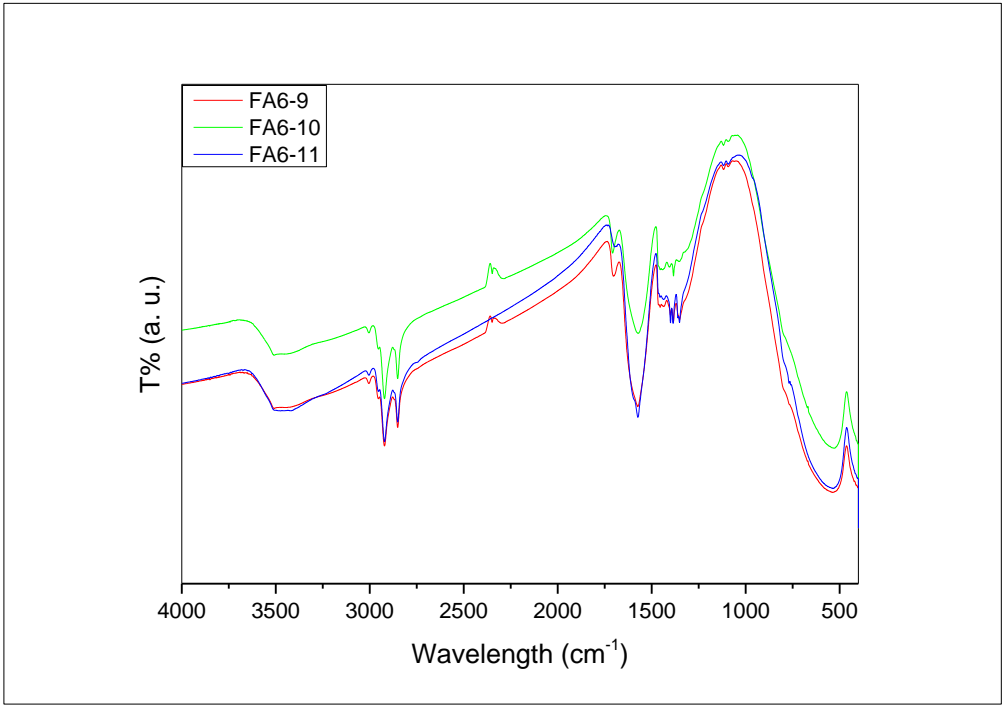


Figure 6-8: FT-IR spectra of the barium titanium oxide nanorods samples FA6-9 - FA6-11, produced using FA3-1 as the starting material.

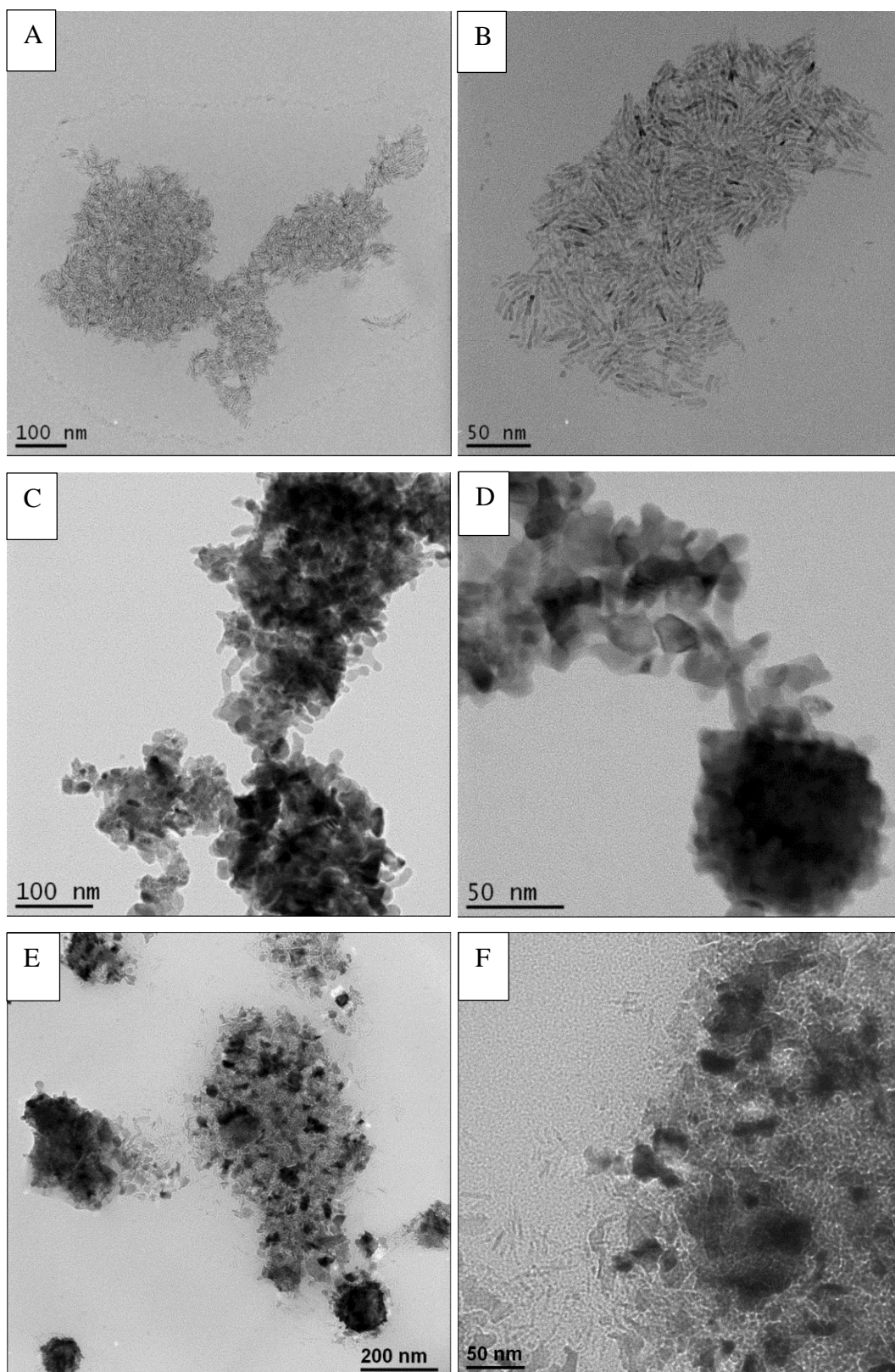


Figure 6-9: TEM images of the oleic acid-stabilised titanium dioxide (TiO₂-OA) nanorods FA3-1 (A-B), barium titanium oxide nanorods FA6-1 (C-D) and FA6-2 (E-F).

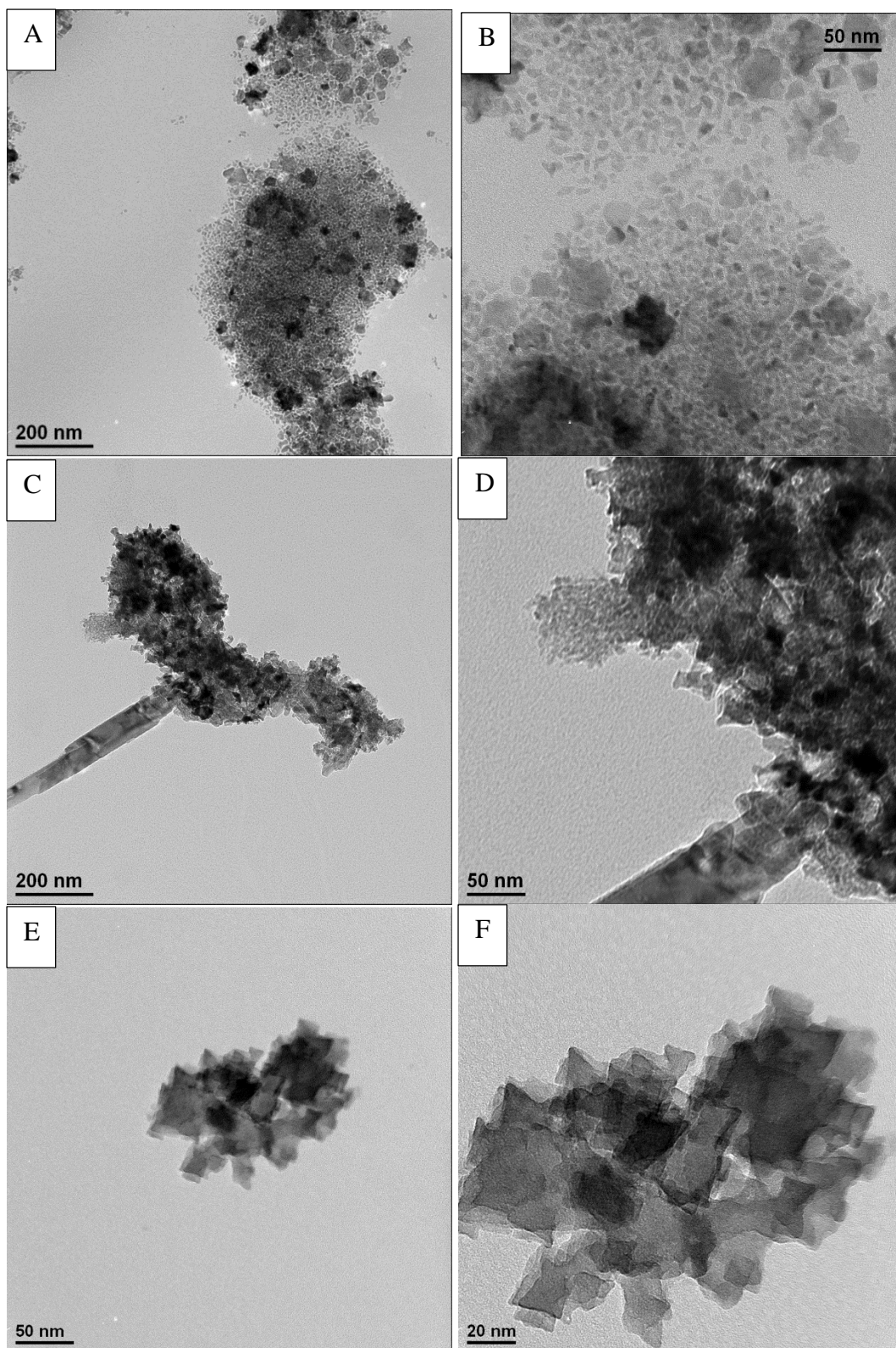


Figure 6-10: TEM Images of barium titanium oxide nanorods FA6-3 (A-B), FA6-4 (C-D) and FA6-5 (E-F).

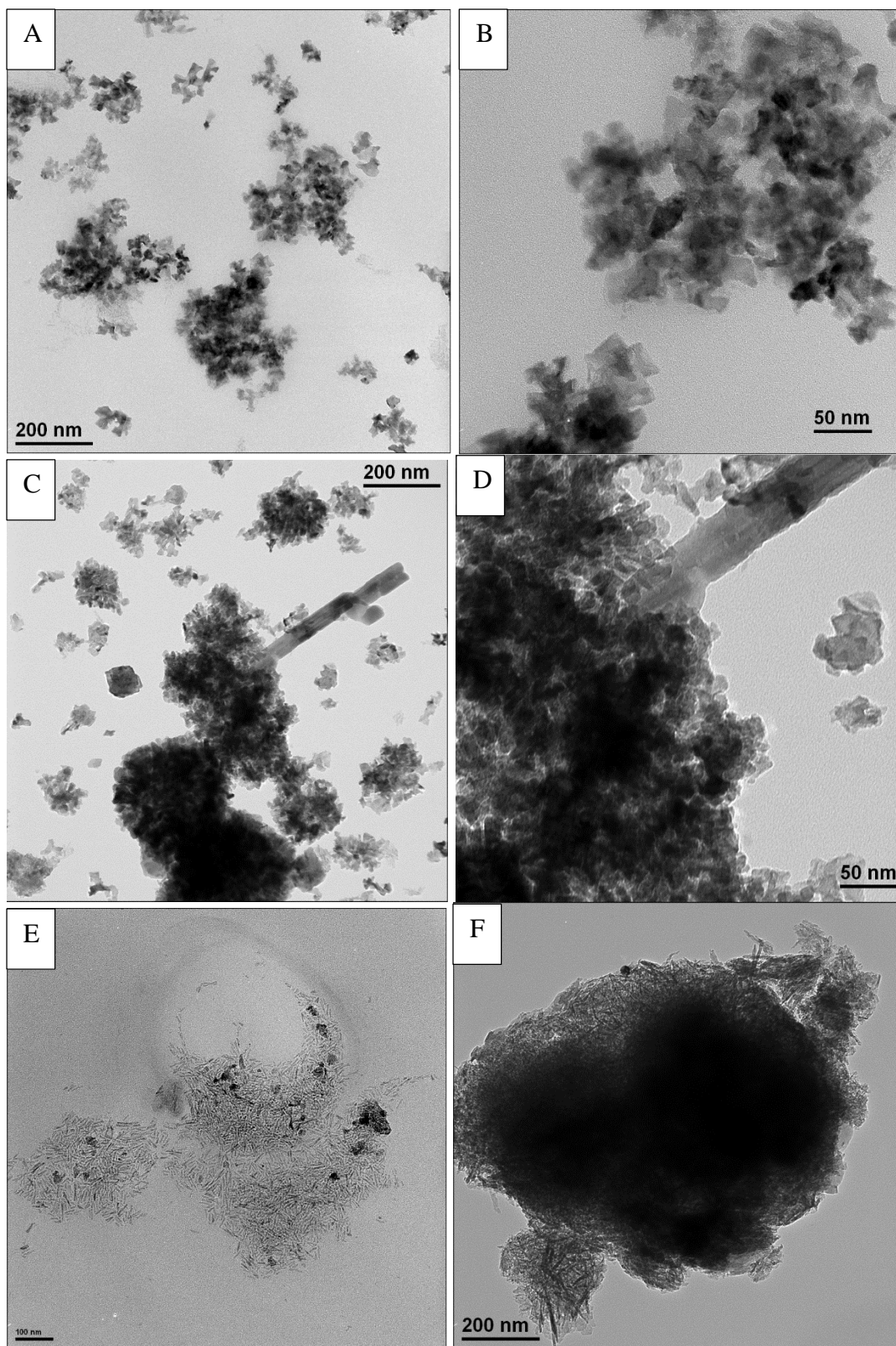


Figure 6-11: TEM Images of barium titanium oxide nanorods FA6-6 (A-B), FA6-7 (C-D) and FA6-8 (E-F).

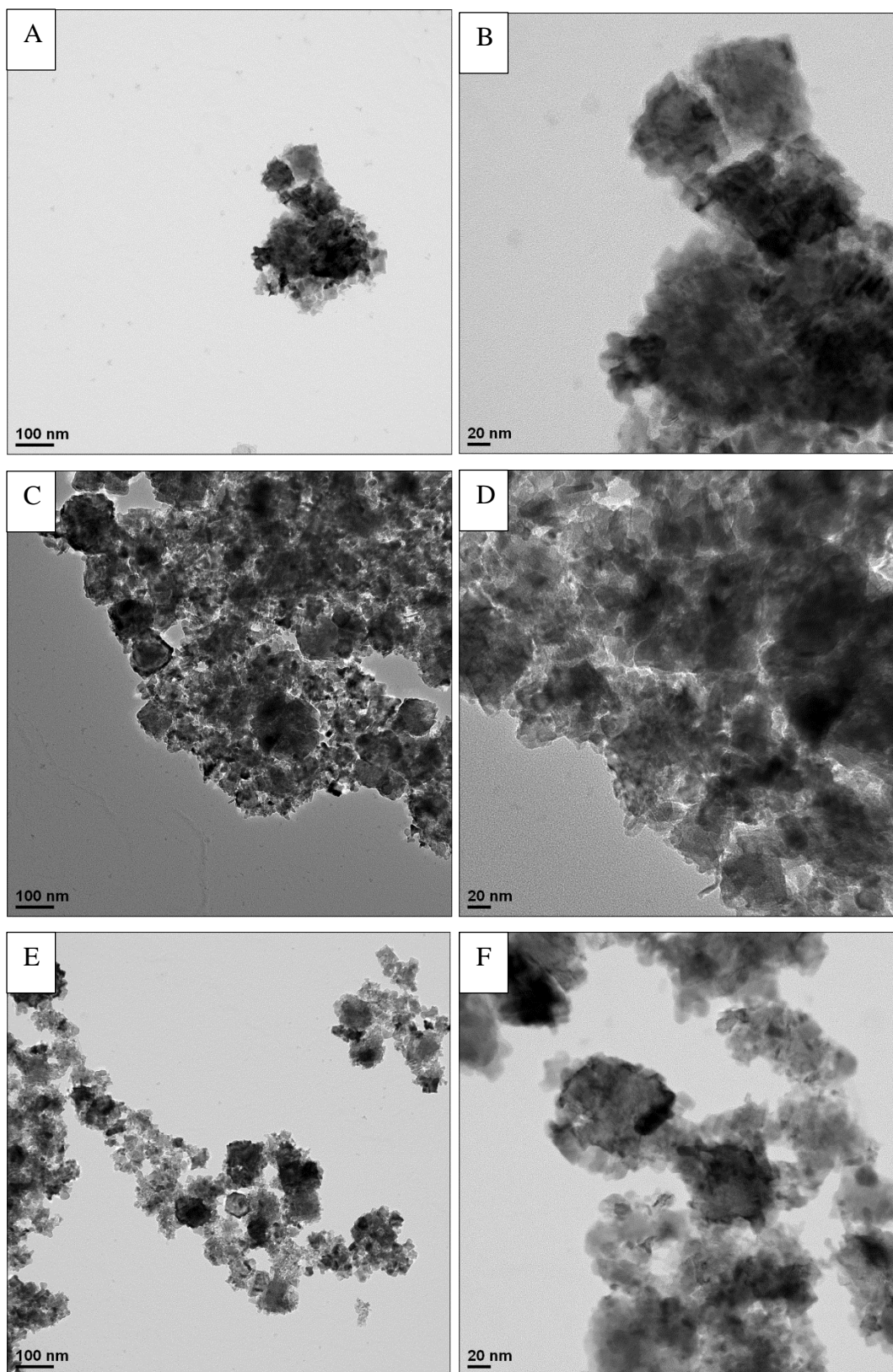


Figure 6-12: TEM images of barium titanium oxide nanorods FA6-9 (A-B), FA6-10 (C-D) and FA6-11 (E-F).

Approach 1-2: Characterisation of Barium Titanium Oxide Nanorods BaTiO₃ from hair-like Rutile Titanium Dioxide Nanorods TiO₂ (NRs-BaTiO₃1-2)

The XRD spectra of the barium titanium oxide samples FA6-12 and FA6-13 prepared using approach 1-2 and the rutile titanium dioxide nanorods FA5-2, used as the starting material in these reactions, shown in figure 6-13, reveal that the rutile phase of the titanium dioxide has been replaced by a cubic phase in the analogous barium titanium oxide nanorods. Only individual reflections are seen at 2θ of 45° , which is characteristic of a cubic barium titanium oxide phase as opposed to the two reflections, corresponding to (200) and (020), expected in this area for the tetragonal phase of barium titanium oxide. In the XRD pattern of FA6-12 and FA6-13, the peaks are sharp and strong, which point to a relative high crystallinity of the powders. ¹¹

The FT-IR spectra of the barium titanium oxide samples FA6-12 and FA6-13 prepared using approach 1-2 and the rutile titanium dioxide nanorods FA5-2, used as the starting material in these reactions, are shown in figure 6-14. Compared with the FT-IR spectrum of the rutile titanium dioxide nanorods FA5-2, a new peak, associated to the formation of O₆ in the BaTiO₃ structure, is apparent at 550 cm^{-1} in FT-IR spectrum of products FA6-12 and FA6-13, supporting the formation of barium titanium oxide. ¹²

The TEM images of rutile titanium dioxide nanorods FA5-2 and barium titanium oxide FA6-12 and FA6-13, shown in figure 6-15 reveal that the shape of the barium titanium oxide nanorods in the sample FA6-12, prepared using a Ti/Ba ratio of 1:1, is almost the same as that of the starting material FA5-2, but with some degree of aggregation. No nanorods can be observed in the sample FA6-13, prepared using higher Ti/Ba ratio of 1:1.5. Sphere-like nanoparticles with a large diameter, i.e., $d = 150\text{ nm}$ to 300 nm , are formed probably due to the aggregation of nanorods.

Analysis using ICP technique reveals that the titanium and barium contents are 24.87 %, 51.75 %, respectively, for FA6-12 and 21.29 % and 59.96 %, respectively for FA6-13. The atomic ratio of Ti/Ba is 1.38 for FA6-12. The Ti/Ba ratio in product FA6-13 is close to 1, indicating pure BaTiO₃ has been obtained.

The barium titanium oxide samples FA6-12 and FA6-13, prepared using approach 1-2, and cannot be dissolved to any significant extent in chlorobenzene. However, instable suspensions can be obtained with these samples in chlorobenzene.

Table 6-5: Chemical analysis of the barium titanium oxide samples FA6-12 and FA6-13 prepared using approach 1-2 using the rutile titanium dioxide nanorods FA5-2 as the starting material in these reactions.

Sample	Ti%	C%	H%	Ba%	Atom ratio of Ti/Ba
FA6-12	24.87	0.42	0.00	51.75	1.38
FA6-13	21.29	0.34	0.20	59.96	1.02

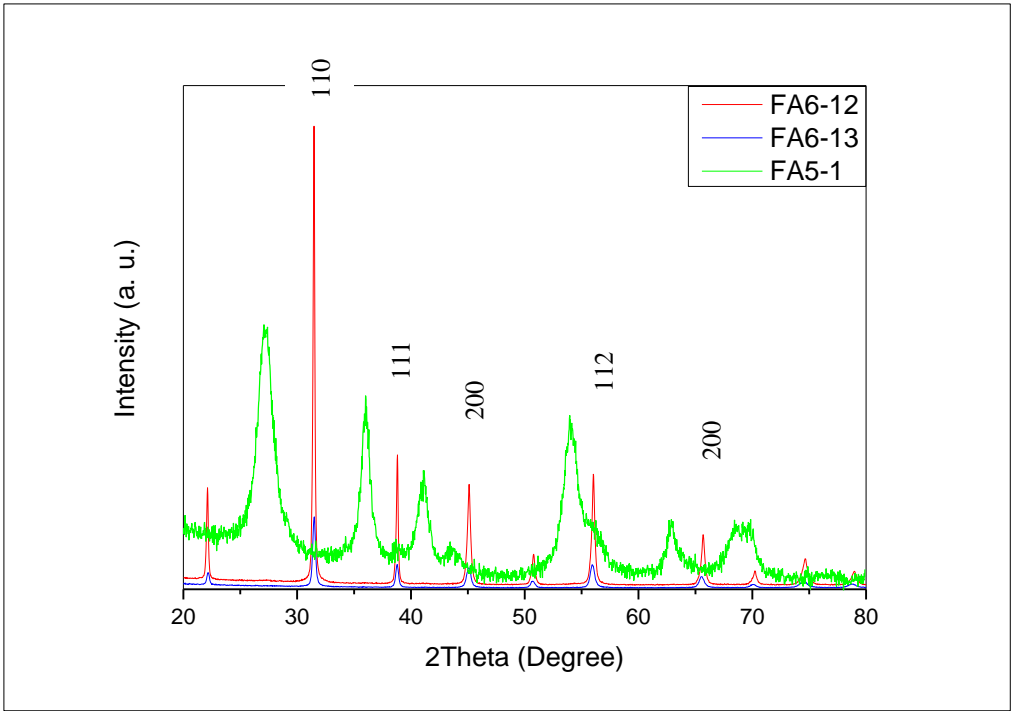


Figure 6-13: XRD spectra of the barium titanium oxide samples FA6-12 and FA6-13 prepared using approach 1-2 and the rutile titanium dioxide nanorods FA5-2 used as the starting material in these reactions.

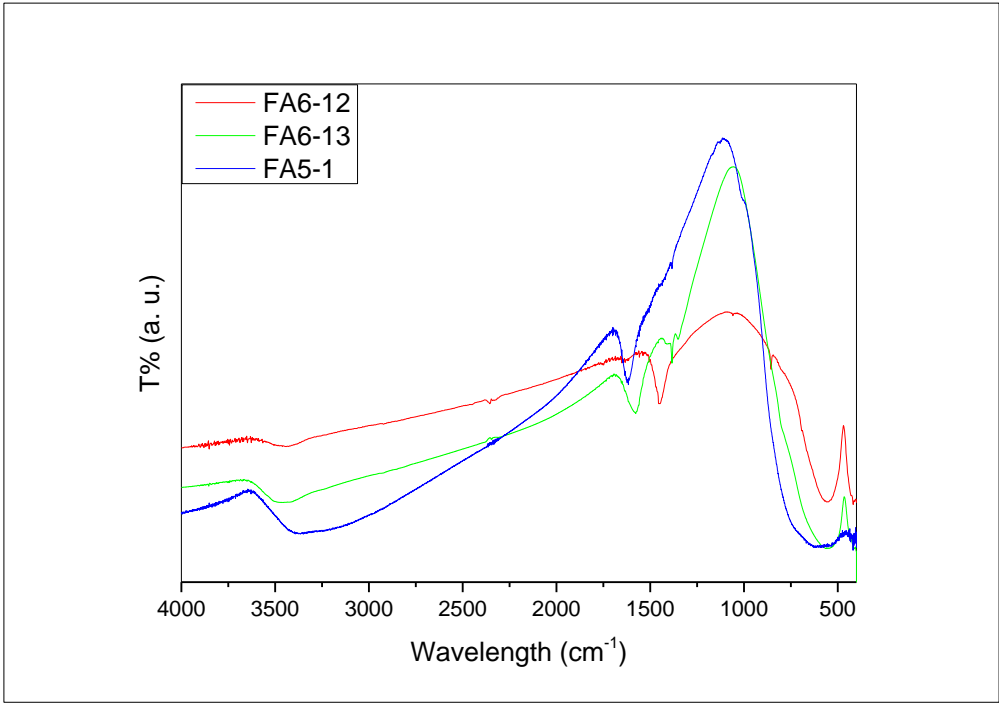


Figure 6-14: FT-IR spectra of barium titanium oxide samples FA6-12 and FA6-13 prepared using approach 1-2 and the rutile titanium dioxide nanorods FA5-2 used as the starting material in these reactions.

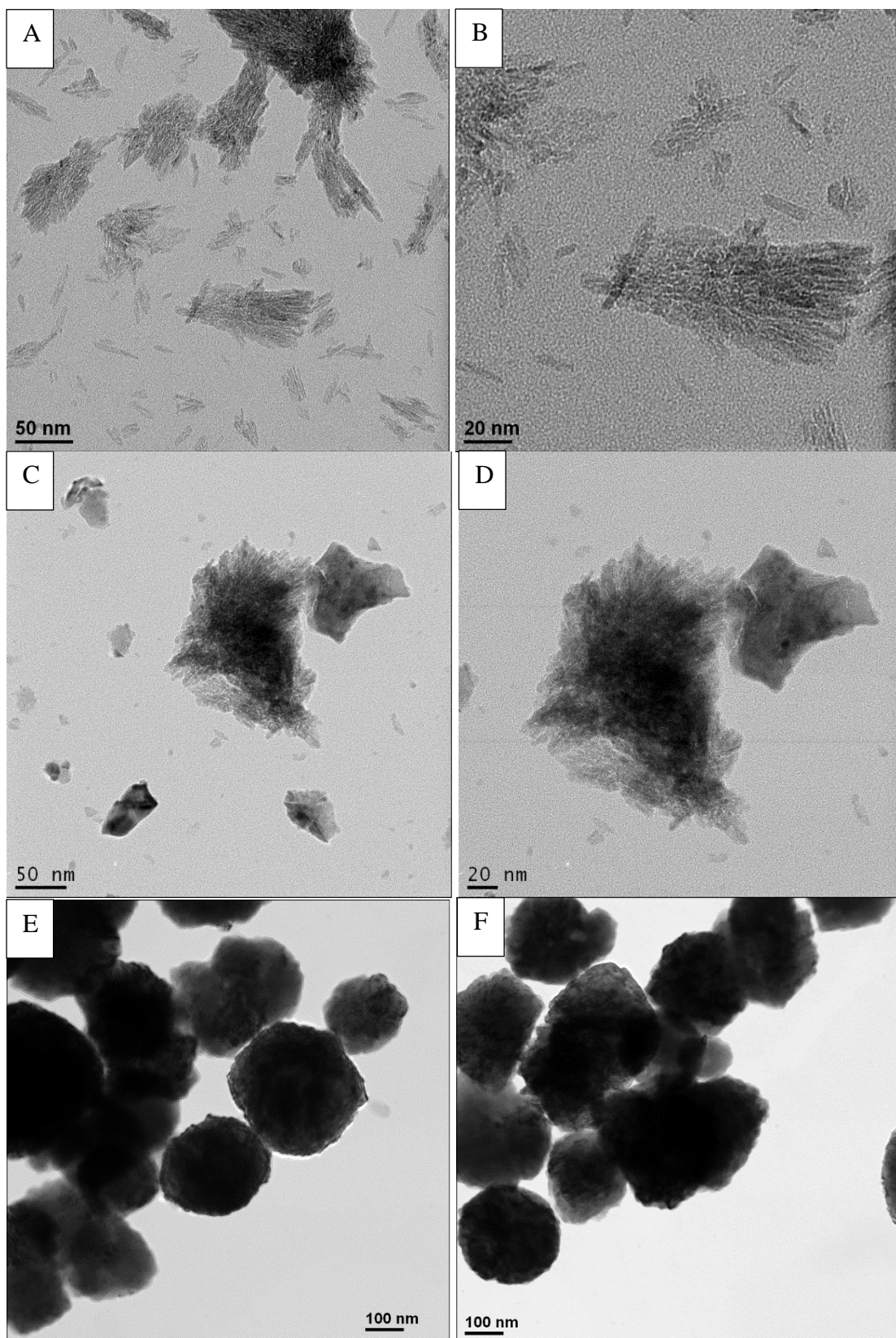


Figure 6-15: TEM images of rutile titanium dioxide nanorods FA5-2 (A-B) and barium titanium oxide nanoparticles FA6-12 (C-D) and FA6-13 (E-F).

Approach 1-3: Barium Titanium Oxide Nanorods Prepared from Large Rutile Titanium Dioxide Nanorods

The XRD spectra of barium titanium oxide products FA6-14 - FA6-17, prepared using different reaction times and Ba/Ti ratios, and the rutile titanium dioxide nanorods FA5-26, used as the starting material, are shown in figures 6-16, 6-17. FA6-14 and FA6-15 are the barium titanium oxide products prepared with a Ba/Ti ratio of 1 and a reaction time of 24 h and 48 h, respectively. FA6-16 and FA6-17 are the barium titanium oxide products prepared with a Ba/Ti ratio of 1.5 and a reaction time of 24 h and 48 h, respectively.

It can be seen that all the barium titanium oxide products FA6-14 - FA6-17 are present in a cubic phase.¹¹ Weak peaks attributable to rutile titanium dioxide nanorods can also be observed in the XRD pattern of the product FA6-14 and FA6-16 prepared with a reaction time of 24 h, indicating that not all rutile titanium dioxide nanorods have completely converted to barium titanium oxide probably due to the large size of rutile titanium dioxide nanorods. An increase of the reaction time from 24 h to 48 h results in the disappearance of these weak rutile titanium dioxide peaks as shown in the XRD spectrum of the barium titanium oxide FA6-15, see figure 6-16. The XRD spectra of the products FA6-16 and FA6-17, prepared using a Ba/Ti ratio = 1.5, show that all of the rutile titanium dioxide nanorods have been completely converted to the barium titanium oxide even using a 24 h reaction time, see figure 6-17.

The FT-IR spectra of barium titanium oxide products prepared using the synthetic approach 1-3, FA6-14 - FA6-17 and the rutile titanium dioxide nanorods FA5-26, used as the starting material in these reactions, are shown in figures 6-18 and 6-19. The FT-IR spectrum of the rutile titanium dioxide nanorods (TiO₂) FA5-26 is also included in the figures in order to facilitate comparisons between the FT-IR spectra of the starting materials and the reaction products created using the synthetic approach 1-3. It is noteworthy that a new peak is apparent at 550 cm⁻¹ in all the FT-IR spectra of the barium titanium oxide nanorods FA6-14 - FA6-17, which can be attributed to the presence of O₆ in the barium titanium oxide structure.¹²

The TEM images of the barium titanium oxide samples FA6-14 and FA6-15 prepared using Ba/Ti ratio = 1 are shown in figure 6-20. The TEM image of FA6-14 prepared using 24 h reaction time is very similar to that of the titanium dioxide nanorods used as the starting materials, indicating that nanorods shape has been successfully retained during the conversion of rutile titanium dioxide nanorods into barium titanium oxide. However, when increasing the reaction time to 48 h results in the disappearance of nanorods and the formation of homogenous

nanoparticles with a relatively large diameter, i.e., $20 < d < 60$ nm for the barium titanium oxide product FA6-15.

Figure 6-21 shows the TEM images of the barium titanium oxide products FA6-16 and FA6-17 prepared using a Ba/Ti ratio = 1.5 and using a reaction time of 24 h and 48 h, respectively. There are some differences in the TEM images of the titanium dioxide nanorods FA5-26 shown in figure 6-20 and figure 6-21 because they represent different batches of FA5-26. It can be seen that the shape and size of the barium titanium oxide product FA6-16 prepared using a reaction time of 24 h is similar to the titanium dioxide nanorods FA5-26 used as the starting material. However, the barium titanium oxide nanorods of FA6-17 prepared using a reaction time of 48 h, are different in shape and size from those of the titanium dioxide nanorods FA5-26 used as the starting material.

Analysis using ICP technique shows that the atomic ratio of Ti/Ba in the barium titanium oxide product FA6-14 prepared using a Ba/Ti ratio of 1.0 and a reaction time of 24 h is 1.59. However, the atomic ratio of Ti/Ba in the barium titanium oxide product FA6-15 also prepared using a Ba/Ti ratio of 1, but a reaction time of 48 h exhibits a much lower Ba/Ti ratio of 1.1 which is consistent with the XRD results. The barium titanium oxide products FA6-16 and FA6-17, prepared using a Ba/Ti ratio of 1.5 reaction times of 24 and 48 h, respectively, exhibit a similar Ti/Ba ratio of ~ 1.3 .

Table 6-6: Chemical analysis of the barium titanium oxide products FA6-14 - FA6-17, prepared using different reaction times and Ba/Ti ratios, using the rutile titanium dioxide nanorods FA5-26 as the starting material.

Sample	Ti%	C%	H%	Ba%	Atom ratio of Ti/Ba
FA6-14	27.10	0.42	0.00	48.77	1.59
FA6-15	21.30	0.41	0.00	55.34	1.1
FA6-16	25.73	0.17	0.14	54.01	1.37
FA6-17	25.05	0.24	0.00	53.43	1.34

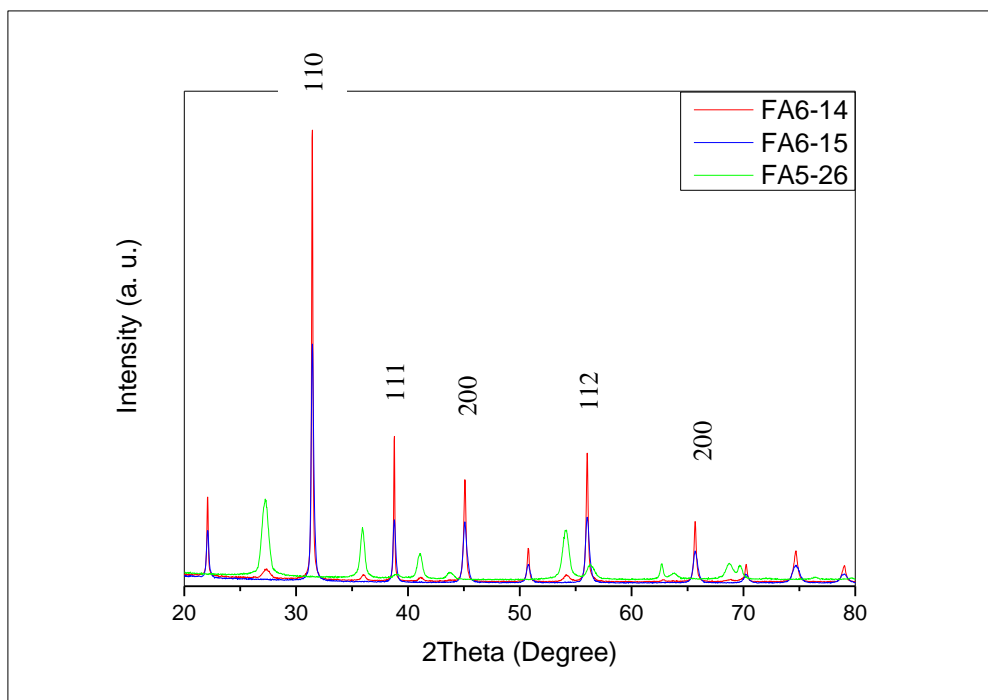


Figure 6-16: XRD spectra of the barium titanium oxide samples FA6-14 and FA6-15 prepared using approach 1-3 and the rutile titanium dioxide nanorods FA5-26 used as the starting material in these reactions.

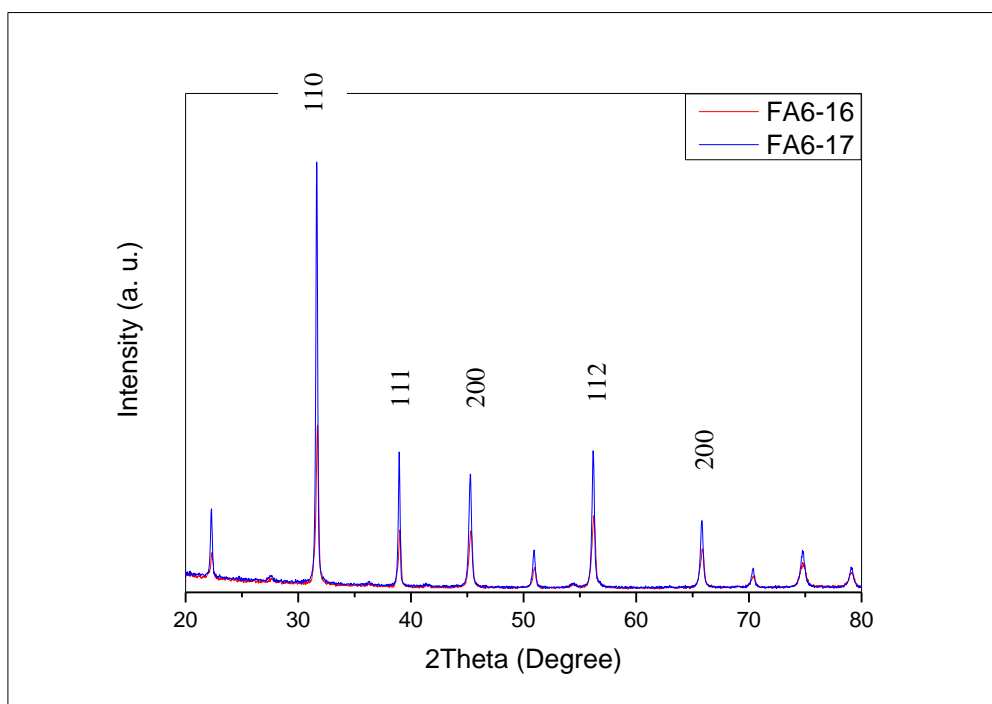


Figure 6-17: XRD spectra of the barium titanium oxide samples FA6-16 and FA6-17 prepared using approach 1-3 using FA5-26 as the starting material in these reactions.

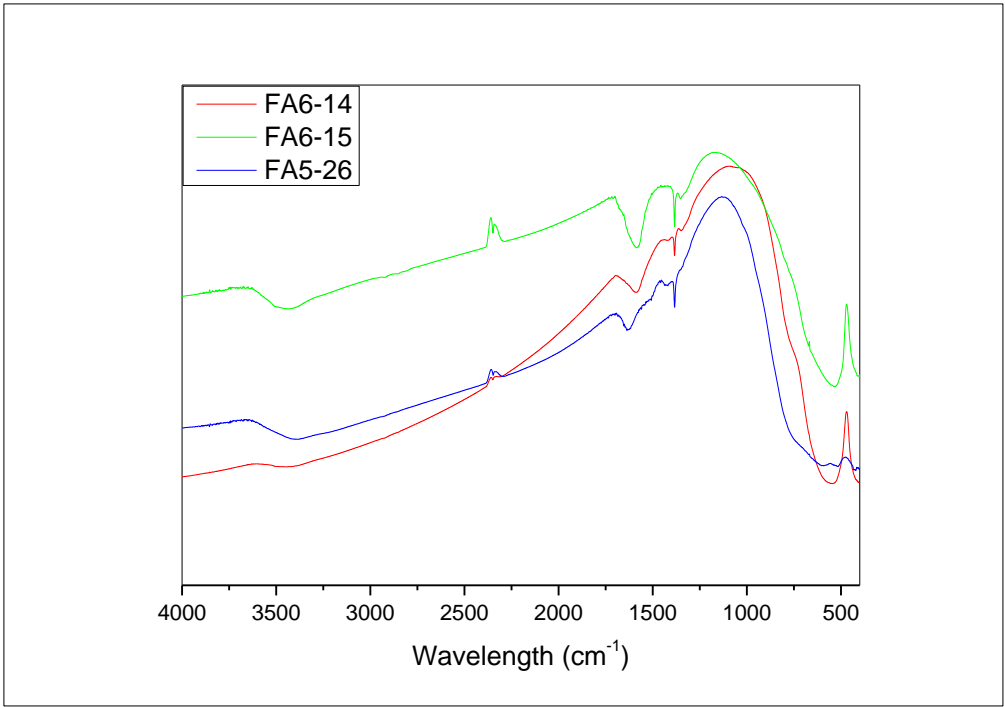


Figure 6-18: FT-IR spectra of the barium titanium oxide samples FA6-14 and FA6-15 prepared using approach 1-3 and the rutile titanium dioxide nanorods FA5-26 used as the starting material in these reactions.

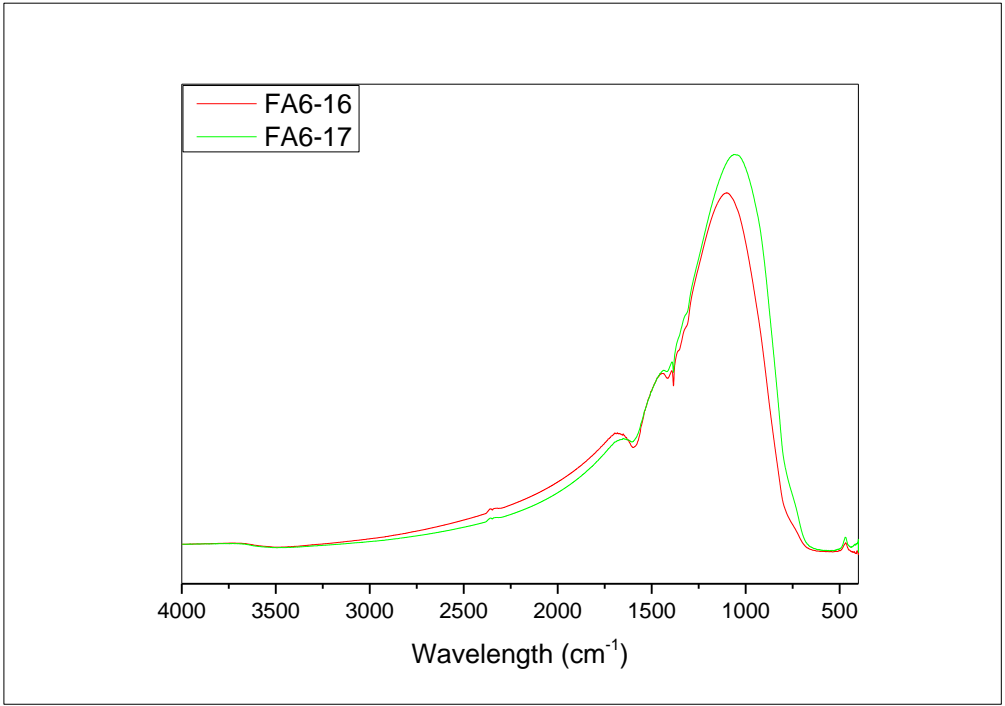


Figure 6-19: FT-IR spectra of the barium titanium oxide samples FA6-16 and FA6-17 prepared using approach 1-3 using FA5-26 as the starting material in these reactions.

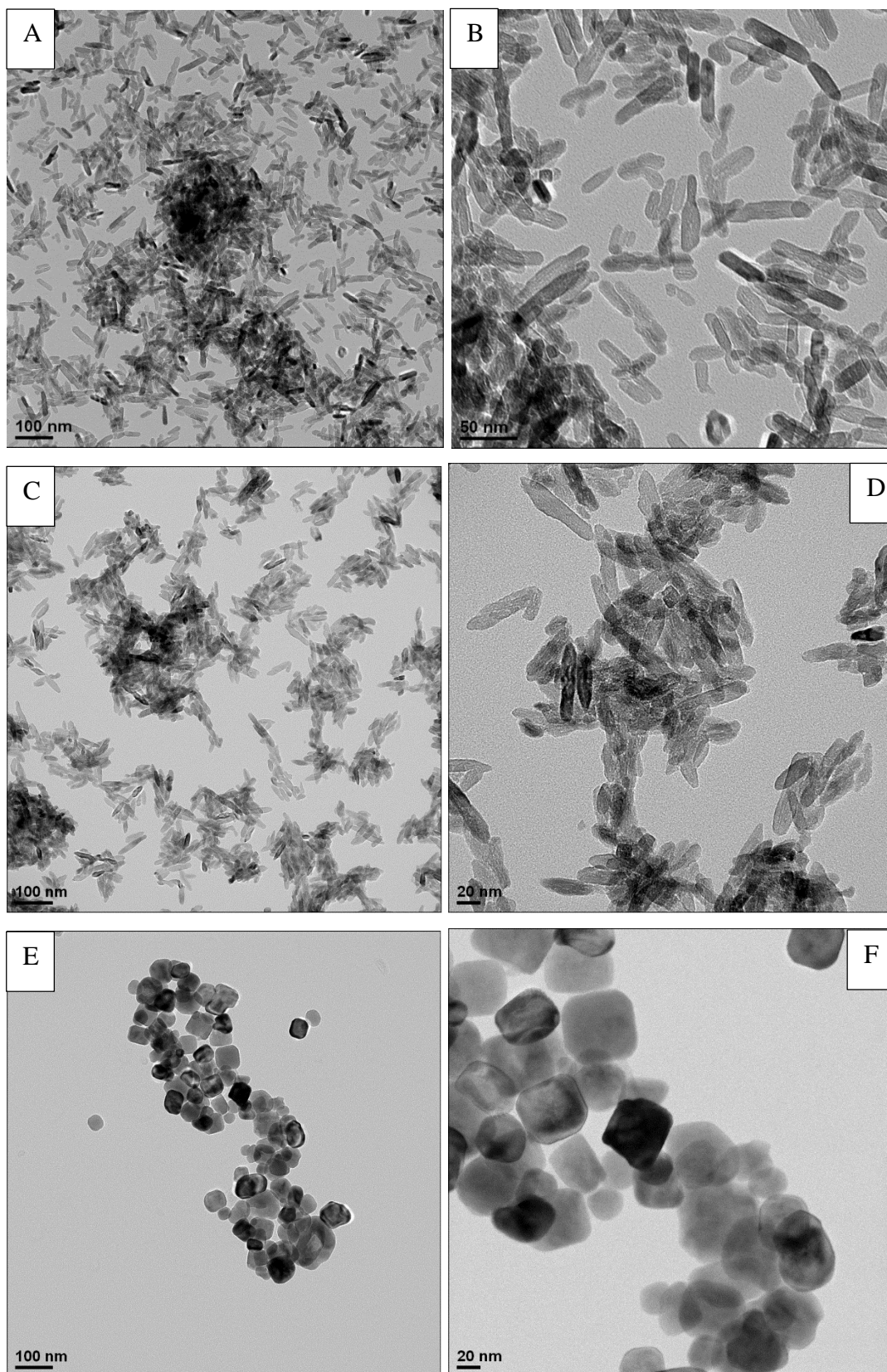


Figure 6-20: TEM images of rutile titanium dioxide nanorods FA5-26 used as the starting material in these reactions (A-B), barium titanium oxide (FA6-14 (C-D) and FA6-15 (E-F).

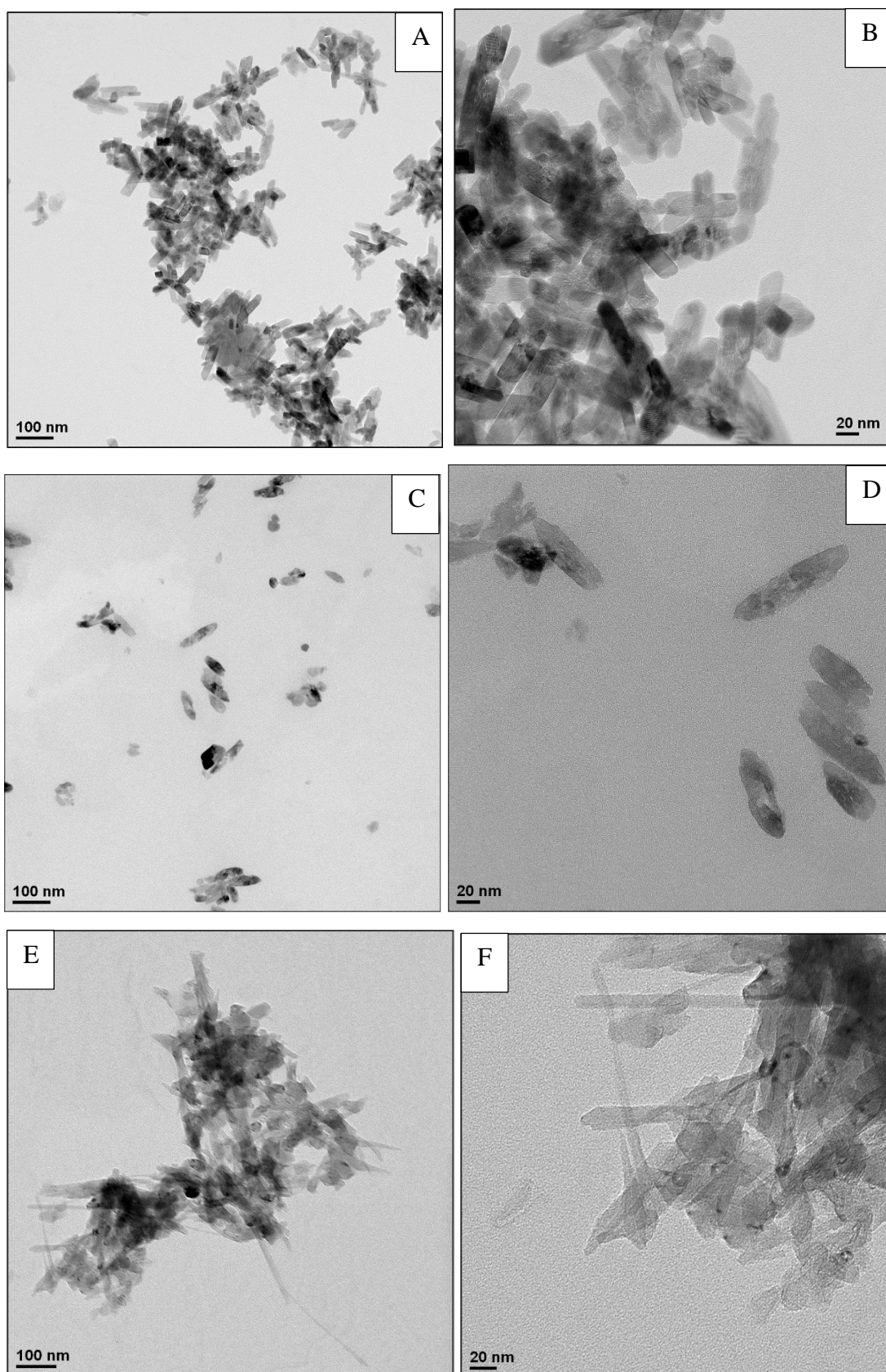


Figure 6-21: TEM images of rutile titanium dioxide nanorods FA5-26 used as the starting material in these reactions (A-B), barium titanium oxide FA6-16 (C-D) and FA6-17 (E-F).

Approach 1 - Reaction Mechanisms

There are two main possible mechanisms for hydrothermal conversion of titanium dioxide into barium titanium oxide: (A) *in-situ* conversion and (B) dissolution precipitation as shown in scheme 6-2.¹⁵

The *in-situ* conversion mechanism would involve titanium dioxide particles reacting first with dissolved cations (Ba^{2+}) in the reaction medium during the hydrothermal reaction to form a continuous layer of barium titanium oxide over the titanium dioxide surface. In order for the reaction to proceed additional barium ions must diffuse through the barium titanium oxide layer to react with the titanium dioxide source until all the titanium dioxide has reacted with the barium ions to form barium titanium oxide. Two rate-governing processes are possible: one is the diffusion of cations (Ba^{2+}) through the barium titanium oxide layer and the other is the reaction between the barium species and titanium dioxide within the nanoparticles. As the reaction proceeds and the surface layer of barium titanium oxide becomes thicker it could reasonably be expected that the conversion reaction would slow down and the reaction rate would approach zero at some point.¹⁶

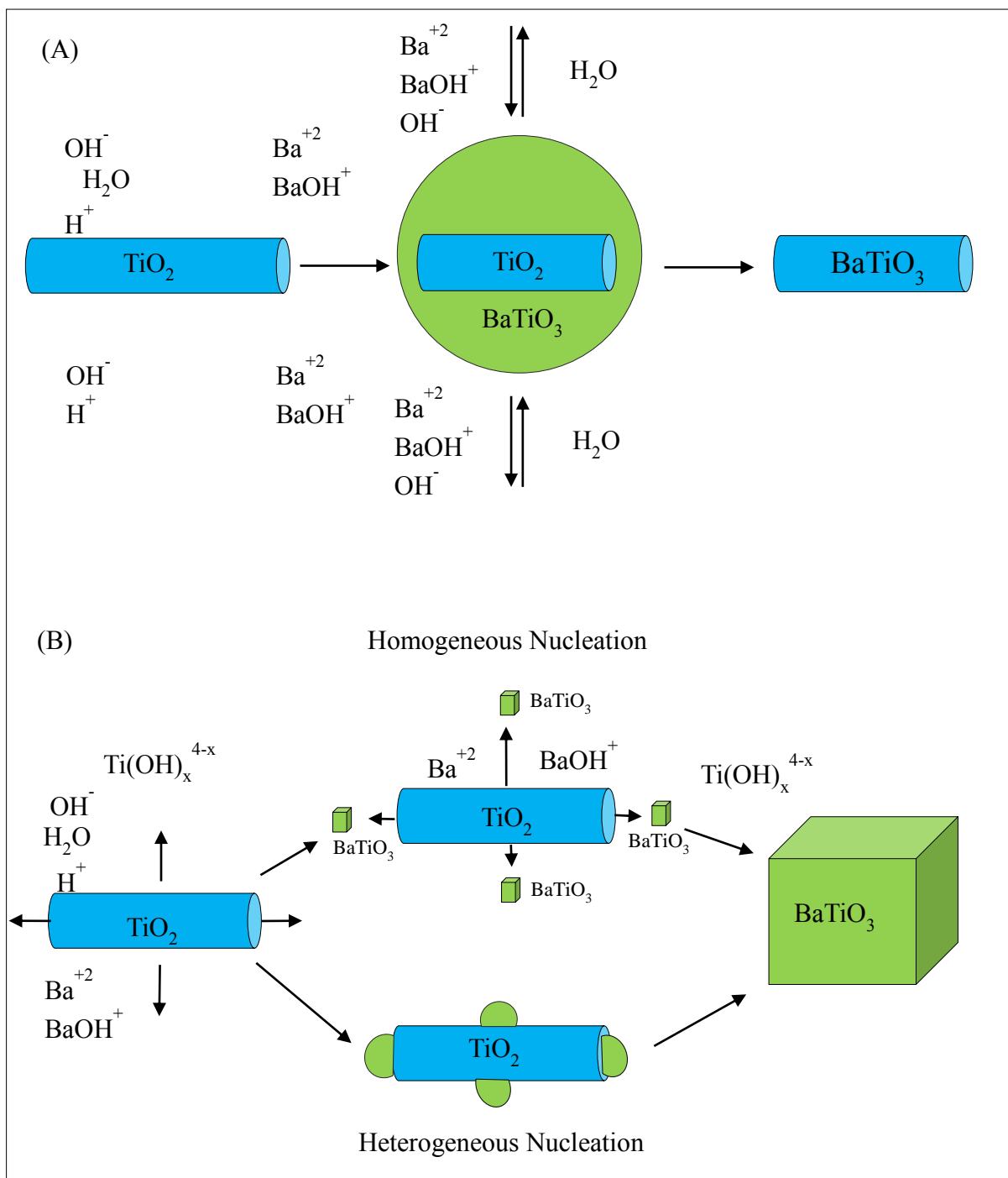
The dissolution precipitation process would involve several stages. Firstly the bonds between Ti and O (Ti-O) in anhydrous titanium dioxide should be broken by hydrolytic attack by hydroxyl anions to produce complexes of titanium hydroxide ($\text{Ti}(\text{OH})_x^{4-x}$) capable of dissolution, which will then react with either barium cations (Ba^{2+}) or barium hydroxide complexes (BaOH^+) in solution to form barium titanium oxide.¹⁵

On the other hand, if using a hydrous titanium dioxide reactant were used in the hydrothermal reaction, some or most of the hydroxylation stage could be avoided. Barium titanium oxide nuclei could either form on the titanium dioxide substrate (heterogeneous nucleation) or form straight in the bulk solution (homogeneous nucleation).

The size and morphology of the barium titanium oxide products, prepared from anatase oleic acid-stabilised titanium dioxide ($\text{TiO}_2\text{-OA}$) nanorods in approach 1-1, are very different from those of the titanium dioxide nanorods used as the starting material suggesting that the reaction in approach 1-1 might occur through a dissolution precipitation mechanism.^{6, 17}

On the other hand, the size and morphology of the barium titanium oxide products prepared using a molar ratio $\text{Ba/Ti} = 1$ in approach 1-2 are similar to those of the rutile titanium nanorods used as the starting material, suggesting that *in-situ* conversion may be the main mechanism for the reaction in approach 1-2.

The size and morphology of the barium titanium oxide products prepared from 24 h reaction are similar to those of the starting rutile titanium dioxide in approach 1-3, however, when the reaction time is increased from 24 h to 48 h, the size and morphology of the barium titanium oxide products changes completely. The titanium dioxide nanorods used to prepare sample FA6-15 using a ratio $Ba/Ti = 1$ and a reaction time of 48 h in approach 1-3 have completely disappeared in the reaction product and barium titanium oxide nanoparticles with a diameter of $\sim 20\text{nm} - 60\text{ nm}$ are formed. The titanium dioxide nanorods used to prepare sample FA6-17 using a ratio of $Ba/Ti = 1.5$ and a reaction time of 48 h in approach 1-3 have been converted to much longer nanorods than those present in the titanium dioxide nanorods used as the starting material. Thus, in situ conversion is the most likely mechanism for the reaction carried out for 24 h in approach 1-3, but it is still unclear what then happens in the reaction after 24 h.



Scheme 6-2: Possible mechanisms for the conversion of titanium dioxide nanorods into barium titanium oxide nanoparticles *via* a hydrothermal reaction.

6.3.2 Approach 2: Barium Titanium Oxide Nanorods from a Single-source Ba/Ti Precursor

The XRD spectrum of the barium titanium oxide sample FA6-18, shown in Figure 6-22 reveals that barium titanium oxide nanorods have been formed in a cubic phase.¹⁸ Some impurities of barium carbonate have also been formed during the reaction, but they can be readily removed by washing with (1 M) formic acid.

The FT-IR spectrum of the barium titanium oxide product FA6-18 shown in figure 6-23 reveals a broad peak at $\sim 550\text{ cm}^{-1}$, which is related to the Ti-O stretching bond for BaTiO_3 ¹⁹, and a peak at 1625 cm^{-1} related to carboxylate group stretching modes. There is also broad absorption peak at $\sim 3500\text{ cm}^{-1}$, which is related to O-H stretching modes.²⁰

The TEM images shown in figure 6-24 for the barium titanium oxide sample FA6-18 show that, although some large nanorods have been formed ($l = 6.3\ \mu\text{m}$ and $d = 0.83\ \mu\text{m}$), most of the nanoparticles are spherical in shape.

Analysis using ICP shows that the content of titanium and barium present in the barium titanium oxide nanorods FA6-18 is 23.49 % and 47.25 %, respectively. The atomic Ti/Ba ratio of 1.43 is higher than one in the crude reaction product due to the presence of barium carbonate, which can be removed easily by washing with formic acid.

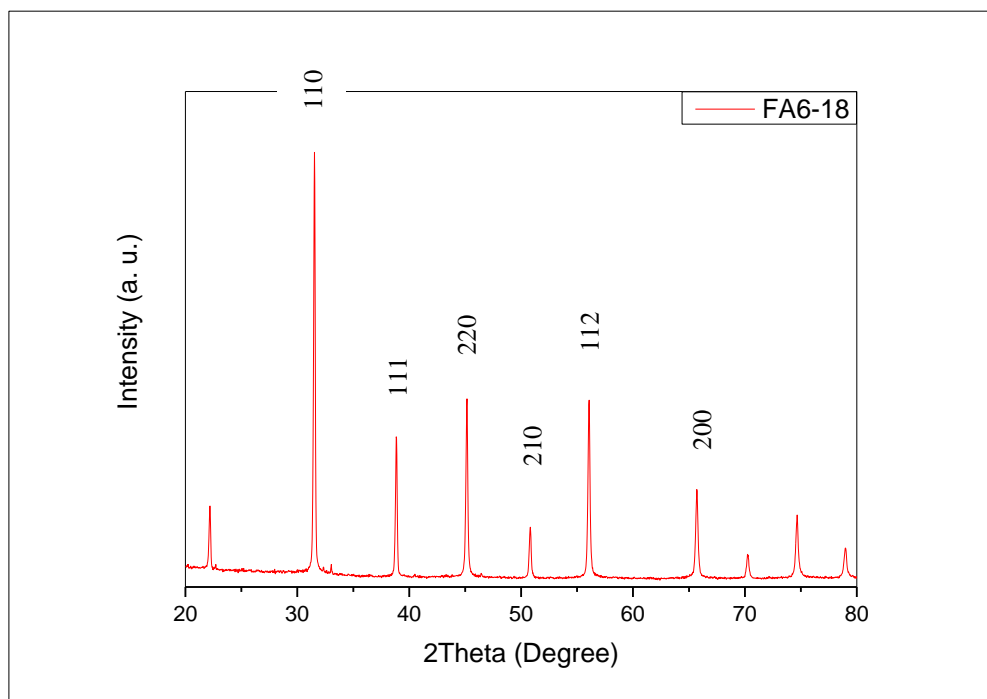


Figure 6-22: XRD spectra of the barium titanium oxide sample FA6-18.

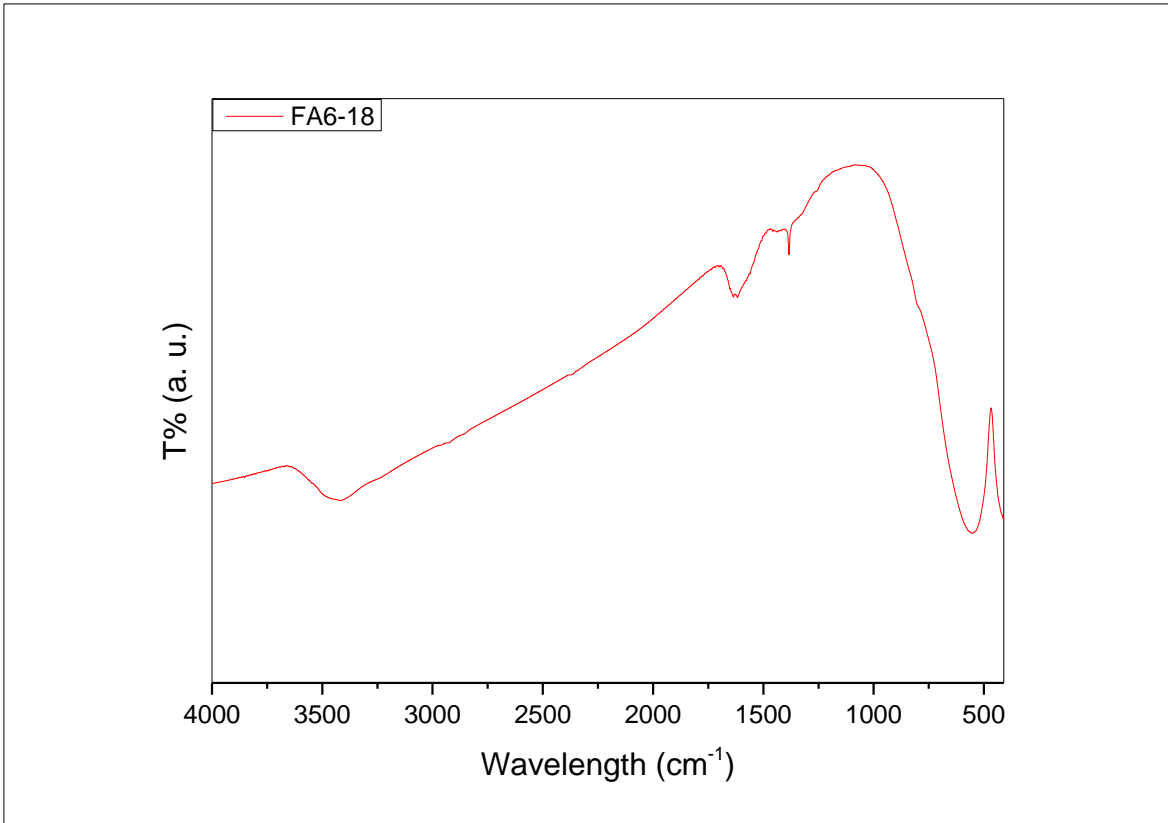


Figure 6-23: FT-IR spectra of the barium titanium oxide sample FA6-18.

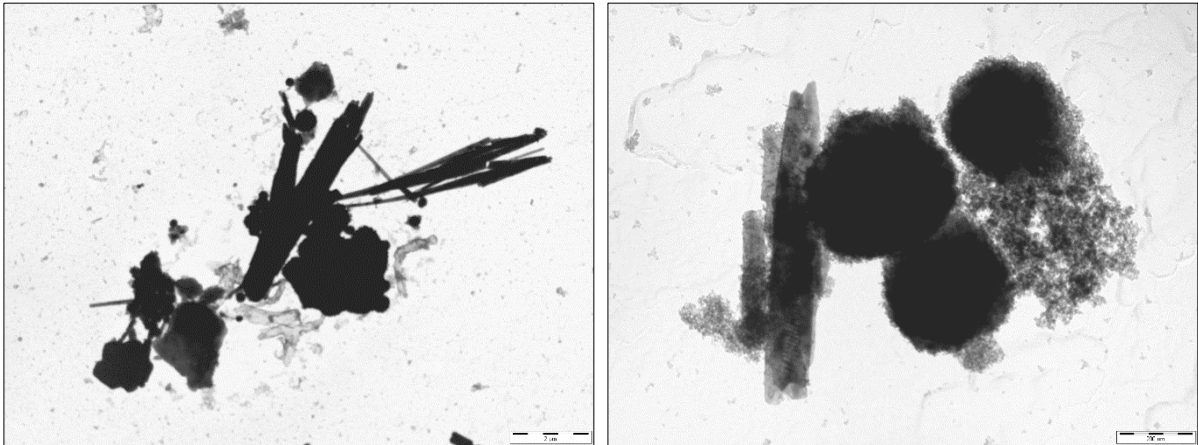


Figure 6-24: TEM images of the barium titanium oxide sample FA6-18.

6.3.3 Approach 3 - Barium Titanium Oxide Nanorods BaTiO₃ using Ethylene Glycol

The XRD spectra of the barium titanium oxide sample FA6-19, before and after the washing treatment, shown in figure 6-25 reveal that barium titanium oxide has been obtained in a cubic phase.²¹ The impurities of barium carbonate also formed during the reaction can be removed by washing with (1 M) formic acid.

The FT-IR spectra of the barium titanium oxide product FA6-19, shown in figure 6-26, contains a broad peak at $\sim 550\text{ cm}^{-1}$ associated with the Ti-O stretching bonds for BaTiO₃.¹⁹ The two peaks apparent at 1625 cm^{-1} and $\sim 3500\text{ cm}^{-1}$ are related to the carboxylate group and O-H stretching modes, respectively.²⁰

The TEM images of barium titanium oxide FA6-19 recorded in figure 6-27 reveal that large nanoplates of barium titanium oxide have been formed ($l = 800\text{ nm}$ and $d = 100\text{ nm}$) in.

Analysis using ICP indicates that the content of titanium and barium present in the barium titanium oxide nanorods FA6-19 is 21.30 % and 55.34 %, respectively, and the Ti/Ba atomic ratio is 1.04, which is indicative of almost complete conversion of the titanium oxy chloride used as the starting material into a barium titanium oxide product.

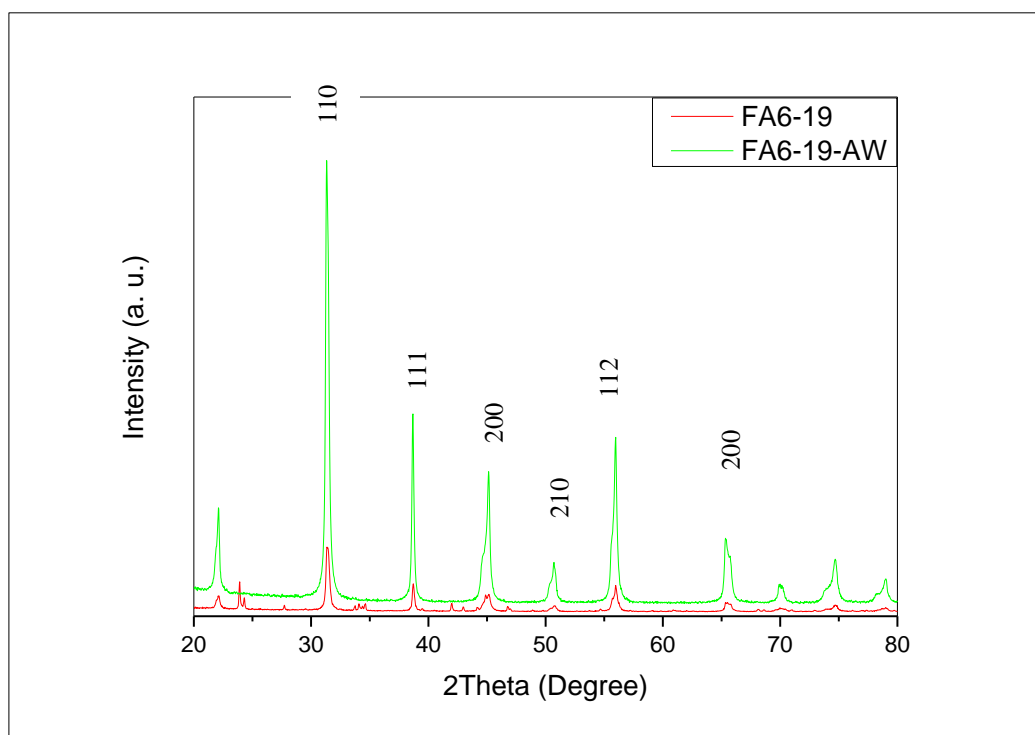


Figure 6-25: XRD spectra of the barium titanium oxide sample FA6-19 and FA6-19 AW, before and after washing with formic acid, respectively.

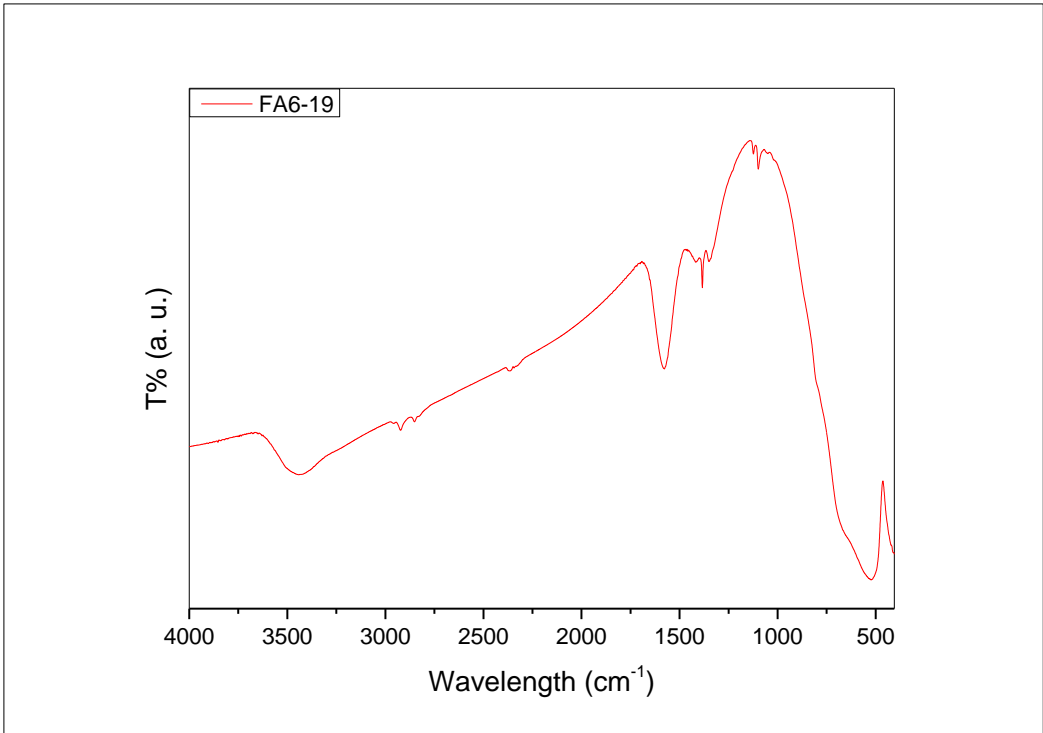


Figure 6-26: FT-IR spectrum of the barium titanium oxide sample FA6-19.

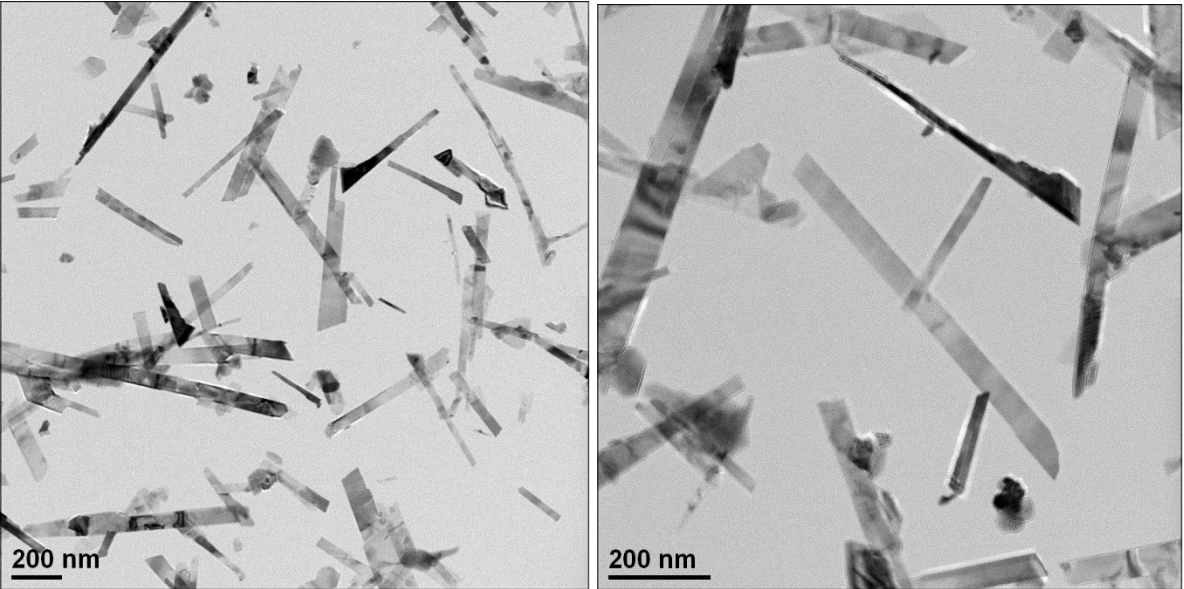


Figure 6-27: TEM images of the barium titanium oxide sample FA6-19.

6.4 Conclusions

Three approaches have been investigated in attempts to prepare barium titanium oxide (BaTiO_3) nanorods efficiently with a given shape and size:

In approach 1, a hydrothermal reaction was carried out to convert titanium dioxide nanorods to BaTiO_3 . Three different sources of titanium dioxide nanorods were used as the starting materials.

In Approach 1-1 the oleic acid-stabilised titanium dioxide nanorods ($\text{TiO}_2\text{-OA}$) with an aspect ratio from 5 - 8, used as the starting material were converted to cubic barium titanium oxide at a $\text{pH} = 12.3$. The shape of nanorods in the starting material was not retained during the conversion reaction. Therefore, taking into account the fact that as the size and morphology of the obtained barium titanium oxide products are very different from those of the starting material ($\text{TiO}_2\text{-OA}$), it is suggested that this reaction may well occur through a dissolution precipitation mechanism.

In Approach 1-2 hair-like rutile titanium dioxide nanorods were used as the starting material. Analysis using XRD shows that the rutile titanium dioxide (TiO_2) nanorods have been completely converted into the corresponding barium titanium oxide nanorods. Analysis using TEM confirms that the shape of the barium titanium oxide nanorods is very similar to that of the titanium dioxide nanorods used as the starting material for the product prepared using a Ba/Ti molar ratio = 1, although some aggregation of the nanorods is observed. This fact suggests that an *in-situ* conversion may be the main mechanism for this reaction. However, only spherical nanoparticles were obtained if prepared using a Ba/Ti molar ratio = 1.5, probably due to the aggregation of nanorods to form nanospheres.

In Approach 1-3 large rutile titanium dioxide nanorods were used as the starting material. The size and morphology of the barium titanium oxide products prepared using a 24 h reaction time are very similar to those of the titanium dioxide nanorods used as the starting material. However, when the reaction time is increased from 24 h to 48 h, the size and morphology of the barium titanium oxide products are completely different. For the sample FA6-15, prepared using a Ba/Ti molar ratio = 1.0 and a 48 h reaction time, the original nanorods have completely disappeared and spherical nanoparticles with a diameter of 20 nm - 60 nm are formed. For the sample FA6-17 prepared using a Ba/Ti molar ratio = 1.5 and a 48 h reaction time, nanorods can also be observed in the TEM images, but they are much longer than those of the titanium dioxide nanorods used as the starting material. An *in-situ* conversion reaction may be the main

mechanism for the first 24 h of the reaction in approach 1-3, but what happens during the reaction after 24 h is still unclear.

In Approach 2 the preparation of barium titanium oxide was carried out by hydrothermal reaction of a single source Ba/Ti precursor, barium titanium ethylhexano-isopropoxide $\text{BaTi}(\text{O}_2\text{CC}_7\text{H}_{15})(\text{OC}_3\text{H}_7)_5$. Some large nanorods are formed ($l = 6.3 \mu\text{m}$ and $d = 0.83 \mu\text{m}$), but the most of the nanoparticles formed are spherical in shape.

In Approach 3 the barium titanium oxide, prepared using a hydrothermal reaction between barium chloride (BaCl_2) and titanium oxy chloride (TiOCl_2) in presence of ethylene glycol as surfactant, are formed as large nanoplatelets ($l = 800 \text{ nm}$ and $d = 100 \text{ nm}$) with a Ti/Ba atomic ratio of 1.04 indicative of almost complete conversion of the titanium oxy chloride used as the starting material into a barium titanium oxide product.

6.5 References

1. Mostaghaci, H.; Brook, R. J., Microstructure development and dielectric properties of fast-fired BaTiO₃ ceramics. *Journal of Materials Science* **1986**, 21, (10), 3575-3580.
2. Dey, S. K.; Lee, J. J., Cubic paraelectric (nonferroelectric) perovskite PLT thin films with high permittivity for ULSI DRAMs and decoupling capacitors. *Electron Devices, IEEE Transactions on* **1992**, 39, (7), 1607-1613.
3. Huybrechts, B.; Ishizaki, K.; Takata, M., The positive temperature coefficient of resistivity in barium titanate. *Journal of Materials Science* **1995**, 30, (10), 2463-2474.
4. Chang-Hua, A.; Shu-Tao, W.; GChun-Ying, L.; Yun-Qi, L., Facile Hydrothermal Single-source Approach to Barium Titanate Nanorods and Nanospheres Preparation. *Chinese Journal of Inorganic Chemistry* **2006**, 22, (6), 1143-1147.
5. Inada, M.; Enomoto, N.; Hayashi, K.; Hojo, J.; Komarneni, S., Facile synthesis of nanorods of tetragonal barium titanate using ethylene glycol. *Ceramics International* **2015**, 41, (4), 5581-5587.
6. Hu, M. Z. C.; Kurian, V.; Payzant, E. A.; Rawn, C. J.; Hunt, R. D., Wet-chemical synthesis of monodispersed barium titanate particles — hydrothermal conversion of TiO₂ microspheres to nanocrystalline BaTiO₃. *Powder Technology* **2000**, 110, (1–2), 2-14.
7. Habib, A.; Haubner, R.; Stelzer, N., Effect of temperature, time and particle size of Ti precursor on hydrothermal synthesis of barium titanate. *Materials Science and Engineering: B* **2008**, 152, (1–3), 60-65.
8. Choi, M.; Yong, K., A facile strategy to fabricate high-quality single crystalline brookite TiO₂ nanoarrays and their photoelectrochemical properties. *Nanoscale* **2014**, 6, (22), 13900-13909.
9. <http://www.crystallmaker.com/crystallmaker/gallery/graphics.html>, (09/06/2015).
10. Tripathy, S. K.; Sahoo, T.; Mohapatra, M.; Anand, S.; Das, R. P., XRD studies on hydrothermally synthesised BaTiO₃ from TiO₂-Ba(OH)₂-NH₃ system. *Materials Letters* **2005**, 59, (28), 3543-3549.

11. Uhlmann, D. R.; Ulrich, D. R.; Engineering, U. o. A. C. o.; Science, M. D. o. M.; Engineering, *Ultrastructure processing of advanced materials*. Wiley: 1992.
12. Samuneva, B.; Jambazov, S.; Lepkova, D.; Dimitriev, Y., Sol-gel synthesis of BaTiO₃ and Ba_{1-x-y}Ca_ySr_x(Zr_yTi_{1-y})O₃ perovskite powders. *Ceramics International* **1990**, 16, (6), 355-360.
13. Nakayama, N.; Hayashi, T., Preparation and characterization of poly(l-lactic acid)/TiO₂ nanoparticle nanocomposite films with high transparency and efficient photodegradability. *Polymer Degradation and Stability* **2007**, 92, (7), 1255-1264.
14. Gao, Y.; Chen, G.; Oli, Y.; Zhang, Z.; Xue, Q., Study on tribological properties of oleic acid-modified TiO₂ nanoparticle in water. *Wear* **2002**, 252, (5–6), 454-458.
15. Eckert, J. O.; Hung-Houston, C. C.; Gersten, B. L.; Lencka, M. M.; Riman, R. E., Kinetics and Mechanisms of Hydrothermal Synthesis of Barium Titanate. *Journal of the American Ceramic Society* **1996**, 79, (11), 2929-2939.
16. Hertl, W., Kinetics of Barium Titanate Synthesis. *Journal of the American Ceramic Society* **1988**, 71, (10), 879-883.
17. Habib, A.; Stelzer, N.; Angerer, P.; Haubner, R., Effect of temperature and time on solvothermal synthesis of tetragonal BaTiO₃. *Bulletin of Materials Science* **2011**, 34, (1), 19-23.
18. Guo, W.; Datye, A. K.; Ward, T. L., Synthesis of barium titanate powders by aerosol pyrolysis of a Pechini-type precursor solution. *Journal of Materials Chemistry* **2005**, 15, (4), 470-477.
19. Last, J. T., Infrared-Absorption Studies on Barium Titanate and Related Materials. *Physical Review* **1957**, 105, (6), 1740-1750.
20. Durán, P.; Capel, F.; Tartaj, J.; Gutierrez, D.; Moure, C., Heating-rate effect on the BaTiO₃ formation by thermal decomposition of metal citrate polymeric precursors. *Solid State Ionics* **2001**, 141–142, 529-539.
21. Sahoo, T.; Tripathy, S. K.; Mohapatra, M.; Anand, S.; Das, R. P., X-ray diffraction and microstructural studies on hydrothermally synthesized cubic barium titanate from TiO₂–Ba(OH)₂–H₂O system. *Materials Letters* **2007**, 61, (6), 1323-1327.

Conclusions

Conclusions

High-*k* dielectric nanorods, which are potentially suitable for low-voltage OFET applications, have been prepared and characterized in this research. The modifications of the nanorods surface with oleic acid, amine and phosphonic acid or phosphonate ligands have also been investigated to improve the solubility of the products in organic solvents.

Oleic-acid-stabilised titanium dioxide nanorods (TiO₂-OA) were prepared using a hydrolysis reaction at 100 °C for 72 h using titanium (IV) tetraisopropoxide (TTIP) as the source of titanium and oleic acid as the surfactant. The TiO₂-OA nanorods prepared using this method have an aspect ratio of 5-8, with a length of ~20nm and a ~3 -4 nm. The specific oleic acid-stabilised titanium dioxide nanorods (TiO₂-OA) FA3-1 were spin coated from a 10% wt solution in chlorobenzene onto pre-patterned metallic electrodes, with a final thickness of the hybrid insulating films of ~200 nm. The dielectric constant of the resultant films is 9-10 at 1MHz, which has been cooperated and provided by Professor Mary O`Neill, Dr Emanuele Verrelli and PhD student, Mohammed A Ibrahim.

After replacement of the oleic acid attached to the surface of the TiO₂-OA nanorods with phosphonic acid or phosphonate, such as octylphosphonic acid (OPA), decylphosphonic acid (ODPA) and 2-phenylethyl phosphonate (DEPPNA), in ligand exchange reactions the phase and morphology of the resultant products were same as those of TiO₂-OA. The ICP and CHN results suggest that the ligands are attached on TiO₂ surface *via* ligand exchange of oleic acid and *via* reaction of P-OH groups of ligands with the hydroxyl groups on the titanium dioxide surface. The ligand exchange rate of phosphonic acid was higher than that of phosphonate and the solubility of the products in organic solvents depends on the structure and the alkyl length of the ligands.

Solution processable, oleic-acid-stabilised, niobium- and indium-doped anatase nanorods TiO₂ (TiO₂-OA-M; M = Nb, In or Nb/In) have been prepared by a novel method based on the co-hydrolysis of titanium (IV) tetraisopropoxide (TTIP) and niobium or/and indium precursors. Niobium isopropoxide (NBIO) and niobium (V) ethoxide (NBEO) were used as niobium precursors and indium (III) isopropoxide (INIO) and indium (III) ethoxide (INEO) as indium

precursors. All the products have a similar morphology of nanorods with length and diameter of 20 and 3 – 4 nm, respectively. Up to 10 % of the products can be dissolved in chlorobenzene.

The Ti/Nb ratio of the products $\text{TiO}_2\text{-OA-Nb}$ was close to the starting molar ratio of TTIP/NBEO when using niobium (V) ethoxide (NBEO) as precursor, but higher than that of TTIP/NBIO when using niobium isopropoxide (NBIO) as precursor. XPS analysis shows that the titanium and niobium anions were present mainly as Ti^{4+} and Nb^{+5} in $\text{TiO}_2\text{-OA-Nb}$. The Ti/In ratio was much higher than the starting molar ratio of TTIP/INIO and TTIP/INEO for the products $\text{TiO}_2\text{-OA-In}$, regardless of using either indium (III) isopropoxide (INIO) or indium (III) ethoxide (INEO) as indium reaction precursors. A mixture of niobium isopropoxide (NBIO) and indium (III) isopropoxide (INIO) was also used as precursors for the preparation of oleic acid-stabilised, niobium/indium-doped anatase nanorods TiO_2 ($\text{TiO}_2\text{-L-M}$; L = OA; M = Nb/In). The ratio Ti/Nb and Ti/In in the products was much higher than the starting molar ratio of TTIP/NBIO and TTIP/INIO used in the reactions.

Ligand exchange reactions were carried out with diethyl 2-phenylethyl phosphonate (DEPPNA) and octadecylphosphonic acid (ODPA) as ligands to produce the corresponding ODPA- or DEPPNA-stabilised, metal-doped nanorods ($\text{TiO}_2\text{-L-M}$; L = ODPA or DEPPNA; M = Nb or In or Nb/In). There was no change in phase, shape or size of the nanorods during the ligand exchange reactions. All of the oleic acid on the surface of the oleic acid-stabilised, niobium-doped nanorods has been replaced by ODPA to yield the corresponding ODPA-stabilised, niobium-doped nanorods ($\text{TiO}_2\text{-ODPA-Nb}$). Up to 10% of these ODPA- or DEPPNA-stabilised, metal-doped nanorods ($\text{TiO}_2\text{-L-M}$; L = ODPA or DEPPNA; M = Nb or In) can be dissolved in common organic solvents, such as chlorobenzene.

Rutile TiO_2 nanorods were synthesised using three different approaches and the surface modification of these nanorods has also been investigated.

In the first approach, hair-like rutile TiO_2 nanorods (Rutile-NRs-1) were prepared using a hydrolysis reaction of TiOCl_2 at 50 °C, 70 °C and 90 °C for 24 h. Surface modification of the rutile TiO_2 nanorods (Rutile-NRs-1) was carried out using wet TiO_2 nanorods with ligands, such as oleic acid and alkyl amines i.e., octyl amine, dodecyl amine and hexadecyl amine. The aliphatic surface coating of the TiO_2 /ligand nanocomposites leads to a relatively high degree of solubility in organic solvents, so some of them can be suspended up to a concentration of 10 % in chlorobenzene. These colloidal solutions are stable for several months. The hybrid

insulator of rutile TiO₂/ligand nanocomposites preparation – surface treatment method 2 product FA5-9 was spin coated from a 10% wt solution in chlorobenzene on prepatterned metallic electrodes, with final thickness of the hybrid insulating films was ~200 nm and the dielectric constant is 9-10 at 1MHz, which has been cooperated and provided by Professor Mary O`Neill, Dr Emanuele Verrelli and PhD student, Mohammed A Ibrahim.

In the second approach, rutile TiO₂ nanorods were prepared by a hydrothermal treatment of TiOCl₂ at 220 °C for 2 h. These rutile TiO₂ nanorods (Rutile-NRs-2) are relatively long, i.e., 150-200 nm and broad, i.e., 25-40 nm. Such large nanorods have a lower effective surface area than those prepared using approach 1 and so less oleic acid is attached in relative terms to the TiO₂/ligand nanocomposite surface, i.e., the carbon content for the resultant TiO₂/ligand nanocomposites is low, e.g., 6 %.

In the third approach, rutile TiO₂ nanorods were prepared by hydrothermal reaction of TiOCl₂ in the presence of 3-hydroxytyramine hydrogen chloride, [(HO)₂C₆H₃CH₂CH₂NH₂·HCl] at 150°C for 13 h. These rutile TiO₂ nanorods (Rutile-NRs-3) are smaller than Rutile-NRs-2, with e.g., 80 nm and 20 nm in length and diameter, respectively. However, the presence of some smaller TiO₂ nanoparticles, e.g., 25 nm long, is also observed. Surface modification was carried out using either oleic acid or phosphonate/phosphonic acid as ligands. Unfortunately, the solubility of TiO₂/ligand nanocomposites is limited due to a lower surface coverage of the ligands bonded onto the nanorod surface.

Barium titanium oxide nanorods (BaTiO₃) have been prepared by three approaches:

In the first approach, a hydrothermal reaction was carried out to convert titanium dioxide nanorods (TiO₂) into barium titanium oxide nanorods (NRs-BaTiO₃-1). Three kinds of titanium dioxide nanorods with different phases and sizes, i.e. anatase TiO₂-OA, rutile TiO₂ (Rutile-NRs-TiO₂-1) and (Rutile-NRs-TiO₂-3), were used as the starting materials. When TiO₂-OA was used as the starting material, the TiO₂ nanorods were converted to cubic BaTiO₃ nanorods at a medium pH = 12.3. The shape of nanorods of the starting material was completely changed during the conversion reaction, i.e., the size and morphology of the BaTiO₃ products obtained are very different from those of the starting TiO₂-OA nanorods, suggesting that the reaction may occur through a dissolution precipitation mechanism. When rutile TiO₂ (Rutile-NRs-TiO₂-1) and (Rutile-NRs-TiO₂-3) were used as the starting materials, the rutile TiO₂ nanorods were also converted to cubic BaTiO₃ nanorods, but the conversion rate depends on the size of the

starting rutile TiO_2 nanorods. *In-situ* transformation may be the main mechanism for the conversion of rutile TiO_2 nanorods to the corresponding BaTiO_3 nanorods

In the second approach the preparation of the barium titanium oxide nanorods (NRs-BaTiO₃-2) was carried out using an hydrothermal reaction using a Ba/Ti precursor, i.e., barium titanium ethylhexano-isopropoxide $\text{BaTi}(\text{O}_2\text{CC}_7\text{H}_{15})(\text{OC}_3\text{H}_7)_5$ to yield nanorods of 6.3 μm in length and 0.83 μm in diameter. However, the most of the nanoparticles produced are sphere-shaped.

In the third approach the preparation of barium titanium oxide nanorods (NRs-BaTiO₃-3) was carried out using a hydrothermal reaction between barium chloride (BaCl_2) and titanium oxychloride (TiOCl_2) in presence of ethylene glycol as surfactant. Nanoplates were formed of 800 nm in length and 100 nm in diameter with a Ti/Ba ratio of 1.04.

Appendix 1

Calculation of ligand exchange rate and analysis of the attachment of ligands on TiO₂.

First, assuming that there are 100 g of TiO₂-OA and TiO₂-ODPA (FA3-4).

Oleic acid molecular weight is 282.46, in which 216.19 is carbon.

Chemical analysis showed 18.6% of C present in TiO₂-OA, thus molar of oleic acid in the 100 g TiO₂-OA is: $18.6/216.19 = 0.086$ mol

Chemical analysis showed that 2.05 % of P and 20.9 % of C were present in TiO₂-ODPA.

If ODPA lost two H to attach on TiO₂ surfaces, the molecule formula is C₁₈H₃₇O₃P with molecule weight of 332.46 in which 216.19 is C and 30.97 is P.

Thus, 2.05 % of P means that 14.31 % of C should be from ODPA:

$$(216.19 / 30.97) \times 2.05 \% = 14.31 \%$$

The remaining 6.59 % of C should be from un-exchanged oleic acid:

$$20.9 \% - 14.31 \% = 6.59 \%$$

Thus the un-exchanged oleic acid is:

$$6.59 / 216.19 = 0.0305 \text{ mol}$$

The exchanged oleic acid is: $0.0860 - 0.0305 = 0.0555$ mol

The ligand exchange rate is: $0.0555 / 0.086 = 64.56 \%$

On the other hand, since 2.05 % of P was present in the TiO₂ – ODPA, the molar of ODPA in 100 g TiO₂ – ODPA is:

$$2.05/30.97 = 0.066 \text{ mol}$$

Since the molar of ODPA (0.066 mol) is higher than the ligand exchanged oleic acid (0.0555 mol), some ODPA should attach on TiO₂ surfaces through a reaction with the hydroxyl groups on TiO₂ surfaces.

Thus ODPA attached on TiO₂ surfaces should be *via* two reaction routes:

- 1) Ligand exchange route (**route 1**): $0.0555/0.066 \times 100 = 83.87 \%$
- 2) Reaction with hydroxyl groups (**route 2**): $100 \% - 83.87 \% = 16.13 \%$